

IR spectroscopy in catalysis

Janusz Ryzkowski*

*Faculty of Chemistry, Department of Chemical Technology, University of Maria Curie-Skłodowska,
Pl. M. Curie-Skłodowskiej 3, 20-031 Lublin, Poland*

Abstract

Infrared (IR) spectroscopy undoubtedly represents one of the most important tools in catalysis research. In this review, recent catalytic applications of the most popular IR techniques will be presented. Each section starts from the very general basis of the spectroscopic method applied. The last section is devoted to the adsorption of chelating compounds on surfaces of mineral oxides. The aim of adding a large number of illustrations and an appendix is to make the presented material more familiar for young researchers and postgraduate students. Most of the papers discussed have appeared in the last 5–6 years, because the older literature has been reviewed in earlier papers. © 2001 Elsevier Science B.V. All rights reserved.

Keywords: Infrared spectroscopy (transmission, reflectance, emission, photoacoustic); Sum frequency generation; Catalysis

1. Introduction

After nearly 50 years of intensive application, infrared spectroscopy (IR) remains the most widely used, and usually most effective, spectroscopic method for characterisation of the surface chemistry of het-

erogeneous catalysts. IR always played an important role in characterisation of heterogeneous catalysts, as it permits direct monitoring of the interaction between sorbed molecules and the catalysts.

The goals of catalytic research are varied. Complete understanding of catalytic reaction mechanisms, including the nature of adsorbed intermediates, is, of course, highly desirable. Catalysis is primarily an applied science, however, and as such should reasonably be expected to provide major assistance in reaching the goals of better catalysts and improved catalytic processes, from a better fundamental understanding of catalyst surface chemistry. This is an area in which IR will undoubtedly make further major contributions.

A variety of IR techniques has been and can be used in order to obtain information on the surface chemistry of different solids. Special meaning have investigations carried out under the reaction conditions. In principle for in situ measurements, all forms of IR spectroscopy are suitable. For most practical experimental reasons, however, the transmission–absorption technique is best suited. This is more related to the

Abbreviations: AIRE, abnormal infrared effect; BATE, boric acid trimethyl ester; CEES, chloroethyl sulphide; CIM, classical impregnation method; DIM, double impregnation method; DSC, differential scanning calorimetry; EDTA, ethylenediaminetetraacetic acid; HTR, high-temperature reduction; IEPS, isoelectric point of the surface; IJVS, Internet journal of vibrational spectroscopy; IRCP, infrared concentration programming; IRE, internal reflection element; IRTP, infrared temperature programming; ISRI, In Situ Research and Instruments; LRS, laser Raman spectroscopy; LTR, low-temperature reduction; MBOH, methylbutynol; ML, monolayer; RT, room temperature; SCO, selective catalytic oxidation; SCR, selective catalytic reduction; SSITKA, steady-state isotopic transient kinetic analysis; TADC, theory of average dielectric constant; TCE, trichloroethylene; TFE, trifluoroethanol; TGA, thermogravimetric analysis; TPD, temperature-programmed desorption; TPO, temperature-programmed oxidation

*Tel.: +48-81-537-55-96; fax: +48-81-537-55-65.

E-mail address: ryzkows@hermes.umcs.lublin.pl
(J. Ryzkowski).

design of cells that are to be used as reactor than with the principal problems of the other techniques.

Recently, several books have been published which are in some way directed at catalysis research. The contents of the books cover theoretical aspects of spectroscopy [1], different techniques and modern molecular spectroscopy [2,3], practical aspects of spectrometers and spectrometry [4], base information related to FT-IR with references and/or recommended bibliography for further reading [5], IR group frequencies [6], IR and Raman of inorganic and coordination compounds [7], interpretation of IR spectra [8,9], a handbook which provides unique data of IR and comparative Raman spectra of inorganic compounds and organic salts including some non-ionic compounds [10], and books for those beginning to work with IR and Raman Spectroscopy in the investigation of surfaces [11,12]. From the internet, the *Internet Journal of Vibrational Spectroscopy (IJVS)* can be found, which is published free of charge exclusively on the World Wide Web [13]. The six editions appearing each year are divided into two parts. The first contains three or four papers on a theme, of graded sophistication, aimed to assist, interest, and also improve the performance of the non-specialist through to the dedicated experienced spectroscopist; news, views, and an unusual feature “Hot Sources” on an ever expanding body of spectroscopic subjects, and Spectroscopists’ Bookshelf, a list of recommended books. Spectroscopy links is a regular, expanding feature of *IJVS*, which compiles a list of *Web sites* with a spectroscopic content [14]. Finally, a series of excellent reviews has been published in 1996, in a special issue of *Catalysis Today* (vibrational spectroscopy of adsorbed molecules and surface species on metal oxides 27 (3–4)).

In the past few years, one can observe a growing interest in the application of IR techniques in catalytic investigations. One of the reasons, among the others, is their wide distribution (nowadays, IR and/or FT-IR spectrometers belong to the standard equipment of each scientific laboratory) and the relatively low costs (compared to the other modern physico-chemical techniques for surface characterisation) of the base instrument.

The aim of this review is to present current investigations in the area of heterogeneous catalysis where different IR techniques are applied.

2. Brief historical background

Since 1905, when Coblenz obtained the first IR spectrum, vibrational spectroscopy has become an important analytical tool in research. By 1940, there was a large body of knowledge concerning IR spectroscopy [15–17]. Three programs of great importance during World War II provided the impetus to begin the manufacture of IR instruments: the synthetic rubber program, largely a US project; the production of aviation fuel, primarily a UK project; and the penicillin program, a joint US–UK endeavour. In 1943, a new technique was introduced for solid samples with Nujol as a mulling agent, and 9 years later KBr was used for solid discs (see Appendix A). In 1954, the analysis of samples in a matrix of liquid argon was introduced. Finally, attenuated total reflection (ATR) was developed independently by Fahrenfort and Harrick between 1959 and 1960. It has been especially useful for thick samples, strong absorbing samples, and surface studies. In the 1960s, the era of Fourier transform IR (FT-IR) began. It was possible due to the application of a “new” optic element (the Michelson interferometer), the development and miniaturisation of lasers, introduction of the algorithm for fast Fourier transform (FFT), development of microcomputers, and the triglycine sulphate (TGS) pyroelectric bolometer.

IR was probably the first vibrational technique to be applied to the analysis of adsorbates on well-defined surfaces. Terenin and Kasparov (1940) made the first attempt to employ IR in adsorption studies. They studied the absorption spectrum of ammonia adsorbed on a silica aerogel containing dispersed iron. The work was continued by Terenin and his collaborators after the Second World War. Carbon monoxide, chemisorbed on metals and metal oxides supported on silica or alumina powder, has been the subject of extensive studies by Eischens et al. [18].

3. Recent applications of IR in catalytic research, and IR cell reactors for in situ studies

Because IR spectroscopy is a regularly used technique for catalyst characterisation, compilations and reviews on the various experimental techniques are numerous. Transmission–absorption, diffuse reflectance, ATR, specular reflectance, and photoacoustic

spectroscopy are among the most frequently used techniques [19]. The principal information obtained with all these techniques is equivalent, and local availability and experimental necessities, such as the sample particle size and the molecular extinction coefficient of the sample, may dominate personal choices. The vast majority of experiments are currently performed in the transmission–absorption and the diffuse reflectance mode. However, as it was pointed out in Section 1, IR plays an important role in characterisation of heterogeneous catalysts, and that is the reason that a large number of publications (including this one) deal with that subject [20–82] [83–145] [146–207]. This includes spectral characteristics of reaction components, catalyst precursors, surface changes due to temperature treatment, and many others. Noticeable examples of spectroscopic application will be given in the following sections.

As the type of probe molecule chosen will influence the obtained characteristics of the probed solid, and will therefore also affect the structure–activity relationship derived, the choice of the appropriate probe molecule is very important [19]. In the last 5 years, one can find in the scientific literature applications of different probe molecules, including those which are the most frequently used as well as very specific, or less frequently used molecules. The literature quotations are examples of applications in catalytic research as follows: ethylamines [166], pyridine [185–207,224–284], pyrrole [274], 2,4,6-tri-*tert*-butylpyridine [285], acetonitrile [182,183,273,274,277], CD₃CN (fully deuterated acetonitrile) [278,286–288], *t*-butylcyanide [283,284], trimethylacetonitrile (pivalonitrile, (CH₃)₃CCN) [183, 184], ammonia [161–165,207–223,279–281,352], carbon monoxide [170–174,205,272–274,287–356], carbon dioxide [175,273,274,276,348–350], nitrogen oxide [167–169,223,282,353–367], methanol [176, 177], ethanol [351], cyclohexanol [178], dibenzenes [179,180], chloroform [181], heavy water (D₂O) [206], dimethylether [274], benzaldehyde [277,350], ethene [347], propene [275,347,367], butenes [347], nitrogen [356], and nitrogen dioxide [368].

Characterisation of selective poisoning of acid sites on sulphated zirconia by ammonia adsorption has been studied [209]. IR spectroscopic studies indicate that the strong acid sites are Brønsted and possibly Lewis acid centres, while the acid sites of intermediate

strength are mainly Brønsted acid sites. The results of selective poisoning of the sulphated zirconia with ammonia indicate that Brønsted acid sites of intermediate strength are active for *n*-butane isomerisation at 423 K while not discounting a possible role of the stronger acid sites.

Binet et al. [274] have investigated surface properties of high surface area ceria samples either in the reduced or unreduced state. For this purpose, as the probe molecules they have utilised adsorption of pyridine, pyrrole, acetonitrile, CO₂, CO, and dimethyl ether.

Carbon monoxide adsorption was a subject of IR studies over Pt/ γ -Al₂O₃ [291], Cu/SiO₂ and Cu/SiO₂–TiO₂ [296,297], Ni/SiO₂ [318], nickel–magnesia catalyst used for CO₂ reforming of methane [304], Au/TiO₂ [330], Pt–Au particle catalysts [302]. Spielbauer et al. [352] have investigated the acidity of sulphated zirconia by adsorption of CO and ammonia. Nitrogen and carbon monoxide were used as probes of zeolite acidity [356].

The IR cell in which the catalyst sample is pre-treated and subsequently studied is extremely important in surface studies. The perfect, all-purpose cell has yet to be devised, and cell design is normally chosen to suit the purposes of a particular study. Some features are usually of overriding importance in a given application. If catalytic reactions are to be studied, the exposure of catalytic metals must be eliminated in cell construction, and bare-heating elements within the cell are ruled out. In some surface characterisation studies such features may be completely acceptable, but even in such studies it is well to avoid any possibility of Ni or other carbonyls being formed from cell components. A variety of relatively simple, but effective, cells has been used for studies. Many of these have been described in the literature and plans of them have been given [369].

As it was mentioned, starting from the pioneering work of Eischens et al. [4,370] on supported metal catalysts (adsorption of ammonia and carbon monoxide), the use of IR in surface science and catalysis has grown rapidly. IR, with its high-energy resolution, can be a very appropriate tool to investigate the internal and external modes of adsorbates and their vibration dynamics. The development of in situ vibrational spectroscopies applicable to metal–support interfaces in recent years has exerted a profound influence on

our understanding of adsorptive chemistry in heterogeneous systems. Some pertinent information can be obtained from the number of bands in the spectra at a single-stage of surface coverage as shown in the original spectra of chemisorbed CO [4]. However, these single-stage spectra do not reveal the relative strength of bonding for the chemisorbed CO contributing to each band or the effect of interaction on the band positions. To obtain this information, the spectra of chemisorbed CO were studied as a function of surface coverage over silica-supported Pt, Pd, and Ni [371]. The authors wrote: “In order to carry out this work efficiently, it was necessary to design apparatus in which the IR spectra could be obtained while the samples were subjected to a wide range of temperatures and pressures. Successful development of this in

situ apparatus not only makes it possible to study the effect of surface coverage but also opens the way to IR studies of chemisorbed molecules while reactions are in progress” [371]. It was one of the first in situ cells for IR studies published in scientific literature [371,372] (see Fig. 1).

More than four decades ago, based on the result thus obtained, Eischens et al. [371] predicted that IR technique would prove to be extremely important in the study of adsorption and catalysis. Parry [373] has applied in situ IR studies for pyridine adsorption on acid solids (see Fig. 2).

He has pointed out that the use of IR technique, and particularly the use of the pyridine spectrum thus appears to be a useful means for delineating protonic and aprotic acidity on surfaces and to find what

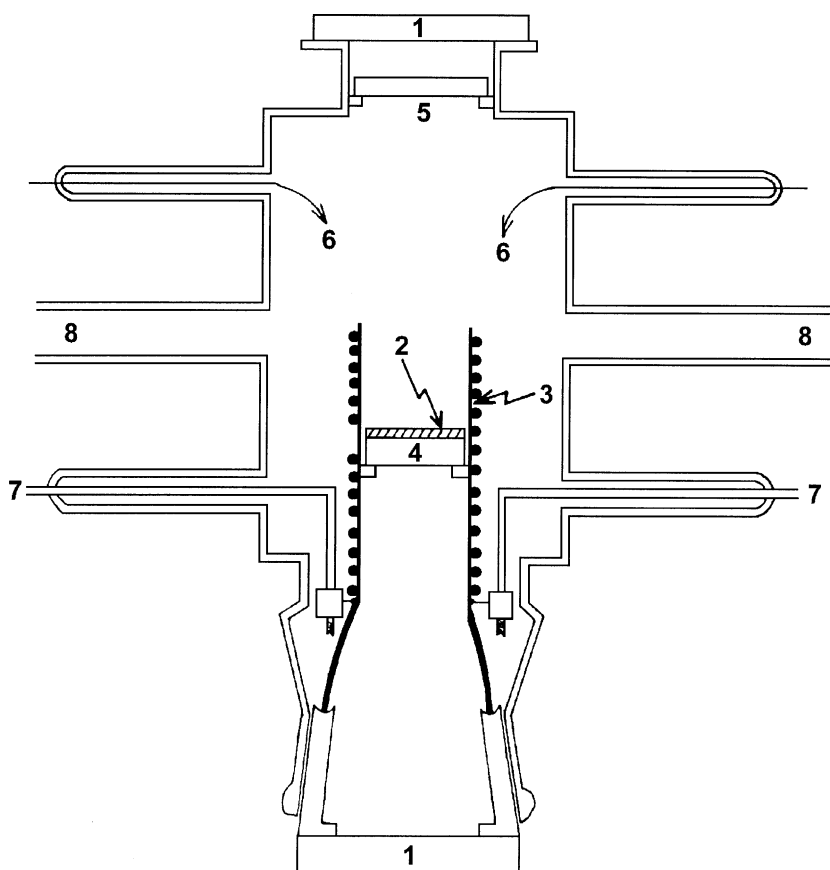


Fig. 1. Simplified scheme of in situ cell for IR study of chemisorbed gases: (1) CaF_2 windows; (2) sample; (3) furnace; (4) CaF_2 plate; (5) gas convection shield; (6) thermocouple; (7) heating wire; (8) connection to the vacuum and gas line [371,372].

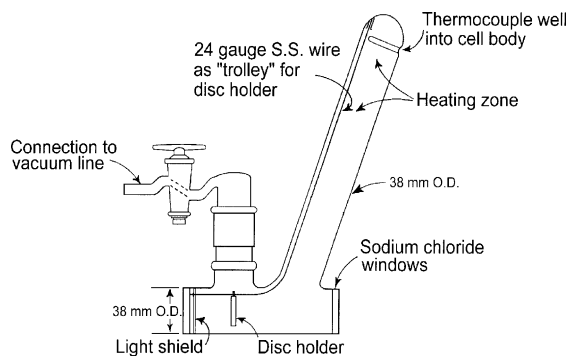


Fig. 2. Design of IR cell for in situ studies of pyridine adsorption on acid solids [373].

effect various treatments have on the surface acidity [373].

Zecchina and Scarano [374] have applied the IR cell reactor for low-temperature studies of CO adsorption at 77 K at the surface of KCl (see Fig. 3). The IR cell has been designed to allow the deposition of the KCl film on an optical window under controlled conditions.

Yates et al. [375,376] have applied the IR cell reactor for a number of studies, e.g., photochemical activation of methane on Rh/Al₂O₃ catalyst (see Fig. 4). Marchese et al. [377] have described an IR cell allowing thermal pre-treatments of the sample in a broad range of temperatures (see Fig. 5). This cell has been utilised for determination of the surface sites of δ -Al₂O₃ by adsorption carbon monoxide.

Chuang et al. [378] have reported the details of a high-pressure and -temperature in situ transmission IR reactor cell. The cell allows for easy assembly and reliable operation up to 773 K and 6.0 MPa (see Fig. 6).

Since the nature of adsorbates is closely related to the surface state of the sites to which adsorbates bind, IR spectra of adsorbates can provide information not

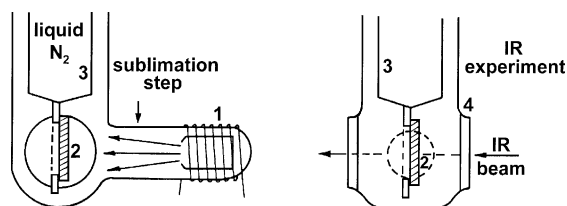


Fig. 3. Schematic representation of IR cell for low temperature in situ IR studies: (1) induction coil; (2) NaCl plate; (3) copper; (4) NaCl window [374].

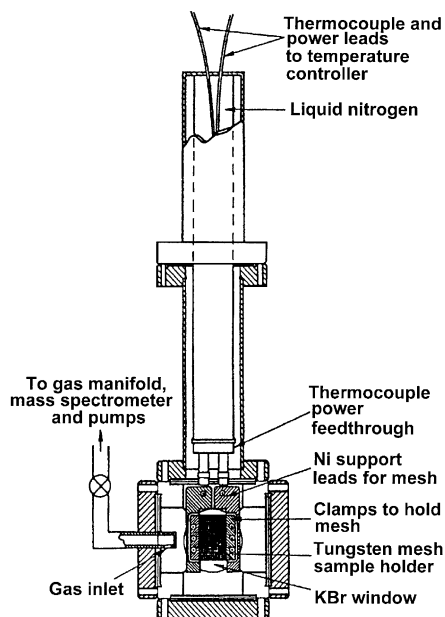


Fig. 4. Schematic diagram showing the high-temperature IR cell (on the top) and schematic diagram showing the optical design of the IR cell for simultaneous photochemistry, and IR spectroscopy on high surface area substrates [375].

only on the structure of the adsorbates but also on the state of the catalyst surface. It is essential to study the nature of adsorbates and the state of the catalyst surface under reaction conditions. Catalytic reactions of industrial interest usually operate at pressures above 0.1 MPa and temperatures above ambient conditions.

Various complex schemes have been designed to seal the reactor cell with IR-transparent windows so that the IR cell can be operated at elevated temperatures and pressures. The development of high-temperature and -pressure transmission IR

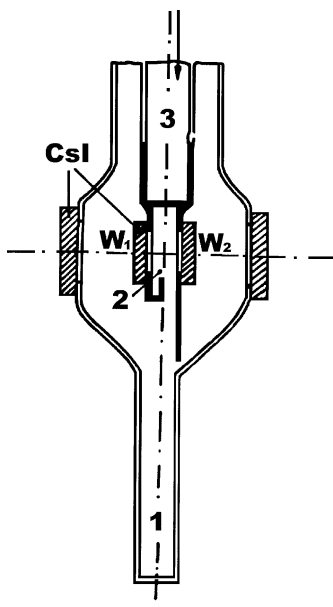


Fig. 5. Cell allowing thermal pre-treatments of the sample up to 1173 K and IR spectra down to 77 K (1 — cooling at RT; 2 — sample position; 3 — Kovar-Pyrex tubing; W_1 , W_2 — copper cages) [377].

cells has permitted observation of adsorbates under reaction conditions. The high-temperature and -pressure cell may serve as a differential reactor for steady-state reaction, temperature-programmed desorption, temperature-programmed reaction, and unsteady-state reaction studies [378].

Investigation of adsorbates by in situ IR spectroscopy coupled with various reaction studies can provide valuable information on the nature of adsorbates under reaction conditions. In situ IR studies of adsorbates under steady-state reaction conditions reveal the structure and the relative coverage of adsorbates on the catalyst surface. The disadvantage of the steady-state technique is that all the adsorbates observed under reaction conditions may not be involved in the catalytic cycle leading to product formation. Steady-state study also does not provide any information regarding the reactivity of adsorbates. Comparing the transient responses of adsorbed species resulting from a perturbation in reactant concentration, temperature, and pressure, may differentiate reactive adsorbates. However, the perturbation in operating conditions upsets the chemical environment of the catalyst surface (i.e., coverage of adsorbates, composition, and structure of the catalyst surface, reaction temperature, total pressure, and partial pressure of the gaseous reactants) has a great effect on the reactivity of adsorbates.

Mariscal et al. [379] have developed a new transmission cell for in situ catalyst pre-treatment and measurements at temperatures between 120 and 773 K (see Fig. 7). The performance of this cell was demonstrated for the characterisation of an oxidic Ni/Al₂O₃ sample and a reduced WO₃/Al₂O₃ sample [379].

Sun et al. [380] have studied the mechanism of methanol synthesis over an ultrafine Cu/ZnO/Al₂O₃

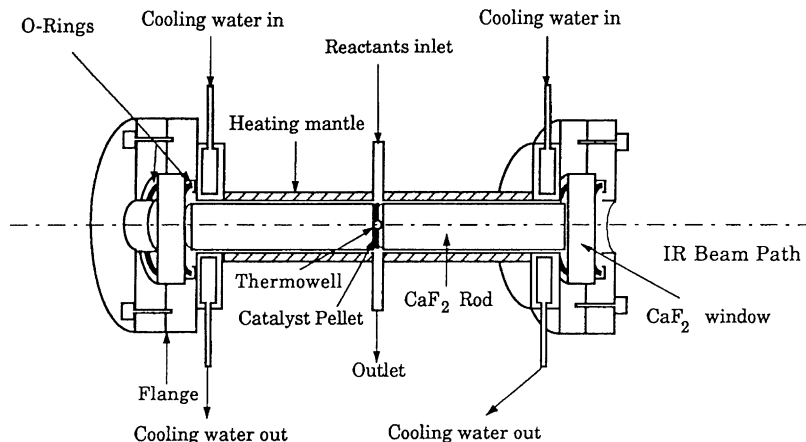


Fig. 6. The IR reactor cell [378].

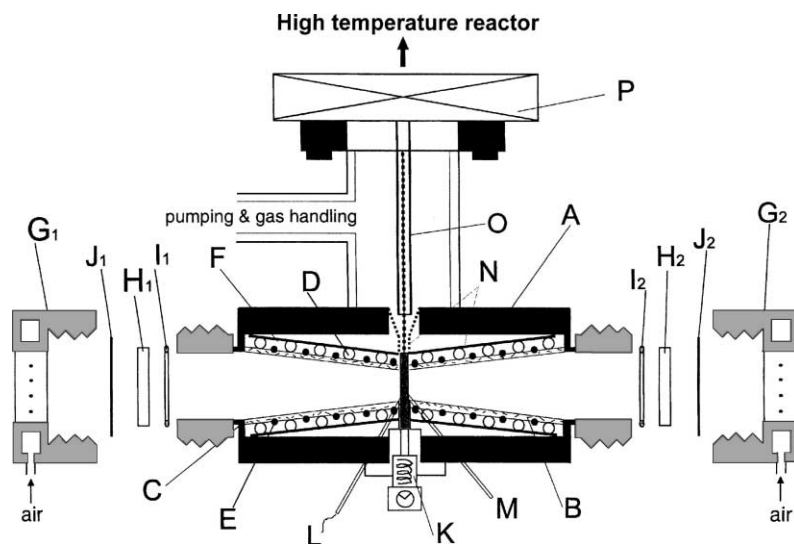


Fig. 7. Scheme of the IR transmission cell. It shows the stainless steel body (A), cooling/heating block (B), ceramic mounts (C), liquid nitrogen cooling circuit (D), heating element (E), the heat shield (F), screw caps (G_1 and G_2) for mounting the CaF_2 windows (H_1 and H_2), Viton gaskets (I_1 and I_2), for sealing the windows to the body, Teflon spacers (J_1 and J_2), sample holder position adjustment (K), thermocouple (L), gas-phase sample line (M), heat shield for the heating/cooling block (N), and the U-shaped rails (O) to keep the sample in position [379].

catalyst. For this purpose, they have constructed a special reactor cell for in situ IR studies (see Fig. 8).

Although in principle all forms of IR spectroscopy are suitable, for most practical experimental reasons, however, the use of the transmission-absorption technique is best. This is more related to the design of cells

(Fig. 9), that are also used as a reactor, than with the principal problems of the other techniques [381].

A cell suitable for investigations of catalysed reactions must fulfil two requirements: (a) it must allow the recording of IR spectra in situ under most reaction conditions, and (b) its volume and construction must

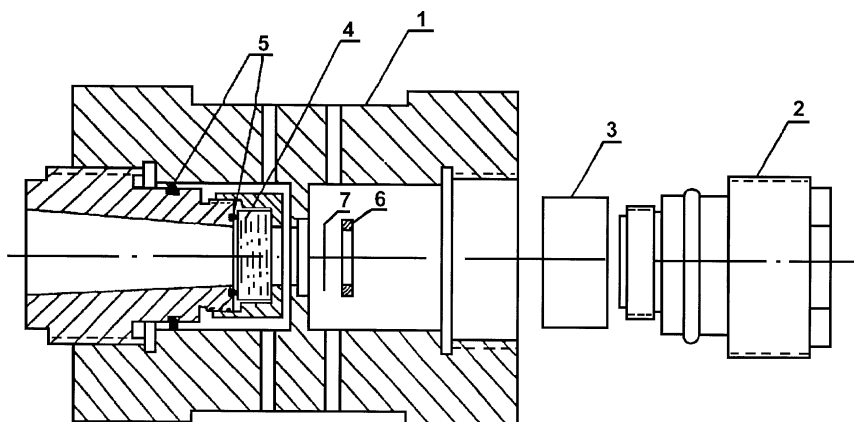


Fig. 8. Schematic diagram of in situ IR reaction cell: (1) cell body; (2) cell core; (3) window frame; (4) NaCl crystal window; (5) O-ring; (6) sample fixing ring; (7) sample wafer [380].

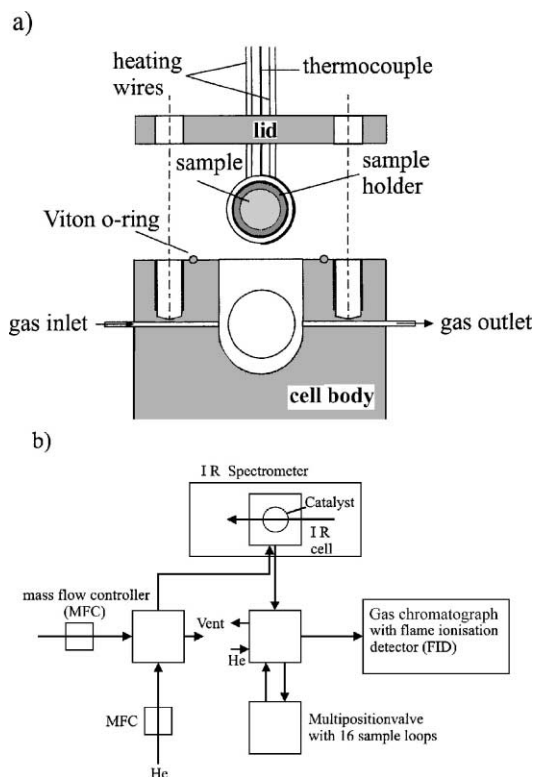


Fig. 9. Schematic outline of a reactor system allowing time-resolved acquisition of kinetic and IR spectroscopic data measurements: (a) IR cell; (b) total set up [19,381,382].

assure good mixing of the gases inside, and the feasible space velocities must allow flexible variations of the conversion. Ideal back mixing in the reactor approximates the cell to a continuously operated tank reactor exposing the catalyst to the concentration of reactants and products that can be analysed precisely at the exit of the reactor. On the other hand, if the design approximates to a tubular reactor, the catalyst would be exposed to a changing gas composition throughout the catalyst bed, and the IR light would sample an average of the surface species making unequivocal conclusions quite difficult [381].

Gorbaty and Bondarenko [383] have presented and described a new high-pressure/high-temperature IR cell with a changeable path length. The cell can be used up to 780 K at a pressure of 100 MPa (see Fig. 10). Another IR cell reactor for diffuse reflectance has been presented by Yoshida et al. [384] (see Fig. 11).

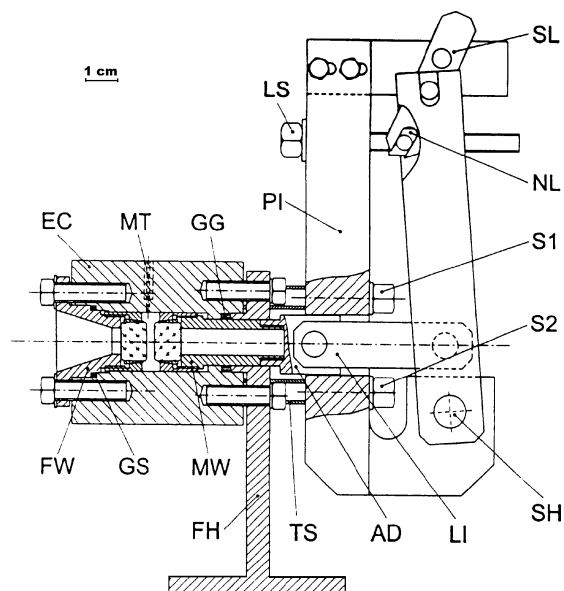


Fig. 10. High-pressure/high-temperature IR cell: EC — the external cylinder; FW — fixed window mounting; MW — movable window mounting; GG — gland made of GraFlex; GS — GraFlex seal; MT — input for pressure and the movable thermocouple; PI — pillar of the driving mechanism; SL — small lever; LS — lead screw; ML — main lever; NL — nut with lugs; S1, S2 — screws; SH — shaft; LI — link; AD — adapter; TS — tube spacers [383].

The construction of the reactor was suitable for the measurement of IR spectra of methane physisorbed on an active carbon at low temperature (153 K) [384]. Weng et al. [385] have studied the partial oxidation of methane to synthesis gas over supported rhodium and ruthenium catalysts using in situ time-resolved FT-IR (TS/FT-IR) spectroscopy. The experiments were performed using a home-built high-temperature in situ IR cell with quartz lining and CaF_2 windows, which could be heated from room temperature (RT) to 973 K. The schematic diagram of the IR cell is shown in Fig. 12.

The internal volume of the IR cell is ca. 25 ml. The gas inlet and outlet of the IR cell were connected to gas line and vacuum system (0.13 Pa), respectively, through a three-way valve and a two-way valve. By proper switching of these valves, the catalyst sample in the IR cell can be evacuated or introduced to different gas atmospheres.

A novel reactor cell with in situ IR analysis was designed and tested experimentally in photocatalytic

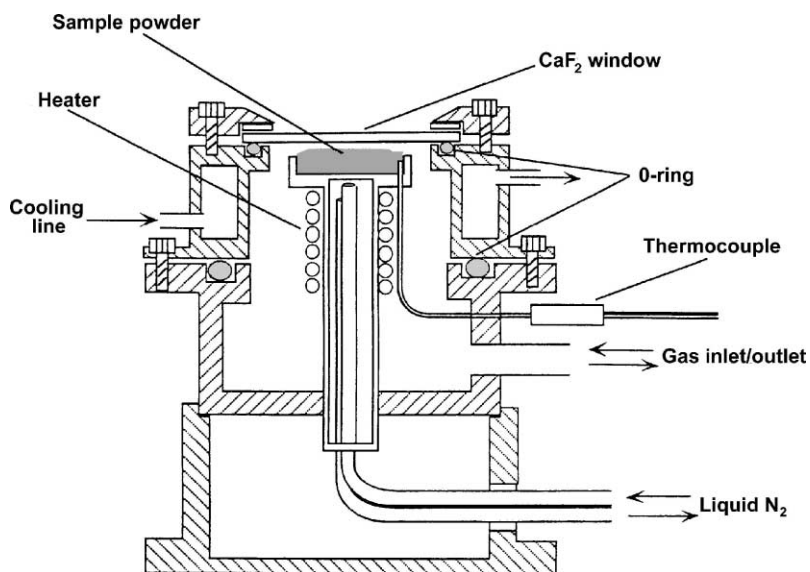


Fig. 11. IR cell reactor for diffuse reflectance [384].

degradation of tetrachloroethene (C_2Cl_4) over TiO_2 in the presence of air [386] (see Fig. 13).

The reactor resembles a commercial gas cell, with NaCl or KBr windows attached to both ends of the cell by clamped-on O-ring fittings. This design allows the

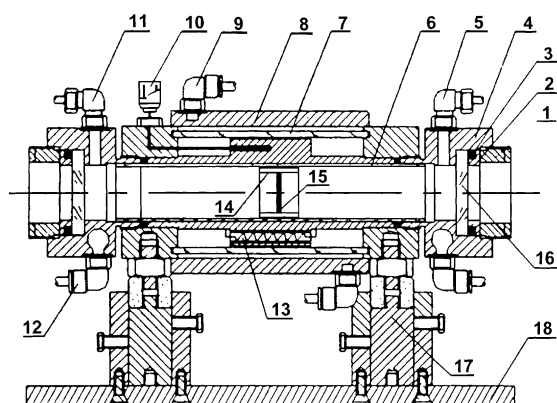


Fig. 12. Schematic diagram of high temperature in situ IR cell: (1) screw cap; (2) pressing ring; (3) Kalrez O-ring; (4) copper assembly; (5) gas inlet copper fitting; (6) inner quartz tube; (7) outside quartz tube; (8) stainless steel outside sleeve; (9 and 12) Legris push-in fittings for cooling water; (10) thermal couple; (11) gas outlet copper fitting; (13) heater; (14) sample holder; (15) sample disc; (16) IR window; (17) supporting rod; (18) bottom plate [385].

easy opening and closing of the cell to exchange the catalyst layer in the reactor. A heatable catalyst holder made of quartz is placed inside the cell; it is equipped with a heating wire, providing the pre-treatment of the catalyst up to 600 K, fastened to the bottom side of the sample holder. The temperature of the catalyst layer is monitored by an attached thermocouple, and thus a regulated heating rate can be attained. All the wires are led through the glass wall via a sealed port, allowing the cell to be evacuated to 10^{-2} Pa. The temperature of the cell can be adjusted (cooled or heated) by running water in an outer jacket. This jacket filters off the IR constituents of the irradiation light. For irradiating the catalyst by UV or Vis light, a lamp fastened to the top of the reactor cell is used. The system allows operation as batch, pulse, or continuous flow reactor. More details can be found elsewhere [386].

A new general purpose high-pressure IR cell has been built, which allows one to work up to 200 MPa pressure with gas, liquid, or supercritical fluid samples, in the temperature range from 203 to 423 K [387] (see Fig. 14).

The optical path can be varied from ~ 0.1 to 4 mm, the different windows allow measurements in a very wide spectral region (from near- to far-IR) [387]. A double-chamber flow cell was developed and applied

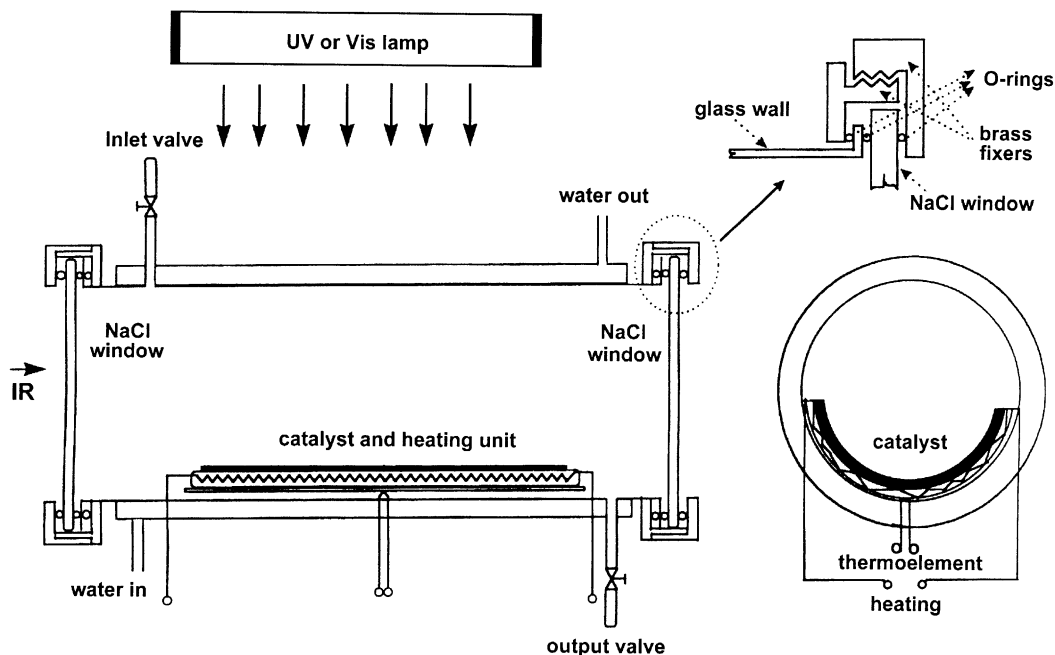


Fig. 13. Scheme of IR cell [386].

to the in situ IR study of chemical reactions in Ziegler–Natta catalyst systems [388]. An in situ IR cell capable of studying reactions over heterogeneous catalysts in the temperature range 77–773 K has been designed and applied to the study of formic acid adsorption on Cu/SiO₂ catalysts [389].

The IR cell reactors presented above (Figs. 1–14) were built in research laboratories for a specific need or application. However, there are available commercial products, which can be purchased directly from the company dealing with such equipment. Below will be given selected examples of the commercial in situ IR cell reactors.

The Harrick Scientific high-temperature cell permits transmission studies of solid samples at temperatures ranging from ambient to 773 K [390]. The high-temperature cell can also be used for external reflection studies, in conjunction with the appropriate transfer optics. Its stainless steel cell body is thermally insulated to prevent heat loss from the sample and water-cooled to eliminate the need for high-temperature window seals (Fig. 15).

The high-temperature cell includes two iron–constantan thermocouples for temperature measurement

of the sample and the heating block, in addition to three heating elements for uniform heating of the sample. The cell is further equipped with two ports with VCO fittings for evacuation of the cell and/or introduction of gases to the sample, two hose fittings for the water cooling ports, and mounting hardware for direct installation into the spectrometer [390].

The high-temperature/high-pressure cell accessory is a multipurpose cell for FT-IR analysis of solid samples in transmission, reflectance, or decomposition modes (Fig. 16).

Sample temperatures of up to 1273 K can be obtained and the cell can operate at pressures from vacuum to 6.89 MPa [391,392]. It is useful for in situ analysis under extreme conditions that replicate industrial processes outside of their normal industrial environment. Gases can be introduced to cell in flow or static operation, either for transmission analysis or use as a purge gas. Fig. 17 illustrates operation of the cell in different modes.

The main applications of the mentioned cell are the following: component failure analysis, decomposition studies, in situ reaction monitoring, raw material

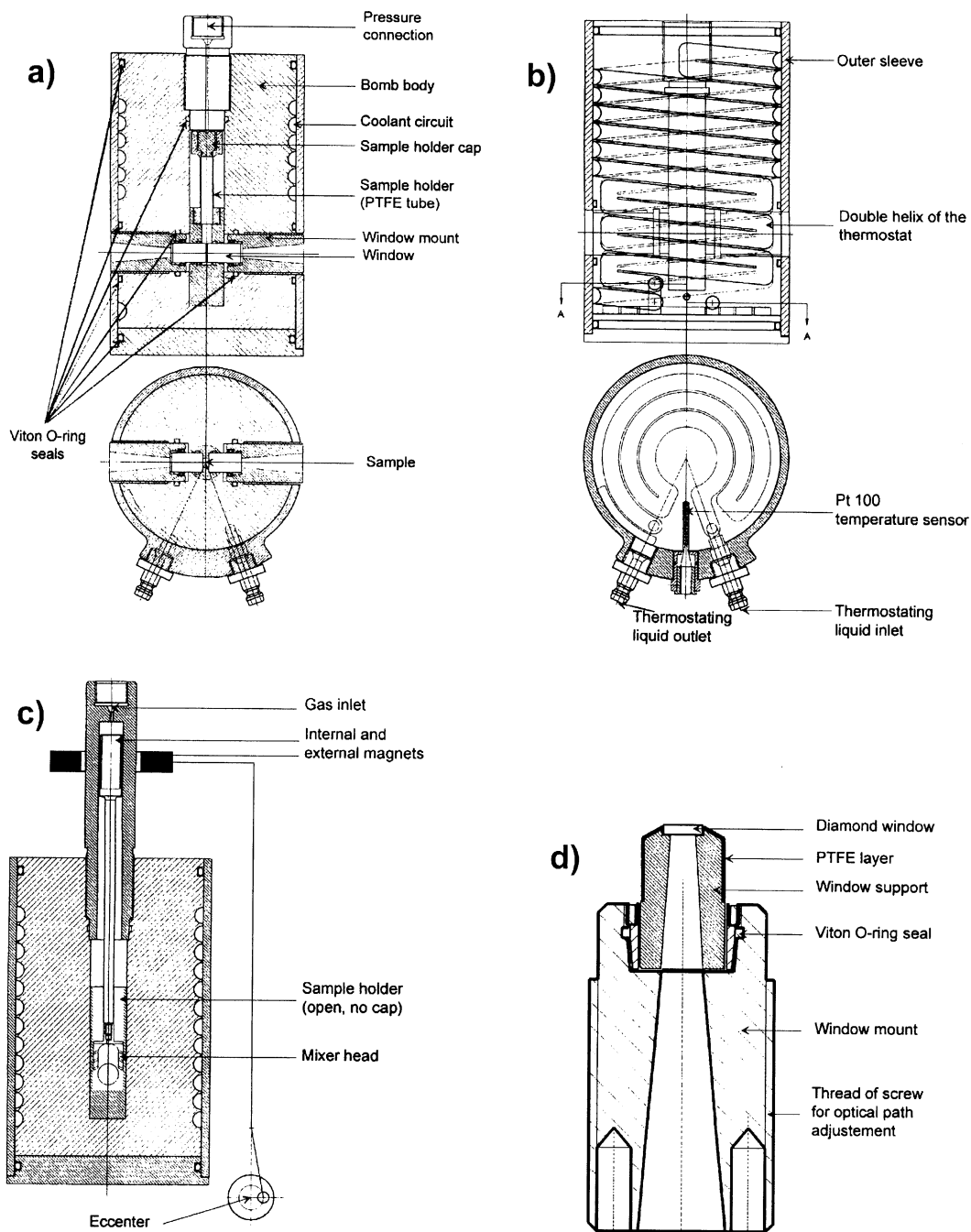


Fig. 14. Design of the high-pressure IR cell: (a) vertical section of the set-up for liquid hydrostatic pressurisation measurements; (b) schematic of the thermostatisation; (c) set-up for measuring/mixing gas-liquid systems; (d) diamond window support [387].

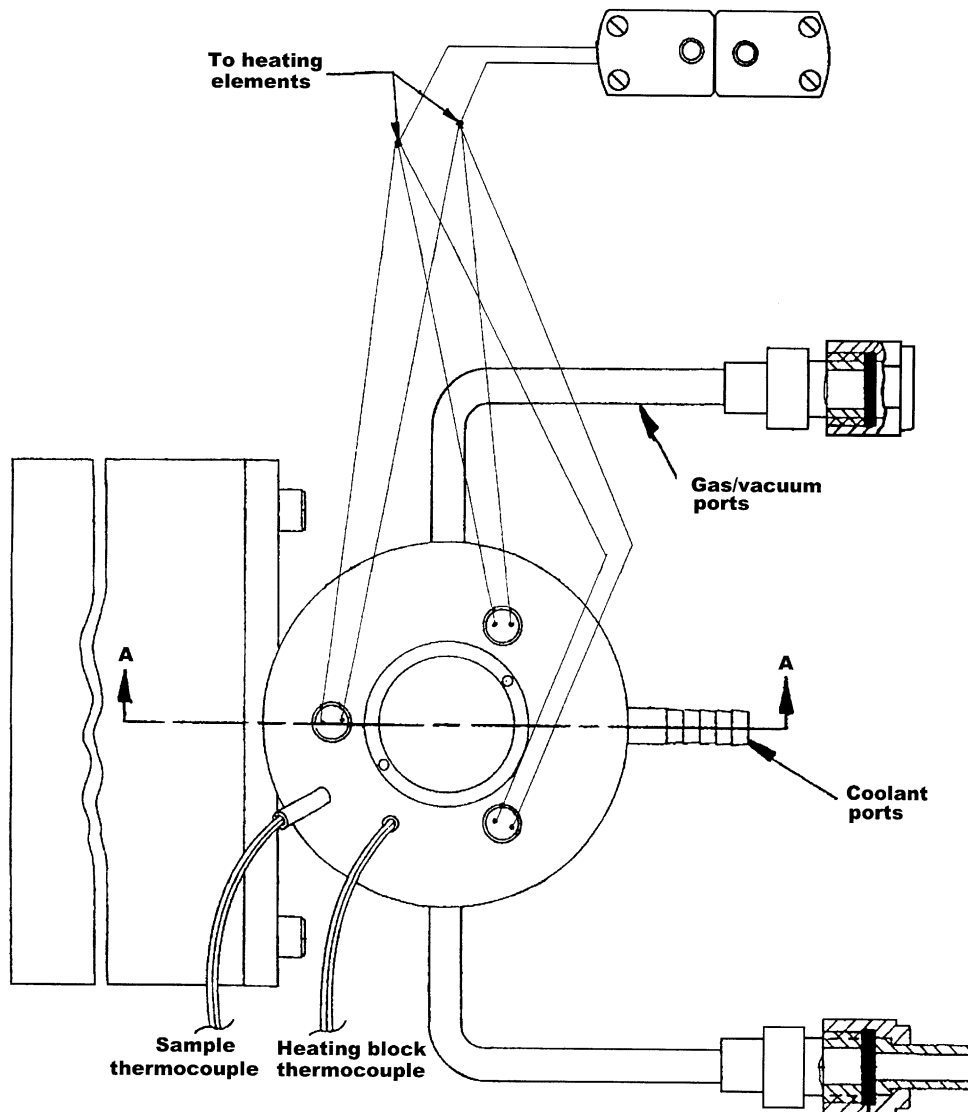


Fig. 15. Profile view of the high-temperature cell [390].

contamination analysis, surface emissivity measurements, and process gas analysis.

In Situ Research and Instruments (ISRI) produces an IR cell reactor (Fig. 18) for in situ transmission IR studies of catalytic reactions [393]. The reactor design allows for a wide range of operating conditions, 1.33×10^{-3} Pa–1.52 MPa. A special design enables heating the sample wafer only, which combined with an internal cooling system, allows the IR cell to

operate up to 773 K. Due to the minimum reactor internal volume, the absorbance of gas-phase species is reduced. For continuous operation, gases flow in and out of the reactor along both sides of the wafer. Alternatively, the cell can be operated in a batch mode, at high pressure or in vacuum. Two thermocouple ports allow for the precise monitoring of the sample and gas-phase temperatures. The reactor is equipped with exchangeable IR windows to cover a wide range of IR

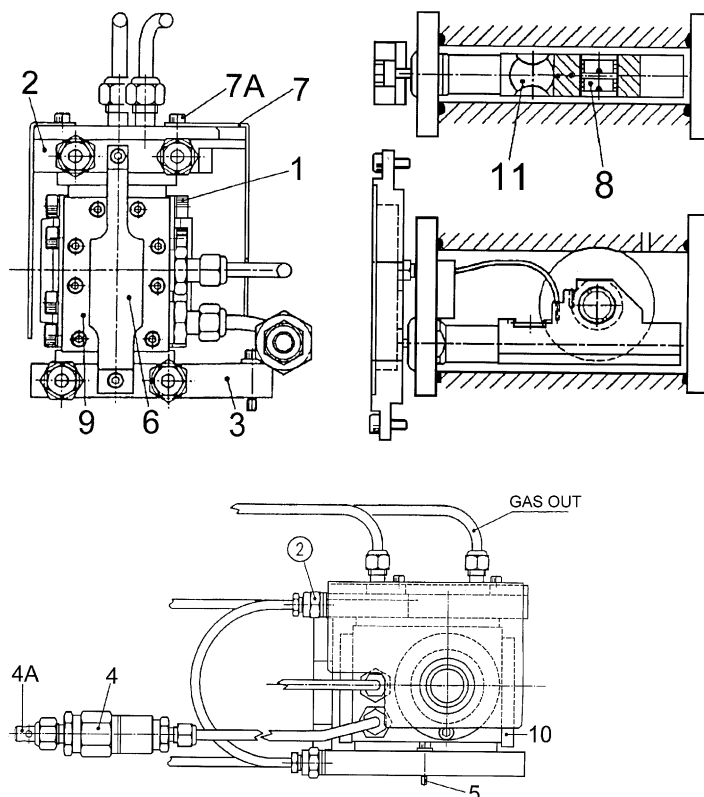


Fig. 16. Assembly of cell in transmission and decomposition modes: (1) M6 caphead window to cell screws; (2) water cooling connectors; (3) cooling plates; (4) pressure burst disc attachment; (4a) burst disc baffle; (5) accessory base captive screw; (6) sample holder/wiring bracket; (7) heat shield; (7a) heat shield securing screws; (8) sample keep ring; (9) sample holder side plate; (10) plain end plate; (11) decomposition sample recess [391,392].

frequencies. Thanks to its compact design and reduced size, the reactor can be fitted in the sample chamber of most commercially available IR spectrometers. The IR cell reactor can be operated with the proper instrumen-

tation to control the temperature and flow during IR experiments with a full spectrum of frequencies collected under a steady-state condition of pressure and temperature. However, maximum advantage of its capabilities

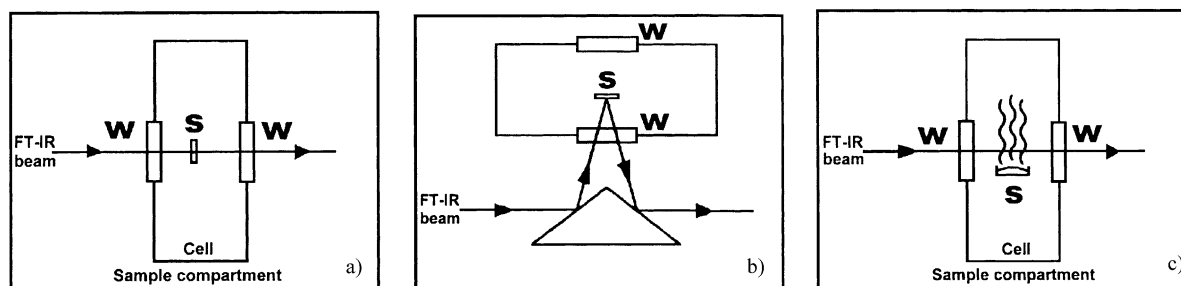


Fig. 17. Simplified diagram of the high-temperature and high-pressure accessory in: (a) transmission mode; (b) reflectance mode; (c) decomposition analysis mode (s — sample; w — window) [391,392].

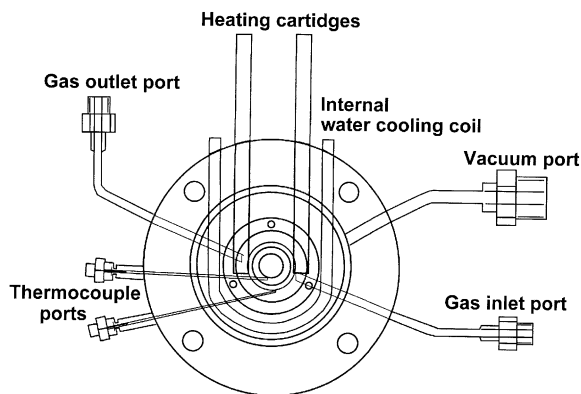


Fig. 18. ISRI IR reactor diagram [393].

is attained when combined with many features of the ISRI RIG-100 temperature and flow control system for transient operation. Two modes of transient operation suggested during IR studies are: IR temperature programming (IRTP) and IR concentration programming (IRCP). In the first mode, the reactor temperature is increased linearly and the IR absorbance is monitored as a function of time or temperature. During IRCP mode, the RIG-100 control system can be used to vary

flow rates of the reactants linearly so the concentration behaviour of different gases can be determined. Finally, a very specific attachment, based on optical fibre technology, can be used for in situ measurements in the gas phase as well as the liquid phase [394] (Fig. 19).

Most of the studies described in the following sections were conducted in situ. The purpose of presenting a short description of different IR cell reactors was to indicate how large is the diversity of these tools utilised in catalytic research nowadays. Each of the following sections will start with the pictogram taken from [390]. These very simple schemes describe the general idea of the spectroscopic technique applied.

4. Transmission spectroscopy

Transmission spectroscopy is the simplest sampling technique in IR spectroscopy and is used for routine spectral measurements (see Fig. 20). A small amount, usually 1–3 mg, of finely ground solid sample is mixed with approximately 400 mg powdered potassium bromide and then pressed in an evacuated

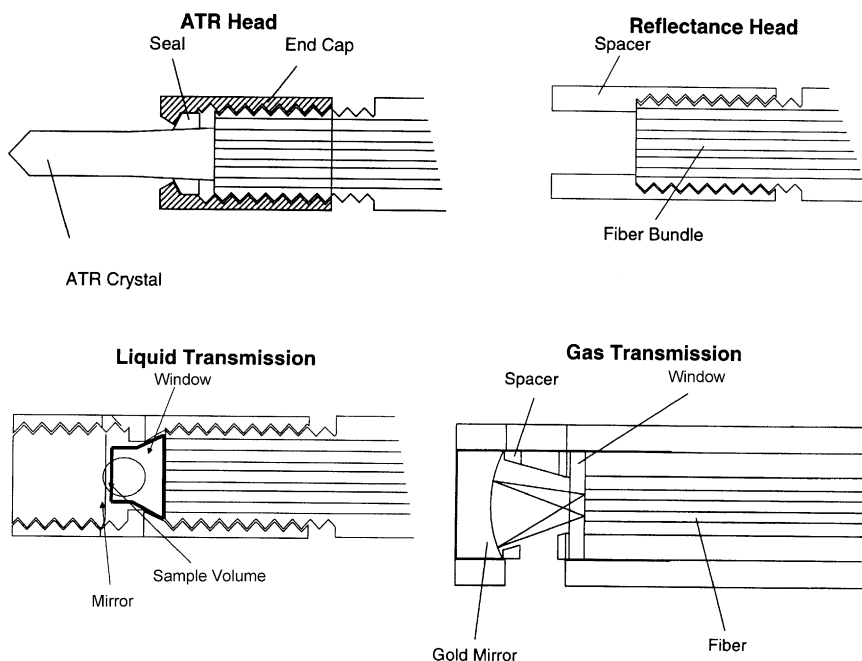


Fig. 19. Mid-IR sensors [394].

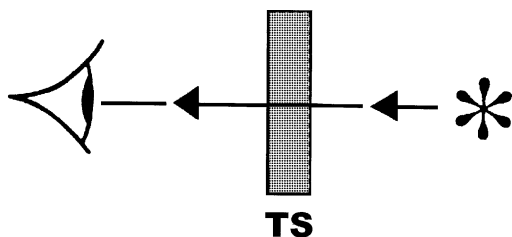


Fig. 20. The principles of transmission spectroscopy [390].

die under high pressure (see Appendix A). The resulting discs are transparent and yield good spectra. The vast majority of experiments are currently performed in the transmission–absorption mode.

The fundamentals of the different IR spectroscopic techniques are briefly outlined in view of their use in the studies of oxide heterogeneous catalysts [395]. Some recent progress in utilisation of IR spectroscopy for the in situ vibrational characterisation of adsorbates at electrochemical interfaces having relevance to catalytic chemistry is briefly outlined in [396].

Lutz and Haeuseler [397] have also reviewed experimental techniques of IR and Raman of solid compounds. The same authors have discussed the application of IR and Raman spectroscopy in inorganic solid-state chemistry [398]. It was concluded that IR and Raman spectroscopy could be a very valuable tool in inorganic and solid-state chemistry research also to the next century. Thus, vibrational spectroscopy methods are valid for determination of:

- the bond strength in molecular units, in particular in hydrogen bond research,
- intermolecular bonding features,
- distortion of molecular units at various lattice sites,
- the structure of molecular units in solids,
- the coordination polyhedra of metal ions,
- space group symmetries,
- determination of isotypism, and
- many other physical properties, such as free carrier concentrations, etc.

Recent developments in the major experimental vibrational spectroscopic techniques (including IR) are reviewed and illustrated with selected results [399]. The use of IR to probe the surface acidity of oxides and molecular sieves is reviewed [19]. As the type of probe molecule chosen will influence the obtained

characteristics of the probed solid and, hence, will also affect the structure–activity relationship derived, the choice of the appropriate molecule is very important. Lercher et al. [19] have summarised the most important criteria:

- The probe molecule should have dominating and rather weak acidic properties;
- The IR spectrum of the sorbed probe molecule should allow to distinguish between sorption and protonic (Brønsted) and aprotic (Lewis) acid sites;
- The probe molecule should allow to differentiate between acid sites of the same type, but of different strength;
- The size of the probe molecule should be comparable to the size of the reactant to probe the concentration of acid sites relevant for a particular reaction (see Table 1).

The most frequently used probe molecules are ammonia, aliphatic amines, pyridine, and substituted pyridines, nitriles, benzene and substituted benzenes, carbon monoxide. Less frequently used probe molecules are ketones, aldehydes, ethers, alkanes, and alkenes [19].

IR spectral analysis of species formed by acid probe adsorption on dispersed metal oxides and alkaline zeolites can lead to information on their surface basicity, particularly on the nature and strength of basic sites [400]. Results obtained from carbon monoxide, carbon dioxide, sulphur dioxide, pyrrole, chloroform, acetonitrile, alcohols, thiols, boric acid trimethyl ether, ammonia, and pyridine are critically reviewed. It was concluded that no probe could be universally used. Pyrrole in the case of alkaline zeolites, CO₂ for weakly basic metal oxides and for basic OH groups, and CO for the characterisation of highly basic structural defects on metal oxides activated at high temperature appear quite suitable probes [400]. Surface chemistry and surface structure of catalytic aluminas as studied by vibrational spectroscopy of adsorbed species has been reviewed by Morterra and Magnacca [401]. Adsorption of ammonia and pyridine on the surface of V₂O₅/MgO catalysts for the determination of Brønsted and Lewis acid sites and adsorption of pyridine and isopropanol on silica-supported heteropolyanions has been studied [402,403]. Irusta et al. [404] have used an acetonitrile as probe molecule for the characterisation VPO catalysts used for selective

Table 1
Conceptual criteria for the selection of probe molecules to characterise solid acids [19]

Lewis acid site		Brønsted acid site	
Sorption complex Detection of complex formation	Electron pair: donor–acceptor Change in the wavenumber of the absorption maximum of ν_B	Hydrogen bond Change in shape and absorption maximum of ν_{OH}	Ion pair (hydrogen bond) Disappearance of the catalysts ν_{OH} ; appearance of ν_{B-H}^+ and/or ν_{B-H}^+
Most exact methods of acid strength determination Determination of concen- tration of acid sites Required spectral properties	Correlations between the changes in ν_B and the heat of adsorption From the intensity of ν_B Shift of ν_B must be significant compared to its half width	Shifts of ν_{OH} for a given probe molecule From the intensity of ν_{OH} Absence of OH groups in the probe molecule	Thermal stability of the hydrogen bonded ipc From the intensity of characteristic bands of the ipc The characteristic band has to be unequivocally attributed to the ipc
Frequently used molecules	Pyridine, ammonia, acetonitrile, benzonitrile, and CO	Benzene, acetone, pyridine, substituted pyridines, amines, and acetonitrile	Ammonia, pyridine, and its derivatives

oxidation of *n*-butane. Basicity of alumina and modified aluminas has been studied by FT-IR using boric acid trimethyl ester (BATE) [405]. BATE was found to interact with basic sites of strong, medium, and even weak basicity on alumina, while CO₂ interacts mainly with strong basic surface hydroxyls.

da Silva et al. [406] have investigated the surface acidic properties of alumina-supported niobia prepared by chemical vapour deposition and hydrolysis of niobium pentachloride. The samples were characterised with respect to chemical composition, surface area, acidity by temperature-programmed desorption of ammonia, nature of acid sites by IR spectroscopy of adsorbed pyridine, and catalytic activity at 643 K in the dealkylation of cumene. The results showed that, for each alumina calcination temperature, the catalysts with the lowest niobium content have a higher density of acid sites than the alumina support, but the acidity decreased, within each series with an increase in the niobium content. A sample of pure niobium oxide had much higher activity than the niobia–alumina samples. Brønsted acidic sites could only be observed by the IR spectra of adsorbed pyridine on the surface of the pure niobium oxide sample. Zhao et al. [407] have studied the acid centres in sulphated, phosphated, and/or aluminated zirconias. On sulphated ZrO₂, the comparison of the effects of adsorbing water or ammonia on the IR bands between 1400 and 1000 cm⁻¹ suggests that besides structural Lewis sites on the surface of ZrO₂, strong Lewis sites are made from

chemisorbed SO₃. Upon adsorption of water, SO₃ is converted, partially, into a surface sulphated species, which may act as strong Brønsted sites. At moderate surface hydration, both types of sites may coexist. The catalytic activity in the isomerisation of isobutane is a function of the overall nominal surface density in SO₄. The acid sites on the surface of phosphated mesoporous zirconia are attributable to surface P–OH groups working as weak Brønsted sites. On both sulphated and phosphated zirconia, surface coating of alumina stabilises the porosity, but it does not modify the nature of their acid centres [407].

Barthos et al. [408] have conducted studies of the acidic and catalytic properties of pure and sulphated zirconia–titania and zirconia–silica mixed oxides. Protonated pyridine was not found on ZrO₂ or ZrO₂–TiO₂ but was detected on sulphated oxides. In contrast, ZrO₂–SiO₂ samples containing about 30–80 mol% ZrO₂ showed Brønsted acidity both in non-sulphated and sulphated forms [408].

A series of titania and silica mixed metal oxide samples modified by H₂SO₄ has been characterised by BET, XRD and XPS, FT-IR, and compared with non-sulphated samples [409]. The shift of the S=O characteristic peak in FT-IR shows that the bond strength of S=O is influenced by the TiO₂–SiO₂ microstructure.

Fig. 21 shows the spectra of the sulphated samples appearing in FT-IR measurements after evacuation at 673 K. A remarkable peak at 1410 cm⁻¹ in 10 mol%

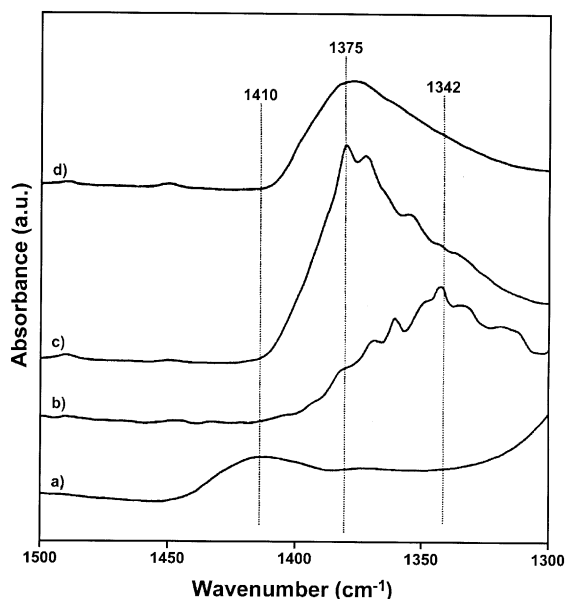


Fig. 21. FT-IR spectra, after evacuation at 673 K: (a) 10 mol% $\text{TiO}_2\text{-SiO}_2/\text{SO}_4^{2-}$; (b) 56 mol% $\text{TiO}_2\text{-SiO}_2/\text{SO}_4^{2-}$; (c) 90 mol% $\text{TiO}_2\text{-SiO}_2/\text{SO}_4^{2-}$; (d) pure $\text{TiO}_2/\text{SO}_4^{2-}$ [409].

$\text{TiO}_2\text{-SiO}_2$ appears. In addition, a small shoulder at 1375 cm^{-1} assigned to S=O induced from titanium sulphate was also detected. Accordingly, the presence of both characteristic peaks provides the fact that the titanium phases are produced during the sulphation, although no crystalline form of TiO_2 was detected in the XRD spectrum of 10 mol% $\text{TiO}_2\text{-SiO}_2$. In 56 mol% $\text{TiO}_2\text{-SiO}_2/\text{SO}_4^{2-}$ sample, a peak at 1342 cm^{-1} appeared whereas the S=O peak at 1410 cm^{-1} is not detected. This shiftdown of S=O position in stretching vibration on FT-IR also indicates a modification of the interaction between the support and surface sulphate complex. In $\text{TiO}_2/\text{SO}_4^{2-}$, it is known that a shift of the S=O peak occurs when a basic material such as pyridine is adsorbed on the sulphated catalyst. The basic molecule can give electron to the support or to the sulphate complex. Sulphate complex has a strong tendency to reduce the bond order of S=O from a highly covalent double bond character to a lesser double bond character when a basic molecule is adsorbed on its central metal cation. Accordingly, if the electron distribution in the surroundings of sulphate is basic, the same influence on the position of S=O can happen. Actually, adsorption of pyridine on 56 mol% $\text{TiO}_2\text{-SiO}_2/\text{SO}_4^{2-}$

does not induce the shift of S=O vibration band. As a result it is concluded that the S=O bond cannot create the acid site since the neighbour electron distribution has an basic-like material that can donate the electron due to the charge uneven distribution of Ti–O–Si. In addition, there is no evidence of a peak attributed to the SiO_2 sulphate found on this sample. It is then proposed that no independent SiO_2 phase exist in this sample.

The 90 mol% $\text{TiO}_2\text{-SiO}_2/\text{SO}_4^{2-}$ sample shows single S=O peak at 1375 cm^{-1} . The position of this peak coincides with that of pure $\text{TiO}_2\text{-SO}_4^{2-}$. As compared with the 10 mol% $\text{TiO}_2\text{-SiO}_2/\text{SO}_4^{2-}$ sample, the peak due to the $\text{SiO}_2/\text{SO}_4^{2-}$ sample was not built up. This result also indicates that the independent SiO_2 phase is not present as already mentioned in 56 mol% $\text{TiO}_2\text{-SiO}_2/\text{SO}_4^{2-}$.

Based on the results obtained by FT-IR, it is suggested that the surface sulphate types depend on the nature of the Ti/Si ratio. In particular, it is suggested that the Ti–O–Si bond in the 56 mol% $\text{TiO}_2\text{-SiO}_2/\text{SO}_4^{2-}$ sample participates in the sulphate formation and generates a new sulphate type with different properties [409].

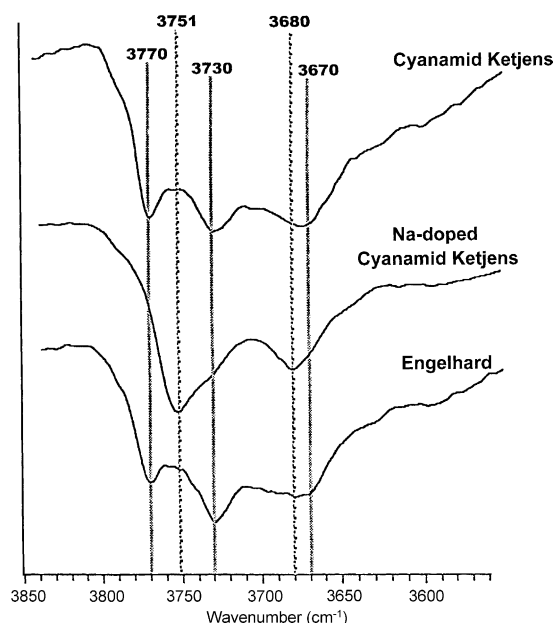


Fig. 22. IR spectrum of different γ -aluminas in the hydroxyl group region. Addition of 5000 ppm of Na removes the 3770 and 3730 cm^{-1} bands and creates a new feature at 3751 cm^{-1} [412].

An acid–base property of Pd–Ca/Al₂O₃ catalysts on the selective hydrogenation of phenol to cyclohexanone has been studied [410]. The addition of Ca as promoter both poisons the Lewis acid sites of the alumina and causes a relevant increase in the number and the strength of basic sites of the Pd/Al₂O₃ system.

The gamma alumina is an aluminium oxide form, which belongs to the so-called transition aluminas. Among the different transition aluminas, γ -Al₂O₃ is perhaps the most widely used mainly as support for a catalyst or as a catalyst itself. The γ -Al₂O₃ structure was considered as a hydrogen spinel and the complex Al–O IR absorption band between 1100 and 350 cm⁻¹ was interpreted under the criteria for the band assignment of the spinels [411].

A series of alumina samples differing in structure (γ , δ , and α) and in Na content was studied by IR spectroscopy (Figs. 22–24) [412]. Transitional aluminas possess well-defined hydroxyl bands whose nature and intensity is affected by alumina structure and impurity content. The most reactive aluminas exhibit a prominent hydroxyl band at 3770 cm⁻¹. Another characteristic of the most reactive aluminas is the formation of a band at 1622 cm⁻¹ after pyridine adsorption and evacuation at RT. Addition of Na as well as thermal treatments that transform γ - to δ -alumina have a similar effect on aluminas, namely, an attenuation of the prominent 3770 cm⁻¹ hydroxyl band and the 1622 cm⁻¹ pyridine band. In both cases,

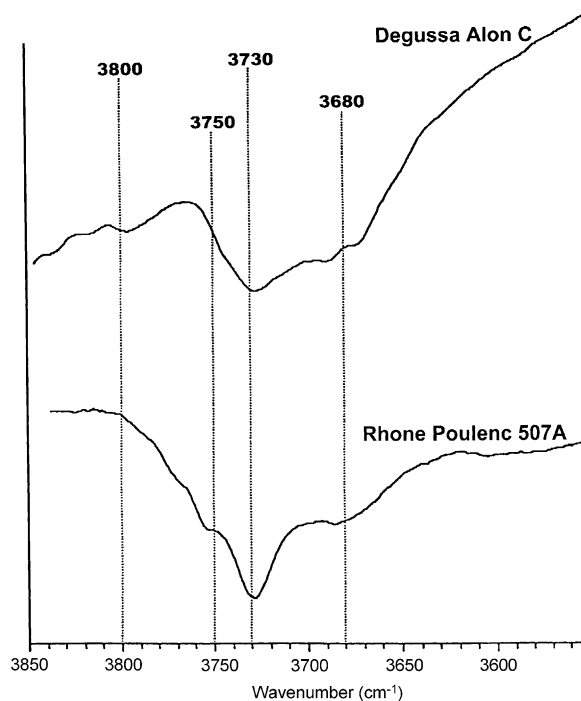


Fig. 23. Hydroxyl band IR spectrum of δ -aluminas. The 3770 cm⁻¹ band seen on the reactive γ -aluminas is seen only as a shoulder while the 3730 cm⁻¹ band is quite prominent [412].

the effect appears to be steric in nature, indicative of hindered access of the probe molecule to the reactive sites. It was mentioned that results from spectroscopy

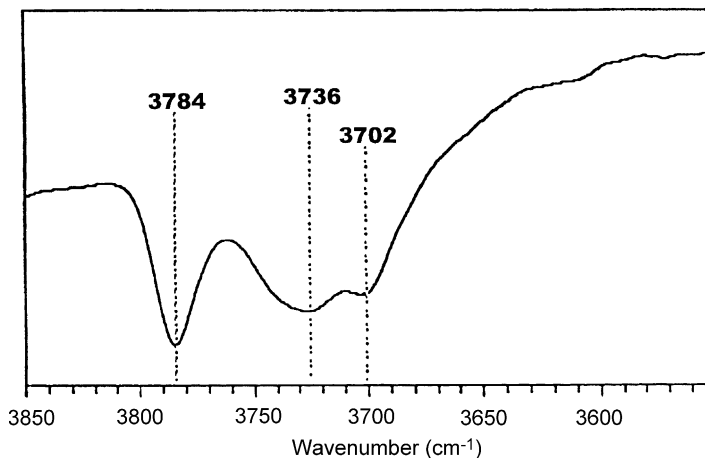


Fig. 24. IR spectrum of α -alumina [412].

correlate well with the trends observed in catalytic reactivity.

The interaction of various hydroxyl groups on the Al_2O_3 surface with bifunctional adsorbate, 2-chloroethylethyl sulphide (CEES), was studied by IR [413]. Three sequential steps have been separated by studies at low temperature, where the rate of the processes was kinetically retarded to allow observation:

- 140–153 K: CEES is frozen on the outer surfaces of the Al_2O_3 powder, interacting primarily with itself and very little with the Al_2O_3 surface.
- 153–273 K: CEES overcomes the barrier to diffusion and migrates into the porous Al_2O_3 network, interacting with both the acidic and basic Al–OH groups.
- $T \geq 273$ K: CEES gains sufficient thermal energy to overcome interactions with the acidic Al–OH groups and desorbs from those sites.
- $T > 298$ K: CEES is bound by the stronger Al^{3+} Lewis acid sites until sufficient thermal energy is introduced into the system to allow the hydrolysis reaction with the neighbouring isolated basic Al–OH groups [413].

The morphology of alumina has been studied [414]. Satisfactory interpretation of experimental IR spectra can be carried out from the theory of average dielectric constant (TADC). This theory was successfully used for determining the morphology of alumina particles larger than $3 \mu\text{m}$ [414].

The modification of MgO with caesium, barium, or yttrium oxide was carried out in order to increase its base strength [415]. The decomposition of 2-butanol and 2-methyl-3-butyn-2-ol, as well as the FT-IR investigation of adsorbed acid probe molecules on the catalysts, were used as basicity characterisation methods. The FT-IR investigations revealed the strongest basic sites in the case of Cs/MgO, while basic sites stronger than on pure MgO were not detected on Ba/MgO and Y/MgO. The IR spectra of adsorbed methane in the region of the ν_1 (gas phase: 2914 cm^{-1}) and ν_3 vibration (gas phase: 3020 cm^{-1}) are shown in Fig. 25.

The totally symmetric ν_1 vibration, which is IR inactive in the gas phase, is activated, which indicates a symmetry reduction of the adsorbed methane molecule. The red shifts of the ν_1 and ν_3 vibrations as compared to the gas phase are the highest in the case

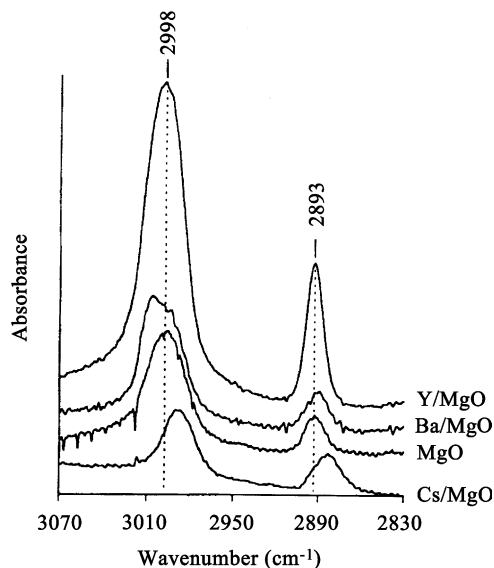


Fig. 25. IR spectra of CH_4 adsorbed on modified MgO samples at 0.08 kPa and 88 K [415].

of Cs/MgO suggesting that the interaction between methane and the caesium-containing magnesium oxide catalyst is the strongest. These shifts are lower and approximately the same for MgO, Ba/MgO, and Y/MgO. The FT-IR spectra of the adsorption of acetylene in the region of the antisymmetric stretching vibration ν_3 (gas phase: 3287 cm^{-1}) are shown in Fig. 26.

The spectra of adsorbed C_2H_2 on Cs/MgO and MgO show a broad band centred $\sim 3148 \text{ cm}^{-1}$. This band is indicative of $\text{H}-\text{C}\equiv\text{C}-\text{H}\cdots\text{O}^{2-}$ hydrogen bonding between acetylene and strong basic sites. The fact that the broad band centred around 3148 cm^{-1} is asymmetric and structured, particularly in the case of MgO, is probably due to the existence of variously coordinated adsorption sites (corners, edges, or planar surface). In contrast, on Ba/MgO and Y/MgO, the band of the antisymmetric ν_3 vibration is narrower and its red shift relative to the gas-phase frequency is smaller than on MgO and Cs/MgO. This suggests that the interaction of acetylene with Ba/MgO or Y/MgO is significantly weaker than with Cs/MgO and with pure MgO. The FT-IR spectra for the adsorption of methylacetylene in the region of the $\equiv\text{C}-\text{H}$ -stretching vibration (gas phase: 3429 cm^{-1}) are shown in Fig. 27.

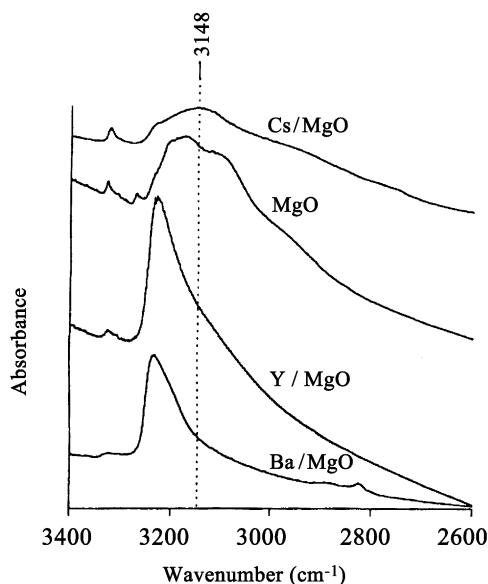


Fig. 26. IR spectra of adsorbed acetylene (0.2 kPa) at 173 K [415].

Two bands which can be assigned to $\equiv\text{C-H}$ -stretching vibrations are evident, namely a narrow band at 3288 cm^{-1} and a second band or shoulder at lower wavenumbers between 3243 cm^{-1} for Y/MgO and 3000 cm^{-1} for Cs/MgO. For MgO and partic-

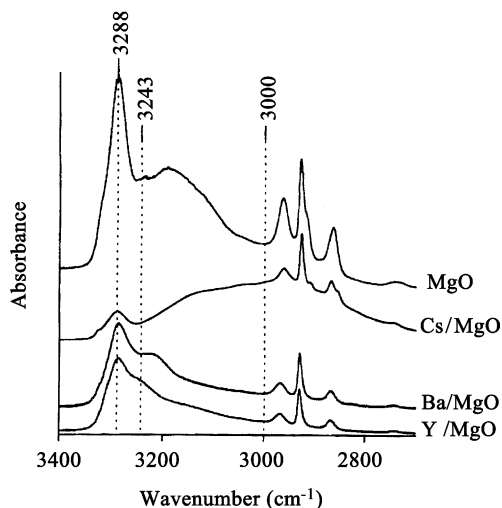


Fig. 27. IR spectra of adsorbed methylacetylene (0.1 kPa) at 173 K [415].

ularly for Cs/MgO, this second band is very broad and significantly shifted toward lower wavenumber as compared to the gas-phase frequency. As for acetylene these broad bands are indicative of a $\equiv\text{C-H}\cdots\text{O}^{2-}$ hydrogen bond formation with strong basic sites. The narrow band at $\sim 3288\text{ cm}^{-1}$ is assigned to an interaction between a coordinatively unsaturated cation and the triple bond of methylacetylene. The absence of the hydrogen-bonded species on Ba/MgO and Y/MgO confirms the observations made for the adsorption of acetylene: there is mainly an interaction between coordinatively unsaturated surface cations and the triple bond of methylacetylene [415].

Gao et al. [416] have studied the preparation and in situ spectroscopic characterisation of molecularly dispersed titanium oxide on silica. Pure silica exhibits the symmetrical Si–O–Si stretching vibration at $\sim 815\text{ cm}^{-1}$, along with a very weak band at 980 cm^{-1} due to the symmetric stretch of Si–OH groups. The addition of titanium surface oxide species decreases the 980 cm^{-1} band, and a new broad band appears at $\sim 965\text{ cm}^{-1}$, which is associated with the formation of Ti–O–Si bridges. A fifth OH-stretching band can be observed in transmission IR spectra of hydrothermal and authigenic kaolinites, which have a high degree of crystallinity [417]. Sugino et al. [418] have utilised IR for studying silica-supported silicomolybdenic acid catalysts and their precursors.

$\text{V}_2\text{O}_5/\text{TiO}_2\text{-ZrO}_2$ catalysts were characterised [419]. The IR spectrum of bulk V_2O_5 shows sharp absorption bands at 1020 and 820 cm^{-1} due to V=O stretching and V–O–V deformation modes, respectively. The FT-IR spectra of the $\text{V}_2\text{O}_5/\text{TiO}_2\text{-ZrO}_2$ catalyst calcined at 773 K indicate that the vanadium oxide is in a highly dispersed state. The spectra show only broad bands at around 980 and 825 cm^{-1} , and further the intensity of these bands decreases with an increase in calcination temperature [419].

Na-doped $\text{V}_2\text{O}_5/\text{ZrO}_2$ catalysts prepared by a two-step impregnation have been studied by FT-IR spectroscopy [420]. The reaction of propan-2-ol was followed by the pulse technique. Addition of sodium to 2 wt.% $\text{V}_2\text{O}_5/\text{ZrO}_2$ catalyst led to the decrease in Brønsted and Lewis acidic sites. Decreasing the Brønsted acidic sites resulted in decreasing propene formation from propan-2-ol. The surface V=O bands in the catalysts shifted to lower wavenumber and reduced in intensity by Na addition. It is concluded

that Na highly disperses on the surface of both 2 and 5 wt.% V_2O_5/ZrO_2 catalysts and inserts into the bulk phase in 5 wt.% V_2O_5/ZrO_2 [420].

The IR spectra of bulk $Nb_2O_5 \cdot H_2O$ and niobia supported on SiO_2 , Al_2O_3 , ZrO_2 , and TiO_2 were recorded in the fundamental and overtone $Nb=O$ regions, as well as in the hydroxyl region, to develop a better understanding of the structural models of surface NbO_x species [421]. The coincidence of the IR and Raman fundamental $Nb=O$ frequency in Nb_2O_5/Al_2O_3 , Nb_2O_5/ZrO_2 , and Nb_2O_5/TiO_2 provides the strongest evidence that the NbO_x surface species ($Nb=O$ fundamental at 980 cm^{-1}) is present as a mono-oxo moiety.

Dong et al. [422] have studied the surface properties of ceria-supported tungsten and copper oxides. Laser Raman spectroscopy (LRS) and IR results of WO_3/CeO_2 samples prepared by using different precursors have shown that calcination has a dramatic effect on the structure of the final product, which might mostly eliminate the differences of the precursors and result in final products with almost a same structure.

Wojciechowska et al. [423] have presented results of studies on the structure of MgF_2 that can be used as non-conventional catalyst support (Fig. 28). In the spectrum of the sample evacuated for 30 min at RT, a series of bands originated from hydroxyl groups can be observed. The increase of the evacuation temperature resulted in a decrease of the bands intensity or even in their complete disappearance. After evacuation at 673 K, only three bands were recorded at ~ 3750 , 3614, and 3400 cm^{-1} . The two former bands originated from the vibrations of isolated OH groups, while the latter was attributed to OH groups bonded via the hydrogen bridge. The further increase of the evacuation temperature resulted in a gradual decrease of the intensity of those bands. The evacuation at 873 K resulted in a complete disappearance of the band at 3400 cm^{-1} . The IR spectra presented show also the bands characteristics of water molecularly adsorbed on magnesium ions at 1639 and 1669 cm^{-1} . The intensities of these bands, similarly as those assigned to OH groups, gradually decreased with increasing evacuation temperature. It was concluded that a temperature of 873 K is sufficient for the total dehydroxylation of the MgF_2 surface [423].

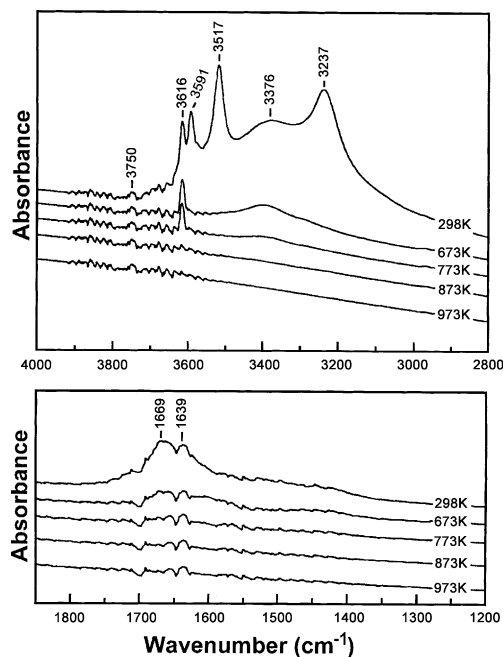


Fig. 28. IR spectra of the MF_2 sample (calcined at 673 K) evacuated at different temperatures for 30 min [423].

The $NiO/\gamma-Al_2O_3$ system has been studied for a long time. In this system there are at least three different oxidic phases: Al_2O_3 , the so-called nickel surface spinel, and NiO . The ratios between the concentrations of these phases depend on the nickel concentration and the temperature at which the system has been calcined. IR and TPD studies of CO and NH_3 adsorption on $NiO/\gamma-Al_2O_3$ were performed to show which are the active sites belonging to the three phases mentioned above, and how the absorptive properties of the system change when, new phases begin to appear due to an increase of Ni concentration [424].

Hydrogen adsorbed on Ru/ZrO_2 was studied [425]. While the $Ru-H$ species was not observed, an H_2O -like species was formed by the H_2 of introduction onto ZrO_2 . The H_2O -like species was characterised by a band at around 1600 cm^{-1} due to the bending mode and by a broad band at $2500\text{--}3800\text{ cm}^{-1}$ attributed to the stretching mode. The H_2O -like species was stable under evacuation at 300 K, but desorbed as H_2 at 370 K. The H_2O -like species was considered to be produced by spillover of hydrogen atoms dissociatively

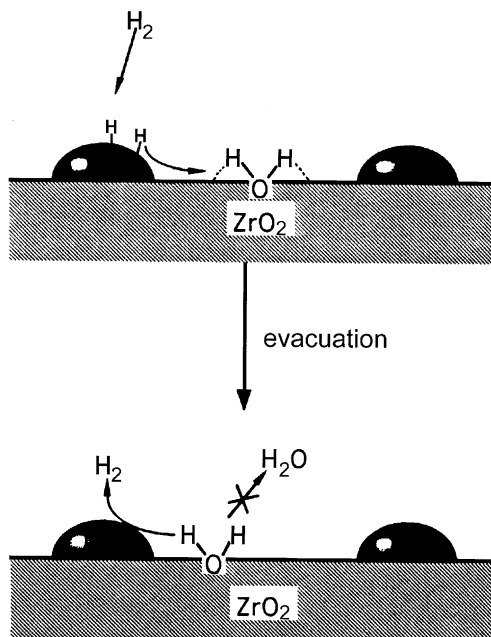


Fig. 29. Hydrogen adsorption and desorption process on Ru/ZrO₂ [425].

adsorbed on Ru particles to react with the surface lattice oxygen atoms of ZrO₂ [425] (Fig. 29).

Methane adsorption on an MgO surface has been studied [426]. Methane has been found to be very

Table 2
Vibrational frequencies of free CH₄ and observed IR bands upon CH₄ adsorption on a MgO surface [426]

Vibrational modes	Gas phase	Adsorbed on MgO
ν_1	2914 ^a	2897
ν_2	2526 ^a	Not observed
ν_3	3020	3002
ν_4	1306	1302

^a IR inactive, Raman band.

weakly bound on the MgO surface and mainly at the low-coordinated ions. Upon interaction with the surface, the C–H symmetric stretching mode (IR symmetry forbidden for the free molecule) becomes IR active and shifts toward lower frequencies. To account for the role of Lewis acid sites in methane adsorption, CO coadsorption has been also considered (Fig. 30, Table 2).

The dynamic behaviour of the ethanol adsorption on γ -alumina was investigated at 453 and 473 K by the transient-response method coupled with FT-IR data of the catalyst surface [427]. The existence of three adsorbates was demonstrated: a reacting species, which is the precursor for the formation of the gas-phase ethene, an inhibiting species responsible for the low steady-state reaction rate, and a spectator species accumulating on the catalyst surface. Their IR spectra indicate an ethoxide-like structure for the three adsorbates.

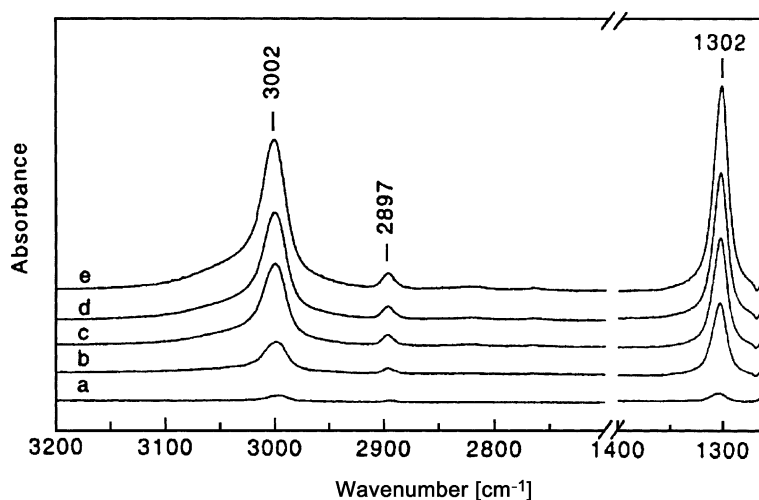


Fig. 30. FT-IR spectra of: (a) 0.01 kPa; (b) 0.02 kPa; (c) 0.05 kPa; (d) 0.1 kPa; (e) 0.2 kPa CH₄ on MgO at 88 K [426].

Adsorption of acetic acid gives rise to very similar species on very different adsorbents, known to be good catalysts for the selective hydrogenation of carboxylic acids to corresponding aldehydes [428]. The species observed by the IR spectra reacts or desorbs at temperatures at which the catalytic reaction occurs, when run at atmospheric pressure. Catalytic data together with the IR spectra allow a consistent picture of the intermediates to be proposed.

Surface complexation of phthalic acid/phthalate has been investigated on synthetically produced, non-aged γ -aluminium oxide by IR and Raman spectroscopy [429]. Effects of time, pH, and ionic strength have been studied both on the total adsorbed amount of phthalate and on the surface complexes. The spectroscopic results indicated the formation of two different types of complexes: outer sphere and inner sphere. The relative concentrations of these complexes were shown to vary considerably with pH but very little with increasing ionic strength, which equally reduced the amount of both types of complexes. Considering the electrostatic interaction between the surface and adsorbate, a complexation model was proposed that is in accordance with the spectroscopic results [429] (see Table 3).

Cox and Tripp [430] have described a transmission IR technique for detecting bands due to adsorbed species on silica gels in the region $4000\text{--}200\text{ cm}^{-1}$. The region below 1300 cm^{-1} contains strong Si–O bulk modes that dominate the much weaker bands due to adsorbed species. Silica gels are strong IR scatters, and adsorbed molecules lead to changes in the spectral artefacts in the region containing the bulk modes. These artefacts dominate and mask out the much weaker bands due to adsorbed species. By embedding the silica gel in a pliable polymer film of similar refractive index, one minimises the artefacts, enabling detection of bands attributed to adsorbed compounds.

Table 3

IR frequencies and band assignments for the surface complex formed during phthalate adsorption on $\gamma\text{-Al}_2\text{O}_3$ [429] (ν_s and ν_{as} are the symmetric and asymmetric stretching, respectively)

Wavenumber (cm^{-1})	Band assignment
1085	$\delta(\text{C-H})$ in plane bending
1148–1150	$\delta(\text{C-H})$
1167	$\nu(\text{C-COO})$
1263	$\nu(\text{C-COO})$
1292–1293	$\delta(\text{C-H})$ coupled to $\nu(\text{C-O})$
1400–1407	$\nu_s(\text{O-C-O})$ of the outer sphere complex
1427–1431	$\nu_s(\text{O-C-O})$ of the inner sphere complex
1451	$\nu(\text{C-C})$ ring
1490–1491	$\nu(\text{C-C})$ ring
1556–1563	$\nu_{as}(\text{O-C-O})$ of the outer sphere complex
1583–1584	$\nu(\text{C-C})$ ring
1610–1611	$\nu(\text{C-C})$ ring

Kantacheva et al. [431] have observed the formation of different surface species during the successive adsorption of small doses of acetone on TiO_2 (anatase). Formed species are due to coordination to Lewis acid sites on titania by the electron pair of oxygen atom from the carbonyl group, or the interaction of titania hydroxyls with acetone molecule (Fig. 31).

The surface concentration of acetone isomeric species (Fig. 31(b) and (c)) depends on the hydroxylation of the sample. The enol form prevails on the anatase surface. It was assumed that coordinatively bonded acetone and its enol surface form are intermediates in the dimerisation of acetone to mesityl oxide [431].

Pathways and generated surface species of adsorption and consequent surface reactions of acetone vapour on characterised silica, alumina, and $\sim 5\text{ wt.}\%$ silica–alumina were examined by in situ IR spectroscopy, following degassing at room and higher temperatures ($373\text{--}673\text{ K}$) [432]. For reference and

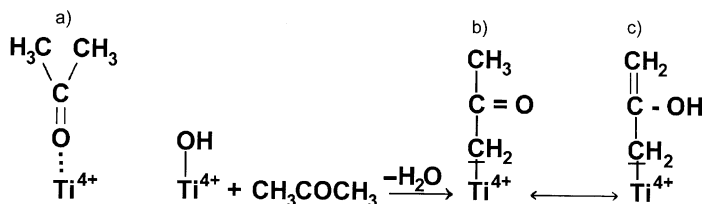


Fig. 31. Adsorbed species of acetone on titania surface: (a) interaction with Lewis acid site; (b, c) interaction with titania hydroxyls to form keto and enol forms, respectively [431].

confirmatory purposes, adsorptives of mesityl oxide and acetic acid, and adsorbents of K-modified and pyridine-covered silica–alumina, were employed. In the absence of Lewis and Brønsted acid sites, as well as of basic sites (i.e., on silica), acetone molecules are weakly hydrogen-bonded to surface $\text{OH}^{\delta+}$ groups and desorb completely at 373 K, without involvement in any further surface reactions. The availability of such acid–base sites on alumina and silica–alumina facilitates acetone chemisorption and activation for aldol condensation-type surface reactions, leading to formation of surface species of mesityl oxide at RT to 473 K and their oxidative conversion into acetate species at 573–673 K. The more obvious availability of Brønsted acid sites on silica–alumina enhances progression of the surface reactions involved [432].

The temperature-dependent adsorption of methyl formate on powdered TiO_2 has been investigated using IR [433]. This study reveals the thermal decomposition process of methyl formate and its reaction kinetics. Methyl formate is adsorbed on the TiO_2 surface in two forms. One is molecularly adsorbed methyl formate showing a red-shifted carbonyl stretching. The other is a structure-reorganised species showing absorption bands at 2841, 2866, and 2942 cm^{-1} in the CH_x stretching region. An orthoester-type intermediate is proposed to explain the observed IR absorption bands. In the thermal reactions, all the detected carbon-containing gas products are derived from $\text{CH}_3\text{O}_{(a)}$ and $\text{HCOO}_{(a)}$, which are generated as surface intermediates in the process of methyl formate decomposition [433].

Chi and Chuang [434] have noticed, that NO/O_2 coadsorbed as a chelating bidentate nitrate on Tb_4O_7 and La_2O_3 , and as a distinctive bridging bidentate nitrate on BaO and MgO via the reaction of adsorbed NO with surface lattice oxygen at 523 K (Fig. 32).

The role of the support nature in chemisorption of $\text{Ni}(\text{acac})_2$ on the surface of silica and alumina has been investigated [435]. Chemisorption of nickel acetylacetonate from the gas phase at 493 K on the surface of silica and alumina supports occurs via chemical reaction of $\text{Ni}(\text{acac})_2$ molecules with surface hydroxyl groups. Acetylacetonate, which is evolved upon chemisorption of $\text{Ni}(\text{acac})_2$, reacts with coordinatively unsaturated Al^{3+} ions on the surface of alumina support.

Molina et al. [436,437] have studied α -alumina-supported Ni catalysts prepared with $\text{Ni}(\text{acac})_2$, too. IR results indicate that the interaction between $\text{Ni}(\text{acac})_2$ and the support involves coordinatively unsaturated Al^{3+} sites, hydroxyls on the support surface, and probably also basic oxygens.

Carboxylic acids are found to adsorb weakly to the native oxide surface of aluminium [438]. Under heat exchange conditions, synergistic carboxylate combinations provide superior high-temperature aluminium corrosion protection and show excellent heat-transfer characteristics. FT-IR was one of the techniques used for the study and characterisation of surface film formed. It was concluded that, under heat-transfer conditions, carboxylates are chemically bonded to the aluminium surface [438].

Adsorption of cobalt carbonyl ($\text{Co}_2(\text{CO})_8$) on the silica surface and decarbonylation during heat treatment were followed by IR [439]. Changes in $\nu(\text{OH})$ and $\nu(\text{CO})$ regions were followed by DRIFTS. The band formation at 3680 cm^{-1} during deposition indicated weak hydrogen bonding between cobalt carbonyls and silanol groups on the silica surface. Rearrangement of $\text{Co}_2(\text{CO})_8$ to $\text{Co}_4(\text{CO})_{12}$ was also seen. Subsequent heat treatment at elevated temperatures (373–423 K) led to decarbonylation, where the completely decarbonylated surface was achieved via the formation of subcarbonyl species. IR bands of carbonate and bicarbonate species were not observed. Formation of carbide compounds was insignificant owing to the very small amount of carbon in the samples. The deposition temperature did not affect the adsorption of cobalt carbonyl on silica, but the pre-treatment temperature affected it [439].

The adsorption of molybdenum hexacarbonyl was studied on thin hydroxylated and partially hydroxylated alumina films [440]. The majority of the $\text{Mo}(\text{CO})_6$ adsorbed on hydroxylated alumina at 80 K desorbs at ~ 200 K; the remainder decarbonylates leading to a molybdenum coverage of $\sim 2\%$ of a monolayer. Subcarbonyl species are detected as the sample is heated to ~ 200 K and, at higher temperatures, the molybdenum is oxidised to an $\sim +4$ oxidation state and deposits primarily oxalate species on the surface. The adsorbed oxalates thermally decompose at ~ 300 K to evolve CO to form adsorbed bidentate carbonate species. These are stable to ~ 560 K and react to evolve CO at this temperature.

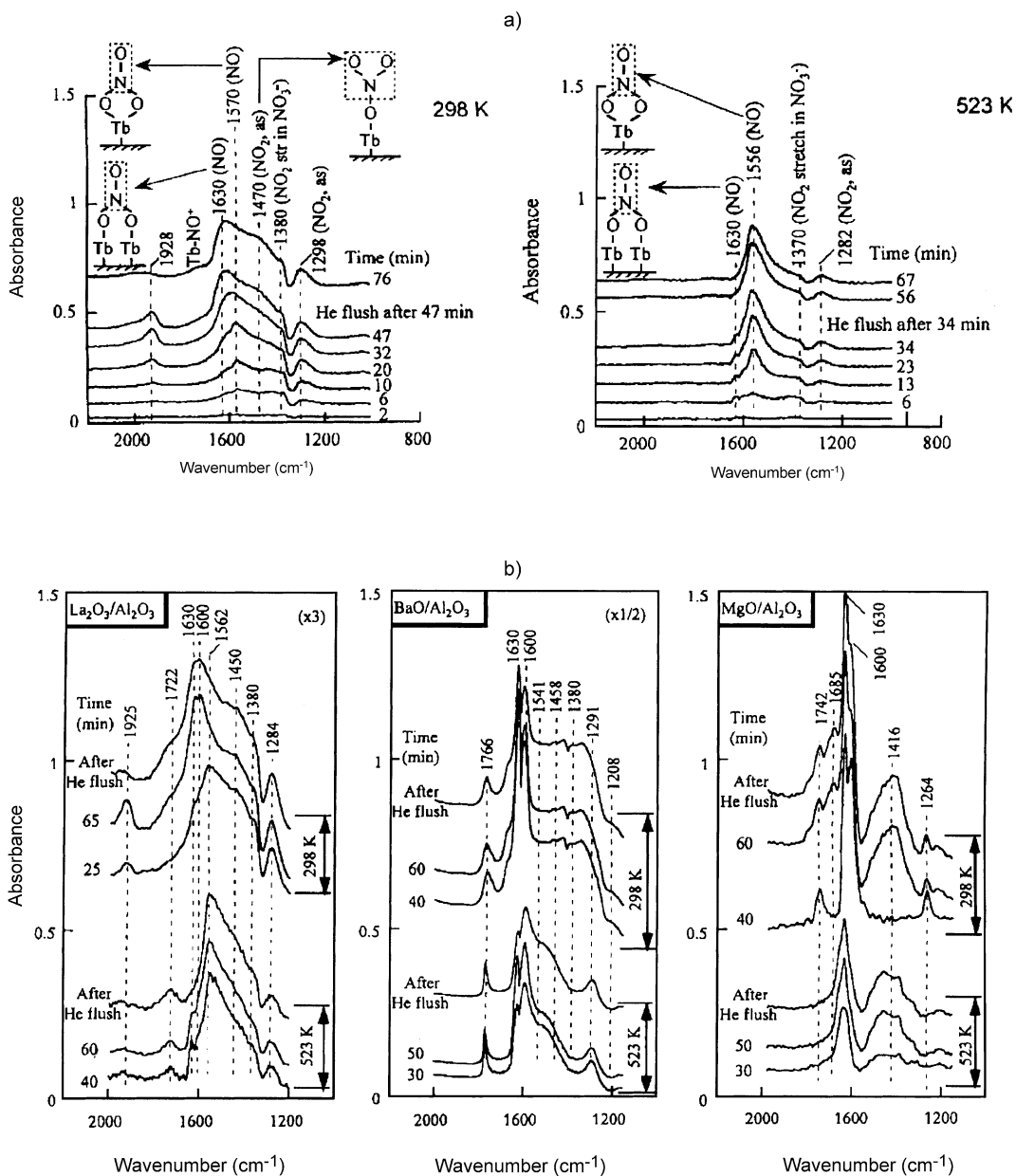


Fig. 32. IR spectra during 0.08% NO and 2% O_2 adsorption at 298 and 523 K on: (a) $Tb_4O_7/\gamma-Al_2O_3$; (b) $La_2O_3/\gamma-Al_2O_3$, $BaO/\gamma-Al_2O_3$, and $MgO/\gamma-Al_2O_3$ [434].

Redox processes induced by interaction of a calcined Cu/CeO₂ catalyst with CO and reoxidation with O₂ have been investigated [441]. Contact of the CO-reduced sample with O₂ at room or higher

temperature produces an important reoxidation of both copper and ceria, revealed by FT-IR and EPR.

Microcalorimetric and FT-IR measurements for the adsorption of ethylene on Pd/SiO₂ and Pd/Sn/SiO₂

catalysts have been performed at temperatures of 300, 263, and 233 K [442]. In addition, microcalorimetric measurements were made for H₂ and CO adsorption and FT-IR studies were conducted for CO adsorption at 300 K on these catalysts. Ethylene adsorption on the catalysts results in the formation of ethylidyne species, di- δ -bonded ethylene, and π -bonded ethylene species at 300 K, with initial heats of adsorption of 160 and 110 kJ/mol for the Pd and Pd/Sn catalysts, respectively. Lower heats of ethylene adsorption caused by the addition of Sn, a new band at 1542 cm⁻¹ is observed in the IR spectra of ethylene on Pd/Sn/SiO₂, and this band is representative of a weakly adsorbed, π -bonded ethylene species.

Microcalorimetric adsorption and FT-IR were used to study the surface species and energy of surface bonding for ethylene adsorption on Ni/SiO₂ and NiBi/SiO₂ catalysts [443]. The FT-IR results show that the surface species on the Ni/SiO₂ at RT are ethylidyne-type (Ni₃≡CCH₃). On the other hand, the heat and coverage for the adsorption of ethylene on the Ni₁₆Bi/SiO₂ sample are significantly lower, indicating a change in the ensemble size of surface Ni in this sample, leading to the change of surface species for the adsorption of ethylene as evidenced by the FT-IR spectrum which reveals the formation of mainly associatively adsorbed ethylene species.

Platinum catalysts supported on TiO₂, ZrO₂, and Al₂O₃ submitted to low-temperature reduction (LTR, 473 K) and high-temperature reduction (HTR, 773 K), and exposed to H₂ and CO at RT were studied by IR [444]. Hydrogen migrates to the bulk of catalysts treated by LTR. This migration results in a strong absorption in the IR region and is dependent on the hydrogen pressure. The same behaviour can be obtained when Pt on reducible oxide catalysts are treated by HTR. A decrease on the carbon monoxide adsorption capacity occurs for Pt/TiO₂ and Pt/ZrO₂ catalysts after HTR treatment as expected for Pt on reducible supports. However, the decrease in the carbon monoxide adsorption capacity is also observed for Pt/TiO₂ and Pt/ZrO₂ catalysts after LTR treatment in the presence of hydrogen. Therefore, a typical SMSI behaviour was also detected after LTR treatment. The electronic effects evidenced by the carbonyl band shifts to lower wavenumbers can be caused by LTR treatment under the presence of hydrogen even for Pt/Al₂O₃, and it was not induced by thermal treat-

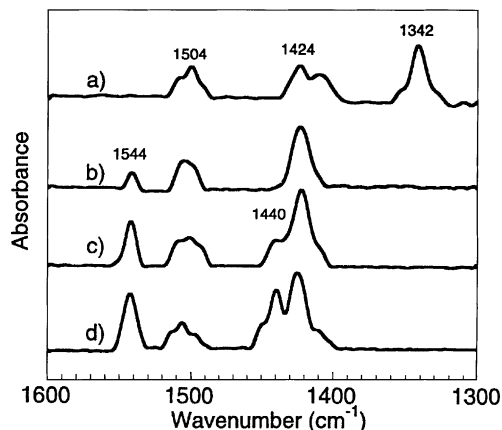


Fig. 33. IR spectra for C₂H₄ adsorption on Pt/Au/SiO₂ catalyst at: (a) 300 K; (b) 263 K; (c) 233 K; (d) 203 K [445].

ment at higher temperatures. This work suggests that the SMSI behaviour observed as a decrease in the carbon monoxide adsorption capacity and carbonyl band shifts to lower wavenumbers is a consequence of hydrogen presence on the support, possibly in the metal–support interface, which can promote electronic effects. Hydrogen spillover increases with support reducibility, but can occur even for Pt on an unreducible alumina support [444]. Shen et al. [445] have investigated ethylene adsorption on Pt/Au/SiO₂ catalysts.

Fig. 33 shows IR spectra for ethylene adsorption on the Pt/Au/SiO₂ catalyst at temperatures from 203 K to RT. The IR spectrum in Fig. 33(a) was collected at RT, and it shows bands at 1504, 1424, and 1342 cm⁻¹, corresponding to π -adsorbed ethylene, di- δ -adsorbed ethylene, and ethylidyne species, respectively. The π -bonded and di- δ -bonded ethylene species on the Pt/Au catalyst probably formed on Pt sites isolated by surrounding Au atoms, whereas ethylidyne species formed on sites with larger ensembles of surface Pt atoms. The significant decrease in the amount of ethylidyne species formed on the Pt/Au catalyst compared to the monometallic Pt catalyst is a strong indication that there is substantial interaction between Pt and Au for our Pt/Au/SiO₂ catalyst.

Spectrum in Fig. 33(b) collected at 263 K shows only π -bonded and di- δ -bonded ethylene species. This behaviour is further evidence for an interaction between Pt and Au, because ethylidyne species require threefold hollow sites composed of adjacent Pt atoms.

If there is interaction between Au and Pt, there will be fewer of these sites than on a Pt catalyst. The band at 1544 cm^{-1} (spectra b–d) was assigned to ethylene adsorbed on Au atoms. The band near 1440 cm^{-1} corresponds to ethylene adsorption on silica.

For methanol synthesis from CO_2 hydrogenation, SiO_2 -, TiO_2 -, and Al_2O_3 -supported Cu catalysts were used [446]. According to in situ FT-IR observations, the peaks of adsorbed formate species observed during the reaction were suppressed for Cu/TiO_2 , although they were dominant for both $\text{Cu/Al}_2\text{O}_3$ and Cu/SiO_2 . In order to understand the relationship between IR spectra and the activity, as well as to find out the essential factors that control the activity, the authors investigated the reactivity of intermediate species mainly by in situ FT-IR spectroscopy. Each Cu site itself had little ability to adsorb CO_2 ; however, Al_2O_3 and TiO_2 readily adsorbed CO_2 by weak bonding to them. CO_2 species adsorbed on Cu sites were rapidly converted to formate species under reaction conditions [446].

Fisher and Bell [447] have studied methanol synthesis from H_2 and CO_2 over Cu-supported catalysts. The locus of methanol synthesis from CO_2/H_2 over Cu/SiO_2 and $\text{Cu/ZrO}_2/\text{SiO}_2$ are found to be quite different. In the former case, the hydrogenation of CO_2 to methanol occurs on Cu. CO_2 adsorbs on Cu to form carbonate species, but in the presence of H_2 these species are rapidly converted to formate species adsorbed on Cu. The latter species undergo stepwise hydrogenation to methanol. For $\text{Cu/ZrO}_2/\text{SiO}_2$, virtually all of the adsorbed species are associated with ZrO_2 . CO_2 adsorbs as carbonate and bicarbonate species, which then react with atomic hydrogen to form formate species, and eventually, methoxide species, all of which are adsorbed on ZrO_2 . The presence of Cu greatly accelerates these transformations, as well as the reductive elimination of methoxide species as methanol. However, the release of methanol via the hydrolysis of methoxide species on ZrO_2 was found to be significantly more rapid than reductive elimination. A bifunctional mechanism for methanol synthesis from CO_2/H_2 was proposed in which CO_2 is adsorbed on ZrO_2 and then undergoes stepwise hydrogenation to formate, methylenebisoxo, and methoxide species, with atomic hydrogen being supplied by spillover from Cu. The final step in this sequence is the hydrolysis of the methoxide groups on ZrO_2 via reaction with water, produced as a co-product of methanol synthesis

and the reverse water–gas shift reaction. The latter reaction is thought to occur exclusively on Cu and is not enhanced significantly by the presence of ZrO_2 [447].

Kusama et al. [448,449] have studied carbon dioxide reactivity and structure of Rh/SiO_2 and Rh-Co/SiO_2 catalysts. The effect of metal precursor using catalyst preparation on CO_2 hydrogenation reactivity was found over Rh/SiO_2 catalysts. Carbon dioxide conversion over the catalyst prepared from chloride precursor was lower than those of acetate and nitrate ones, because there were fewer active sites on the catalyst, as estimated by H_2 chemisorption and in situ FT-IR. The main product was carbon monoxide over the catalysts prepared from acetate and nitrate precursors, but was methane over the catalyst prepared from the chloride one [448].

Rh-Co/SiO_2 catalysts, which showed remarkable methanol formation in CO_2 hydrogenation, were characterised by various methods such as TEM, EDX, XPS, and in situ FT-IR [449]. A good correlation was obtained between methanol selectivity and the surface Rh composition of Rh-Co/SiO_2 catalysts determined by XPS analysis. The selectivity to methanol increased with the surface composition of Rh. Adsorbed CO species on the Rh–Co alloy (cobalt rhodium carbonyl) were observed on Co-promoted catalysts in the spectra of in situ FT-IR during CO_2 hydrogenation reaction. These results indicated that methanol formation was promoted on the interface between Rh and Co. The electron-donating effect from Co to Rh was observed in situ FT-IR observation of CO_2 adsorption on Rh-Co/SiO_2 . Fig. 34 shows the observed in situ FT-IR spectra for 5 wt.% Rh/SiO_2 catalyst. When CO_2 was introduced to the catalyst, two bands appeared at 2047 and 1796 cm^{-1} (Fig. 34(a)). The first band was assigned to $\nu(\text{CO})$ for linear CO species and the second band was attributed to $\nu(\text{CO})$ for bridged CO species. Additionally, a shoulder peak assigned to $\text{Rh}_2-(\text{CO})_3$ was observed at 1883 cm^{-1} (Fig. 34(a)). As the temperature was increased, the linear CO species began to react with H_2 at 473 K (Fig. 34(e)). The bridged CO species also began to react with H_2 at 533 K (Fig. 34(f)). These species disappeared completely at 573 K (Fig. 34(g)).

The results of in situ FT-IR observation for 5 wt.% $\text{Rh-Co}(1:0.1)/\text{SiO}_2$ catalyst are illustrated in Fig. 35. After CO_2 adsorption, two peaks appeared at 2020 and

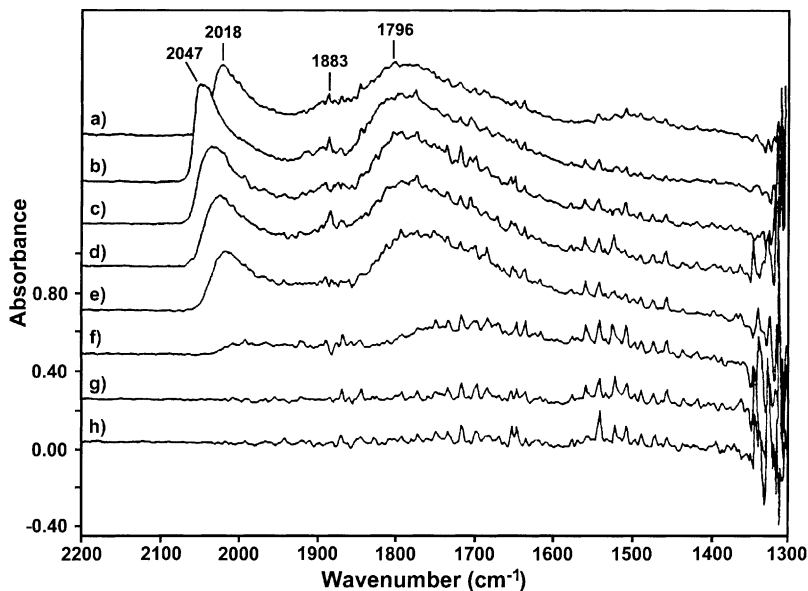


Fig. 34. In situ FT-IR spectra of hydrogenation of adsorbed CO_2 derivatives on the 5 wt.% Rh/SiO₂ catalyst: (a) CO_2 adsorption, 308 K; (b) hydrogenation, 308 K; (c) 373 K; (d) 423 K; (e) 473 K; (f) 533 K; (g) 573 K; (h) 623 K [449].

1769 cm^{-1} (Fig. 35(a)). As the temperature was raised in H_2 , the peak at 2031 cm^{-1} began to react with H_2 at 533 K. The peak at 1769 cm^{-1} also began to react with H_2 at 573 K (Fig. 35(g)). These adsorbed CO species disappeared completely at 623 K (Fig. 35(h)).

The results indicated that methanol synthesis was promoted on the interface between Rh and Co. The more the Rh ratio on the surface of Rh-Co/SiO₂ catalysts was, the more is the interface ratio between Rh and Co was on the catalyst surface, resulting in

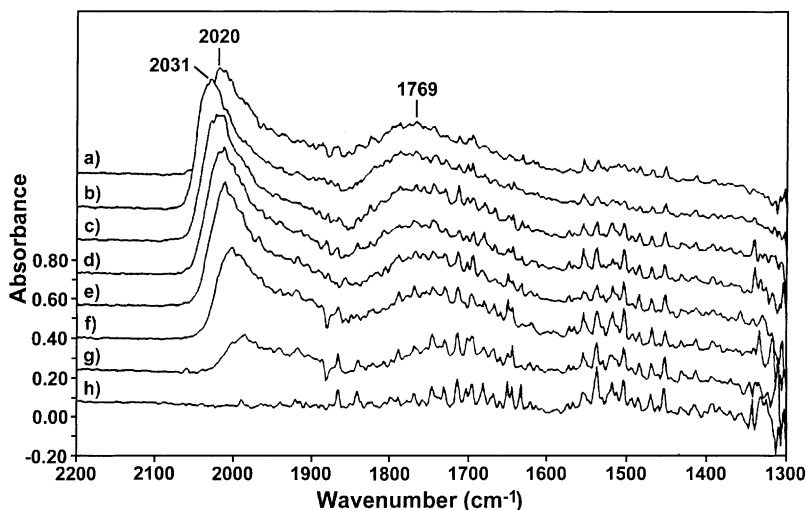


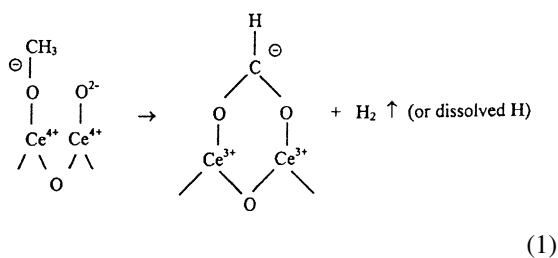
Fig. 35. In situ FT-IR spectra of hydrogenation of adsorbed CO_2 derivatives on the 5 wt.% Rh-Co(1:0.1)/SiO₂ catalyst: (a) CO_2 adsorption, 308 K; (b) hydrogenation, 308 K; (c) 373 K; (d) 423 K; (e) 473 K; (f) 533 K; (g) 573 K; (h) 623 K [449].

promotion methanol formation. The temperature at which adsorbed CO species reacted with H₂ over Co-promoted Rh/SiO₂ catalysts was higher than that over unpromoted catalyst. Judging from these findings of in situ FT-IR and CO₂ hydrogenation reactivity, the authors concluded that Co additive stabilised adsorbed CO species derived from CO₂, resulting in promotion of methanol formation [449].

The effects of co-catalyst were studied on the methanol synthesis reaction from CO₂ and H₂ over various TiO₂-supported copper catalysts [450]. By in situ FT-IR, the formate species formed on Cu was observed over CuO/TiO₂ catalyst. The amount of the formate species depended on the kinds of additive. Addition of K, Zr, and Zn showed high activity and increased the intensities of the formate species. On the other hand, addition of P decreased the activity and the intensities of the formate species. Among them, Zn addition increased the amount of adsorbed formate species markedly and resulted in the highest methanol yield.

The synthesis of methanol from CO₂ and H₂ over YBa₂Cu₃O₇ catalyst was studied [451]. Intermediate species such as formate, methoxide (2957 cm⁻¹), methylenebisoxo, formyl, and formaldehyde (2880, 2707, and 1763 cm⁻¹) were observed in situ FT-IR and FT Raman studies.

Finocchio et al. [452] have investigated the thermal reduction of a series of Ce_xZr_{1-x}O₂ solid solution samples by methanol adsorbed at RT. Methoxy species resulting from methanol dissociation and adsorbed as on-top or bridging species, either on Zr⁴⁺ or Ce⁴⁺ ions, are well differentiated. Upon the thermal treatment, Ce⁴⁺ sites appear to be exclusively the reactive ones through their reduction into Ce³⁺:



First, on-top methoxy species adsorbed on Ce⁴⁺ sites are oxidised to mobile formate species in the 423–473 K temperature range, with the subsequent partial cerium reduction. Second, bridging methoxy

and formate species decomposed in the 473–523 K temperature range through processes involving CO, CO₂, H₂, and H₂O gaseous evolution. The reduction of surface cerium ions is then complete. The different temperature range at which mixed oxide reduction and hydrogen evolution take place demonstrates that the catalysts are not reduced by H₂ uptake, but by framework oxygen consumption, due to methoxy oxidation into formate species [452].

The alkylation of aniline with methanol over γ -alumina was studied [453]. Based on the FT-IR results and those reported in the literature, it was proposed that both aniline and methanol are adsorbed undissociatively on the Lewis acid–base dual sites of γ -alumina. The electrophilic attack of the methyl group of methanol on the nitrogen atom of aniline or *N*-methylaniline yields *N*-methylaniline and *N,N*-dimethylaniline, respectively.

Zhang and Smirniotis [454] have studied oxide-based catalysts for the oxidative transformation of acetonitrile to acrylonitrile with methane. FT-IR and TPD experiments indicated that an increase in the number and strength of the basic sites of the catalysts plays a negative role in the coupling of CH₄ and acetonitrile to acrylonitrile.

The interconversion of isomeric unsaturated C₄ nitriles in solution in the presence of butyllithium was investigated [455]. The generation and existence of a carbanionic intermediate in the base-induced interconversion of C₄ nitriles were unequivocally proven and characterised by the shifts in the $\nu(\text{CN})$ and $\nu(\text{C}=\text{C})$ vibration regions of the IR spectra.

In situ IR spectroscopy coupled with dynamic and steady-state isotopic transient kinetic analysis permitted observation of the transient response of IR-observable adsorbates as well as gaseous reactants and products [456]. This technique was used to examine the reaction pathway, reactivity of adsorbates, and nature of sites for the CO/H₂/C₂H₄ reaction on Mn–Rh/SiO₂. Dynamic IR study reveals that Rh⁰ sites, which chemisorb linear CO actively catalyse CO insertion, a key step for the formation of propionaldehyde from the CO/H₂/C₂H₄ reaction.

The influence of added isobutane on the formation of unsaturated carbenium ions (considered to be precursors of carbonaceous deposits) from 1-butene was studied [457]. The unequivocal results obtained by IR and UV–Vis spectroscopy show that the formation of

alkenyl ions is strongly suppressed in the presence of isobutane. The role of isobutane was explained by its enhanced hydride ion donor character.

The oxidation of propane over a Mn_3O_4 catalyst has been investigated [458]. Data on the mechanism and on the reaction pathways have been derived from an evaluation of the reaction kinetics and from FT-IR experiments. The main by-reaction with respect to oxy-dehydrogenation is propene over-oxidation to CO_2 . Direct total oxidation of propane to CO_2 can become predominant only in oxygen excess. Iso-propoxide species act probably as surface intermediate species in propene synthesis.

Studying the butyne hydrogenation on Pd and Pt catalysts, it was found that the formation of a surface hydrocarbon overlayer regulates the semi-hydrogenation selectivity [459]. It might be composed of η^2 -butyne species. These species are equilibrated with the reactive intermediates, which are thought to be vinylic adsorbed species. However, if the reactive intermediates are initially quickly hydrogenated, the coverage of the surface in equilibrium with the gas fugacity is so low that the hydrocarbon overlayer does not form and the catalyst is not selective.

Polymerisation of acetone and acetylene, the decomposition products of methylbutynol (MBOH), on the surface of Y/MgO catalyst was inferred [460]. It was found that MBOH decomposes into acetone and acetylene revealing the basic surface character of Y/MgO catalyst. However, modification of MgO with Y^{3+} cations decreased the catalyst activity towards MBOH decomposition relative to that observed for pure MgO. The consecutive polymerisation of the decomposition products is responsible for this low activity, since polymerised acetone is strongly adsorbed on the catalyst surface, and hence, blocks the surface active sites. FT-IR spectroscopy has been used to study the adsorption and reactivity of MBOH on the surfaces of pure and Cs^+ - and Ba^{2+} -modified MgO [461]. It has been found that MBOH is adsorbed via two different mechanisms. Dissociative adsorption at acid–base (M–O) pair-sites with the creation of new H-bonded surface OH_s groups is the most favourable adsorption mode in the case of Cs/MgO. This is attributed to the strong Lewis basic sites generated on the catalyst surface upon impregnation with Cs^+ cations which facilitate abstraction of hydrogen from MBOH, leading to

the formation of alcoholate species. On the other hand, the Ba/MgO catalyst adsorbs MBOH preferentially via interaction with surface hydroxyl groups. Both these adsorption modes are operative on the surface of pure MgO. The acetylenic group is also involved in the adsorption of MBOH. The acidic acetylenic hydrogen interacts with the Lewis basic sites, whereas the Lewis acid sites interact preferably with the acetylenic π -electron system. With regard to surface reactivity, the catalysts are active towards the decomposition of MBOH to acetone and acetylene, revealing their basic properties. It was concluded that the basicity of the series of studied catalysts can be ranked as follows: $\text{Cs/MgO} > \text{MgO} > \text{Ba/MgO}$ (Figs. 36 and 37).

Carbon dioxide reforming of methane has been studied over Ru/ SiO_2 and Ru/ $\gamma\text{-Al}_2\text{O}_3$ catalysts [462]. Catalytic activity measurements, IR spectroscopic analysis, and isotopic tracing experiments applied to the study of the surface hydroxyl groups of the supports have allowed different reaction mechanisms to be proposed on the bases of the detected surface species, their mobility, stability, and reactivity. Activation of both reactants takes place on the ruthenium surface for Ru/ SiO_2 catalyst. The accumulation of carbon adspecies formed from methane decomposition on the metallic particles finally impedes carbon dioxide dissociation and induces rapid deactivation of this catalyst. The alumina support provides an alternate route for CO_2 activation by producing formate intermediates on its surface that subsequently decomposes releasing CO. This bifunctional mechanism, in which the hydroxyl groups of the support play a key role, induces greater stability on the Ru/ Al_2O_3 catalyst by significantly decreasing the rate of carbon deposition on the metal [462].

Heterogeneous stoichiometric oxidation and catalytic partial oxidation of methane are studied at the surfaces of MgO, $\alpha\text{-Al}_2\text{O}_3$, and CeO_2 containing small Rh clusters [463]. Experiments performed in a reaction chamber equipped with IR and mass spectrometry have shown that CO and H_2 are produced as primary reaction products with selectivity close to 100% by alternating reactions with flowing streams of CH_4 and O_2 . When CH_4 and O_2 were admitted simultaneously into the reaction environment, CO_2 and H_2O were also formed through reactions involving Rh hydridocarbonyl species and gaseous O_2 molecules. CO_2 and H_2O formation was reduced

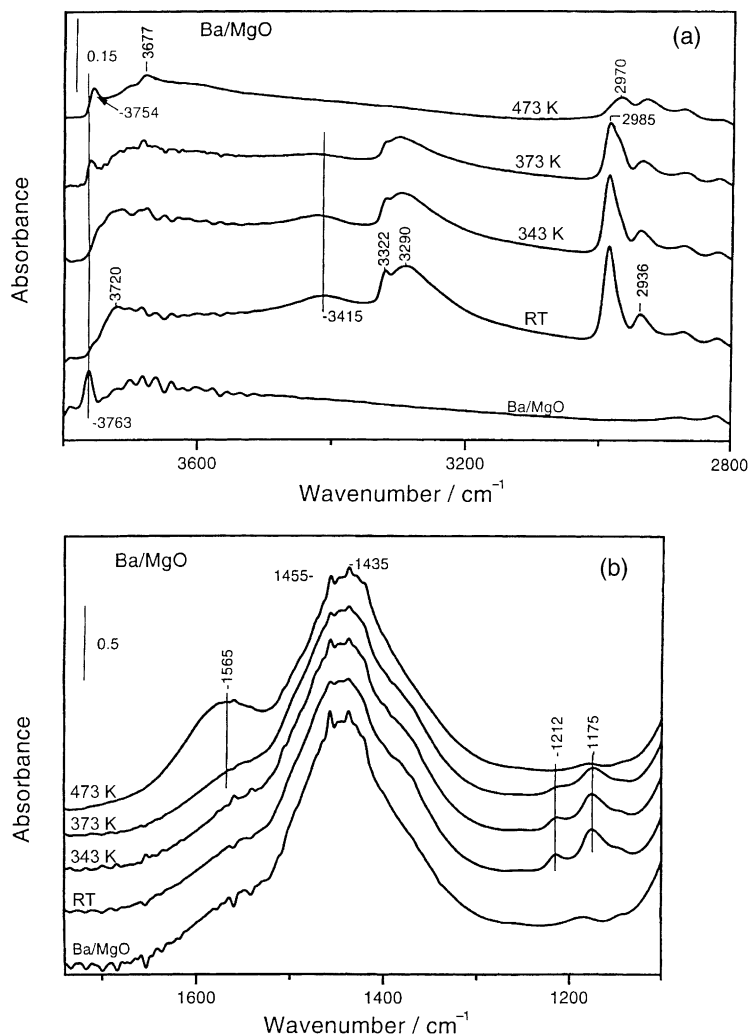


Fig. 36. (a) FT-IR spectra recorded for MBOH adsorbed on the Ba/MgO surface at different reaction temperatures. (b) The Ba/MgO spectrum is given for comparison [461].

at high surface temperatures, suggesting that at high temperatures thermally activated desorption of primary reaction products (CO, H₂) prevailed over total oxidation [463].

Ulla et al. [464] have studied catalytic combustion of methane on Co/MgO catalysts. Bulk characterisation was carried out using XRD, TPR, and Raman spectroscopy, and showed that the solids were made up of a CoO–MgO solid solution and a MgO phase. A detailed examination of catalysts' surfaces was achieved through FT-IR spectroscopy of adsorbed CO probe molecules, which indicated that at low cobalt

loadings only a small proportion of the Co going into the solid solution was present on exposed faces as either Co²⁺ oxo-species or pentacoordinated Co²⁺. However, as the cobalt content of the samples increased, a larger amount was exposed on the surface. This effect levelled off at 9 wt.% Co, after which the increase in exposed Co²⁺ sites was countered by the masking effect of islands of MgO [464].

Busca et al. [465] have studied the total oxidation of propane and its oxy-dehydrogenation to propene on spinel-type catalysts Mn₃O₄, Co₃O₄, and MgCr₂O₄ in a flow reactor and in an IR cell. Analogous stud-

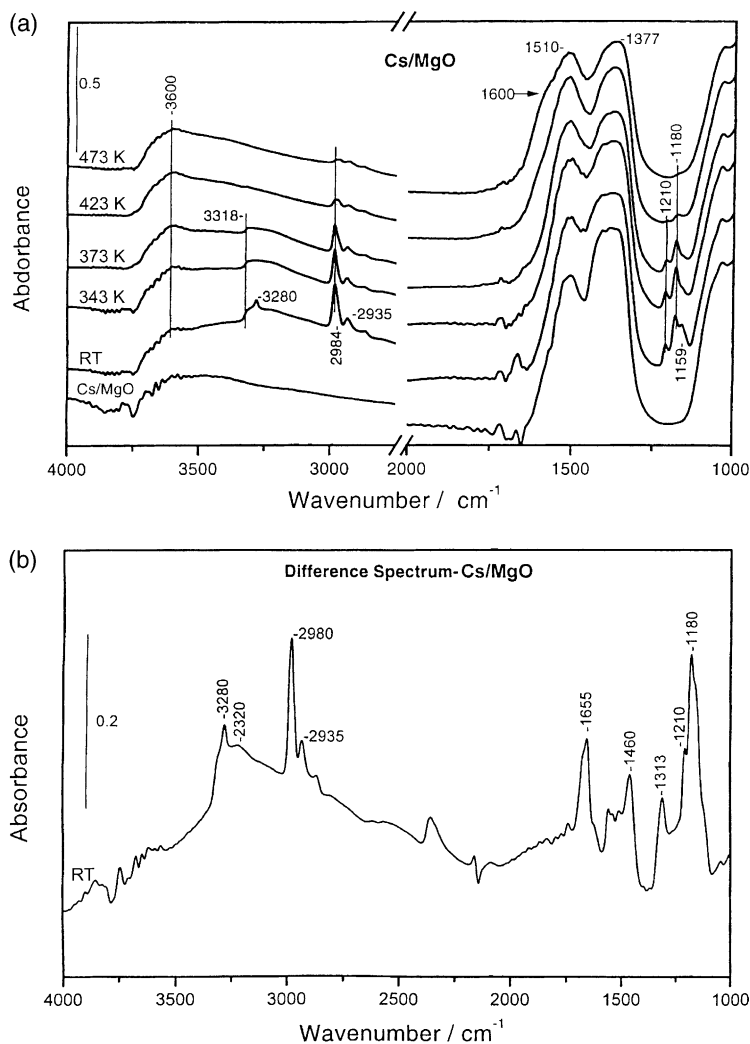


Fig. 37. (a) FT-IR spectra recorded for MBOH adsorbed on the Cs/MgO surface at different reaction temperatures. The Cs/MgO spectrum is given for comparison. (b) Difference spectrum recorded for MBOH adsorbed on the Cs/MgO surface at RT [461].

ies were performed on the oxy-dehydrogenation of *n*-butenes to 1,3-butadiene over MgFe_2O_4 . The activation of the hydrocarbons is thought to occur by abstraction of hydrogen from the weakest C–H bond, with a simultaneous reduction of a surface site and with the formation of a surface alkoxy-group (Fig. 38).

Selective oxidation of C_2H_6 to acetaldehyde and acrolein over silica-supported vanadium catalysts has been studied by Zhao et al. [466]. UV–Vis and IR measurements in samples identified the different types of vanadyl species with different vanadium loadings.

It was estimated that isolated vanadyl species with tetrahedral coordination, which were found mainly on the catalysts with vanadium loading lower than 0.5 at.%, became the active site for the aldehyde formation through the interaction with Cs.

Kinetic and in situ FT-IR studies of the catalytic oxidation of 1,2-dichlorobenzene over $\text{V}_2\text{O}_5/\text{Al}_2\text{O}_3$ catalysts. The IR studies have been conducted suggest that the benzene ring remains intact during the adsorption of 1,2-dichlorobenzene, while no surface species containing C–Cl bonds were detected [467].

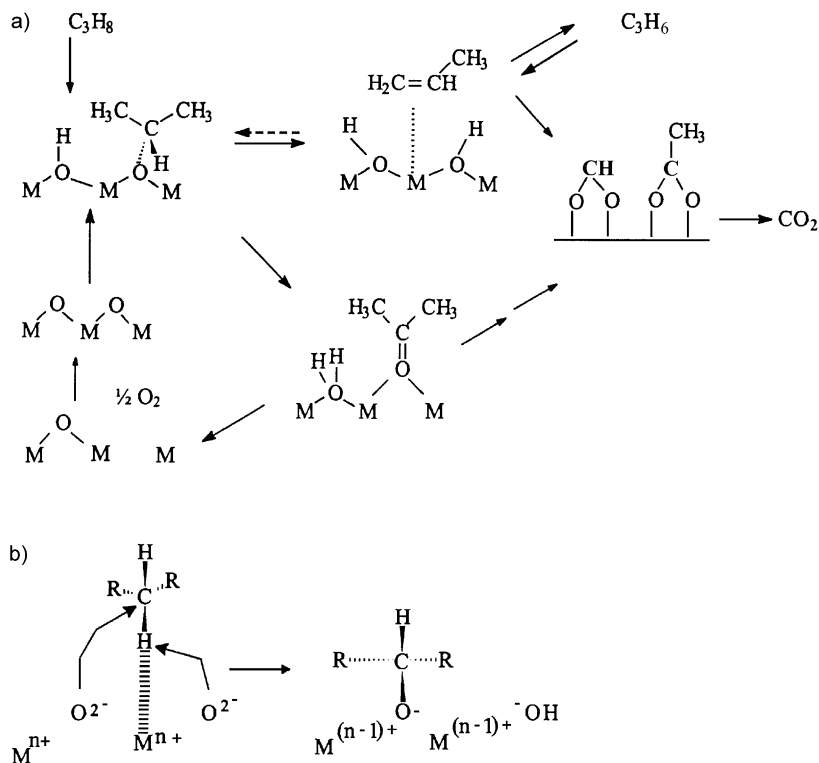


Fig. 38. Proposed generalised reaction pathway for propane oxidation over spinel-type oxide catalysts (a) and proposed mechanism for C-H bond activation over metal oxide catalysts (b) [465].

The authors suggested that chlorine abstraction is the first step in the reaction. Several partial oxidation products were observed on the catalyst surface under reaction conditions. The catalytic oxidation of 1,2-dichlorobenzene has been systematically investigated over a series of transition metal oxides (i.e., Cr_2O_3 , V_2O_5 , MoO_3 , Fe_2O_3 , and Co_3O_4) supported on TiO_2 and Al_2O_3 [468]. In situ FT-IR studies indicate the presence of carboxylates (i.e., acetates and formates), maleates, and phenolates on the surfaces of all catalysts studied under reaction conditions. These surface species were reactive in the presence of gas-phase oxygen and are potential intermediates for the oxidation of 1,2-dichlorobenzene.

FT-IR was used to investigate the catalytic performance of vanadyl pyrophosphate ($(VO)_2P_2O_7$) in the partial oxidation of toluene to benzaldehyde [469]. Generated benzaldehyde is strongly adsorbed on the catalyst surface and, therefore, consecutive reaction products such as cyclic anhydrides and radi-

calic degradation products of the aromatic ring can be formed easily. Higher reaction temperatures promote the total oxidation.

The conversion of ethylchloride into ethylene + HCl on pure and doped alumina supports and on $CuCl_2-Al_2O_3$ -based oxychlorination catalysts has been investigated by pulse reactor and FT-IR spectroscopy [470]. FT-IR spectra of ethylchloride adsorbed on $\gamma-Al_2O_3$ show weakly molecularly adsorbed species and ethoxy groups formed by nucleophilic substitution; adsorbed diethylether is also observed. The analysis of the gas-phase species shows that ethoxy groups decompose, giving rise to ethylene at 523 K. Under the same conditions, gaseous HCl is also released from the surface and diethylether is also observed in the gas phase. Chlorination of alumina with HCl only partially hinders the dehydrochlorination mechanism occurring through ethoxy groups [470].

$CuCl_2/Al_2O_3$ ethylene oxychlorination catalysts have been characterised by using IR spectroscopy of

the surface hydroxy groups and of adsorbed pyridine and CO₂ [471]. Ermini et al. [472] have studied the conversion of propane on γ -Al₂O₃. The interaction of the same catalyst with propane, propene, isopropanol, and acetone has also been investigated, with additional gas-phase monitoring, in an FT-IR cell.

Baldi et al. [473] have studied the selective catalytic oxy-dehydrogenation of C3 alcohols on Mn₃O₄. IR studies showed that the high yields obtained in carbonyl compound production over this catalyst are mainly due to their very weak adsorption. The main factor limiting the selectivity to acetone and, mainly, propanol is the tendency of both to give enolate anions that are further converted into acetaldehyde. Over-oxidation of aldehydes to the corresponding carboxylate species is a less efficient mechanism limiting selectivity. The selectivity/activity behaviour is definitely different from both that observed for the stoichiometric oxidation of alcohols with Mn(III) compounds, and that observed on other catalysts. This difference is associated to the low surface acidity of the Mn₃O₄ catalyst [473].

Jung and Park [474] have studied enhanced photoactivity of silica-embedded titania particles prepared by sol-gel process for the decomposition of trichloroethylene. From XRD and FT-IR results they concluded that added silicon formed segregated amorphous silica and embedded into anatase titania matrix. When the Si content was over 30 at.%, the distinct band for Ti–O–Si vibration (960 cm⁻¹) was observed.

Heterogeneous photochemical activation of CH₄ over a substrate containing Rh(CO)₂ species (Rh(CO)₂/Al₂O₃) and formation of an acetyl moiety on the surface has been investigated [375]. In situ FT-IR has been used to study the mechanistic details of adsorption and photocatalytic oxidation of acetone on TiO₂ surfaces at 298 K [475]. The adsorption of acetone has been followed as a function of coverage on clean TiO₂ surfaces (dehydrated TiO₂). IR spectra at low acetone coverages show absorption bands at 2973, 2931, 1702, 1448, and 1363 cm⁻¹ which are assigned to the vibrational modes of molecularly adsorbed acetone (Fig. 39).

At higher coverages, the IR spectra show that adsorbed acetone can undergo an aldol condensation reaction followed by dehydration to yield (CH₃)₂C=CHCOCH₃, 4-methyl-3-penten-2-one (commonly called mesityl oxide). The ratio of surface-bound

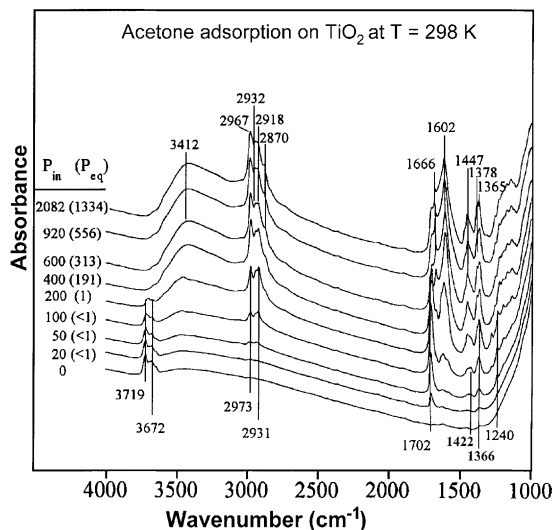


Fig. 39. IR spectra of acetone adsorbed on dehydrated TiO₂ at 298 K as a function of acetone pressure. The pressure introduced into the IR cell (P_{in}) and the equilibrium pressure established in the IR cell (P_{eq}) are given in units of mTorr. Absorptions assigned to adsorbed acetone are observed at 2973, 2931, 1702, 1422, 1366, and 1240 cm⁻¹. Absorptions assigned to adsorbed mesityl oxide are observed at 2967, 2932, 2918, 2870, 1666, 1602, 1447, 1378, and 1365 cm⁻¹ [475].

mesityl oxide to acetone depends on surface coverage. At saturation coverage, nearly 60% of the adsorbed acetone has reacted to yield mesityl oxide on the surface. In contrast, on TiO₂ surfaces with pre-adsorbed water (hydrated TiO₂), very little mesityl oxide forms. IR spectroscopy was also used to monitor the photocatalytic oxidation of adsorbed acetone as a function of acetone coverage, oxygen pressure, and water adsorption. Based on the dependence of the rate of the reaction on oxygen pressure, acetone coverage, and water adsorption, it is proposed that there are potentially three mechanisms for the photo-oxidation of adsorbed acetone on TiO₂. In the absence of preadsorbed H₂O, one mechanism involves the formation of a reactive O_(ads)⁻ species, from gas-phase O₂, which reacts with adsorbed acetone molecules. The second mechanism involves TiO₂ lattice oxygen. In the presence of adsorbed H₂O, reactive hydroxyl radicals are proposed to initiate the photo-oxidation of acetone [475].

Photo-oxidation of toluene has been carried out in gas-solid regime by using polycrystalline anatase TiO₂ as the catalyst [476]. FT-IR investigation was

carried out simulating the experimental conditions used during the photoreactivity experiments. The results indicated that toluene is weakly stabilised on the hydrated TiO₂ particles by hydrogen-bonding with surface hydroxyl groups, and that it is photo-oxidised to benzaldehyde only in the presence of surface OH groups.

Early et al. [477] have investigated the gas-phase hydrodechlorination of CF₃CFCl₂ to CF₃CFH₂ and CF₂Cl₂ to CF₂H₂ catalysed by Pd supported on Al₂O₃, a series of fluorinated Al₂O₃, and AlF₃. FT-IR investigations suggest the occurrence of direct reaction between the CFC and the support material, which results in the consumption of hydroxyl groups during the early stages of reaction.

In situ FT-IR spectroscopy has been used to study the adsorption at ~77 K of CO on tetragonal, non-calcined sulphated tetragonal, and calcined sulphated tetragonal zirconia [478]. CO adsorption at low temperature turned out to be a suitable probe to test the surface charge-withdrawing properties of the various zirconia-based systems. Similar studies have been conducted on the adsorption (at ~77 K) of carbon monoxide on (i) tetragonal zirconia (t-ZrO₂), (ii) non-calcined sulphated tetragonal zirconia (t-SZ), and (iii) calcined sulphated tetragonal zirconia ([t-SZ]_C) [479]. CO adsorption at low temperature turned out to be a suitable probe to test the surface charge-withdrawing properties of the various zirconia-based systems. On t-ZrO₂ it has been possible to distinguish the H-bonding adsorption of CO on at least two families of acidic surface OH groups and the coordinative adsorption of CO on surface Lewis acidic sites (i.e., coordinatively unsaturated Zr⁴⁺ surface centres) located either in regular patches of low-index crystal planes (the “top” termination of ZrO₂ crystallites) or in defective terminations of the particles (the “side” termination of ZrO₂ crystallites). On t-SZ, virtually only CO uptake by H-bonding on some surface OH groups is observed, as virtually all of the non-hydroxylated parts of the surface are occupied and maintained coordinatively saturated by sulphate groups. On [t-SZ]_C, the calcination process selectively eliminates the sulphates that were initially located in the defective crystal terminations. As a consequence CO uptake reveals, besides two well-resolved families of OH groups yielding adsorption by H-bonding, two well-resolved families of

Lewis acid sites located in defective crystal terminations (strong Lewis sites), whereas no CO uptake occurs in the regular terminations of the crystallites. The latter crystal positions remain occupied by a family of sulphates, that turn out to be responsible for the catalytic activity of [t-SZ]_C systems [479].

Low-temperature (85 K) CO adsorption on V-containing aluminophosphates (VAPO-5 and VMgAPO-5) [480]. Mild reduction of VAPO-5 with hydrogen (673 K) generates two kinds of V⁴⁺ sites, which can be detected by CO only at low temperature by bands at 2200 and 2194 cm⁻¹. In these complexes, CO is coordinated via a σ-donor bond. Deeper reduction of VAPO-5 with hydrogen (773 K and above) leads to the formation of V³⁺ sites. These cations form two kinds of carbonyl complexes (bands at 2197 and 2186 cm⁻¹) in which a weak π-back bonding is realised. As a result, the V³⁺-CO carbonyls are more stable than the V⁴⁺-CO species and can be detected at RT. The V³⁺ sites in VAPO-5 are fully oxidised by oxygen even at 85 K thus forming V⁴⁺ and eventually V⁵⁺ species. At higher reoxidation temperatures (up to 373 K), the major part of the V⁴⁺ sites is also oxidised to V⁵⁺. Some V⁴⁺ sites are created on VMgAPO-5 during the evacuation of the samples at 673 K. CO can monitor these sites by a band at 2204 cm⁻¹ only at low temperature. Deeper reduction with hydrogen creates a new kind of site (most probably V³⁺), which is characterised by a carbonyl band at 2197 cm⁻¹. The spectral regions in which V⁴⁺-CO (at least 2204–2194 cm⁻¹) and V³⁺-CO (2197–2186 cm⁻¹) species are detected are superimposed [480].

The interaction of CO with two aerogel solids have been investigated by in situ FT-IR spectroscopy in order to obtain experimental data on the mechanism of formation of the formate species which can be considered as the intermediate adsorbed species in the synthesis of methanol from CO/H₂ [481]. The adsorption of CO on ZrO₂ and ZnO/ZrO₂ aerogel solids was studied in the temperature range 298–623 K. At temperatures lower than 373 K, CO is mainly reversibly adsorbed on a cationic site M₁ (either Zr⁴⁺ or Zr³⁺), leading to an IR band at 2192 cm⁻¹ on ZrO₂, and 2183 cm⁻¹ on ZnO/ZrO₂. It is shown that this adsorption follows the Langmuir's model on both solids. At higher temperatures (*T* > 400 K), formate species are detected characterised on ZrO₂ by IR bands at 2967,

2882, 1576, 1382, and 1367 cm^{-1} . It is shown that the formation of this species decreases the number of cationic sites M_1 , which adsorb CO at temperatures lower than 373 K, and creates a new cationic site M_2 . This is interpreted as a mechanism of formation of the formate species involving two sites of the surface; an OH group, and a cationic site M_1 . The CO is first adsorbed on the cationic site M_1 , followed by a reaction with an OH group to produce a formate species. This last species is adsorbed on the cationic site M_1 , and a new cationic site is formed M_2 [481].

Savelieva et al. [482] have studied the reaction mechanism of CO oxidation on alumina-supported palladium catalysts. They have found the oxidation of adsorbed CO at $T < 423\text{ K}$ includes joint activation of the molecules. Moreover, two reaction mechanisms of the oxidation with different kinetic parameters and structures of CO and O_2 were found for temperatures below 423 K and over 423 K.

FT-IR spectroscopy of chemisorbed CO is suitable for determining strong metal–support interaction (SMSI) even in an incipient state when it is not detectable by other methods [483,484]. The chemisorption capacities of silica-supported nickel and platinum for CO is drastically decreased due to SMSI, i.e., silicide formation during high-temperature reduction [485].

The specific activity of supported metals in structure-sensitive reactions depends on the degree of metal dispersion. The state of Ni in reduced and oxidised Ni/SiO₂ catalysts was studied by IR spectra of adsorbed CO [486]. Nagase et al. [487] have studied the oxidation state of Cu in the course of CO oxidation over powdered CuO and Cu₂O.

The adsorption of CO at low temperatures (130–293 K) has been investigated on Rh/Al₂O₃ catalysts of low (0.001–1 wt.%) Rh loadings [488]. The surface structure of Rh produced at different reduction temperatures (573 and 1173 K) was shock-cooled to 130 K, where the addition of CO caused the appearance of the band due to bridge-bonded CO ((Rh⁰)₂–CO) on all samples. The appearance of the bands due to gem-dicarbonyl (Rh⁺(CO)₂) and linearly bonded CO (Rh_x–CO) depended on the Rh content and the reduction temperature of the catalysts. The positions and the integrated absorbances of the symmetric and asymmetric stretching of the Rh⁺(CO)₂ changed with temperature. On the basis of the above find-

ings, the rearrangement of the adsorbed CO species (indirectly that of surface Rh) was discussed [488].

The adsorption of CO at RT on a Ru/SiO₂ catalyst has been studied [489]. Spectral evidence was found for the formation of water molecules and a quantity of very dispersed ruthenium on the catalyst surface during CO adsorption. On the basis of these experimental results, a new reaction scheme for the interaction of CO with a silica-supported ruthenium catalyst was proposed. The adsorption of CO on a Ru/SiO₂ catalyst causes disruption of the Ru–Ru bond in the metal clusters and, as a result, mobile Ru⁰–CO species are formed. Some part of them interacts with the isolated Si–OH groups and replaces the protons of the hydroxyl groups. This process leads to transformation of the isolated hydroxyl groups to associated ones and to water molecule formation. In addition to this, O²⁻–Ru(CO)₃ species are produced which are directly bonded to the silica surface. The mobile Ru⁰–CO species form nearly isolated Ru⁰–CO species, i.e., a quantity of very small Ru particles is produced on which CO is chemisorbed. As a consequence of these processes, the metal dispersion in Ru/SiO₂ catalyst is increased [489].

IR spectra of adsorbed CO have been used as a probe to monitor changes in Pt site character induced by the coking of Pt/Al₂O₃ and Pt–Sn/Al₂O₃ catalysts by heat treatment in heptane/hydrogen [490]. Four distinguishable types of Pt site for the linear adsorption of CO on Pt/Al₂O₃ were poisoned to different extents showing the heterogeneity of the exposed Pt atoms. The lowest coordination Pt atoms ($\nu_{\text{CO}} < 2030\text{ cm}^{-1}$) were unpoisoned whereas the highest coordination sites in large ensembles of Pt atoms (2080 cm^{-1}) were highly poisoned, as were sites of intermediate coordination ($2030\text{--}2060\text{ cm}^{-1}$). Sites in smaller two-dimensional ensembles of Pt atoms ($2060\text{--}2065\text{ cm}^{-1}$) were partially poisoned, as were sites for the adsorption of CO in a bridging configuration. The addition of Sn blocked the lowest coordination sites and destroyed large ensembles of Pt by a geometric dilution effect. The poisoning of other sites by coke was impeded by Sn, this effect being magnified for Cl-containing catalyst [490].

The adsorption of CO on ZrO₂ and 0.5% Pt/ZrO₂ catalysts has been studied by means of FT-IR spectroscopy between 300 and 740 K at constant partial pressures of CO [491].

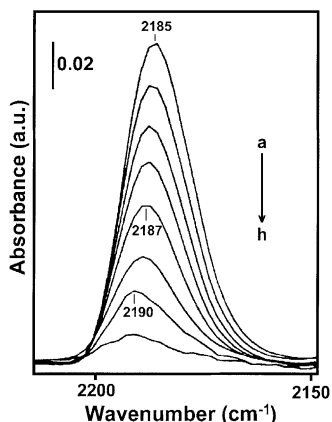


Fig. 40. Evolution of the IR band of the linear CO species adsorbed on ZrO_2 (L_{Zr} species) with adsorption temperatures (10% CO/He): (a) 300 K; (b) 313 K; (c) 320 K; (d) 329 K; (e) 340 K; (f) 358 K; (g) 378 K; (h) 413 K [491].

Fig. 40 shows the FT-IR spectra recorded on the pure ZrO_2 in the course of the CO adsorption with the 10% CO/He mixture for several values of the adsorption temperature (T_a). The IR band at 2185 cm^{-1} observed at $T_a = 300\text{ K}$ corresponds to a linear CO species (denoted by L_{Zr}) on Zr^{+3} or Zr^{4+} sites (denoted by $\text{Zr}^{+\delta}$). At 300 K, a switch 10% CO/He \rightarrow He leads to the disappearance of the IR band indicating that the L_{Zr} species is reversibly adsorbed.

The increase in T_a (spectra b–h in Fig. 40) with the 10% CO/He mixture, leads to a progressive decrease in intensity of the IR band alongside a slight shift to higher wavenumbers (2187 cm^{-1} at 340 K and 2190 cm^{-1} at 378 K).

Fig. 41 gives, for the 10% CO/He mixture, the evolution with T_a of the IR band of the L_{Zr} species formed on the PdZrO_2 solid. The increase in T_a leads to the decrease in the intensity of the IR band as observed on the pure ZrO_2 , alongside a slight shift to higher wavenumbers.

Fig. 42 shows, in the $2100\text{--}1900\text{ cm}^{-1}$ range, the FT-IR spectra recorded on the Pt/ZrO_2 solid in the course of the CO adsorption (1% CO/He) at various adsorption temperatures. The IR band at 2068 cm^{-1} after adsorption at 300 K (Fig. 42(a)) is similar to that observed at 2073 cm^{-1} on a 2.9% $\text{Pt/Al}_2\text{O}_3$ solids and corresponds to the linear CO species on Pt sites (denoted by L_{Pt}). The increase in T_a leads to an increase in the IR band intensity for $T_a < 500\text{ K}$ (spectra b and

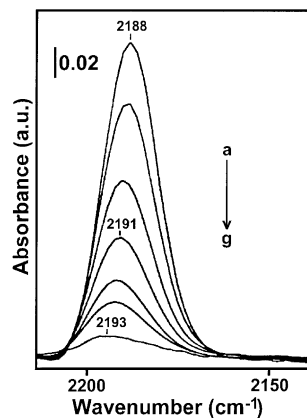


Fig. 41. Evolution of the IR band of the L_{Zr} species adsorbed on Pt/ZrO_2 with adsorption temperatures (10% CO/He): (a) 300 K; (b) 313 K; (c) 320 K; (d) 329 K; (e) 340 K; (f) 358 K; (g) 378 K; (h) 413 K [491].

c in Fig. 42) associated to a shift to lower wavenumbers (2064 cm^{-1} at 403 K and 2058 cm^{-1} at 503 K). This has been also observed on various Pt containing solids and some studies report similar observations. The authors have suggested that this was due to a reconstruction of the CO/Pt particles system in the course of the adsorption at high temperatures. The intensity of the IR band remains constant during cooling down of the sample in 1% CO/He from $T_a = 503$ to 373 K and this indicates that the modification

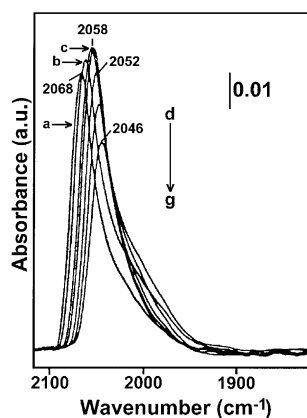


Fig. 42. Evolution of the IR band of the L_{Pt} species adsorbed on Pt/ZrO_2 with adsorption temperatures (1% CO/He): (a) 300 K; (b) 403 K; (c) 503 K; (d) 573 K; (e) 645 K; (f) 698 K; (g) 738 K [491].

of the surface is irreversible. For $T_a > 500$ K, the intensity of the IR band progressively decreases associated to a shift to lower wavenumbers (2055 cm^{-1} at 573 K, 2052 cm^{-1} at 645 K, 2049 cm^{-1} at 698 K, and 2046 cm^{-1} at 738 K) [491].

Pt–Sn/ Al_2O_3 catalysts have been studied by CO chemisorption and FT-IR of adsorbed CO after each cycle in a series of six oxychlorination–reduction cycles or six oxidation–reduction cycles followed by oxychlorination–reduction [492].

Dulaurent et al. [493] have studied the heat of adsorption of CO on a Pd/ Al_2O_3 using in situ IR at high temperatures (300–800 K). Two main IR bands were detected above and below 2000 cm^{-1} , ascribed to linear and bridged adsorbed CO species on Pd atoms, respectively. The change in IR band intensities with adsorption temperature was used to determine the evolution in the coverage θ of the various adsorbed species with this parameter.

CO species adsorbed on the surface of oxidised bimetallic Rh–Pd catalysts, prepared by coimpregnation and sequential impregnation methods, were analysed in situ by IR spectroscopy, during the reaction of CO with O_2 in an oxidising atmosphere [494]. The results show that the two methods of impregnation lead to the existence of oxidised Rh on the surface of the bimetallic catalyst, however, in the case of the sequential impregnation method, the Pd surface is more reduced than in the case of catalysts prepared by coimpregnation.

Lin et al. [495] have studied catalysis of CO electro-oxidation at Pt, Ru, and PtRu alloy. IR spectroscopy data indicate that the surface structure of the CO adlayer strongly differs for Pt, PtRu, and Ru. The pure metals present a relatively compact adlayer structure while the alloy exhibit a loose CO_{ad} structure thus offering the best distribution of $\text{CO}_{\text{ad}}/\text{OH}_{\text{ad}}$ reactive pairs.

The adsorption of CO on a Pt/Rh/ $\text{CeO}_2/\text{Al}_2\text{O}_3$ three-way catalyst was studied in the temperature range 300–800 K by FT-IR spectroscopy using a suitable IR cell of small volume [496]. The quantitative treatment of the spectra leads to the determination of the evolution of the coverage of the adsorbed species with the temperature. The main adsorbed species is the linear CO form characterised by an IR band at 2063 cm^{-1} , probably formed on platinum atoms.

Ruthenium catalysts exhibit high-specific activity in CO hydrogenation to CH_4 and long-chain hydrocarbons. Todorova and Kadinov [497] have studied CO and H_2 interaction on Ru/ Al_2O_3 catalyst. They have observed that the multicarbonyl species on isolated Ru atoms or clusters in Ru/ Al_2O_3 catalysts exhibits the highest thermal stability and the lowest reactivity to hydrogen. The CO species single bonded to reduced ruthenium atoms on the surface of metal particles exhibits the highest reactivity to hydrogen. CO hydrogenation on Ru/ Al_2O_3 catalysts could also proceed with the formation of oxygen-containing intermediates (formyl groups) [497].

Tripathi et al. [498] have conducted adsorption and reaction studies of CO, O_2 , and $\text{CO} + \text{O}_2$ over Au/ Fe_2O_3 , Fe_2O_3 , and polycrystalline gold catalysts.

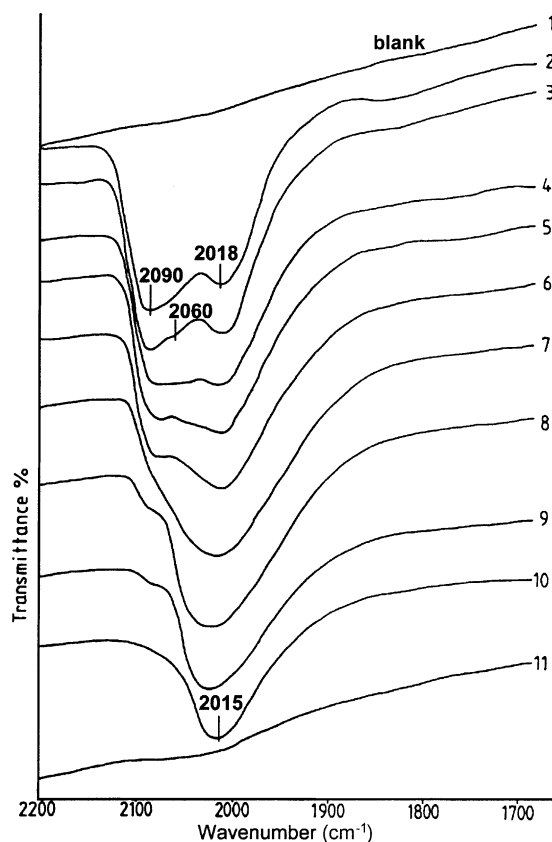


Fig. 43. IR spectra of 5% Ir/ Al_2O_3 observed at RT following 10 Torr CO adsorption (1) at 300 K for 15 min (2) and evacuation at 298 K (3), 373 K (4), 423 K (5) 473 K (6), 533 K (7) 573 K (8), 623 K (9), 673 K (10), and 723 K (11) for 15 min [499].

The results demonstrate that the oxidation of CO on both Fe_2O_3 and $\text{Au/Fe}_2\text{O}_3$ occur by means of similar redox mechanisms involving the removal and replenishment of lattice oxygen, where the presence of gold promotes these processes. The FT-IR data reveal that gold facilitates the chemisorption of CO on $\text{Au/Fe}_2\text{O}_3$, leading predominantly to the formation of $\text{Au}^0\text{-CO}$ species. The carbonate-like species, formed on both Fe_2O_3 and $\text{Au/Fe}_2\text{O}_3$ during the adsorption of CO or $\text{CO} + \text{O}_2$, are stable below 375 K and are regarded to be mere by-products that do not play a major role in the CO oxidation process, particularly at low-reaction temperatures (<400 K).

The adsorption of CO, the interaction and the reaction of CO and water have been investigated over supported Ir catalysts [499]. The dominant spectral features for $\text{Ir/Al}_2\text{O}_3$ at 298 K are the bands at 2090, 2060, and 2018 cm^{-1} but on Ir/TiO_2 , Ir/SiO_2 , and Ir/MgO only a band at $2060\text{--}2075\text{ cm}^{-1}$ was detected (Figs. 43 and 44). The IR spectra of the adsorbed CO in the presence of water differed from that observed during the adsorption of CO; the band due to linearly bonded CO was shifted to lower wavenumbers.

Catalytic hydrogenation of CO and CO_2 was studied over copper/zirconia and silver-promoted copper/zirconia catalysts [500]. Vibrational spectroscopy was used to obtain information on the reaction mechanism leading to methanol by in situ identification of the adsorbed species and intermediates in the pressure range from 0.3 to 2.5 MPa.

The interaction of carbon monoxide and hydrogen with $\text{Fe/Al}_2\text{O}_3$ catalyst during Fischer–Tropsch synthesis has been studied at temperatures ranging from 300 to 523 K and at a pressure of 103 kPa [501]. The formation of hydrocarbons is evident from the well-developed absorption bands in the $3000\text{--}2800\text{ cm}^{-1}$ range, due to stretching vibrations of CH_2 and CH_3 groups. Assignment of the various absorption bands in the $1700\text{--}1200\text{ cm}^{-1}$ wavenumber range is speculative, due to (partial) coincidence of the bands and the gradual change in chemical composition of the catalyst particles. Interaction of the reduced iron catalysts with ethylene or methane at 523 K gives rise to absorption bands at 1555, 1345, and 1050 cm^{-1} , which are assigned to CH_x -adsorbed species [501].

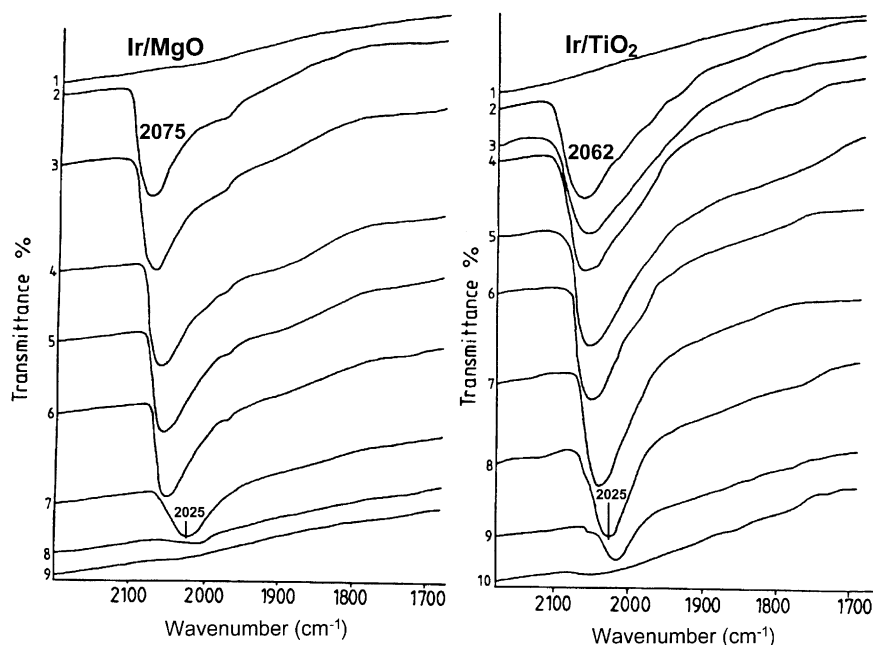


Fig. 44. IR spectra of 5% Ir-supported magnesia and titania observed at RT following 10 Torr CO adsorption (1) at 300 K for 15 min and evacuation at 298 K (2), 373 K (3), 473 K (4), 523 K (5), 573 K (6), 623 K (7), 673 K (8), 723 K (9), and 773 K (10) for 15 min [499].

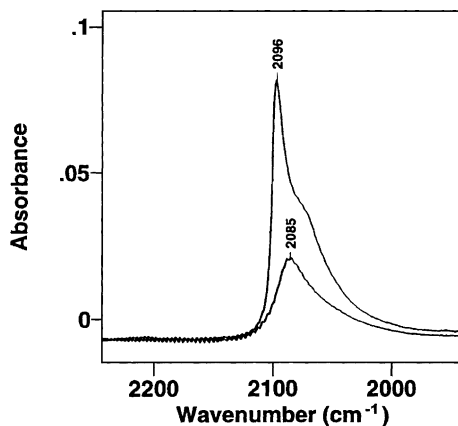


Fig. 45. IR spectra of CO adsorbed at RT on 1% Cu/ZnO (lower spectrum), and 5% Cu/ZnO (upper spectrum) [502].

IR studies of CO adsorption have been used to elucidate the surface structure of Cu/ZnO methanol synthesis catalysts [502].

Fig. 45 shows the IR spectra of CO adsorbed at RT after reduction at 493 K on 1% Cu/ZnO and 5% Cu/ZnO, respectively. Mainly one CO band at 2085 cm^{-1} is seen on the 1% Cu/ZnO, whereas a band at 2096 cm^{-1} with a lower frequency shoulder at around 2080 cm^{-1} is seen for the 5% Cu/ZnO. In both cases, the absorption bands are readily removed upon brief evacuation at RT signifying weakly adsorbed CO.

The results for the 1% Cu/ZnO (Fig. 46) clearly show a progressive intensity decrease with increasing

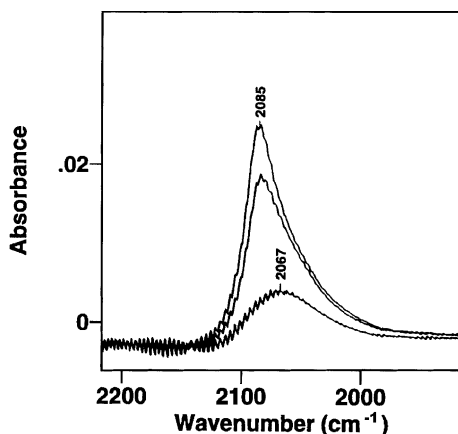


Fig. 46. IR spectra of CO adsorbed at RT on 1% Cu/ZnO after reduction treatment at 493 K (top), 533 K (middle), and 573 K (bottom) [502].

reduction temperature. Beside changes in the intensity, the band position is seen to shift downwards from 2085 to 2083 cm^{-1} and subsequently to 2067 cm^{-1} as the reduction temperature was raised from 493 to 533 K and to 573 K.

The variations in CO band frequencies observed for the different Cu/ZnO catalysts indicate that the surface composition or surface structure of the Cu particles may vary depending on the Cu loading and the reduction conditions. Thus, the band may contain contributions from several CO bands as, for example, seen in the results for the high loading Cu/ZnO (Fig. 45) catalyst as well as in the spectral changes observed upon increasing the reduction temperature (Fig. 46). Shifts in CO band frequencies have often been related to changes in exposed Cu surface planes [502].

Rasko [503] has studied the photoinduced dissociation of CO_2 on titania-supported noble metals. The photoinduced dissociation of CO_2 resulting in adsorbed CO occurred on Pt, Rh, and Ir titania-supported catalysts at 190 K far below the temperature, at which the thermal CO_2 dissociation was observed. The extent of this process depends on the nature of the noble metals and the supports. The oxygen vacancy of the support, the electronic interaction between noble metals and titania, and the extended electron transfer originating from the photoexcitation of titania play decisive role in the dissociation of adsorbed CO_2 .

The effect of metal loading on CO_2 hydrogenation reactivity over Rh/SiO₂ catalysts was studied [504]. The main product transformed from CO to CH₄ with the loading amount of Rh, retaining similar total activity. For 1 wt.% Rh/SiO₂ catalyst, the concentration of surface Rh particles was low, so Rh species were surrounded by hydroxyl groups of SiO₂. CO-saturated Rh species reacted with surface hydroxyl groups to form relatively fine Rh carbonyl clusters, and adsorbed CO was not subjected to further hydrogenation, resulting in desorption as molecular CO. On the other hand, from the results of H₂ chemisorption, 10 wt.% Rh/SiO₂ had about 5.8 times more surface coverage of Rh species than 1 wt.% Rh/SiO₂, accordingly less surface hydroxyl groups of SiO₂ existed around Rh particles. Therefore, once a CO domain was formed on the surface, Rh carbonyl species could not be liberated from a large particle to form Rh carbonyl clusters (Fig. 47).

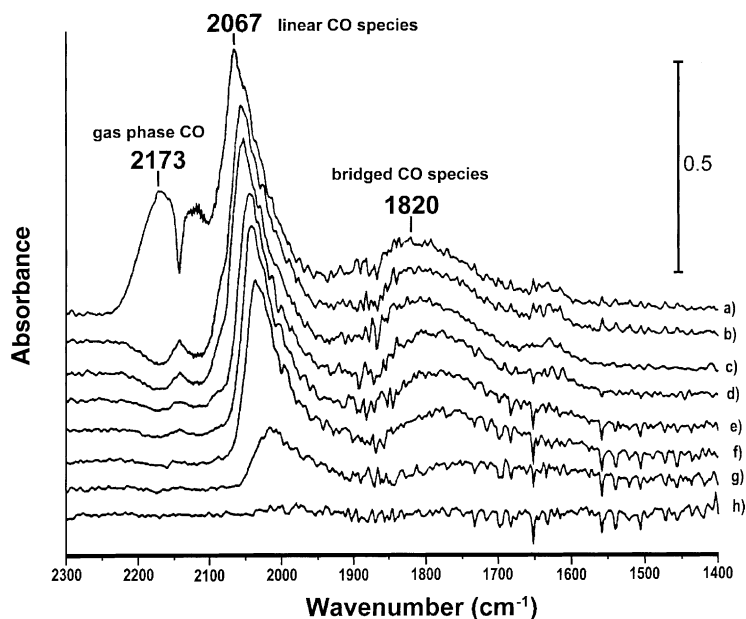


Fig. 47. In situ FT-IR spectra of hydrogenation of adsorbed CO derivatives on the 1 wt.% Rh/SiO₂ catalyst: (a) CO adsorption, 303 K; (b) hydrogenation, 303 K, 0 h; (c) 303 K, 0.1 h; (d) 373 K; (e) 423 K; (f) 473 K; (g) 533 K; (h) 573 K [504].

Adsorption of carbon dioxide over nickel–magnesia solid solution catalysts applied in CO₂ reforming of CH₄ has been studied [505]. Carbon dioxide reforming of methane over Ni–Ru and Ni–Pd bimetallic catalysts has been studied by Crisafulli et al. [506]. On the basis of FT-IR spectra of adsorbed CO, H₂ chemisorption, and TPR measurements, it has been proposed that the different behaviour of the Ni-based bimetallic catalysts can be related to different metal–metal interactions occurring on the catalysts. In particular, the strong improvement in the activity and stability observed in the case of ex-nitrate Ni–Ru catalysts has been attributed to an enrichment of the catalyst surface in nickel due to the formation of Ni–Ru clusters with the surface mainly covered by Ni. This leads to an increase in the metallic dispersion of Ni and favours the formation of more reactive intermediate carbonaceous species.

Carbon dioxide adsorption on Li/MgO and Sn–Li/MgO catalyst applied in the oxidative coupling of methane was investigated [507]. The oxidative adsorption of SO₂ on ceria has been studied using gravimetry and IR spectroscopy [508]. SO₂ oxidation gives rise to two main types of sulphates; surface- and bulk-like species. The former are characterised by IR

bands in the 1400–1340 cm⁻¹ range while the latter lead to a very broad band near 1200 cm⁻¹. Their relative amount depends on the sample surface area and the total sulphate amount formed. It is also found that oxidation of SO₂ adsorbed species into sulphate can occur without O₂ addition.

Sulphate species formed by heating SO₂ in excess of O₂ at 723 K on TiO₂, ZrO₂, Al₂O₃, and Al₂O₃ promoted by Fe, Cu, Ni, Mo, W, or V were studied by FT-IR spectroscopy [509]. The presence of Ni, Cu or Fe enhances sulphate formation on the Al₂O₃ support.

The effect of sulphur on the deactivation of palladium catalysts for methane oxidation has been investigated [510]. A PdO deactivation mechanism due to sulphur was proposed over the 373–673 K range. H₂S-induced catalyst poisoning of PdO/γ-Al₂O₃ is attributed to the formation of aluminium sulphate. Surface sulphite and sulphate groups were observed by FT-IR on poisoned catalysts.

Studies conducted by low wavenumber IR spectroscopy (750–450 cm⁻¹) can provide useful information on the interaction between H₂S and SO₂ on a Claus catalyst [511]. The spectral assignments have been proposed taking into account the spectra of

different $S_xO_y^{n-1}$ salts in solution or as solids. Some spectra of these ions have been revised ($Na_2S_2O_4$) or recorded for the first time ($Na_2S_3O_6$). The adsorption of SO_2 leads mainly to disulphite (bands at 657 and 560 cm^{-1}) and sulphite (635 and 495 cm^{-1}) species. The adsorption of H_2S alone produced $NaSH$ species. SO_2 reacted with chemisorbed H_2S to yield a stable thiosulphate species (680 cm^{-1}).

Studies conducted by Laperdrix et al. [512] were devoted to the comparison between the activity of γ -alumina and titania (anatase) toward CS_2 hydrolysis. It was shown that, without any other sulphur compound, like H_2S and SO_2 , and without O_2 traces in the feed, alumina is more active than titania at 593 K. The IR study of CS_2 adsorption on alumina evidenced the participation of the most basic OH groups and the formation of hydrogen thiocarbonate and hydrogen carbonate species, providing some information on the nature of the active sites and the reaction mechanism. Chemisorbed COS appeared as a reaction intermediate. Realistic industrial Claus conditions imply, in addition to CS_2 and H_2O , the presence of H_2S , SO_2 , and O_2 traces in the feed. It appears that the presence of O_2 traces in the CS_2 - H_2O mixture brings about a decrease in activity of the alumina and titania. This is due to sulphate formation as shown by the IR analysis of the catalysts after the reaction. Moreover, IR evidence shows that sulphate species are reduced by H_2S at 593 K on TiO_2 , contrary to results obtained on Al_2O_3 , explaining why TiO_2 is much more effective than Al_2O_3 when the $CS_2 + H_2O$ feed also contains H_2S and O_2 traces [512].

It is well known that the problem of H_2S utilisation and processing is one of the most urgent tasks in the creation of environmentally safe processes in gas and oil extracting and processing. The investigation of the reaction of direct oxidation of H_2S over different catalysts ($Fe_2O_3/\gamma-Al_2O_3$, $MgCr_2O_4/\gamma-Al_2O_3$, $TiO_2-SiO_2-Al_2O_3$, and $\gamma-Al_2O_3$) was studied [513]. It has been shown using IR spectroscopy that H_2S adsorption is dissociative at RT on the titania-silica-alumina catalyst and at 373 K on magnesium-chromium and iron oxide catalysts. Further increase of the temperature leads to an interaction between H_2S and surface oxygen to form sulphur and surface adsorbed SO_2 . Adsorption of intermediates and the reaction products formed take place on the Lewis acidic centres of all studied catalysts [513].

The deactivation of catalysts by coke deposition invariably takes place in many industrial processes. Operating conditions and type of catalyst have a marked influence upon the characteristics of coke deposits [514–516]. Knowledge of the coke structure and of mechanisms of its deposition is required in order to prevent its formation and to design strategies for the regeneration of the catalyst.

Sarbak [517] has studied the effect of Cr, Mo, and W on carbon deposition on Pt/Al_2O_3 catalysts. The results show that ethylene deposition on low-loaded samples yield two strong bands with maxima near 1580 and 1460 cm^{-1} in the FT-IR spectra. These bands, identical to those observed for chemisorbed acetic acid were assigned to the asymmetric and symmetric stretching vibrations of C–O bonds in carboxylate structure. Moreover, for a sample of Pt with 2 wt.% Mo/Al_2O_3 , the bands assigned to the conventional coke were also observed. For high-loaded samples, the bands attributed to carboxylate were only observed for $Pt-Cr/Al_2O_3$. However, the FT-IR spectra of all samples from this series showed bands assigned to alkyl naphthalenes and polyphenylenes. It was suggested that in low-loaded $Pt-Me/Al_2O_3$ samples coke has a more carboxylate character whereas for high-loaded samples coke is more aromatic [517].

The process of coke deposition during the dehydrogenation of butene to butadiene over a chromia-alumina catalyst at temperature ranging from 753 to 873 K has been studied by FT-IR [518]. The aromatic C–C stretching region (1630 – 1500 cm^{-1}) and the aliphatic C–H bending region (1450 – 1300 cm^{-1}) in the FT-IR spectra were studied by curve-fitting analysis. The slight modifications produced by the process of coke deposition can be observed in the 1700 – 1300 cm^{-1} range. The expanded spectrum of the fresh catalyst in the 1700 – 1500 cm^{-1} region (Fig. 48) reveals the presence of a strong band at 1634 cm^{-1} attributed to O–H bonds of adsorbed water.

The presence of oxygen-containing structures (C=O) can also be observed by several small bands in the 1750 – 1650 cm^{-1} region. These bands disappear with increasing reaction temperature. At low temperature (753 K), the beginning of the coke deposition on the catalyst produces the appearance of bands in the 1570 – 1520 cm^{-1} region while the band at 1634 cm^{-1} remains unaltered. Small bands at 1750 – 1650 cm^{-1} (C=O structures) can still be observed. At 793 K, the

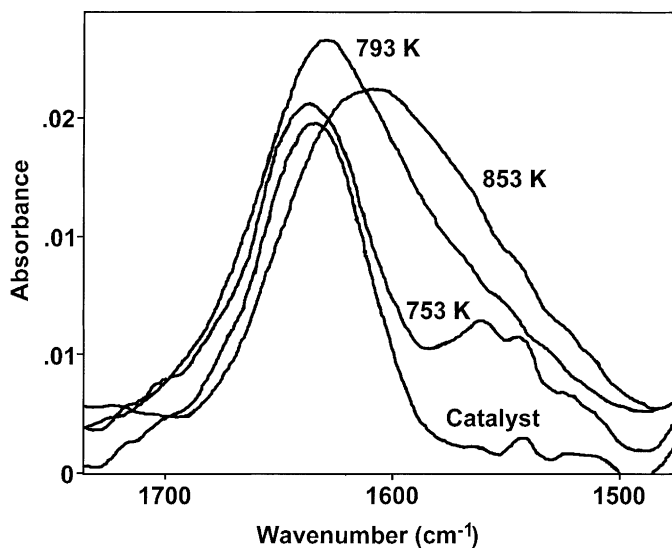


Fig. 48. Expanded FT-IR spectra of the fresh catalyst ($\text{Cr}_2\text{O}_3\text{-Al}_2\text{O}_3$) and the catalyst cooked at different temperature [518].

deposition of coke on the catalysts causes a slight shift of the peak towards 1632 cm^{-1} . The curve-fitting analysis shows a marked increase of this band. The 1632 cm^{-1} band should be assigned to stretching vibrations of double bonds in polyolefinic structures rather than $\text{C}=\text{C}$ bands in aromatic rings. Likewise, a new band at 1590 cm^{-1} can be observed. This band, also named “coke band” can be assigned to $\text{C}=\text{C}$ bands in aromatic and highly conjugated structures. At 853 K, the coke peak has increased markedly, while the 1632 cm^{-1} band has decreased to values very close to the fresh catalyst. These facts should be related to the transformation of olefinic materials into more aromatic structures (aromaticity of the coke increases with increasing reaction temperature).

The time of operation at given temperature may have a significant effect on the characteristics of the coke deposited on the catalyst. The ageing in nitrogen of the coke deposited at high temperatures (853 K) does not seem to produce significant changes in the FT-IR spectrum, even after 180 min at this temperature.

Fig. 49 shows the evolution of the aliphatic structures in the $1450\text{--}1350\text{ cm}^{-1}$ for studied cokes. The band at 1400 cm^{-1} can be ascribed to C-H stretching in $\text{C}-(\text{CH})_2$ or $\text{C}-(\text{CH})_3$ groups. This band achieves a maximum at 793 K and then decreases with increasing

temperature and ageing time. These facts suggest that the 1400 cm^{-1} band could be related to C-H bands in polyolefinic structures. The 1385 cm^{-1} band assigned to symmetric deformation of methyl groups reflects the changes produced during the process of coke deposition. Thus, this band increases markedly with the process of coke formation and decreases at 853 K when long reaction times are used. These facts suggest that aliphatic CH_3 structures are present in coke deposit probably attached to aromatic structures and that they

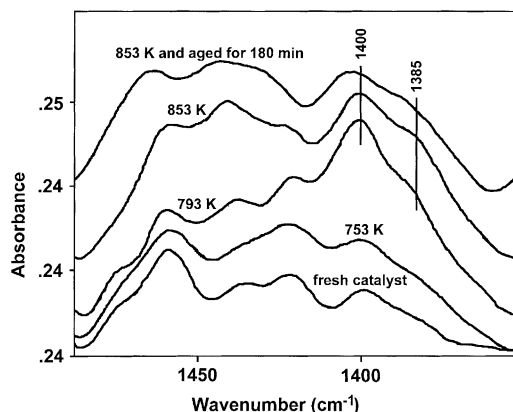


Fig. 49. FT-IR spectra of the fresh catalyst and catalysts cooked at different temperatures [518].

disappear during dehydrogenation process which take place during long ageing times [518].

Wang et al. [519] have studied the decomposition of methane and the subsequent reaction of carbonaceous residues over Rh/Mo/Al₂O₃ catalysts. CH₄ decomposes over these catalysts at 673 K to produce C_xH species and other amorphous carbon species, with the latter primarily responsible for metal site blocking. Hydrogenation of C_xH species (3045 cm⁻¹) releases few metal sites and leads to the formation of long-chain alkyl groups which are retained by the catalyst.

FT-IR has been used for the characterisation of coke formed in C₅/C₆ alkane isomerisation on Pd/H-modernite catalysts [520]. The results obtained confirmed the presence of both aromatic rings and alkyl groups in the insoluble coke sample.

Carbonaceous deposits (coke) formed during the catalytic deep oxidation of benzene over copper and palladium zeolites Y have been analysed [521]. The coke fractions insoluble in methylene chloride consist of polyaromatic compounds with different oxygen contents. The fact that the main constituent 1,4-naphthoquinone and five more identical components are found in the soluble coke fractions of PdY as well as CuY points to a similar reaction mechanism on both catalysts.

The effect of coke formed by conversion of ethylbenzene as well as ethene on the sorption capacity and diffusivity of benzene and ethylbenzene in H-ZSM-5 was investigated [522]. A set of spectra obtained during coke deposition due to ethylbenzene conversion by in situ FT-IR in the C–H deformation vibration range is shown in Fig. 50.

With increasing time on stream (t_c) prominent bands developed, in particular at 1610, 1540, and 1490 cm⁻¹. The band at 1610 cm⁻¹ is the so-called coke band. The band around 1540 cm⁻¹ is ascribed to alkylnaphthalenes or polyphenylene structures, whereas the one at 1490 cm⁻¹ is indicative of $\delta_s(\text{CH}_2)$, $\delta_{\text{as}}(\text{CH}_3)$, =C⁺H, –C⁺H₂ (deformations of primary or secondary carbocations) or to CCC stretching of allylic carbocations. The absorbances of the 1610 and 1490–1510 cm⁻¹ bands can be used as a measure of the amount of coke deposited [522].

Guisnet et al. [523] have studied oxidation of xylene over a 0.2 wt.% Pd/HFAU(17) catalyst. During this reaction a coke formation was observed. The part of

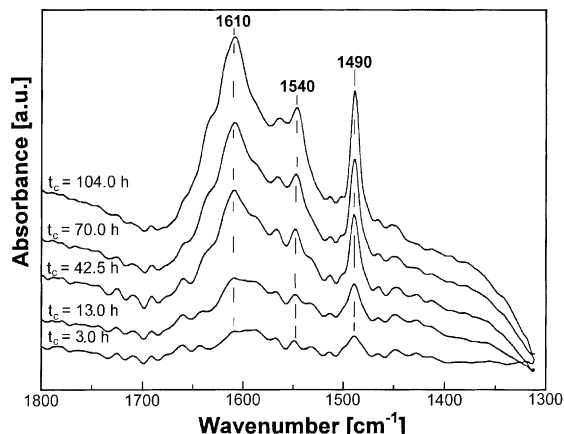


Fig. 50. IR spectra obtained after coking due to ethylbenzene conversion at 575 K over H-ZSM-5 [522].

coke soluble in methylene chloride was characterised by IR, GC, and GC/MS coupling. The IR spectrum of coke formed at 473 K (Fig. 42) shows the presence of bands characteristic of C=O (1665, 1738 cm⁻¹), C–O (1264 cm⁻¹), aromatic C=C (1490, 1600 cm⁻¹), and OH (3611 cm⁻¹) groups (see Fig. 51). GC analysis shows that soluble coke is a complex mixture.

Carqueira et al. [524] have studied the influence of coke deposits on activity, acidity, and porosity of USHY zeolite during *m*-xylene transformation in the temperature range 523–723 K. At both temperatures, *m*-xylene undergoes two main reactions; isomerisation into *o*- and *p*-xylenes and disproportionation into toluene and trimethylbenzenes. In addition, at 723 K, C₂–C₄ alkenes are also found at high concentrations. Whatever the temperature and the contact time, a rapid deactivation of the catalysts is observed. However, the conversion on the fresh catalyst can be estimated by carrying out various analyses at short time-on-stream (TOS) values. For both temperatures, the composition of coke was determined by dissolving the zeolite in hydrofluoric acid solution and recovering the coke molecules in two parts; one soluble in methylene chloride and the other insoluble, hence constituted of highly polyaromatic compounds. Practically no coke can be recovered through a simple soxhlet treatment of the coked zeolite samples; hence coke was essentially located within the pores. The integrated absorbance of the bands in the 1655–1530 cm⁻¹ region is proportional to the percentage of coke deposited

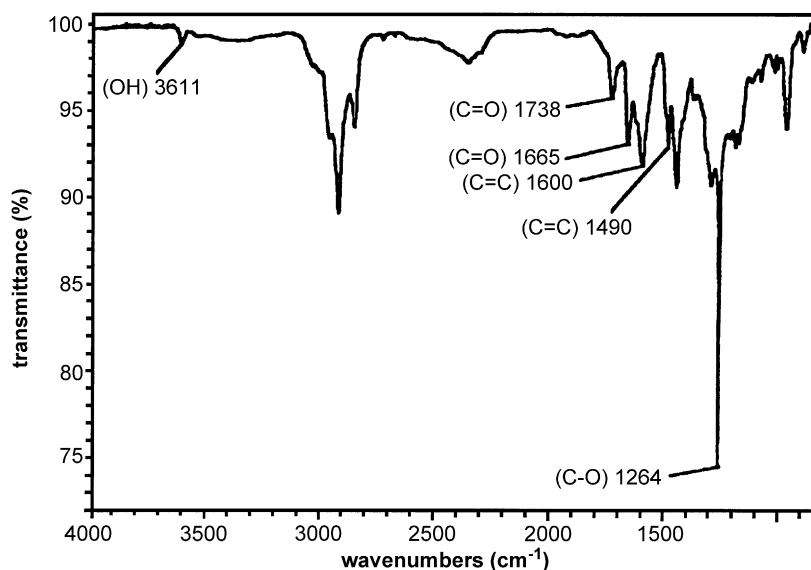


Fig. 51. IR spectrum of the “coke” retained at 473 K on 0.2 wt.% Pd/HFAU(17) during *o*-xylene oxidation [523].

on the zeolite. The quantitative distributions of coke molecules were estimated by GC [524]. IR spectroscopy confirms that the coke formed at 723 K is more polyaromatic than the coke formed at 523 K.

Adsorption of N_2 on NaY zeolites at 85 K and equilibrium pressures higher than 1 kPa results in the formation of geminal dinitrogen complexes characterised by an IR band at 2333.5 cm^{-1} [525]. With decreasing equilibrium pressure, the complexes tend to lose one N_2 ligand, thus forming linear species characterised by an IR band at 2336.8 cm^{-1} . All species disappear completely after evacuation. Co-adsorption of N_2 and CO revealed that the dinitrogen complexes are formed on Na^+ cations.

Kazansky et al. [526] have studied the nature of the sites of dissociative adsorption of dihydrogen and light paraffins in Zn-HZSM-5 zeolite. The use of the low-temperature adsorption of dihydrogen as a probe indicated the appearance, after high-temperature vacuum pre-treatment, of three different Lewis acid sites connected with coordinatively unsaturated Zn^{2+} ions. The strongest Lewis sites, with an H–H stretching frequency of adsorbed molecular hydrogen of 3940 cm^{-1} , dissociatively adsorbed hydrogen, methane, and propane at both room and elevated temperatures. These sites are represented either by Zn^{2+}

ions on the walls of the main channels of the zeolite or by Lewis base pairs on the surface of nanometric clusters of zinc oxide.

CO and N_2 adsorbed, at nominally liquid-nitrogen temperature, on Mg^{2+} exchanged ETS-10 molecular sieve were found to form $Mg^{2+} \cdots CO$ and $Mg^{2+} \cdots N_2$ adducts involving cations located in the main channels (12-membered rings) of the ETS-10 [527]. These adducts gave main IR absorption bands at 2190 and 2203 cm^{-1} for CO, and at 2336 and 2339 cm^{-1} for N_2 , which were assigned to the fundamental stretching mode of the diatomic molecules polarised by the electric field created by Mg^{2+} ions. Corresponding adducts with Na^+ and K^+ ions, not exchanged with Mg^{2+} , were also present.

Konduru and Chuang [528] have carried out transient IR studies of active and spectator adsorbates during NO decomposition over Cu-ZSM-5. Silanol groups existing on the outer surfaces of zeolites, whose OH stretching band appears at the same frequency as that of silanol groups on amorphous silica, are recognised as neutral or very weakly acidic [529]. The acid property of silanol groups on zeolites has been estimated by the adsorption of probe molecules. The IR spectra of ferrierite before and after CO adsorption are shown in Fig. 52(a) and (b), respectively.

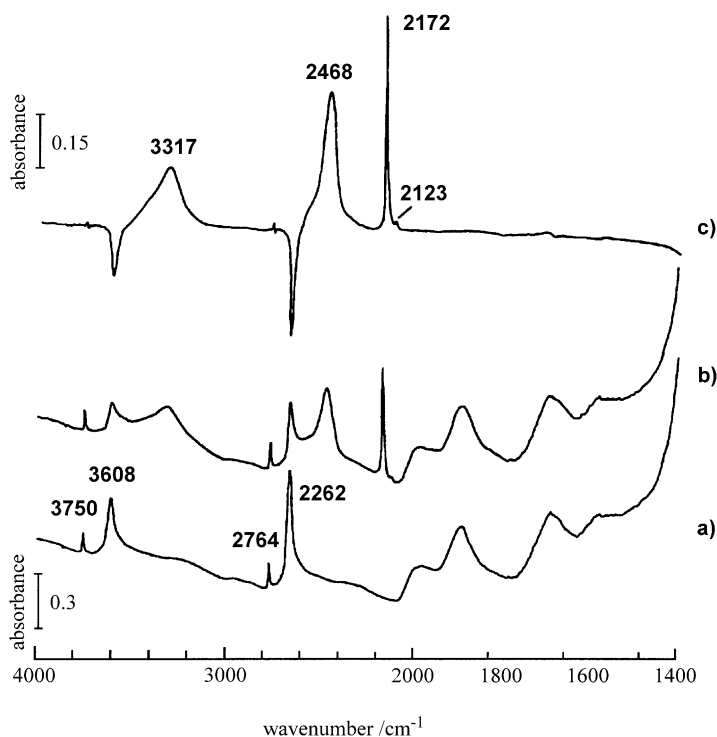


Fig. 52. IR spectra of ferrierite: (a) before and (b) after adsorption of CO. Spectrum (c) was obtained by subtracting spectrum (a) from (b) [529].

The external silanol groups and the acidic hydroxy groups were observed at 3750 and 3608 cm^{-1} , respectively, after the pre-treatment. The involvement of the acidic OH groups in CO adsorption was confirmed by the shifts of their bands from the isolated positions to the hydrogen-bonded (3317 and 2468 cm^{-1}) positions. The hydrogen-bonded CO showed a band at 2172 cm^{-1} , while the band at 2123 cm^{-1} is attributed to the physically adsorbed CO. In general, CO adsorbed on to Lewis acid sites of zeolites or strongly cationic sites of oxides is known to show the CO stretching band at a higher frequency than hydrogen-bonded CO. The absence of such a band in Fig. 52(c) indicates that no Lewis acid sites existed on the ferrierite zeolite under the experimental conditions used.

The existence of silanol groups and the absence of acidic OH groups on the external surface of ferrierite were confirmed by pyridine adsorption. In Fig. 53, as-observed spectra before (a) and after (b) probe

adsorption, as well as the difference spectrum (c), are shown.

The band attributed to silanol groups almost disappears, while that due to the acidic OH groups stays unchanged. These are clearly observed in the difference spectrum, where the consumed isolated silanol groups showed a sharp negative band, but the bands of the acidic OH groups shifted slightly (differential peak shape). Since the experiment was conducted at 235 K in order to avoid the thermal diffusion of pyridine into the pores, pyridine molecules adsorbed on silanol groups by hydrogen bonding. Consequently, a broad hydrogen-bonded silanol band was observed around 3000 cm^{-1} , as well as bands due to molecular pyridine in the CH stretching region higher than 3000 cm^{-1} and in the ring-breathing vibration region at 1400–1610 cm^{-1} . The small pore size of ferrierite inhibited the access of large pyridine molecules to the acidic OH groups, and the strong basicity of pyridine resulted in adsorption on the external silanol

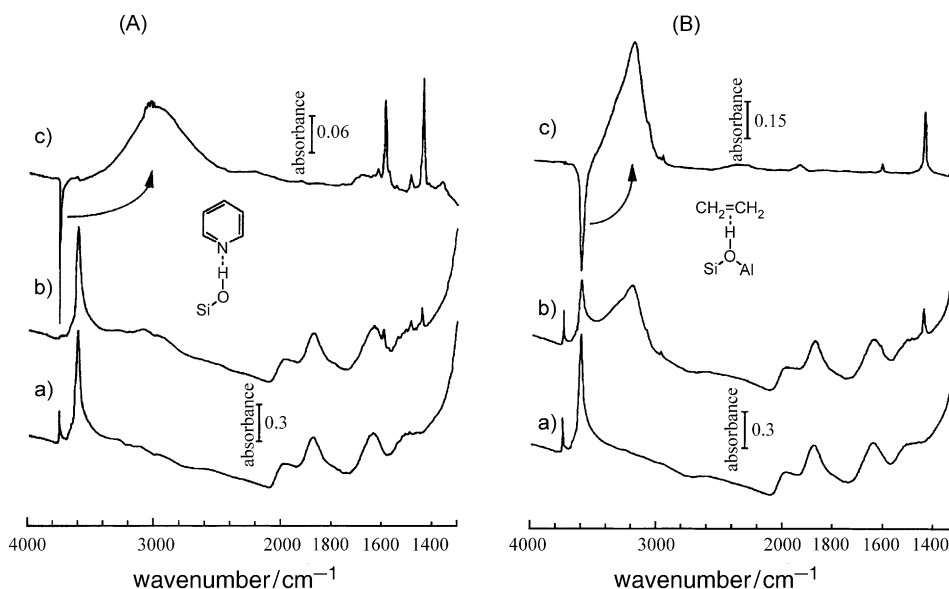


Fig. 53. IR spectra of pyridine (A) and ethene (B) adsorbed on ferrierite at 235 and 221 K, respectively. In both series, spectra (a) and (b) were measured before and after adsorption, respectively, and (c) represents the difference spectrum [529].

groups. Therefore, all the acidic OH groups were assigned to be inside the small pores of ferrierite. When ethene was used as a probe, ethene molecules irreversibly adsorbed exclusively on the acidic OH groups (Fig. 53). Accordingly, it is possible to estimate the numbers of the external silanol groups and the acidic OH groups by using pyridine and ethene adsorption [529].

FT-IR spectroscopy shows that the first step of interaction of pyrrole, furan, and thiophene with H- β and H-ZSM-5 zeolites is the formation of hydrogen bonded species involving the Brønsted acid sites of the zeolite and the π -electron system of the heterocyclic molecule [530].

The effect of chemisorbing water on three catalysts (alumina and HY, USY zeolites) previously evaluated in the acetone condensation reaction has been studied [531]. The active sites in that reaction are Lewis acid sites present either on the surface of alumina or of non-framework alumina in zeolites. These sites are poisoned by water and the reaction rate decreases at the pace of the loss of Lewis sites.

The thermal reactivity behaviour of $\text{Mn}(\text{CO})_5\text{Br}$ on the surfaces of zeolites Y and A has been investigated [532]. Sorption of *para*-, *meta*-, and *ortho*-

diethylbenzene from the gas phase over H-ZSM-5 was studied by means of in situ IR [533].

IR study of on the location of benzene in KL zeolite upon coadsorption of ammonia and methylamine has been carried out [534]. It has been shown that ammonia and methylamine can interact not only with K^+ ions via the lone pair on the nitrogen atoms but also with residual silanols present in KL zeolite after pre-treatment at 723 K. The interaction of KL zeolite with methylamine is found to be much stronger than that with ammonia and is so strong that the lattice parameter of the zeolite is modified, indicating the deformation of the zeolite framework. This deformation of the framework induced by adsorption of methylamine gives a beneficial effect for the location of benzene on 12R windows of KL. The deformation renders the 12R windows of KL zeolite, which are initially not adsorption sites for benzene, favourable for the location of benzene on these sites. This indicates that structural compatibility is the most important key factor in the location of benzene on 12R windows. It shows also that, in some zeolites, both the structural and chemical properties of 12R windows can be accommodated by introduction of a coadsorbate to the location of benzene.

Marturano et al. [535] have used FT-IR for studying preparation procedure of overcharged Fe-ZSM-5 zeolites. The results obtained suggested that overcharged iron zeolites could not be prepared easily by conventional ion exchange in aqueous solution. Moreover, the effectiveness of this method does not seem to depend on the source of the parent ZSM-5 used.

The state of the iron in two different Fe-ZSM-5 samples prepared by sublimation of FeCl₃ was investigated [536]. IR showed that binuclear Fe complexes are located at the ion exchange positions of the zeolite, compensating one or two lattice charges.

In situ FT-IR has been used to observe the species deposited on Co-ZSM-5 during the decomposition of nitromethane [537]. At 553 K deactivation commences after 60 min. This is accompanied by the formation of bands due to NCO species between 2150 and 2300 cm⁻¹ and the sudden development of a very strong band at 1662 cm⁻¹. The latter band can be assigned to the s-triazine compound, melamine, and/or derivatives of it, which cause deactivation by blocking zeolite channels. The most likely chemistry is an initial dehydration of nitromethane to isocyanic acid (HNCO) which forms melamine by reaction with ammonia derived by hydrolysis of HNCO. Cyanuric acid, the cyclic trimer of HNCO, may be an intermediate in the process [537].

Adsorption of CO and NO on Co²⁺ ions dispersed on Al₂O₃, SiO₂, ZSM-5 was studied by means of IR spectroscopy [538]. It was found that Co²⁺ ions exchanged in ZSM-5 zeolite are characterised by a higher coordinative unsaturation than Co²⁺ ions dispersed on Al₂O₃ or SiO₂. As a result CO forms carbonyls on Co-ZSM-5 even at ambient temperature, whereas the Co²⁺-CO complexes on Co/SiO₂ and Co/Al₂O₃ samples are stable at low temperature only. Surface dinitrosyl complexes are formed after NO adsorption on supported Co whatever the support. The Co²⁺(NO)₂ species on Co-ZSM-5, however, are stable up to 623 K, but the nitrosyls formed on Co-supported silica or alumina are easily destroyed by evacuation at ambient temperature [532].

Yoo et al. [539] have characterised properties of Ti-ZSM-5 prepared by chemical vapour deposition. Based on FT-IR results it was concluded that Ti is incorporated in the zeolite surface with tetrahedral coordination (965 cm⁻¹).

Dimeric copper acetate and chloroacetate complexes (CuAc and CuClAc, respectively), were encapsulated in zeolite-Y by the flexible ligand synthesis method [540]. Spectroscopic techniques and thermal analysis provide convincing evidence for the formation of acetato-bridged dimeric copper(II) complexes in the supercages of zeolite-Y. The separation ($\Delta\nu$) between $\nu_{\text{as}}(\text{COO}^-)$ and $\nu_{\text{s}}(\text{COO}^-)$ bands in the FT-IR spectra changes from 182 to 213 cm⁻¹ for CuAc and 185 to 205 cm⁻¹ for CuClAc upon encapsulation and corresponds to the *syn-syn* mode of coordination for the bridging carboxylato groups.

Copper ion-exchanged zeolites ZSM-5 with SiO₂/Al₂O₃ molar ratios 33 and 53 have been subjected to activity tests for direct decomposition of NO [541]. In situ IR measurements were used to follow the reaction, and surface and gas-phase compositions. IR studies were also done in excess oxygen with rapid NO₂ formation in the gas phase. A high level of overexchange of copper in the zeolite in combination with a low concentration of acid sites, concurrent with a high SiO₂/Al₂O₃ ratio, enhances the conversion of NO. A vibrational band at 1631 cm⁻¹ is observed below the light-off temperature and interpreted as a bridged nitrate group bound to Cu²⁺-O-Cu²⁺ dimers. This band disappears above the light-off temperature but the intensity below this temperature correlates with the catalytic activity. The interpretation given was that these bridge bound nitrate groups act as siteblockers on the active sites for NO conversion and that a tentative reaction intermediate, N₂O₃, also binds in a bridge configuration to the same Cu²⁺-O-Cu²⁺ dimers. A second nitrate group with unidentate coordination and vibrational bands at 1598/1575 cm⁻¹ probes isolated copper ions. A third IR band at 2130 cm⁻¹ confirms previous observations of NO²⁺-ions bound to the zeolite. The conclusion was that these species are coordinated to deprotonated and negatively charged sites on the zeolite and that these sites for NO²⁺ adsorption are blocked by Cu²⁺ ion exchange. The 2130 cm⁻¹ species appear to have no role in direct NO decomposition but the adsorption sites are crucial for the stability of the zeolite and intimately related to ion mobility in the lattice [541].

Several Cr exchanged ZSM-5 zeolites of varying SiO₂/Al₂O₃ ratio were prepared and investigated for ambient adsorption and subsequent oxidative destruction (523–673 K) of gaseous trichloroethylene (TCE,

Table 4
Summary of assignments resulted from interaction of 1-butene with H-ferrierite zeolite [545]

Hydrocarbon/species	Wavenumber (cm ⁻¹)
1-butene	1629
2- <i>cis</i> -butene	1643
2- <i>trans</i> -butene	1657
Aliphatic products	2957, 2937, 2863, 1378, 1368
Allyl carbocation	4154, 4084, 1580
Dienyl carbenium ions	1450–1550
Trienyl carbenium ions	1450–1550
Enyl carbenium ions, $n \geq 3$	1450–1550
Neutral di- and triens	1450–1550
Aromatics	3000–3070, 2921, 2865, 1650–1450

Cl₂C=CHCl) in a humid air stream [542]. In order to gain knowledge of physisorption sites for TCE molecules in the ZSM-5 structure, TPD and in situ FT-IR studies, among others, at ambient conditions were carried out. These studies revealed that in almost all studied zeolites TCE interacted with terminal silanol (SiOH) and AlOH groups.

IR detection and distinction of In cations of different oxidation states in zeolites (Y, ZSM-5, mordenite) has been carried out [543]. The catalysts (Pt organometallic complex encapsulated in Y zeolite) utilised in selective dimerisation of ethylene were characterised by FT-IR [544].

The interaction of 1-butene with zeolite H-ferrierite has been studied at increasing temperatures (between 300 and 670 K) with the aim to isolate in situ the species precursors to isobutene and high-temperature coke (Table 4) [545]. The bimolecular mechanism of conversion of butene to isobutene on the fresh catalyst has been confirmed, since low-branched C8 chains are observed. At 300 K, the main products of the interaction are the butene isomers 2-*cis*- and 2-*trans*-butene. At temperatures between 300 and 393 K, the presence of monoenic allylic carbocations is observed, and at temperatures between 473 and 573 K, neutral and carbocationic polyenes are present. At temperatures ≥ 623 K, the polyenyl unsaturated chains cyclise to form mono- and polycyclic aromatics.

The interaction of H-ZSM-5 zeolite with *n*-butane, *iso*-butane, *n*-heptane, 1-butene, *cis*-2-butene, *trans*-2-butene, *iso*-butene, benzene, and toluene in the tem-

perature range 100–773 K has been investigated [546]. Low-temperature experiments allowed characterising hydrogen-bonded species of all adsorbates both with the internal bridging OH of H-ZSM-5 and with the external terminal OH. H-bonds apparently involve C–C σ -type orbitals of alkanes and C=C π -type orbitals of alkenes and aromatics. Evidence was provided for a partial steric hindrance in the interaction of benzene and toluene with the internal OH.

Adsorption and reaction of 2-methylpropene (*iso*-butene) on zeolites (ZSM-5 and faujasite (Y zeolite)), a silica–alumina, and silica were investigated below RT [547]. On silica, isobutene molecules that adsorbed on silanol groups simply desorbed below 230 K in vacuum, while isobutene π -bonded to the acidic OH groups (π -complex) on acid catalysts reacted to dimer alkoxy (2,4,4-trimethylpentoxy) groups. The structure of the reaction product, dimer alkoxy groups, was found to be restricted by the pore size of zeolites. 2,4,4-trimethyl-2-pentoxy species were identified on silica–alumina and Y zeolite similarly to those on mordenite, while the reaction of *iso*-butene resulted in 2,4,4-trimethyl-1-pentoxy species on the acidic OH groups in the pores of ZSM-5. Therefore, the space restriction of the pore size of zeolites on the reaction product was directly observed by the low-temperature IR study [547].

Weyrich and Holderich [548] have studied dehydrogenation of α -limonene over Ce-promoted zeolite-supported palladium catalysts. Pyridine adsorption was used to study change of acidity following ion exchange and catalyst activation. Pure zeolite Na-ZSM-5 did not exhibit any Brønsted acidity as evidenced by the missing pyridine absorption band at around 1545 cm⁻¹. Only a few Lewis acid sites have been observed (1445 cm⁻¹). With the incorporation of Ce into the zeolite (catalyst Ce/Na-ZSM-5), Lewis acidity is strongly increased, as evidenced by the increase of the absorption band at around 1445 cm⁻¹. Only a low Brønsted acidity has been generated, as seen from the small absorption band at around 1545 cm⁻¹. Insertion of Pd (catalyst Pd/Na-ZSM-5) leads to the generation of Brønsted sites, as evidenced to the rise of the absorption band at around 1545 cm⁻¹. No change of Lewis acidity compared with the pure Na-ZSM-5 is observed upon Pd exchange. Ce- and Pd-exchanged catalysts exhibit both Lewis and Brønsted acid sites. Comparison of Brønsted absorption bands of Pd

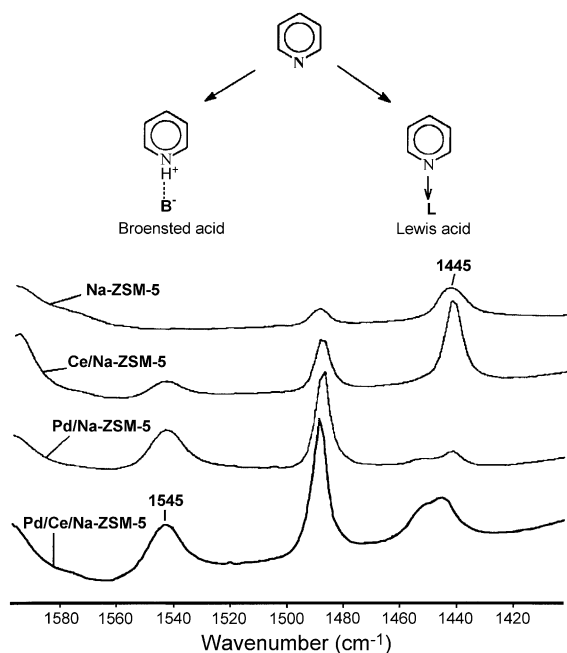


Fig. 54. Pyridine adsorption on different zeolites samples [548].

containing Na-ZSM-5 and Ce and Pd containing Na-ZSM-5 does not exhibit major differences in acid strength (see Fig. 54).

FT-IR study of coked HY zeolite regeneration using O_2 or O_3 has been carried out [549]. It was found that oxygen regeneration occurred at 770 K or above, whereas ozone was effective at 450 K or less.

A study was made of the interconversion of isomeric unsaturated C_4 nitriles over strongly basic Na/NaY, and for comparison on neutral NaY and acidic CaY catalysts at 623 K [550]. FT-IR studies of the adsorbed molecules revealed the possible involvement of anionic intermediates.

The vibrational properties of triflic (CF_3SO_3H) acid and of triflic acid-deuteroacetonitrile (CF_3SO_3H/CD_3CN) adducts adsorbed in silicalite channels are described [551]. The spectroscopic modifications induced on triflic acid by the acid–base interaction are compared with those of the HCl/acetonitrile adducts formed in situ in the silicalite channels, and with those of the H-ZSM-5/acetonitrile and of the H-Nafion/acetonitrile systems. It was concluded that triflic acid in silicalite shows acidity almost comparable to that of H-ZSM-5 and of H-Nafion.

Kowalak et al. [552] have studied the catalytic properties of SmY zeolite modified with trifluoroethanol (TFE). The spectra of adsorbed pyridine indicate almost negligible contribution of the Lewis sites in the parent SmY. The fluorination brings about a noticeable reduction of the protonic acid sites concentration and an increase in contribution of the Lewis acid centres.

Fu et al. [553] have studied copper and titanium substituted mesoporous silicas (Cu-HMS and Ti-HMS) as catalysts for hydroxylation of phenol. FT-IR measurements indicate that the calcined Cu-HMS and Ti-HMS samples all exhibit a weaker absorption band near 960 cm^{-1} which may be rather a fingerprint of the heteroatom on the matrix of $[SiO_4]$ units, whatever its crystallisation state. Zhang et al. [554] have characterised the structure of titanium silicate molecular sieves (TS-1) by means of FT-IR.

In situ IR spectra were recorded during the selective reduction of NO by C_3H_6 , on Al_2O_3 at 573 K, and strong bands due to the adsorbed acetate were observed, accompanying weak bands due to formate and nitrate [555]. The acetate was also formed in $C_3H_6 + O_2$, while nitrate was formed in $NO + O_2$. Characterisation and catalytic properties of CuO– SiO_2 sol–gel catalysts applied for NO reduction were described by Diaz et al. [556]. Holles et al. [557] have studied the influence of Ce and La promoters on the kinetics of NO and N_2O reduction by CO over alumina-supported Pd and Rh. In situ IR spectroscopy showed the presence of isocyanate surface species on Rh/ Al_2O_3 but not on Pd/ Al_2O_3 , which suggested two different reaction mechanisms for the $N_2O + CO$ reaction. No synergistic effect on NO_x reduction was observed for a Pd/Rh bimetallic sample. The effects of NO on the CO-induced structural changes of Rh deposited on SiO_2 , MgO, and TiO_2 were investigated in the temperature range 110–503 K [558]. It was observed that the addition of NO to CO dramatically enhanced the development of *gem*-dicarbonyl, $Rh^I(CO)_2$, from Rh_x-CO species at 233–300 K. This was explained by the formation of a strong bond between NO and Rh_x crystallites which weakens the Rh–Rh bond. It was assumed that the NO and its dissociation product, the adsorbed O, participate in the oxidation of isolated Rh^0 atoms to Rh^I ions. The presence of NO slowed down the conversion of *gem*-dicarbonyl into Rh_x-CO at and above 448 K to

a great extent, indicating that NO retards the reductive agglomeration of Rh^{I} to Rh_x crystallites on these supports.

Synthesis, characterisation, and catalytic activity in the reduction of NO by CO on alumina–zirconia sol–gel derived mixed oxides has been conducted by Moran-Pineda et al. [559]. FT-IR absorption bands assigned to Zr–O–Al bonds (872 and 618 cm^{-1}) were observed in the mixed oxides.

The CO + NO on the Pt/SiO₂ reaction was studied using a new pulse technique [560]. This method allows one to simultaneously follow the surface species and the gas-phase composition evolutions at atmospheric pressure and high temperature with a time resolution of about 1 s. When CO is pulsed in a NO continuous flow on the Pt/SiO₂ catalyst, the NO reduction occurs mainly at the end of the pulse. The N₂ selectivity of the reduction increases with the CO amount in the pulse. The authors show that these results correspond to a NO dissociation mechanism: CO reduces the platinum surface; NO adsorbs and dissociates on reduced Pt sites with recombination into N₂ and N₂O. The NO dissociation itself is a fast step and the N₂ selectivity increases with the availability of dissociation sites [560].

Almusaiteer and Chuang [561] have studied the dynamic behaviour of adsorbed NO and CO under transient conditions on Pd/Al₂O₃. Below the light-off temperature (i.e., 561 K), Pd⁰–NO and Pd⁰–CO are the dominant NO and CO adsorbates. Pd⁰–NO competes favourably over Pd⁰–CO for the same Pd⁰ site when the temperature is increased. Pulse reaction studies at 473 K suggest that Pd⁰–NO dissociates to form adsorbed nitrogen and adsorbed oxygen. Adsorbed oxygen further reacts with Pd⁰–CO to produce CO₂. Dynamic behaviour of adsorbed NO and CO as well as gaseous products suggests that removal of adsorbed oxygen from the Pd surface to produce CO₂ is the rate-limiting step. Prolonged exposure of the catalyst to the NO flow at 473 K results in oxidation of Pd⁰ to Pd⁺ and produces Pd–NO⁺; the presence of gaseous CO reduces Pd⁺ to Pd⁰ and increases the surface coverage of Pd⁰–NO. Above the light-off temperature, Pd–NO⁺, Al–NCO, nitrate, and carbonate are the dominant adsorbates. The presence of Pd–NO⁺ indicates that the process of oxidation of Pd⁰ to Pd⁺ by NO is faster than that of the reduction of Pd⁺ to Pd⁰ by CO. All the gaseous reaction products are produced on Pd⁰ sites.

Exposure of Rh⁺(CO)₂ on Rh/Al₂O₃ to NO causes CO desorption and adsorption of NO as Rh–NO⁺ [562]. Exposure of Rh⁺(CO)₂ to NO/H₂ produced N₂O at 573 K. The presence of both reductant (i.e., CO) and oxidant (i.e., NO or O₂) in the reactant pulse is needed to initiate and sustain the NO–CO redox reaction cycle for CO₂ formation.

The effect of oxygen on the nature, population, and reactivity of surface species formed during reduction of NO by CO over Rh/TiO₂ catalysts has been examined employing FT-IR and transient MS techniques [563]. It has been found that the activity of Rh is hindered by accumulation of surface oxygen originating from NO decomposition and gas-phase oxygen in the feed. Adsorbed CO and reduced TiO_{2–x} species in the vicinity of Rh particles act as oxygen atom scavengers and, under fuel-rich conditions, remove atomic oxygen from the surface and restore the catalytic properties. Results from the present study provide additional evidence that production of N₂ is related to dissociation of adsorbed Rh–NO[–] while production of N₂O is related to the presence of Rh(NO)₂. The presence of reduced Rh⁰ sites is necessary for the formation of both reduction products. In the absence of oxygen in the feed, surface isocyanate species are also observed under reaction conditions. Their formation requires the presence of adjacent Rh⁰–CO and reduced Rh⁰ sites. Although these species are favoured under conditions in which NO conversion to reduction products is observed, there is no evidence that they are catalytically active species.

The formation, stability, and reactivity of surface isocyanate species with CO, NO, and O₂ has been examined over Rh/TiO₂(W⁶⁺) catalysts, under conditions of NO reduction by CO, using FT-IR and transient MS techniques [564]. It has been found that W⁶⁺ doping of TiO₂ results in stabilisation of the Rh–NCO species and in the expansion of the temperature window of N₂O formation toward lower temperatures. Surface isocyanates react with NO to yield gas-phase N₂O, thus providing an alternative route for the production of nitrous oxide:



A novel experimental approach, which couples in situ IR with selective enhancement and poisoning, has been developed to identify the active adsorbate for the NO–CO reaction on Pd/Al₂O₃ [565]. In situ IR stud-

ies of the steady-state NO–CO reaction show that NO adsorbs as $\text{Pd-N}\equiv\text{O}^{\delta+}$, $\text{Pd-N}=\text{O}$, and $\text{Pd-N}=\text{O}^{\delta-}$. CO adsorbs as $\text{Pd-C}\equiv\text{O}$ and $\text{Pd}_2\text{C}=\text{O}$. Addition of H_2 to the NO–CO flow as a reaction enhancer, which reacts with adsorbed nitrogen and oxygen, results in depletion of $\text{Pd-N}=\text{O}$, while addition of O_2 to the NO–CO flow as a reaction poison leads to accumulation of $\text{Pd-N}=\text{O}$ on the Pd surface. These observations suggest that $\text{Pd-N}=\text{O}$ is the active adsorbate involved in NO dissociation. The observed variation in the concentrations of CO_2 and $\text{Pd-C}\equiv\text{O}$ suggests that $\text{Pd-C}\equiv\text{O}$ is the active adsorbate leading to CO_2 .

Adsorption of nitric oxide and carbon monoxide and the Co-adsorption of $(\text{NO} + \text{CO})$ and $(\text{CO} + \text{NO})$ over the transition metal-exchanged SAPO-34 have been studied by IR spectroscopy [566]. Detailed FT-IR studies were carried out on the disproportionation reaction of NO and the decomposition of CO over the Mn-, Co-, Cu-SAPO-34 catalysts. The IR spectra indicated the formation of various CO/NO species or complexes with active metal species. NO adsorption leads to band formation of at least four metal- NO_x complexes [566].

Gerlach et al. [567] have studied the mechanism of the reaction between NO_2 and propene over acidic modernites. It was shown that nitrosonium ions, which are formed upon reaction of NO_2 with NO over acidic zeolites, are likely to be important intermediates of NO_x reduction over this type of catalyst; they react rapidly with propene, thereby forming acrylonitrile.

Hydrolysis of acrylonitrile yields adsorbed ammonium ions, which are known to reduce NO_x to nitrogen efficiently. Furthermore, the results show that the acid sites of the catalyst are important catalytic centres for the formation of acrylonitrile. The involvement of acid sites appears to shift the mechanism from radical-type processes in the case of gas-phase nitrogen oxide to an electrophilic mechanism involving chemisorbed nitrosonium ions.

Lobree et al. [568] have investigated the interactions of NO, O_2 , and NO_2 with Fe-ZSM-5, as well as the reduction of NO by C_3H_8 in the presence of O_2 . In situ IR observations of NO reduction by C_3H_8 in the presence of Fe-ZSM-5 indicate that adsorbed NO_2/NO_3 species are active intermediates, whereas adsorbed NO is not. NO_2/NO_3 species are formed via the reaction of NO with adsorbed O_2 and by the adsorption of NO_2 formed in the gas phase via homogeneous reaction of NO with O_2 . The reaction of gas-phase C_3H_8 with adsorbed NO_2/NO_3 species results in the formation of a nitrogen-containing deposit. It was proposed that CN or NCO species derived from this deposit act as intermediates and that the oxidation of these species results in the formation of N_2 and CO_2 (Fig. 55).

The role of gaseous NO and C_3H_8 has been studied over low-exchanged Cu-ZSM-5 zeolite with the alternate introduction of NO or C_3H_8 on to the catalyst surface [569]. The rate of the N_2 formation is directly proportional to the content of gaseous NO and the surface coverage with 2-nitrosopropane. There was no

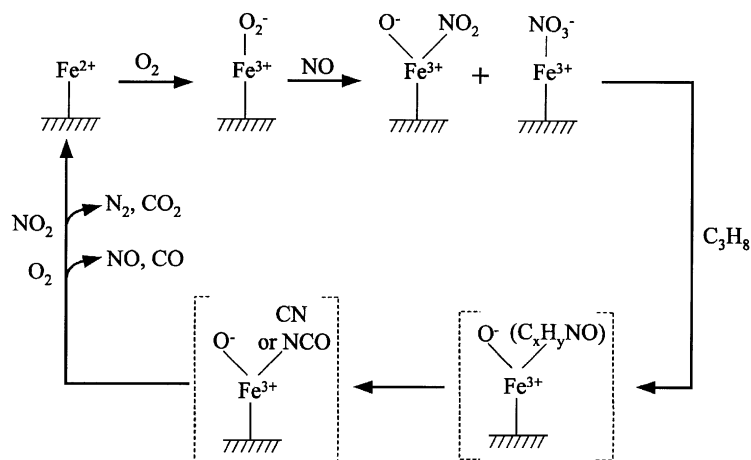


Fig. 55. Proposed mechanism for the reduction of NO by C_3H_8 over Fe-ZSM-5 [568].

formation of N_2 during interaction of gaseous C_3H_8 with NO adsorbates. However, 2-nitrosopropane and its isomer, acetone oxime, were also formed in this reaction.

Wang et al. [570] have studied selective reduction of NO_x with hydrocarbons over MFI-supported cobalt catalysts. Co/MFI catalysts were prepared by various methods, including wet-ion exchange, either as such or in combination with impregnation, solid-state ion exchange, and sublimation of $CoCl_2$ (at 973 K) or $CoBr_2$ (at 873 K) onto H/MFI. The catalysts were tested for the reduction of NO_x with methane or *iso*-butane in excess oxygen. Characterisation by physicochemical methods (including IR) reveals that wet-ion exchange catalyst contains isolated Co^{2+} and $(Co-OH)^+$ ions that are only reducible at 973 K. The N_2 yields of NO_x reduction in excess O_2 over Co/MFI catalysts depend dramatically on the catalyst preparation method and the nature of the reductant. With *iso*- C_4H_{10} and catalysts prepared by sublimation or wet-ion exchange, the N_2 yields are near 100%. With CH_4 the yields over the same catalysts are near 30%. Other preparation methods, such as solid-state ion exchange and impregnation give substantially inferior catalysts [570].

The effect of sulphur on the $C_3H_6-NO-O_2$ and $C_3H_8-NO-O_2$ reactions over Pt/Al_2O_3 was investigated [571]. Ex situ treatment of the catalyst with SO_2 under oxidising conditions results in the formation of sulphate species on the Al_2O_3 but not on the Pt. This results in strong poisoning of the NO_x reduction activity in the $C_3H_8-NO-O_2$ reaction, where NO_x reduction occurs on the Al_2O_3 , but has no effect on the $C_3H_6-NO-O_2$ reaction, where the reaction occurs exclusively on the Pt surface.

An investigation of the interaction of NO and NO_2 with Pd-H-ZSM-5, as well as the reduction of NO by CH_4 , has been conducted using mass spectrometry and in situ IR [572]. Prior to reaction most of the Pd in Pd-H-ZSM-5 is present as Pd^{2+} cations. NO reduction by CH_4 in the absence of O_2 results in the progressive reduction of Pd^{2+} cations above 610 K and the formation of small Pd particles. Reduction of Pd^{2+} cations is significantly suppressed when O_2 is added to the feed of NO and CH_4 . In situ IR reveals the presence of NO^+ and NO as the principal adsorbed species. NO^+ does not react with CH_4 at temperatures up to 773 K. Adsorbed NO reacts with CH_4 above 650 K, and

CN species are observed as intermediates. The latter species reacts with both NO , O_2 , and presumably NO_2 .

NO_x adsorption/desorption capacities of barium aluminates and $BaSnO_3$ were measured under representative exhaust gas mixture at temperatures below 823 K and compared to those of bulk BaO [573]. An N-bounded nitrate, with IR frequencies at 1360 and 1415 cm^{-1} , is formed on barium aluminate and $BaSnO_3$ and not on bulk BaO .

The mechanisms for storing NO_x in platinum–barium–alumina catalysts during lean-rich transients were investigated [574]. Oxidation of NO to NO_2 was found to be an important step. NO_2 was found to be important for oxidation of the catalyst or of nitrites to form nitrates. NO_x is then stored in the form of surface nitrates. FT-IR studies show no formation of bulk nitrates in experiments carried out.

Friedell et al. [575] have presented a systematic investigation of the effect on NO_x storage in a model Pt–Rh/ BaO/Al_2O_3 catalyst of several parameters. Significant amounts of NO_x were found to be stored in the catalysts containing both barium oxide and noble metals. A maximum in NO_x storage was observed at about 653 K. Around this temperature no significant differences between NO and NO_2 with respect to NO_x storage capacity could be observed. A slow increase in the amount of NO_x stored could be observed with increasing oxygen concentration during the lean phase. At about 653 K, the in situ FT-IR spectra showed characteristic nitrate peaks in the region 1300–1400 cm^{-1} when NO_x catalysts were stored under lean conditions, and isocyanate peaks around 2230 cm^{-1} when the catalysts were regenerated under rich conditions, in the presence of hydrocarbons. The reaction step leading to stored NO_x is believed to involve NO_2 and the presence of atomic oxygen. During the rich period, the noble metal surfaces are probably reduced; leading to breakthrough peaks when NO desorbs.

The formation of various species formed during the adsorption of NO_x issued from a synthetic lean-burn exhaust gas upon barium aluminates was studied using FT-IR and TGA [576]. The structure of the nitrates formed upon either BaO or barium aluminate are completely different. On BaO , bridged, unidentate, or free nitrates are formed preferentially whereas upon barium aluminate nitrates have a different structure; although a fraction of free nitrates does exist, the most abundant species is an N-bound nitrate. To

form such a species, barium aluminate must play the role of an Lewis acid.

Hadjivanov et al. [577] have studied the effect of water on the reduction of NO_x with propane on Fe-ZSM-5. Adsorption of NO on Fe-ZSM-5 leads to formation of $\text{Fe}^{n+}\text{-NO}$ ($n = 2$ or 3) species (1880 cm^{-1}), $\text{Fe}^{2+}(\text{NO})_2$ complexes (1920 and 1835 cm^{-1}), and NO^+ (2133 cm^{-1}). Water strongly suppresses the formation of NO^+ and $\text{Fe}^{2+}(\text{NO})_2$ and more slightly the formation of $\text{Fe}^{n+}\text{-NO}$. Introduction of oxygen to NO converts the nitrosyls into surface nitrates (1620 and 1575 cm^{-1}) and this process is almost unaffected by water. The nitrates are thermally stable up to ca. 573 K , but readily interact with propane at 473 K , thus forming a surface C–H–N–O deposit showing bands in the $1700\text{--}1300\text{ cm}^{-1}$ region. Water does not hinder the process. The C–H–N–O deposit is relatively inert (it does not interact with NO or $\text{NO} + \text{O}_2$ at ambient temperature) but, at temperatures higher than 523 K , it is decomposed to NCO^- species (bands at 2215 (Fe–NCO) and 2256 cm^{-1} (Al–NCO)). In the presence of water, however, only the Fe–NCO species are formed. At ambient temperature the NCO^- species are inert towards NO and O_2 , but easily react with a $\text{NO} + \text{O}_2$ mixture. The mechanism of the selective catalytic reduction of nitrogen oxides on Fe-ZSM-5 and the effect of water on the process was discussed too [577].

Strongly bound nitrite–nitrates have been studied as intermediates in the reaction of NO_x selective reduction by hydrocarbons under oxygen excess over cation-exchanged zeolites [578]. Participation of strongly bound nitrates in the rate-limiting-stage of the NO_x selective reduction by propane under oxygen excess, catalysed by Cu- and Co-containing zeolites, was firmly established and a scheme was proposed the reaction mechanism [578].

Copper species present in Cu-ZSM-5 catalysts for NO_x reduction have been identified [579]. FT-IR spectroscopy of CO adsorption has indicated that CuO species are present on the surface of zeolite (2143 cm^{-1}).

The main cause of deterioration for the NO_x storage-reduction catalyst has been shown to be sulphur poisoning [580]. On the basis of the thermogravimetric (TG) and FT-IR analyses of aged catalysts, it was assumed sulphur poisoning of NO_x storage-reduction catalyst consists of two main

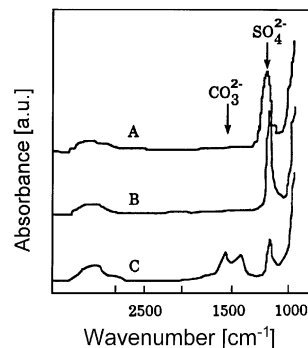


Fig. 56. IR spectra of the catalyst poisoned by sulphur after heat treatment in 25% H_2/He . Catalyst A: Pt/Ba/ $\gamma\text{-Al}_2\text{O}_3$ as poisoned, Catalyst B: after treated catalyst A at 873 K , catalyst C: after treated catalyst A at 973 K [580].

factors. One is that SO_2 in the exhaust gas is oxidised on precious metals and reacts with the support, forming aluminium sulphate; another is that SO_x reacts with the NO_x storage components such as Ba to form BaSO_4 (see Fig. 56).

These consequences lead to the concept that sulphur poisoning should be suppressed by the enhancement of sulphur desorption from the support and BaSO_4 . Using a mixture of TiO_2 and $\gamma\text{-Al}_2\text{O}_3$ as the support, minimised the amount of SO_x deposit on a catalyst after the sulphur-poisoning test. As to $\gamma\text{-Al}_2\text{O}_3$, sulphur desorbed at a lower temperature from the catalyst with lithium-doped $\gamma\text{-Al}_2\text{O}_3$ than the other alkaline or alkali-earth $\gamma\text{-Al}_2\text{O}_3$ after the sulphur-poisoning test. Hydrogen was the most effective gas for enhancing the reduction of BaSO_4 in the aged catalyst, and adding Rh/ZrO₂ with high steam reforming reactivity enhanced hydrogen generation on the catalyst.

FT-IR studies of the deposits formed on Fe/ZSM-5 during SCR of NO_x were carried out [581]. The SCR of nitric oxide NO by propylene over a 0.8 wt.% Pt/ Al_2O_3 catalyst was studied [582]. NO adsorption resulted in the formation of nitrate species associated with the Al_2O_3 support, as well as surface NO species associated with Pt. Similarly, C_3H_6 adsorption resulted in the formation of carboxylate species associated with Al_2O_3 , as well as surface CO associated with Pt. Experiments conducted with the reactive $\text{NO-C}_3\text{H}_6\text{-O}_2$ mixture resulted in the formation of surface –CN and –NCO species.

Rh-exchanged Al-MCM-41 was studied for SCR of NO by C_3H_6 in the presence of excess oxygen [583].

It showed a high activity in converting NO to N₂ and N₂O at low temperatures. In situ FT-IR studies indicate that the Rh–NO⁺ species (1910–1898 cm⁻¹) is formed on the Rh–Al–MCM-41 catalyst in flowing NO/He, NO + O₂/He, and NO + C₃H₆ + O₂/He at 373–623 K. This species is quite active in reacting with propylene and/or propylene adspecies (e.g., π-C₃H₅, polyene, etc.) at 523 K in the presence or absence of oxygen, leading to the formation of the isocyanate species, Rh–NCO (signal at 2174 cm⁻¹), CO, and CO₂. Rh–NCO was also detected under reaction conditions. A possible reaction pathway for reduction of NO by C₃H₆ was proposed. In the SCR reaction, Rh–NO⁺ and propylene adspecies react to generate the Rh–NCO species, then Rh–NCO reacts with O₂, NO, and NO₂ to produce N₂, N₂O, and CO₂. Rh–NO⁺ and Rh–NCO species were two main intermediates for the SCR reaction on Rh–Al–MCM-41 catalyst.

The distribution of gaseous products and the nature of the surface species generated during the SCR of NO with C₃H₆ in the presence of excess O₂ were studied over both a 0.4% Co/γ-Al₂O₃ catalyst and a sulphated 1.2% Ag/γ-Al₂O₃ catalyst [584]. It was shown that the initial step of the C₃H₆-SCR of NO over a 0.4% Co/γ-Al₂O₃ was not the oxidation of NO to NO₂ (Fig. 57). The high concentration of NO₂ observed during the course of the reaction was produced via another route, possibly via the combustion of organo-nitrito compounds. A similar conclusion could be drawn for a sulphated 1.2% Ag/γ-Al₂O₃ material. Over these samples and the parent materials, NO was probably first reacted to form strongly bound inorganic ad-NO_x species such as nitrites and nitrates. It is suggested that the ad-NO_x species reacted with the reductant and derived species to form both organo-nitro and organo-nitrito compounds, the reaction products of which combined to yield N₂. The sulphation of the 1.2% Ag/γ-Al₂O₃ reduced the surface concentration of strongly bound ad-NO_x species, probably by decreasing both the number of adsorption sites available to NO_x and the oxidation activity of the silver promoter. A global C₃H₆-SCR of the NO reaction scheme was proposed, which accounts for the various side products and surface species observed on the different samples [584].

The selective catalytic reduction of NO with propane was studied using metal oxide (Pt, Mn, Fe, Ni, Cu, and Ga) loaded sulphated zirconia as catalysts

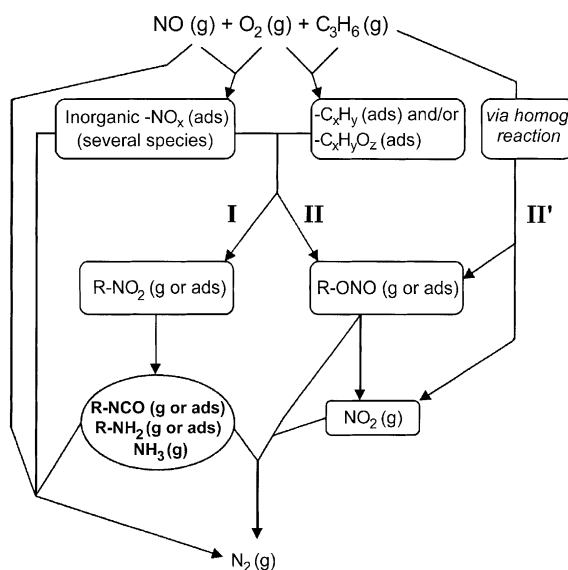


Fig. 57. Simplified reaction scheme of the C₃H₆-SCR of NO over γ-Al₂O₃ and the low loading Ag and Co/γ-Al₂O₃ giving the nature of the different species likely to be involved. It is proposed that the reduction to N₂ occurs through the reaction of oxidised and reduced nitrogen compounds [584].

under lean conditions at reaction temperatures between 573 and 873 K [585]. Pure and sulphated zirconia showed only a low activity for SCR with propane. After loading sulphated zirconia with Cu and especially Ga oxide, a high catalytic activity with NO conversion of 80% in the case of the Ga loading was achieved. The selectivities towards the main product of the SCR product N₂ were very promising. The catalytic activity only slightly decreased upon introduction of SO₂ into the reaction mixture (see Fig. 58).

The mechanism of SCR of NO by C₃H₆ on Al₂O₃ was investigated [586]. Attention was focused on the reactivity of the adsorbed acetate and nitrates on the Al₂O₃ surface. IR spectra showed that the reaction starts with the formation of nitrates from NO + O₂ followed by their reaction with C₃H₆ to form acetate. This becomes the predominant surface species in the steady-state condition. The acetate band, which was stable in He or NO, significantly decreased when the flowing gas was switched to NO + O₂. A complementary set of experiments monitoring gas composition showed that N₂ and CO_x were produced by the reaction of acetate with NO + O₂. The rate of acetate consumption in NO + O₂ exhibited the same order of

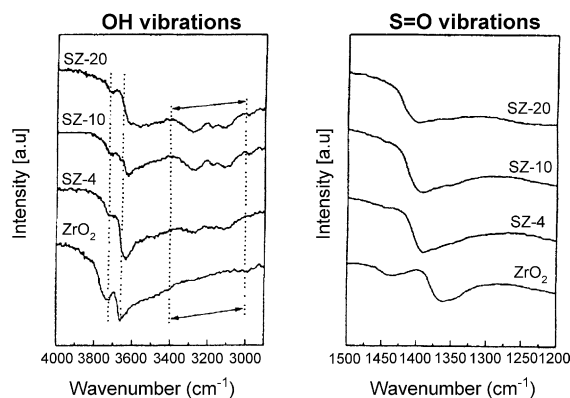


Fig. 58. IR spectra of pure and sulphated zirconia [585].

magnitude as the NO reduction rate, indicating that the acetate is active as a reductant and takes part in the N_2 formation. Nitrates can oxidise both C_3H_6 and acetate, and are mostly reduced to N_2 [586].

The EUROCAT SCR (V_2O_5 – WO_3 /TiO₂) catalyst has been characterised by IR spectroscopic methods [587]. Both V^{5+} and W^{6+} ions in $V=O$ and $W=O$ species on the surface act as Lewis acid sites towards ammonia molecules. Furthermore, the formation of ammonium ions by NH_3 adsorption indicated that Brønsted acid sites are also present. Both types of acid site were detected by pyridine adsorption also. The adsorption of nitric oxide alone and its coadsorption with ammonia indicated that NO molecules interact only weakly with the catalyst surface, while their reduction easily occurs in the presence of NH_3 . No clear evidence on whether coordinated or protonated ammonia molecules are the active species in such process was obtained.

Only minor differences between the surface features of the fresh and used catalyst were observed. In particular, the use of the catalyst in an industrial stream resulted in a slight decrease in the strength of the Lewis acid sites and the appearance of some nucleophilic centres. This behaviour suggests that a limited poisoning of the catalyst occurred, by deposition of basic species [578].

Fe-exchanged ZSM-5, the most active catalyst known for the SCR of NO with ammonia, was characterised. FT-IR spectra showed that NO molecules could be oxidised by O_2 to adsorbed N_2O_3 , NO_2 , and nitrate [588]. The NO_x adspecies were not stable at

above 573 K in He, but the adsorbed NO and NO_2 could be observed in flowing $NO + O_2/He$. NH_3 molecules were adsorbed on Brønsted acid and Lewis acid sites of Fe-ZSM-5 to generate, respectively, NH_4^+ ions (majority) and coordinated NH_3 (minority).

Long and Yanh [589] have studied the mechanism of Fe^{3+} exchanged TiO₂-pillared clay catalyst for SCR of NO with NH_3 . FT-IR spectra showed that NO molecules were oxidised by O_2 to form adsorbed NO_2 and nitrate species on the Fe-TiO₂-PILC catalyst. NO_2 adspecies was the dominant species and was more stable than nitrate species at high temperatures (i.e., >523 K). It could be reduced by NH_3 at high temperatures. Ammonia molecules were adsorbed on the Brønsted acid sites and Lewis acid sites of the catalyst to generate, respectively, NH_4^+ ions and coordinated NH_3 species. Both of them could react with NO, $NO + O_2$, and NO_2 at high temperature, but the reactions with $NH_3 + NO + O_2$ and $NH_3 + NO_2$ were much faster than the reaction with $NO + NH_3$. In situ FT-IR experiments revealed that the surface of Fe-TiO₂-PILC was covered mainly by NH_4^+ ions and coordinated NH_3 , and no NO_x adspecies was detected under the reaction conditions.

Kantcheva et al. [590] have studied selective catalytic reduction (SCR) of nitrogen oxides by NH_3 by means of IR spectroscopy. The studies were carried out on V_2O_5 /TiO₂, Cr_2O_3 , TiO₂, and the following conclusions were made:

- NH_3 adsorption on TiO₂, V_2O_5 /TiO₂, and Cr_2O_3 samples leads to formation of strongly bound coordinated ammonia (reversible formation of NH_4^+ occurs on V_2O_5 /TiO₂ and Cr_2O_3), which evidences weak Brønsted acidity.
- Adsorption of NO_2 on TiO₂, V_2O_5 /TiO₂, and Cr_2O_3 samples results in formation of different nitrates (NO^+ is also produced on TiO₂ and V_2O_5 /TiO₂ surfaces; strong Brønsted acidity is generated on all of the catalysts).
- Coadsorption of NO_2 and NH_3 leads to appearance of NH_4NO_3 -like surface species. They are intermediates in the SCR process. On TiO₂ these species decompose to N_2O (non-selective reduction), whereas on the V_2O_5 /TiO₂ and Cr_2O_3 catalysts the process occurs with a simultaneous reoxidation of a surface active site (V^{4+} , Cr^{3+}) and the final decomposition product is nitrogen (selective reduction).

- One of the main roles of the oxygen in the SCR is to ensure the production of surface nitrates which, reacting with ammonia, form NH_4NO_3 -like surface species [590].

Surface acidity of MCM-41 and clays has been determined by pyridine adsorption [591,592]. Brunner [593] has characterised solid acids by IR and other spectroscopic methods. H/D isotope exchange between *n*-alkanes and the Brønsted acidic hydroxyl groups in ferrierite ($\text{SiO}_2/\text{Al}_2\text{O}_3 = 17.0$) was observed by IR [594]. The formation of $\text{RhI}(\text{CO})_2$ from $\text{Rh}_6(\text{CO})_{16}$ impregnated on SiO_2 and its reactivity toward $\text{C}_2\text{H}_4/\text{H}_2$ has been investigated using in situ IR spectroscopy [595].

In situ IR spectroscopy was utilised to identify adsorbed species on zinc copper chromium oxide and potassium carbonate promoted zinc copper chromium oxide catalysts [596]. Bielanski et al. [597] have studied the hydration of dodecatungstosilic acid ($\text{H}_4\text{SiW}_{12}\text{O}_{40} \cdot 15.6\text{H}_2\text{O}$). Catalysts with several loadings of NiMoO_4 supported on silica were prepared using different methods and characterised by FT-IR spectroscopy [598]. The adsorption of formic acid on a polycrystalline Ag catalyst after various degrees of oxidation was investigated using in situ IR spectroscopy [599]. CO adsorption and oxidation over Cu_2MnO_x catalyst from RT to 373 K was studied [600]. Carbon monoxide/hydrogen reactions over Rh/TiO₂ catalysts at high temperature and pressure were studied by means of IR spectroscopy [601]. Rh-based catalysts to be used for the synthesis of C₂-oxygenates from syngas were characterised by CO adsorption [602]. FT-IR studies of dynamic surface structural changes in Cu-based methanol synthesis catalysts have been studied [603]. IR studies of CO adsorption and transmission properties have provided evidence for the nature of species in Cu/Al₂O₃, Cu/ZnO, and Cu/SiO₂ catalysts. The results obtained suggest that the active copper species present during methanol synthesis is metal-like [603]. For relatively small amounts of ZrO₂ to Cu/SiO₂ in situ IR spectroscopy shows that methanol synthesis occurs on both Cu and ZrO₂ components [604]. Methanol decomposition over Cu/SiO₂, ZrO₂/SiO₂, and Cu/ZrO₂/SiO₂ has been studied [605]. Bando et al. [606] has investigated the CO₂ hydrogenation over RhY catalyst. The role of the catalyst support in methane reforming with

carbon dioxide over rhodium catalysts was studied using in situ IR spectroscopy [607]. Rakkamaa et al. [608] carried out an FT-IR study on the adsorption of NO and reactions of NO and H₂ on a modified alumina-supported Pd monolith catalyst. The in situ DRIFTS analysis of adsorbed gases on studied catalysts was performed, too. The species formed by the adsorption of methanethiol and dimethyl sulphide on zirconia were studied [609]. Cornaglia et al. [610] have investigated cobalt-impregnated VPO catalysts precursors by means of FT-IR. FT-IR and Raman spectroscopy were used to investigate the surface chemistry of several magnesium vanadate and V₂O₅-TiO₂ catalysts [611,612]. Studies of a phosphine-palladium catalyst for the hydrocarboxylation of olefins were performed in situ using IR spectroscopy [613]. IR spectroscopy was used in conjunction with kinetic measurements in order to clarify the mechanism of the methylation of aromatics over zeolitic catalysts [614]. High-temperature in situ IR spectroscopy was used to investigate the surface species present on Cu-ZSM-5 catalysts during the reduction of NO_x with propylene in a lean environment [615]. In situ IR spectroscopy was employed to study the system of rhodium-exchanged NaX zeolite with different metal dispersion during syngas reactions [616]. Coke deposition on a Cr₂O₃-Al₂O₃ catalyst during dehydrogenation of butene to butadiene was followed by FT-IR, using coked catalyst dispersed on KBr pellets [617]. Driessen and Grassian [618] have studied the gas-phase photo-oxidation of trichloroethene (TCE) on Pt/TiO₂. A detailed investigation of a well-known photoreaction, phenol photodegradation, in the presence of TiO₂ was carried out [619]. Basini has described spectroscopic methods for the study of inter-phase zones under reaction conditions [620]. IR and molecular simulation studies of adsorption of simple gases such as methanol and water on aluminophosphates were reported [621]. An in situ dynamic study of the hydrogenation of but-1-yne on Pt/SiO₂ catalysts using IR spectroscopy was performed [622]. Ford et al. [623] has presented an overview of the use of time-resolved techniques for the investigation of reactive organometallic intermediates generated by laser flash photolysis. Time-resolved techniques provide valuable, otherwise unobtainable, structural and kinetic information about intermediates in the reaction sequence. IR, NMR, and EPR

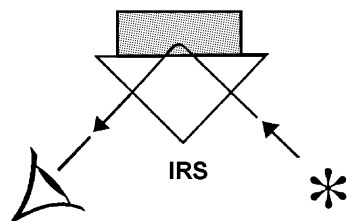


Fig. 59. The principles of ATR spectroscopy [390].

techniques have been used to analyse reduction under H_2 of Rh/CeO₂ catalysts prepared from chloride and nitrate precursor salts [624].

Recently, a study of coprecipitated Mn–Zr oxides and their behaviour as oxidation catalysts has been conducted [625]. Lewis acidity has been found below 423 K for Mn–Zr mixed oxides. The acid strength of these systems is quite low, and tends to grow upon increasing the zirconium content. Mn–Zr mixed oxides appear to be very active catalysts for isopropanol vapour total oxidation giving rise to CO₂ as the exclusive product. They are more active and more selective to carbon dioxide than Mn–Ti mixed oxides and are more stable than pure Mn oxides.

5. ATR spectroscopy

Internal reflection spectroscopy (IRS) became a popular spectroscopic technique in the early 1960s. It has become more widely known by the name ATR spectroscopy (see Fig. 59). ATR spectroscopy permits any surface to be brought in to contact with a high index of refraction internal reflection element (IRE). However, since the radiation is trapped by total internal reflection inside the IRE and only interacts with the sample surface, it is not propagated through it.

The ATR technique has found abundant application for the analysis of a wide variety of sample types and for a wide range of spectral ranges. The surface of samples may be probed from as little as a few tens of nanometers to several micrometers by the ATR technique. The chemical composition, layer structure, diffusion, adsorption, chemical reaction monitoring, orientation, and physical state of surfaces are a few of the types of qualitative and quantitative analyses that can be done by ATR.

Spectroscopic investigation of the reactions and equilibria of Mo(CO)₆ and molybdenum halocarbonyls under reaction conditions of ethylene carbonylation were done by ATR method [626]. From the in situ IR experiments, it was clear that the identifiable Mo species present during the course of the iodide-promoted carbonylation of C₂H₄ with Mo catalysts are Mo(CO)₆, Mo(CO)₅I[−], and Mo(CO)₄I₃[−]. The zero-valent species, Mo(CO)₆ and Mo(CO)₅I[−], are in equilibrium with one another, with Mo(CO)₆ being the favoured species under catalytic reaction conditions. An innovative approach has been used to probe the molecular nature of metal oxide/aqueous solution interface [627]. IRS of thin colloidal TiO₂ films, under aqueous solutions of pH 11.7–2.3 has been used to obtain differential in situ IR spectra related to interfacial species (Table 5).

Differential absorbance spectra generated by pH changes have revealed considerable spectral detail related to interfacial species including the TiO₂ surface groups, adsorbed ions, and associated water. This powerful approach gives new insights into the molecular structure of the metal oxide/aqueous interface and provides a basis for IR spectroscopic analysis of adsorption mechanisms. The IR horizontal ATR technique was adapted to be applied for in situ monitoring even at high pressure and high temperature [628]. Different types of reactors and flow cells are presented which

Table 5
Assignments of IR absorptions of hydrous TiO₂ surface groups [627]

Species	pH range	Wavenumber (cm ^{−1})	
		in H ₂ O	in D ₂ O
Ti–OH	10.7–4.3 (max ~8)	~3400	~2450
Ti–OH ₂	≤10.7	~3200	~2350 (masked by CO ₂)
Ti–OH ₂ ⁺	<5	1623, ~3000 (br)	1193, ~2240
Ti–OH ⁺ –Ti	<4.3	~3000 (br), 927	~2240, 920

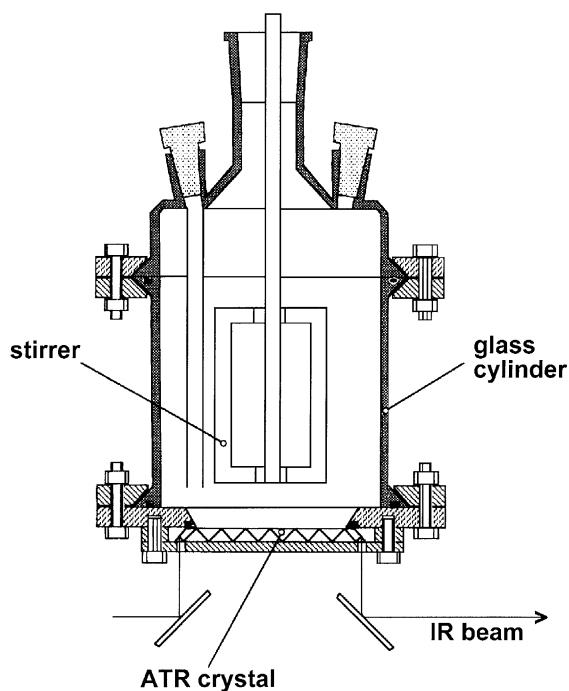


Fig. 60. Schematic diagram of the horizontal ATR laboratory reactor [628].

can be used for recording IR ATR spectra at pressure up to 20 MPa and temperatures up to 573 K (Figs. 60 and 61).

The use of the horizontal ATR technique has been shown for the following application examples:

- Addition reaction of *n*-butyl isocyanate with butyric alcohol;
- Investigation of equilibrium of isocyanate, HCl, and carbamic acid chloride at elevated pressure and temperature;
- Monitoring of polycondensation of bifunctional alcohols and carbonic acids;
- Recording spectra of polymer (polycarbonate and polyamide-6) melts at 553 K.

The use of ATR/FT-IR microspectroscopic techniques for the verification of the structure of chemical compounds synthesised on polystyrene beads in combinatorial chemistry was described [629]. Compared to other IR techniques, the ATR micro-IR technique shows clear advantage with respect to sensitivity and resolution. Thomasson et al. [630] have applied ATR

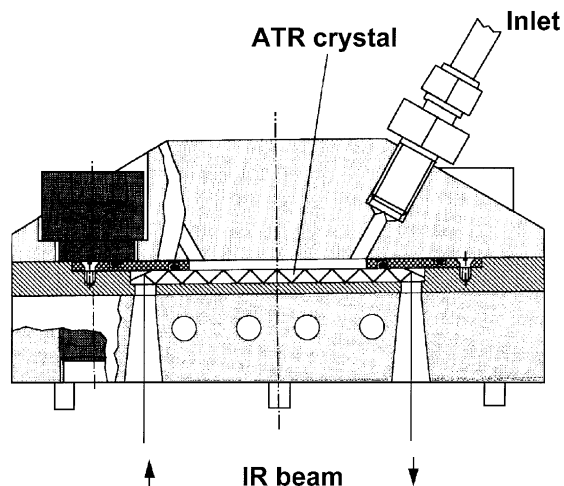


Fig. 61. Schematic diagram of the high-pressure horizontal ATR flow cell [628].

IR microspectroscopy for coal measurements. ATR microspectra of coal could be easily measured in less than 1 min on the polished block samples utilised by petrographers, without further preparation. Spectra are similar to absorption spectra but band intensities are different because of the relationship between penetration depth and wavelength that exists in ATR spectra. The ratio of the aromatic C–H stretching intensity at 3045 cm^{-1} to the aliphatic C–H stretching intensity at 2945 cm^{-1} correlated well with the mean maximum vitrinite reflectance R_{vmax} showing that the spectra contain similar information to other IR spectra collected by macrotechniques, such as diffuse reflectance. Comparison of the available internal reflection elements for ATR microspectroscopy, silicon, and germanium showed that while both gave acceptable spectra, the silicon gave higher quality, more intense spectra because it has the greater penetration depth owing to its lower refractive index. In comparison with the commonly used IR microscopy technique of specular reflection, the ATR approach has the advantage that useful spectra are obtained directly from the polished block without the need for complex mathematical procedures. The major disadvantage of the ATR technique is the spatial resolution of around $100\text{ }\mu\text{m}$ compared with as high as $20\text{ }\mu\text{m}$ for specular reflection. IRAS was applied to study the adsorption structures of 1,3-butadiene on Au(111) and Ag(111) in the temperature range from 25 to

95 K [631]. Rodes et al. [632] have studied CO microscopic adlayer structure on the Pt(111) terrace width and the step orientation. Sioku and Nix [633] have studied the interaction of methanol with well-defined Ce surfaces. IRAS was applied for the studies of ethylene adsorption structures on Ag(110) [634]. Wijnja and Schulthess [635] have applied ATR/FT-IR and DRIFTS spectroscopy for studying carbonate species at the aged γ -Al₂O₃/water interface. The spectra of ageing suspensions of γ -Al₂O₃ confirm the formation of bayerite on the surface of the Al-oxide particles [635]. Site blocking effects in ethylidene decomposition kinetics on Ru(001) was studied using in situ reflection-absorption IR spectroscopy [636]. Information on the bonding of organic ligands to hydrous metal oxide surfaces in order to gain insight into the mechanisms of surface reactivity was studied using in situ ATR spectroscopy [637]. Heger and Marx [638] have described the application of IR reflection spectroscopy for the analysis of hard coatings on metallic substrates. Pt, Pd, and Rh films of a few nanometers in thickness supported on glassy carbon and other substrates were prepared by electrochemical voltammetry [639]. Studies of in situ FT-IR spectroscopy on chemisorption of CO and SCN⁻ and formation of a polymer of *o*-phenylenediamine on electrodes of nanometer thin films have been conducted to explore the abnormal infrared effects (AIREs), which consist of two main characteristics: (a) inversion of IR bands, and (b) the enhancement of IR absorption of adsorbates. The results demonstrated that the AIREs depend mainly on the structure and the chemical nature of nanometer thin films. In all cases of chemisorption on thin films of platinum-group metals supported on glassy carbon, or supported on polymer-covered GC, the direction of IR bands of adsorbates is inverted in comparison with the direction of IR bands of the same adsorbates on corresponding massive metal electrodes. The results in this paper demonstrated also that the AIREs belong to a new phenomenon of IR reflection spectroscopy, which is related to the nanometer scale of the material. This study manifests the remarkable advantages of AIREs for studying surface processes and may contribute considerably to fundamental studies of electrocatalysis and reflection spectroscopy.

IRAS was used to study the reaction kinetics of CO oxidation on Pd(100) and Pd(111) catalysts [640,641], and to investigate NO and CO coadsorption

on Pd(100), Pd(111), and a Pd catalyst supported on silica [642]. In situ IR spectra for dilute (i.e., low-coverage) CO and NO adlayers on (111) and (100) Pt, Rh, Ir, and Pd surfaces in acidic aqueous solution were compared with vibrational spectra and other structural information for the corresponding systems in ultrahigh vacuum (UHV), with the objective of assessing the roles of the solvated double layer on the preferred binding sites and vibrational frequencies [643]. Results are considered for eight CO and five NO adlayers, involving C–O (ν_{CO}) and N–O (ν_{NO}) stretching bands, respectively.

6. Diffuse reflectance spectroscopy

The optical phenomenon known as diffuse reflectance is commonly used in the UV–Vis, NIR, and MIR regions to obtain molecular spectroscopic information (see Fig. 62). When it is applied in MIR area with an Fourier transform it is known as diffuse reflectance infrared Fourier transform spectroscopy (DRIFTS). It is usually used to obtain spectra of powders with minimum sample preparation. The collection and analysis of surface-reflected electromagnetic radiation as a function of frequency or wavelength obtain a reflectance spectrum. Two different types of reflection can occur: regular or specular reflection usually associated with reflection from smooth, polished surfaces like mirrors, and diffuse reflection associated with reflection from so-called mat or dull surfaces textured-like powders. In diffuse reflectance spectroscopy, electromagnetic radiation reflected from

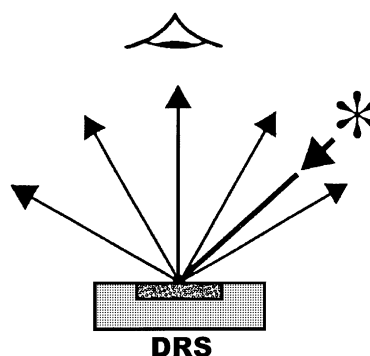


Fig. 62. The principles of diffuse reflectance spectroscopy [390].

dull surfaces is collected and analysed. If a sample to be analysed is not shiny, and for whatever reason is not amenable to conventional transmission spectroscopy, diffuse reflectance spectroscopy is a logical alternative.

Studies of the surface of γ -aluminas dehydrated at different temperatures with the conventional pyridine adsorption DRIFTS technique have revealed their very important surface structure features [644]. Presented results demonstrate that the three types and strengths of Lewis acid sites correspond to the three possible Al^{3+} coordination configurations predicted in the model given [644]. The five-coordinate Al^{3+} sites are weak Lewis acid sites, while the three- and four-coordinate Al^{3+} sites are strong and medium strong Lewis acid sites. The observation of Lewis acid sites close to hydroxyls on the surface of γ -alumina provides experimental evidence for migration of protons/OH groups on the surface during dehydration. Analysis of DRIFTS spectra can generate useful information concerning the nature and concentrations of different types of hydroxyls, carbonate, or bicarbonate species found on the surface of alumina powders [645]. Lee and Condrate [645] showed that the bands at 3305, 1570–1520, and 1390 cm^{-1} are associated with a dawsonite-like species which forms by interaction between Na^+ ions, which are present as an impurity on the alumina surface, and CO_2 and H_2O vapour adsorbed from the atmosphere. Then, adsorbed CO_2 forms bidentate carbonates. The presence of Na^+ ions on the alumina surface enhances the ability of adsorbing CO_2 . Hutchings et al. [646] have studied by means of DRIFTS aluminium phosphate (AlPO_4) catalysts surface during dehydration of 2-methylbutanol to isoprene. They have found that the intense band at 1300 cm^{-1} , associated with P–OH deformation, is absent following reaction. This indicates that there was a loss of surface P–OH groups during reaction. Extensive DRIFTS study of the catalytic oxidation of carbon black by K_2CO_3 , K_2MoO_4 , and the nitrates of the alkali metals (Na, K, Rb, and Cs) was described [647]. The spectra of potassium benzoate, potassium phenoxide and catalytically oxidised fullerene C_{60} were recorded as model systems to enable the assignment of the various absorption bands. Alkali benzoate-type species are likely to be formed upon decomposition of the alkali metal precursors in air, as well as alkali metal oxide species

attached to the carbon surface. Absorption bands in the 1100–1150 cm^{-1} region and around 620 cm^{-1} are assigned to CO_2 , chemisorbed on these oxidic alkali metal clusters. A review of literature dealing with alkali-catalysed carbon gasification was presented, to validate that assignment. A strong absorption band around 1140 cm^{-1} has been observed in the spectra of partially converted CaO/carbon black samples, which might also be related to chemisorbed CO_2 . A kinetic and DRIFTS investigation of crotonaldehyde adsorption and hydrogenation was conducted over TiO_2 -supported Pt and Ni with the intent of gaining insight into the adsorption modes of molecules with carbonyl groups on these catalysts in the SMSI and non-SMSI states [648]. DRIFTS spectra under reaction conditions identified crotonaldehyde species strongly adsorbed through the C=C bond and weakly coordinated through both the C=C and the C=O bonds on these catalysts after reduction at 573 K, which gave a peak at 1693 cm^{-1} (Fig. 63).

After reduction at 773 K, an additional adsorbed species with a strong band at 1660 cm^{-1} , indicating a significant interaction between the carbonyl group and the surface, was observed, which is presumed to be stabilised at interfacial Pt– TiO_x and Ni– TiO_x sites (Fig. 64).

The adsorption and catalytic behaviour of Cu supported on different forms of carbons were examined during crotonaldehyde hydrogenation [649]. Both DRIFTS and kinetic data obtained during crotyl alcohol and butyraldehyde hydrogenation indicated stronger adsorption and higher reactivity of crotyl alcohol on Cu, presumably leading to these low steady-state selectivities. DRIFTS spectra taken under reaction conditions revealed adsorbed crotonaldehyde, provided evidence for a monohydrogenated reactive intermediate with detectable surface coverage, and detected no adsorbed butyraldehyde.

IR spectra of propionaldehyde were studied over silica-supported Rh–Sn bimetallic catalysts [650]. Two absorption bands of the carbonyl group were observed at 1670 and 1720 cm^{-1} , and the aldehyde hydrogen (–CH=O) was also observed at 2748 and 2848 cm^{-1} over the Sn/Rh/ SiO_2 catalysts on which propionaldehyde was preadsorbed (Fig. 65). One of the absorption bands of carbonyl groups at 1670 cm^{-1} readily disappeared by contact with H_2 , whereas the other band at 1720 cm^{-1} remained. The band of the

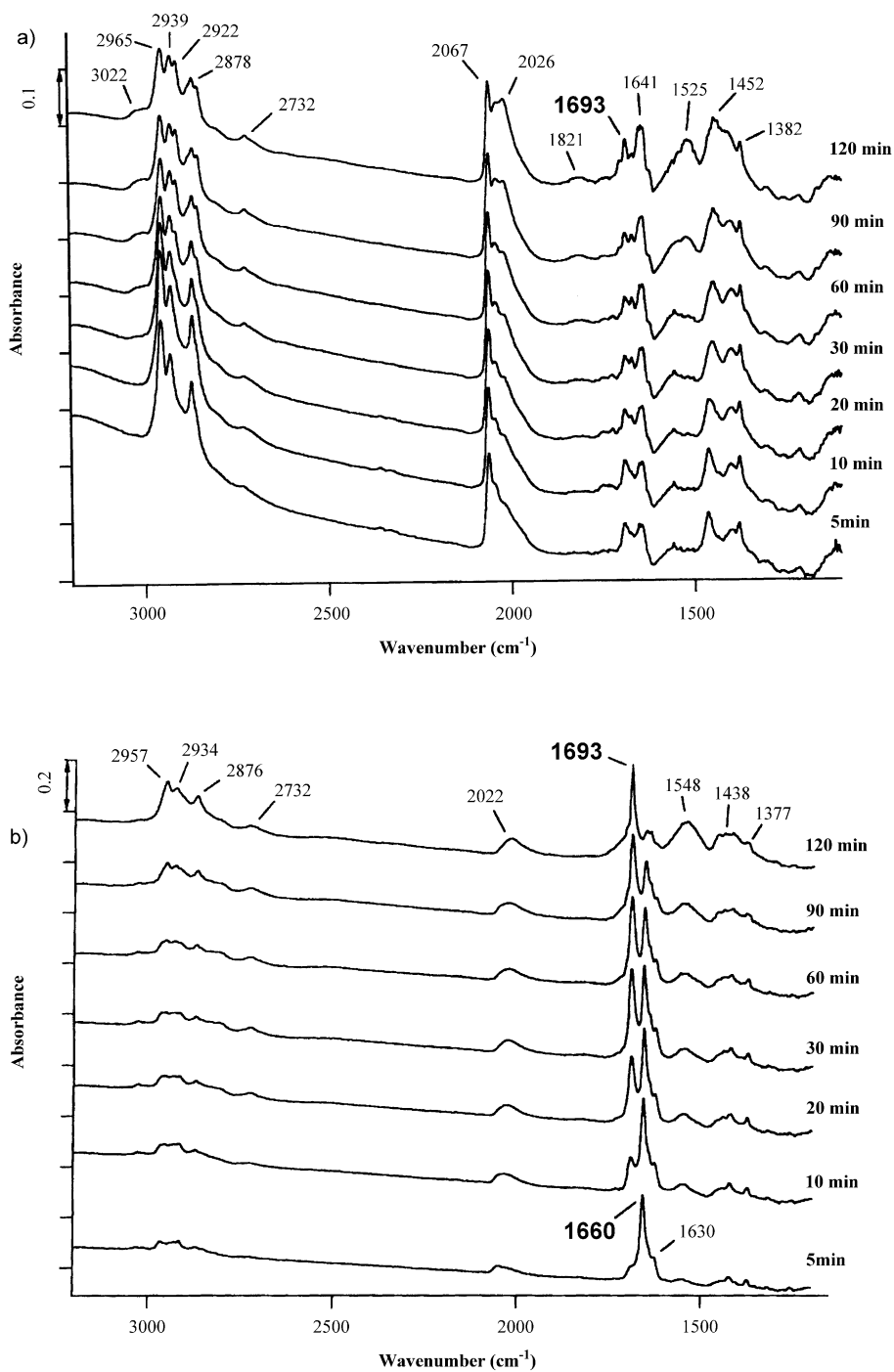


Fig. 63. In situ DRIFTS spectra during crotonaldehyde hydrogenation over Pt/TiO₂ reduced at (a) 573 K, (b) 773 K as a function of time on stream [648].

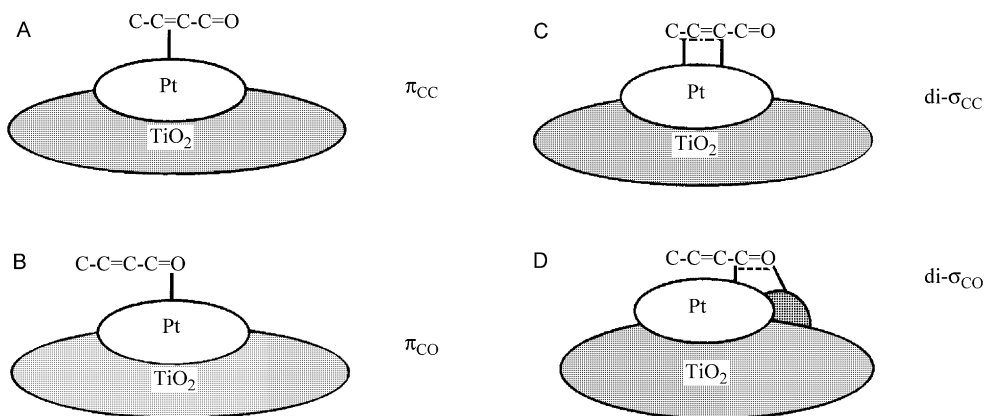


Fig. 64. Different possible adsorption modes of crotonaldehyde over Pt/TiO₂ [648].

aldehyde hydrogen also disappeared by the contact with H₂. The band observed at 1720 cm⁻¹ was assigned to a species weakly adsorbed on the catalyst surface. The intensity of the band at 1670 cm⁻¹ was increased with a Sn/Rh ratio up to unity and then was gradually decreased with the Sn/Rh ratio of the catalysts.

Silica-supported bimetallic Pt–Cu and Pt–Au catalysts were prepared using bimetallic molecular cluster precursors as the metal source [651]. The DRIFTS spectrum of carbon monoxide adsorbed to Pt₂Cu₄

catalyst contains a very broad and asymmetric peak associated with CO bound to Pt (see Fig. 66).

One possible interpretation of this peak is that it results from overlapping linear Pt–C≡O stretches and lower energy C≡O stretches from bridging or semibridging modes between Pt and Cu.

Tsyganenko et al. [652] have performed a variable-temperature IR spectroscopic studies of CO adsorbed on Na-ZSM-5 and Na-Y zeolites. They have found that CO interacts with extra-framework alkali metal cations (M⁺) of zeolites to form both M⁺ ··· CO

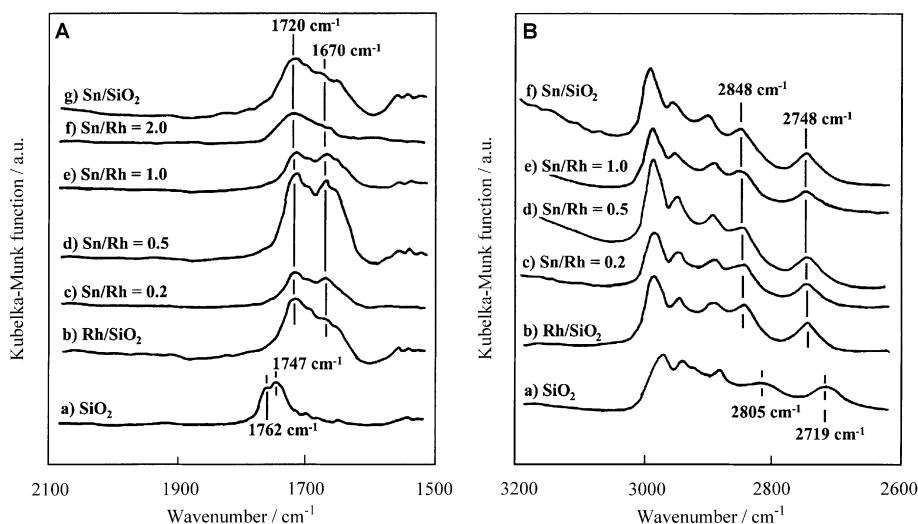


Fig. 65. IR spectra of propionaldehyde adsorbed at RT on Sn/Rh/SiO₂ catalysts: A–C–O stretching band, B–C–H stretching band [650].

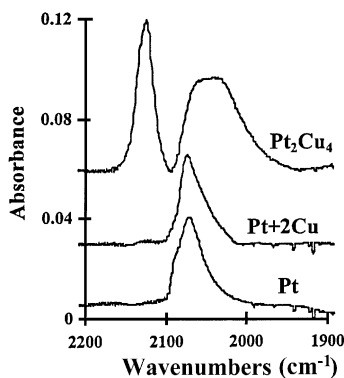


Fig. 66. DRIFTS spectra of the C≡O stretching region for CO adsorbed to the 0.15 Pt, 0.15-Pt + 2Cu, and 0.15 Pt₂Cu₄ catalysts [651].

and $M^+ \cdots CO$ species. By using variable-temperature FT-IR spectroscopy, these C-bonded and O-bonded species were found to be in a temperature-dependent equilibrium.

In situ DRIFTS study of the reduction/activation of Ga/H-ZSM-5 and variants thereof has been performed

[653]. These studies have shown a synergy between acidic supports (zeolitic and non-zeolitic) and Ga₂O₃, which leads to the reduction of the latter in either a H₂ or propane stream, as evidenced by the loss in intensity of the $\nu Ga-O$ band. No reduction of Ga₂O₃ was observed when it was unsupported or supported upon non-acidic supports. In all cases the reduction process was accompanied by loss of Brønsted acid groups due to reaction between the acidic site and gallium suboxide. Moreover, the appearance of a strong sharp band coincident with the known frequency of the $\nu Ga-O$ band was also recorded and is presumed to indicate the presence of Ga₂O.

Changes in the surface structure of sulphated zirconia prepared by sol-gel method were studied using nitrogen adsorption, in situ DRIFTS and other spectroscopic methods [654]. These studies were performed following deactivation and regeneration of the catalyst (Figs. 67 and 68).

The physical properties of sulphated sol-gel zirconia were unchanged as a result of reaction and catalyst regeneration. The isomerisation of *n*-butane was used as a probe reaction. Both Brønsted and Lewis

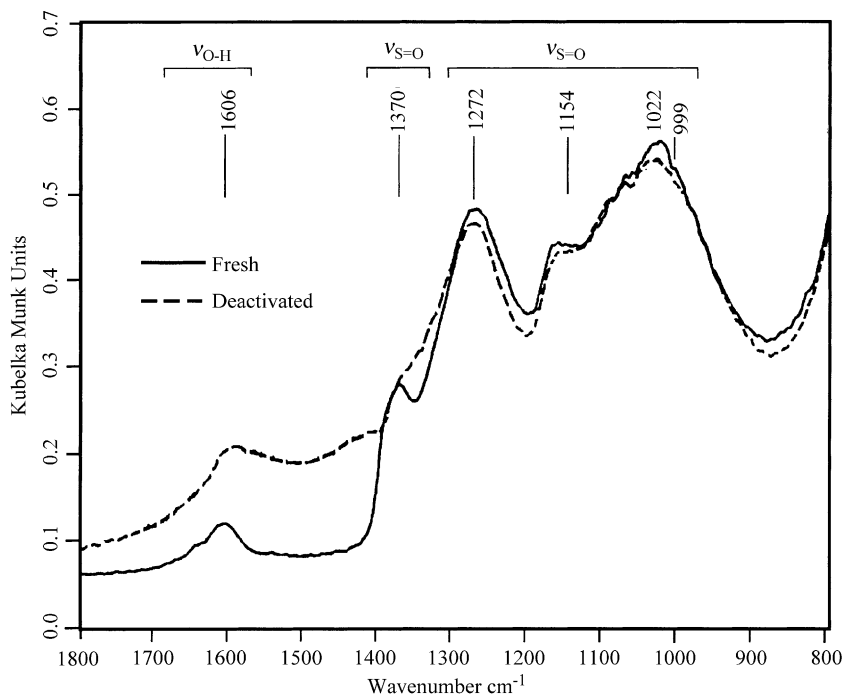


Fig. 67. In situ DRIFTS spectra of fresh and deactivated sulphated sol-gel zirconia [654].

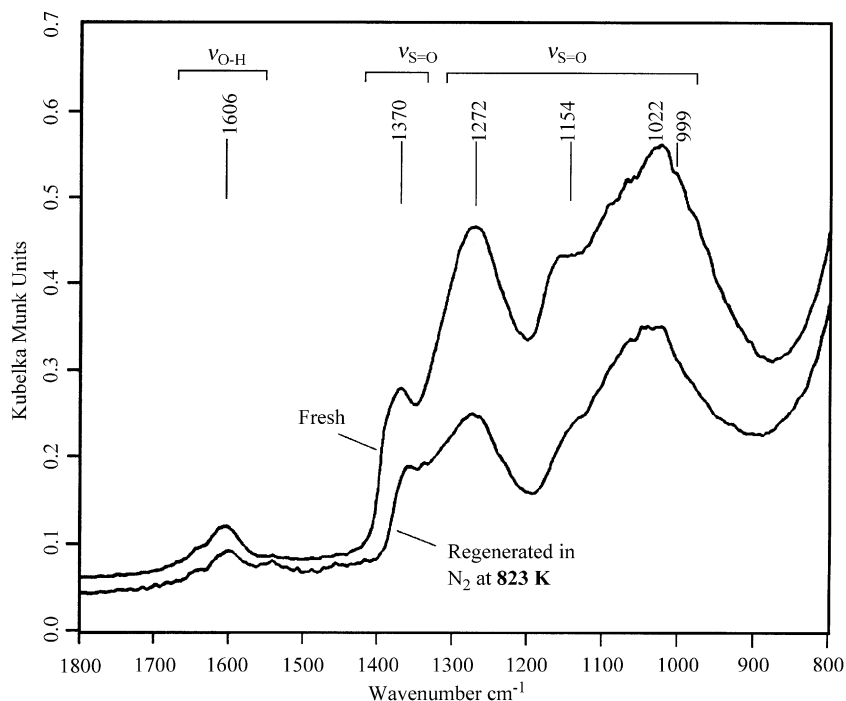


Fig. 68. In situ DRIFTS spectra of fresh and regenerated sulphated sol-gel zirconia [654].

acid sites using pyridine adsorption at 373 K were observed on sulphated zirconia (Fig. 69).

Catalytic activity of sulphated zirconia was affected by both sulphur loading level and surface crystal phase [655]. Incorporation silica or alumina into the catalyst system stabilised the tetragonal crystal phase and prolonged activity. Stabilised sulphated zirconia prepared with 20 wt.% alumina maintained catalytic activity for the isoparaffin alkylation reaction six times longer than pure sulphated zirconia. Based on in situ transient measurements using DRIFTS, a reaction mechanism was proposed for the CO₂ methanation reaction on 2% Ru/TiO₂ at 383 K, involving the existence of a precursor for adsorbed CO, a reaction intermediate in the pathway to methane, while formate is a side product adsorbed on the support [656]. It was further suggested that this surface intermediate corresponds to a formate adsorbed at the metal-support interface, and that the formate infrared bands measured correspond to the formate species that has diffused from the interface to the support. The hydrogenation of the adsorbed carbon monoxide is presented in a lumped form involving six adsorbed hydrogens, which is obviously not

an elementary reaction, but the different hydrogenation steps cannot be distinguished by IR. A pathway involving hydrogen carbonate was presented for the formation of the interfacial formate because DRIFTS experiments have shown that this species is formed on the support during the reaction and that its transient response is consistent with the response of a CO precursor. The partial oxidation of methane to synthesis gas over an α -Al₂O₃ and a γ -Al₂O₃-supported Rh catalyst has been studied at atmospheric pressure using in situ DRIFTS between 823 and 973 K [657]. A surface intermediate species with IR band at 2000 cm⁻¹, correlating with the CO formation, was observed during the partial oxidation. DRIFTS spectra of adsorbed CO at 323 K were used to study the state of Rh during the partial oxidation. The state of Rh at 973 K is proposed to be a matrix of metallic rhodium with clusters of partially reduced oxide phase with isolated Rh⁺ atoms dispersed on the support. Rh oxide with Rh⁺ cations is the state of Rh during partial oxidation of methane at 823 K. In situ DRIFTS was performed to study the reaction mechanism of NO decomposition on La₂O₃ [658]. Peak assignments were verified by establishing

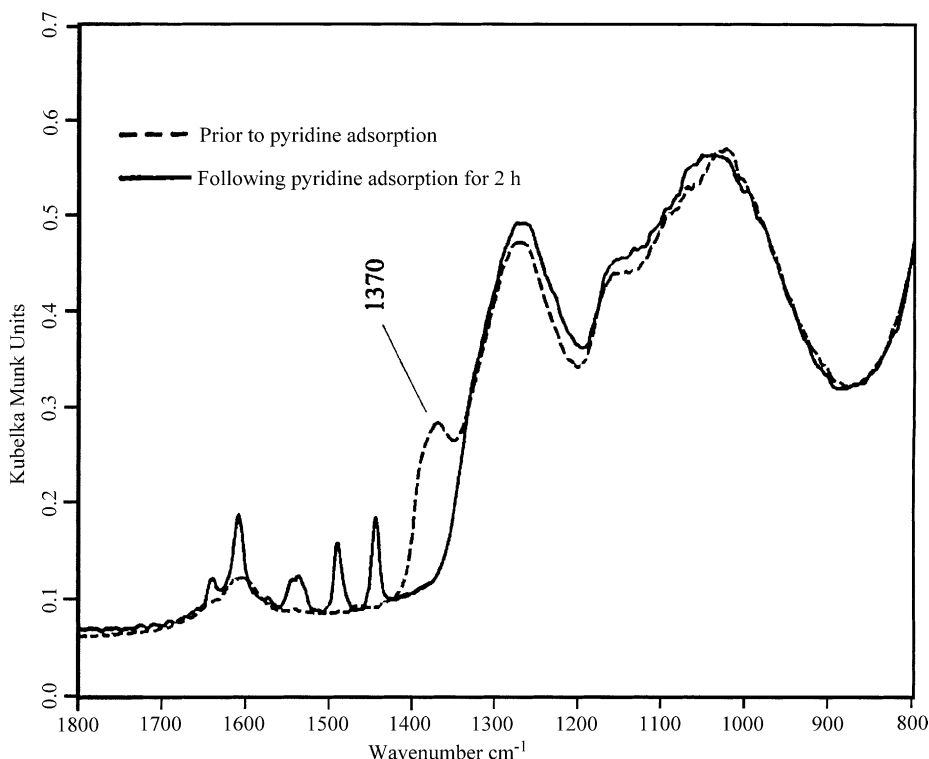


Fig. 69. In situ DRIFTS spectra of fresh sulphated sol-gel zirconia before and after the adsorption of pyridine [654].

isotope shifts of species formed after adsorption of ^{15}NO . Peak deconvolution was employed to resolve complex spectra. The adsorption behaviour of NO was established at 298 K as well as temperatures up to 773 K. Upon adsorption at RT, NO^- , $\text{N}_2\text{O}_2^{2-}$, chelating NO_2^- , nitrito (NO_2^-), and unidentate and bidentate NO_3^- groups are observed, whereas at higher temperatures, nitrate and smaller amounts of NO_2^- groups prevail. A surface reaction model developed on the basis of the solid-state properties of La_2O_3 reveals that the anionic NO species (NO^- , $\text{N}_2\text{O}_2^{2-}$) are formed by adsorption on anion vacancies and that they decompose at higher temperatures to yield nitrogen and oxygen. NO adsorption onto basic oxygen anion creates NO_2^- and NO_3^- spectator species. However, NO_2^- groups may also be involved in the decomposition process by reacting with the remaining oxygen to form nitrates (Table 6).

Huang et al. [659] have conducted DRIFTS studies of adsorption and reduction of NO on La_2O_3 dispersed on Al_2O_3 (Fig. 70). The surface properties of La_2O_3

supported on $\gamma\text{-Al}_2\text{O}_3$ showed features more and more similar to unsupported La_2O_3 as the La_2O_3 loading increased. DRIFTS spectra have shown that a highly dispersed La_2O_3 phase exists on $\gamma\text{-Al}_2\text{O}_3$ when present at submonolayer coverages, whereas bulk-like La_2O_3 features were observed with a 40% $\text{La}_2\text{O}_3/\gamma\text{-Al}_2\text{O}_3$ sample, which contained more than one theoretical monolayer of La_2O_3 (Figs. 71 and 72).

The shift of a surface vibrational mode of strained Al–O–Al bridges to lower frequencies as the La_2O_3 loading increases was attributed to an Al–O–La interaction. Characterisation by TPD and DRIFTS using NO or NO_2 as a probe molecule also showed the same trend, i.e., adsorption behaviour on 10% $\text{La}_2\text{O}_3/\gamma\text{-Al}_2\text{O}_3$ was similar to that on $\gamma\text{-Al}_2\text{O}_3$, whereas adsorption on 40% $\text{La}_2\text{O}_3/\gamma\text{-Al}_2\text{O}_3$ was similar to that on bulk La_2O_3 .

The chemistry between NO_x species adsorbed on La_2O_3 and CH_4 was probed by temperature-programmed reaction (TPR) as well as in situ DRIFTS [660]. During NO reduction by CH_4 in the presence of O_2 ,

Table 6
Peak positions and assignments for adsorption of ^{14}NO at various conditions and temperatures [658]^a

Species	Peak position (cm^{-1})					
	^{14}NO at 298 K for 35 min	After heating to 473 K	After heating to 773 K	^{14}NO ads. at 573 K	^{14}NO ads. at 673 K	^{14}NO ads. at 773 K
NO^-	a	1100–1000sh?	b	a	1150?vw	b
$\text{cis-N}_2\text{O}_2^{2-}$	1108sh	1100–1000sh?	b	a	b	b
Nitrate NO_3^- unidentate	1020	1020	1020vw			
	1273	1258	1260	a	a	
	1530	1508	1511	1523	1513	1522
Nitrate NO_3^- unidentate	1210sh	b	b	c	c	c
	1613					
Nitro NO_2^- chelating	a	1324	1324	1375	1373	1329
		1100–1000		a	1150?	
Nitrito NO_3^-	818					
	1433	1424	1420	1420	1420vw	1420vw

^a a: not resolved; b: not observed; c: not observed or covered by carbonate loss; sh: shoulder; vw: very weak.

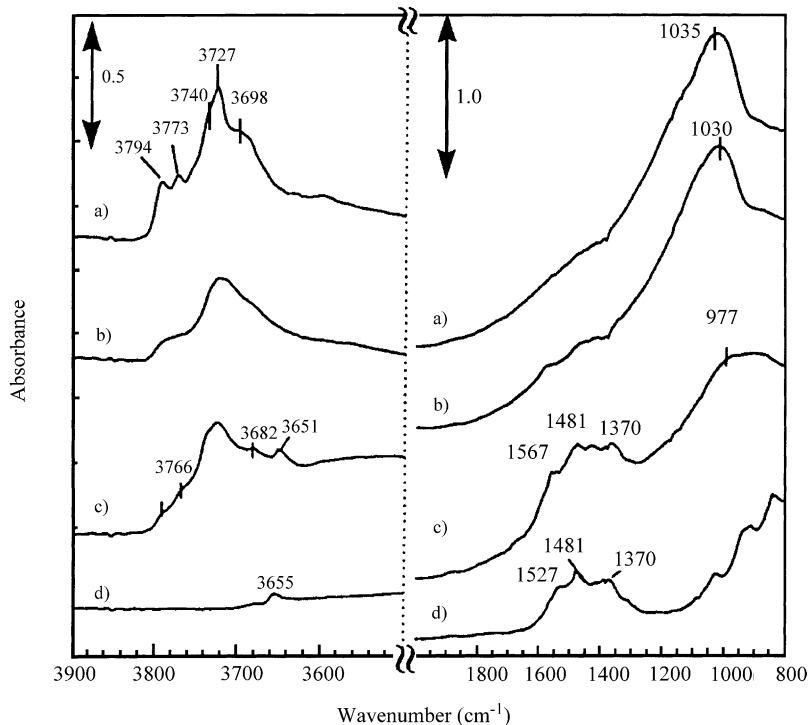


Fig. 70. IR spectra of: (a) $\gamma\text{-Al}_2\text{O}_3$; (b) $\text{La}_2\text{O}_3/\gamma\text{-Al}_2\text{O}_3$; (c) 40% $\text{La}_2\text{O}_3/\gamma\text{-Al}_2\text{O}_3$; (d) La_2O_3 [659].

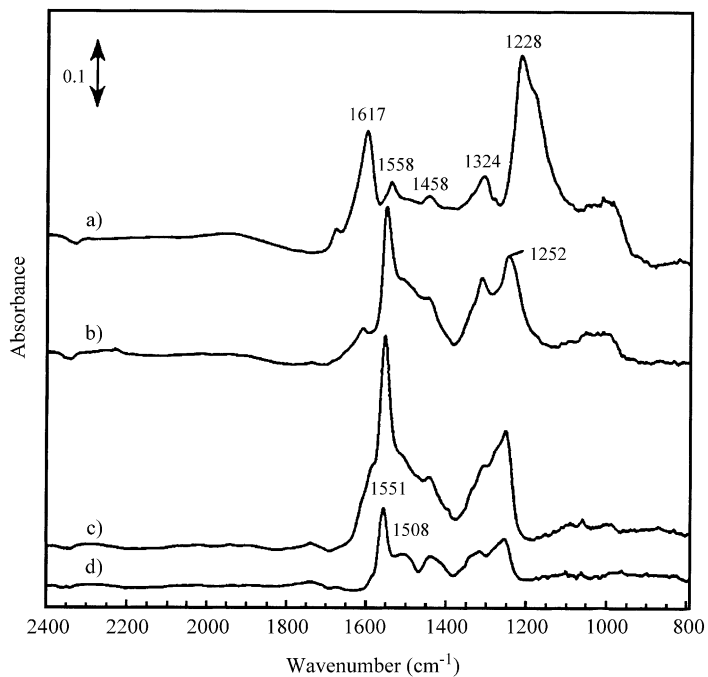


Fig. 71. DRIFTS spectra on 10% La₂O₃/γ-Al₂O₃ after exposing to 4% NO at 300 K for 30 min: (a) after purge in Ar for 30 min. The sample was then heated in Ar to: (b) 473 K; (c) 673 K; (d) 800 K and cooled to 300 K to obtain spectra [659].

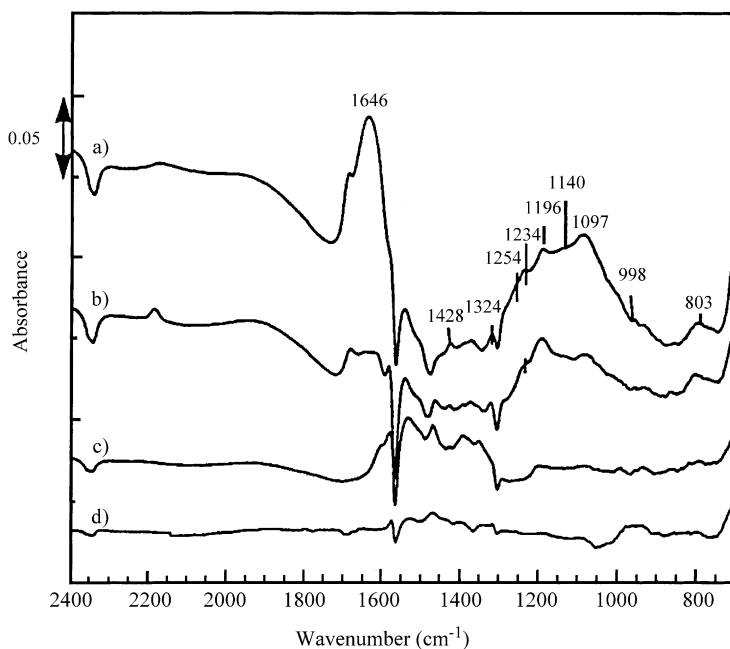


Fig. 72. DRIFTS spectra on 40% La₂O₃/γ-Al₂O₃ after exposing to 4% NO at 300 K for 30 min: (a) after purge in Ar for 30 min. The sample was then heated in Ar to: (b) 473 K; (c) 673 K; (d) 800 K and cooled to 300 K to obtain spectra [659].

NO_3^- does not appear to activate CH_4 , thus either an adsorbed O species or an NO_2^- species is more likely to activate CH_4 . In the absence of O_2 , a different reaction pathway occurs and NO^- or $(\text{N}_2\text{O}_2)^{2-}$ species adsorbed on oxygen vacancy sites seem to be active intermediates, and during NO reduction with CH_4 unidentate NO_3^- , which desorbs at high temperature, behaves as a spectator species and is not directly involved in the catalytic sequence.

Koizumi et al. [661] by means of DRIFTS have studied TPD of NO adsorbed on Co–Mo/ Al_2O_3 sulphided at high pressure. It was found that two kinds of nitrosyl species were formed on Co–Mo/ Al_2O_3 . One is dinitrosyl species adsorbed on coordinatively unsaturated sites of Co (doublet band at 1835 and 1785 cm^{-1}), and the other is unidentified nitrosyl species (singlet band at 1785 cm^{-1}). The singlet band also appeared in DRIFTS spectra of Co–Mo/ Al_2O_3 sulphided at atmospheric pressure. So far, IR spectrum of NO adsorbed on sulphided Co–Mo/ Al_2O_3 has been interpreted as superposition of two doublet bands. But the results obtained in the work of Koizumi et al. indicate that such an interpretation is not adequate.

Comparing DRIFTS spectra of Co–Mo/ Al_2O_3 with those of the physical mixture of Mo/ Al_2O_3 and Co/ Al_2O_3 , it was suggested that the singlet band was assigned to NO adsorbed on the coordinatively unsaturated sites of Co–Mo interaction species. As concerns the effect of sulphiding pressure, it is noted that the relative intensity of the singlet band in the spectrum of Co–Mo/ Al_2O_3 sulphided at high pressure seems to be different from that of Co–Mo/ Al_2O_3 sulphided at atmospheric pressure. Therefore, it is possible that the

formation of Co–Mo interaction species depends on the pressure of sulphiding. This might be the reason for the difference between DRIFTS spectrum of NO adsorbed on Co–Mo/ Al_2O_3 sulphided at high pressure and that on Co–Mo/ Al_2O_3 sulphided at atmospheric pressure.

The SCR of NO with C_3H_6 in the presence of a large excess of O_2 was studied over alumina and silver–alumina catalysts [662]. The $\gamma\text{-Al}_2\text{O}_3$ and the low-loading silver material exhibited high conversions to N_2 whereas the high-loading sample predominantly yielded N_2O . Surprisingly, a comparison of actual NO_2 yields to thermodynamically predicted yields of NO_2 showed that the formation of NO_2 during the C_3H_6 -SCR of NO over $\gamma\text{-Al}_2\text{O}_3$ was not achieved through the direct oxidation of NO with O_2 . An alternative mechanism involving the formation of organonitrite species followed by their decomposition/oxidation was suggested to be the main route for the formation of NO_2 (Fig. 73).

The promoting role of low loadings of silver on alumina on the activity for N_2 production was attributed to the higher rate of formation of inorganic ad- NO_x species (e.g., nitrates) as evidenced by in situ DRIFTS and thermogravimetric analyses. It was proposed that these inorganic ad- NO_x species further react with the reductant or a derived species to form various organo- NO_x compounds. In particular, organo-nitro and organo-nitroso compounds and/or their derivatives (e.g., isocyanate, cyanide, amines, and NH_3) were suggested to react with NO or the organo-nitrite and/or its derivative NO_2 to yield N_2 . When no reductant was present, the low-loading

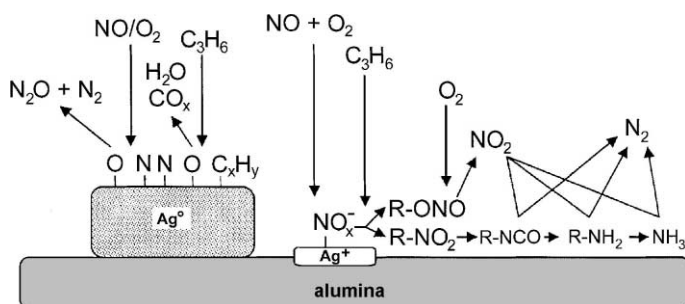


Fig. 73. The different roles of Ag during the C_3H_6 -SCR over $\text{Ag}/\gamma\text{-Al}_2\text{O}_3$: large Ag^0 particles catalyse the decomposition–reduction of NO whereas Ag^+ species favours the oxidation of NO to ad- NO_x species which subsequently react through the intermediacy of organonitrogen compounds [662].

Ag/ γ -Al₂O₃ material was poisoned by strongly bound nitrates and its activity for NO₂ formation was similar to that observed over the alumina.

An in situ DRIFTS study of the SCR of NO with NH₃ in the presence of O₂ has been carried out over vanadia/alumina and vanadia/lanthanide-doped alumina catalysts [663]. In the case of lanthanide-doped vanadia/alumina catalysts, there seems to exist a direct relationship between the activity of the catalyst in the SCR reaction and the Brønsted acidity shown by the catalyst. In this sense, the addition of lanthanide ions to vanadia/alumina catalysts change the electronic densities of vanadium, oxygen and lanthanide ions involved in the V–O–Ln bonds hence altering the acid–base nature of the catalysts which results in enhancing Lewis acidity with respect to the undoped catalyst thus leading to an activity decrease. The SCR reaction seems to occur via an Eley–Rideal-type mechanism, where gaseous NO reacts with adsorbed ammonia species, preferentially as NH₄⁺ groups.

The deactivation of Ce-zeolite deNO_x catalysts has been studied [664]. Catalysts were aged in exhaust gases of a diesel engine and a natural gas engine. The deactivation in real exhaust gas has been compared to deactivation in simulated exhaust gas. Ammonia and urea were used as reducing agent. Deactivated catalysts were characterised with DRIFTS.

Mahzoul et al. [665] have studied the NO_x adsorption over NO_x trap catalysts. The maximum storage capacity was obtained at 623 K. The storage capacity increases when the oxygen concentration in the feed increases from 0 to 3%. The storage capacity increases when NO₂ is injected instead of NO or NO/O₂. A higher Ba content or/and the presence of Pt in the catalyst increases the storage capacity. Two kinds of platinum sites seem to operate, the sites close to BaO crystallites are active in barium nitrate formation while the other sites are responsible for NO₂ formation.

DRIFTS spectra of ammonia adsorption (acidity) on a cobalt-catalysed amination of 1,3-propanediol have been studied by Fisher et al. [666].

Selective catalytic reduction of NO by NH₃ over vanadia–titania aerogels [667] and catalysts [668] was studied using in situ DRIFTS. DRIFTS has been used to study NH₃ and NO adsorption over vanadia/titania catalysts [669]. Those study of the NH₃ adsorption over an oxidised 15% w/w vanadia/titania catalyst reveals that NH₃ is adsorbed on both Lewis and Brønsted

acid sites as, respectively, coordinate NH₃ and NH₄⁺ species, leading to a reduction of the V⁵⁺=O groups of the vanadium surface. At 573 K, adsorbed nitrosyl species are detected on the surface of the catalyst under ammonia flow, suggesting that the oxidation of gaseous or adsorbed ammonia species takes place over the V=O sites. On the contrary, NO is not adsorbed on the oxidised catalyst. The required reduction degree of the vanadium surface for which NO adsorption takes place, is estimated to be between 50 and 95%, through the measure of the area of the 2ν(V=O) DRIFTS bands [669]. DRIFTS measurements on shallow-bed-treated HY and H-ZSM-5 zeolite revealed the combination of stretching and bending modes of bridging OH groups as well as their combination with vibrational modes of the zeolite framework [670].

A DRIFTS was used in situ in order to identify the active sites in the reaction of CO and H₂ over lanthanide-modified Rh/Al₂O₃ catalysts [671]. The activity and good selectivity (>90%) of γ -Al₂O₃-supported Ni for the selective catalytic oxidation (SCO) of NH₃ to N₂ with excess of O₂ has been shown by microreactor studies [672]. Two IR absorption bands appear during the TPO of NH₃ in the temperature range of N₂ formation (1546 and 1280 cm⁻¹) and have been assigned to stable bidentate nitrate surface species. This represents strong evidence that under the studied conditions, formation of N₂ occurs via the in situ SCR mechanism.

A correlation between spectra and catalyst activity was investigated via in situ diffuse reflectance IR spectroscopy of probe molecules adsorbed onto CoMo–alumina hydrotreating catalysts [673]. Robert et al. [674] have studied chemisorption of phenols and acids on TiO₂ (P25 Degussa) surface.

In the case of substituted phenols adsorption, the most important changes between adsorbates and solid starting phenols are, in all cases, the following (Fig. 74): (1) disappearance of O–H bending bands (two bands at 1430–1440 and 1350–1370 cm⁻¹), (2) decrease of the intensities and shift of the C–O stretching bands (1240 and 1090 cm⁻¹), and (3) strong decrease of the band attributed to “skeletal ring breathing mode” between 1600 and 1500 cm⁻¹. The authors suggest that the strong decrease of this band could be attributed to the formation of phenolate and/or to flat adsorption of the phenols on TiO₂. The relative decrease of asymmetric and

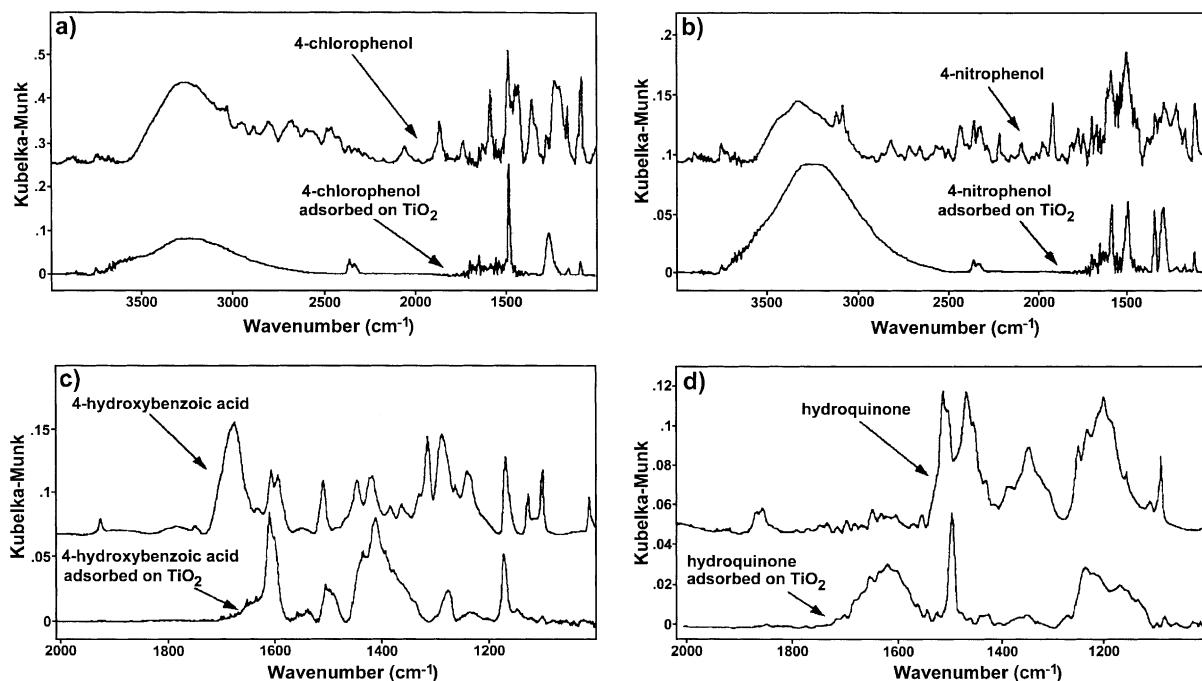


Fig. 74. DRIFTS spectra of some phenolic compounds adsorbed and non-adsorbed on the TiO_2 [674].

symmetric stretching vibrations of the NO_2 group for 4-nitrophenol ($1550\text{--}1340\text{ cm}^{-1}$; Fig. 74(b)) could also be explained by the adsorption of the aromatic ring parallel to the TiO_2 surface. For acidic functions, the disappearance of the intense $\text{C}=\text{O}$ stretching band (1678 cm^{-1} for 4-hydroxybenzoic acid in the example; Fig. 74(c)) and the strong increase of the band at $1580\text{--}1610\text{ cm}^{-1}$ attributed to carboxylate show the complete dissociation of adsorbed acid and chelate or bidentate formation. One of the assumption done by the authors suggests the adsorption of phenols and phenol acid on the TiO_2 surface proceeds via phenolate and carboxylate formation.

Measurements of OH fundamentals and combination bands were performed using in situ diffuse reflectance spectroscopy in order to investigate MFI-type zeolites [675]. A review of the characterisation of heterogeneous catalysts by DRIFTS was published [676].

DRIFTS and mass spectrometry were used to relate the catalytic properties of iridium clusters on polycrystalline alumina to the formation of gaseous reaction products [677]. A bimetallic Fischer–Tropsch

catalyst, consisting of Co–Re on Al_2O_3 support, was studied by DRIFTS [678]. The reaction products of the hydrogenation of CO and the reactivity of $\text{Rh}/\text{Al}_2\text{O}_3$ used as the catalyst for the hydrogenation were studied via in situ DRIFTS [679]. The results of a DRIFTS study of CO linearly adsorbed on $\text{Ir}/\text{Al}_2\text{O}_3$ catalyst were reviewed [680]. $\text{Pt}/\text{MgO}\text{--}\text{Al}_2\text{O}_3$ catalysts, used for the selective ammoxidation of *n*-alkanes, were shown by a DRIFTS study to contain two types of metallic Pt particles [681].

A precursor for an aluminophosphate catalyst family was characterised by XPS and DRIFTS [682]. A DRIFTS was used in a study of the products formed by the oxidation and ammoxidation of toluene over a vanadium catalyst [683]. Information about the OH groups in MFI-type zeolites was obtained by means of in situ DRIFTS [684]. The same technique was used for the analysis of CO linearly adsorbed on Pt particles in a zeolite [685]. DRIFTS was used to investigate the decarbonylation products of $\text{Mo}(\text{CO})_6$ supported on silica [686]. The structure of the complex formed by deposition of copper acetylacetonate on the surface of silica was characterised [687]. The decomposition

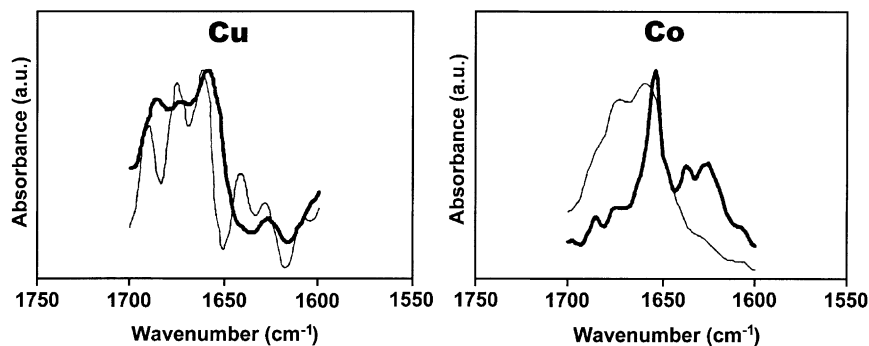


Fig. 75. DRIFTS spectra of the impregnated (thin line) and covalently bonded (thick line) complexes [700].

kinetics of ethylene glycol dinitrate adsorbed on zinc oxide was monitored by DRIFTS [688].

DRIFTS studies of the adsorption and reaction of 4-nitrobenzoic acid on ω -functionalised alkanethiol monolayers on powdered silver were conducted [689]. Analysis of adsorbed species present on the surface of Pd–Cu catalysts under reaction conditions of CO and NO elimination was performed by DRIFTS [690]. Petkovic and Larsen [691] have utilised DRIFTS for studying the transformation of isobutene into linear butenes. Toluene oxidation over reduced Pd/Al₂O₃ and acetone oxidation over Mn₂O₃/Al₂O₃ was carried out performing DRIFTS spectra under reaction conditions [692]. A DRIFTS was used to study *n*-hexane cracking over H-ZSM-5 and H- β zeolites [693]. Kiviahio et al. [694] have conducted studies on carbon carbonyl cluster derived Co–Ru/SiO₂ catalysts. Centeno et al. [695] have conducted DRIFTS study of the surface structure and nitridation process of mixed galloaluminophosphate oxynitride (AlGaPON) catalysts. Carbon-supported copper catalysts and CoMo/alumina prepared from carbonyl precursors were characterised [696,697]. The decarbonylation of Co_{4–n}Rh_n(CO)₁₂/SiO₂ and (Co₄(CO)₁₂ + Rh₄(CO)₁₂)/SiO₂ catalysts was studied by temperature-programmed reduction (TPR) and in situ DRIFTS [698]. Special attention was paid to the effect of the decomposition atmosphere on the supported catalysts. NO reduction of CO over Pd–*x*Mo/Al₂O₃ catalysts has been studied by DRIFTS [699]. Recently, Valente et al. [700] have studied oxidation of pinane using copper and cobalt acetylacetonate complexes immobilised on modified activated carbon.

The FT-IR spectra of adsorbed and bonded Cu(acac)₂ and Co(acac)₂ complexes on the activated carbon supports are shown in Fig. 75. The spectra of the bonded and adsorbed samples are different. The former clearly shows a band at 1658 cm^{–1} that does not appear in the spectra of the adsorbed complexes. This band may be assigned to the new C=N bond resulting from the Schiff condensation between the complexes and the amines [700].

7. Emission spectroscopy

There are numerous examples of manufacturing processes where the ability to perform a rapid, non-destructive determination of product quality is of great value. IR spectral data of a sample contain compositional as well as physical property information hence can often provide the information required determining product quality. Infrared emission spectroscopy (IRES) is a technique that can often be applied to conveniently collect IR data from a sample in a process (see Fig. 76). All that is required to measure an IR emission spectrum is to generate a situation where the sample is at a different temperature than that of the IR detector.

IRES has some significant advantages when compared to the much more common technique of IR absorption spectroscopy, especially when used in a process monitoring application. In many cases, the samples are large relative to the area of the sample viewed by the spectrometer, a situation that eliminates the need for precise alignment or, alternatively, allows determination of properties as a function of

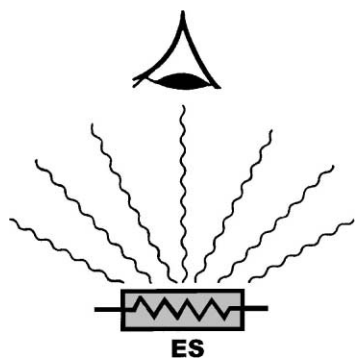


Fig. 76. The principles of emission spectroscopy [390].

position on a sample. No sample preparation is required and the sample is the source, alleviating the need of a conventional source. Modern IR instruments are, however, exceptionally good in these areas, making it possible to obtain an IR emission spectrum very rapidly with high signal-to-noise ratio even when the sample temperature is only slightly above the detector temperature. Even high signal-to-noise ratio IR emission data are complex. The complexity is due to the many parameters that affect the data. Sample composition, thickness, refractive index, and geometry influence the data.

This spectroscopic technique is not popular in the catalytic research, and in the last years only few examples can be found [701]. Bodis et al. [702] have applied emission FT-IR (FT-IRES) for studying adsorption of CO on dark metal powders (Pt, Pd, Rh) and supported catalysts (Rh/C) (see Fig. 77).

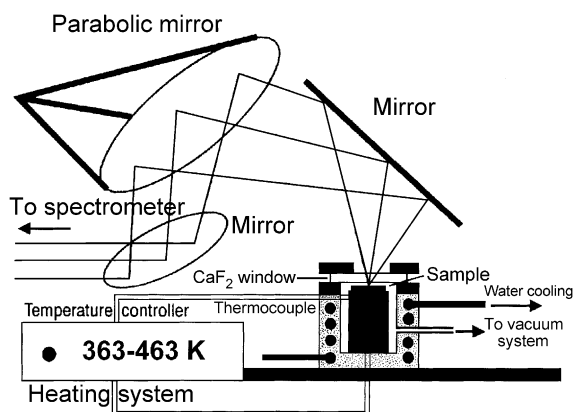


Fig. 77. Experimental set-up for FT-IRES measurements [702].

Frost and Klopogge [703] have used both IR absorption and emission spectroscopy to assign the vibrational bands of brucite ($\text{Mg}(\text{OH})_2$). IR emission bands were observed at 3686, 3571, 3251, and 2940 cm^{-1} . The intensity of these bands decreases upon thermal treatment corresponding to the dehydration and dehydroxylation of the brucite. Low-frequency IR emission bands were observed at 876, 706, 622, and 559 cm^{-1} . IR emission spectroscopy enabled the study of the dehydroxylation in situ at the elevated temperatures (473–1023 K), and also confirmed the absorption bands assigned to brucite. The same authors by means of thermogravimetric analysis and IES have studied the thermal behaviour of synthetic Mg-, Ni- and Co-hydrotalcite catalyst [704]. The Mg-hydrotalcite IRES shows major changes around 623–673 K indicating the end of the dehydroxylation (Fig. 78).

In this temperature range, Al–OH bands disappear and some new bands are observed indicating the formation of spinel (MgAl_2O_4) together with MgO, which is another product formed after dehydroxylation. Similar results are obtained for the Co-hydrotalcite, which shows the formation of CoAl_2O_4 spinel and/or cobalt oxide. IRES supports the reaction of Ni-hydrotalcite to a NiAl_2O_4 spinel phase + NiO and not $\text{Al}_2\text{O}_3 + \text{NiO}$ (Fig. 79).

The dehydroxylation of alumina gels prepared from the hydrolysis of trisecbutoxyaluminium has been studied using a combination of differential thermal analysis and IR emission spectroscopy [705]. The alumina phases in the gel (gibbsite), the structure, and dehydroxylation of the gel was determined by FT-IR absorption and FT-IRES.

A spectral method (IES) to characterise thermal properties of silica aerogel was described [706].

8. Photoacoustic spectroscopy

Photoacoustic spectroscopy (PAS) measures a sample's absorbance spectrum directly with a controllable sampling depth and with little or no sample preparation (see Fig. 80). This rapid direct analysis capability is applicable to nearly all samples encompassing a wide range of absorbance strengths and physical forms. Among the other key features of PAS are that it is non-destructive, noncontact, applicable to

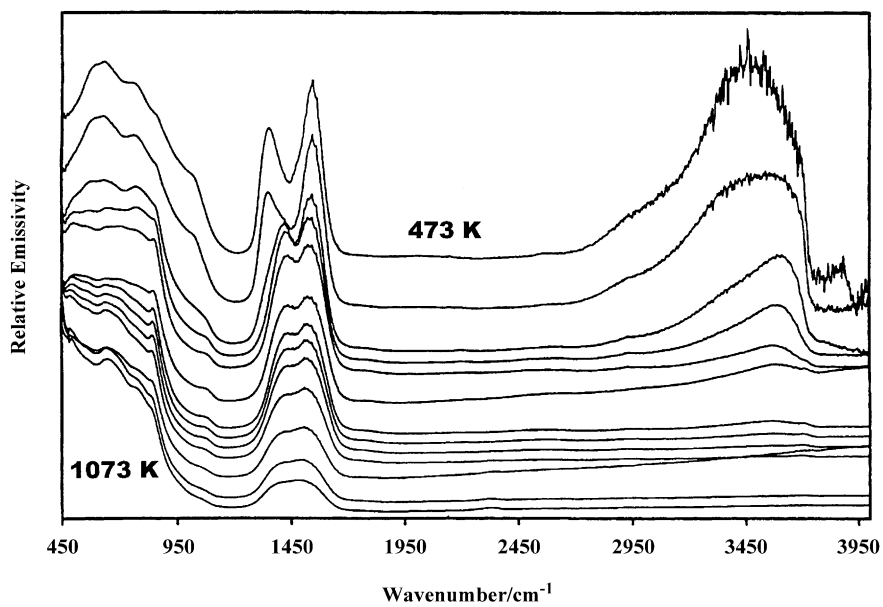


Fig. 78. IRES spectra of Mg-hydroxalcite from 473 to 1073 K at 50 K intervals [704].

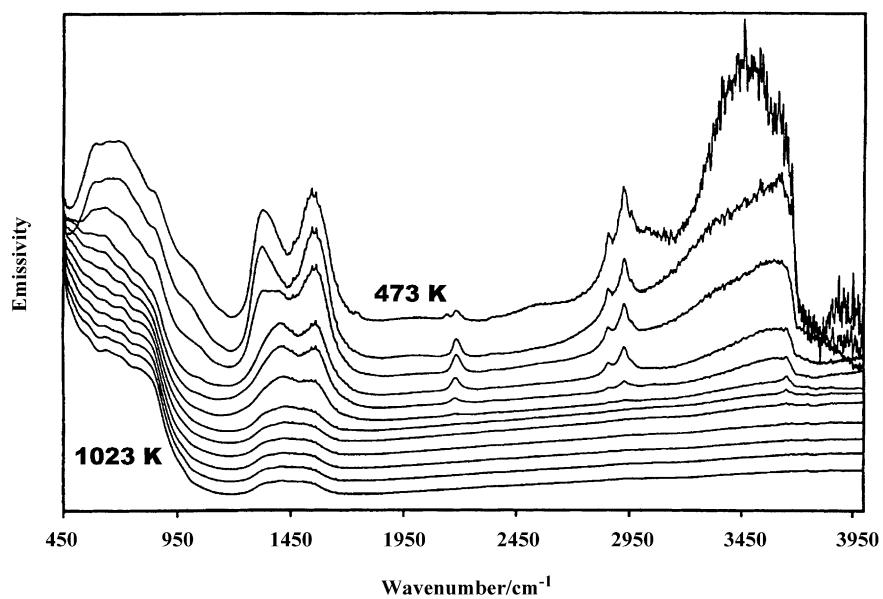


Fig. 79. IRES spectra of Ni-hydroxalcite from 473 to 1023 K at 50 K intervals [704].

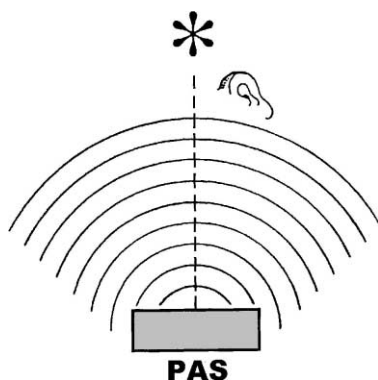


Fig. 80. The principles of photoacoustic spectroscopy [390].

macrosamples and microsamples, insensitive to surface morphology. It has a spectral range from the UV to far-IR, and is operable in photoacoustic absorbance, diffuse reflectance, and transmission modes, and is capable of measuring spectra of all types of solids without exposure to air or moisture. A commercial photoacoustic detector, which operates with all FT-IR manufacturer's instruments, is available [707]. There are no commercial reactor cells, which can operate under FT-IR/PAS measurements. In the literature it can be find single examples of such "home-made" reactors (Fig. 81) [708].

What you cannot see or see through you can sometimes hear. That is the idea behind PAS [709]. The practical aspects of using FT-IR photoacoustic spectroscopy (FT-IR/PAS) was reviewed [710] as well as quantitative applications of PAS [711].

The applications of photoacoustic/photothermal detection to molecular spectroscopy were reviewed, with special emphasis on the use of step-scan FT-IR/PAS for chemical analysis and depth profiling [712].

The development and applications of a photoacoustic phase theory for multilayer materials were discussed [713]. Several papers discuss depth profiling with a step-scan FT-IR and PAS detector, particularly focusing on the application of phase analysis [714–717]. Eyring et al. [718] have described application of PAS for catalyst surfaces. IR PAS of silica and aluminium oxide and study of the free hydroxyl group vibration of silica gel was described, too [719,720]. The interaction of $\gamma\text{-Fe}_2\text{O}_3$ powder with several adsorbates and their adsorption sites on the iron oxide surface was investigated [721]. The PAS absorption spectra of carbon dioxide were studied as a function of temperature [722]. Li et al. [723] have described organophosphorus compounds adsorption on heat-treated MgO. FT-IR/PAS and DSC studied the adsorption of pyridine on Cu–silica catalysts, with spectral changes correlating with the observed DSC scans [724]. Adsorbed pyridine was used to probe the acidic sites of a silica-supported Cu/MoO₃ catalyst in a study carried out by photoacoustic spectroscopy FT-IR/PAS [725,726]. Fejes et al. [727] have used FT-IR/PAS for the investigation of heat-treated isomorphously substituted ZSM-5 zeolites.

Hess and Kemnitz [728] have studied surface acidity of modified zirconium and titanium dioxides (Figs. 82 and 83). The nature of acid sites was determined by

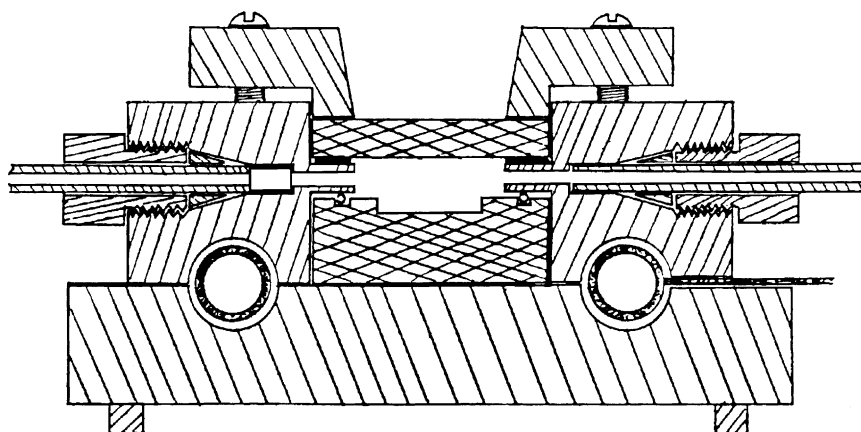


Fig. 81. Scheme of high-temperature PAS sample cell [708].

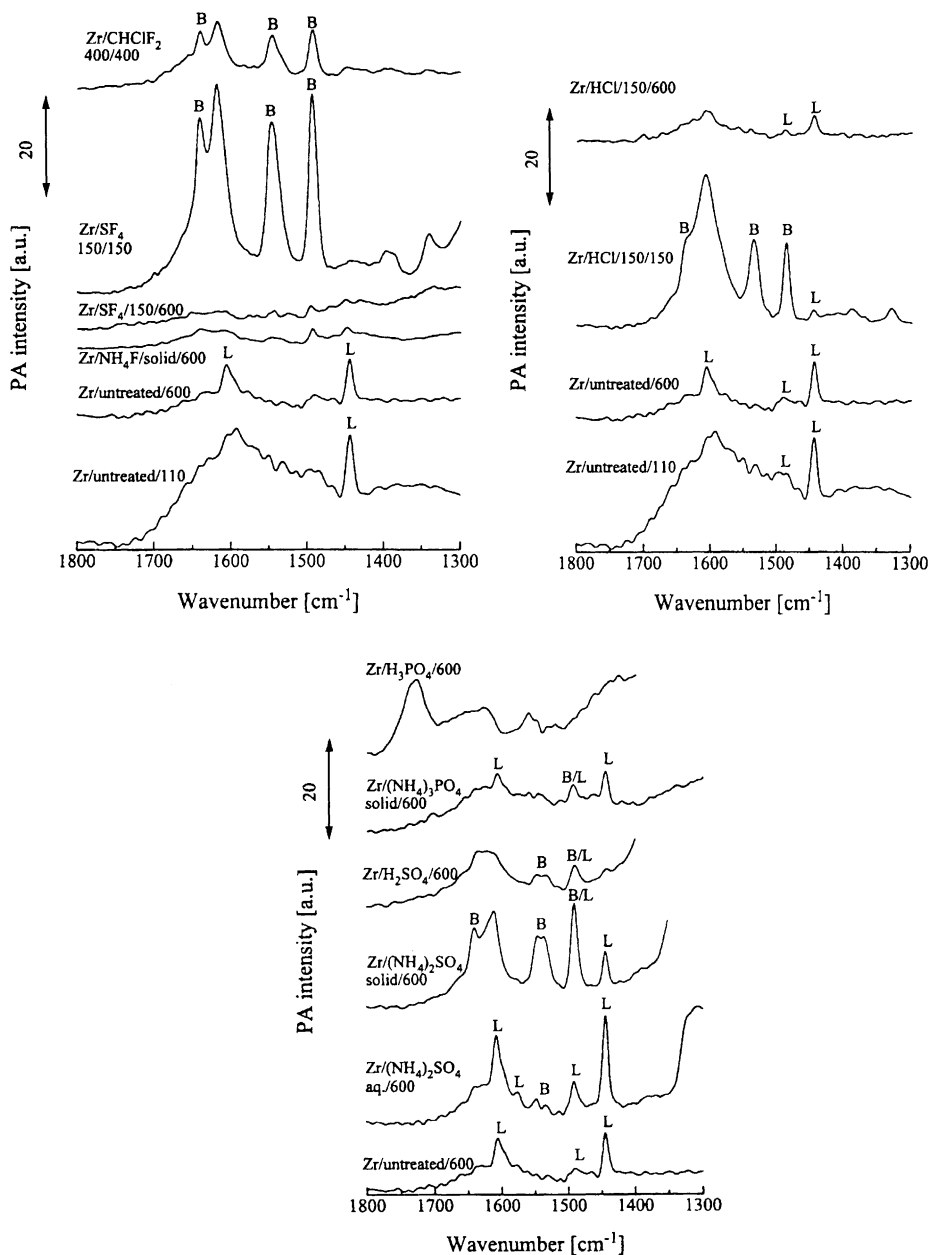


Fig. 82. FT-IR/PAS spectra of pyridine chemisorbed on modified ZrO_2 samples (L, B — pyridine chemisorbed on Lewis and Brønsted acid sites, respectively) [728].

FT-IR/PAS of pyridine adsorption and correlated with the catalytic behaviour.

Those studies are the continuation of those carried out earlier where in a similar way the acidity of

γ -alumina, α - Cr_2O_3 and β - AlF_3 samples was determined [729].

FT-IR/PAS was used to study the interaction of adsorbed EDTA with an alumina substrate [730]. A

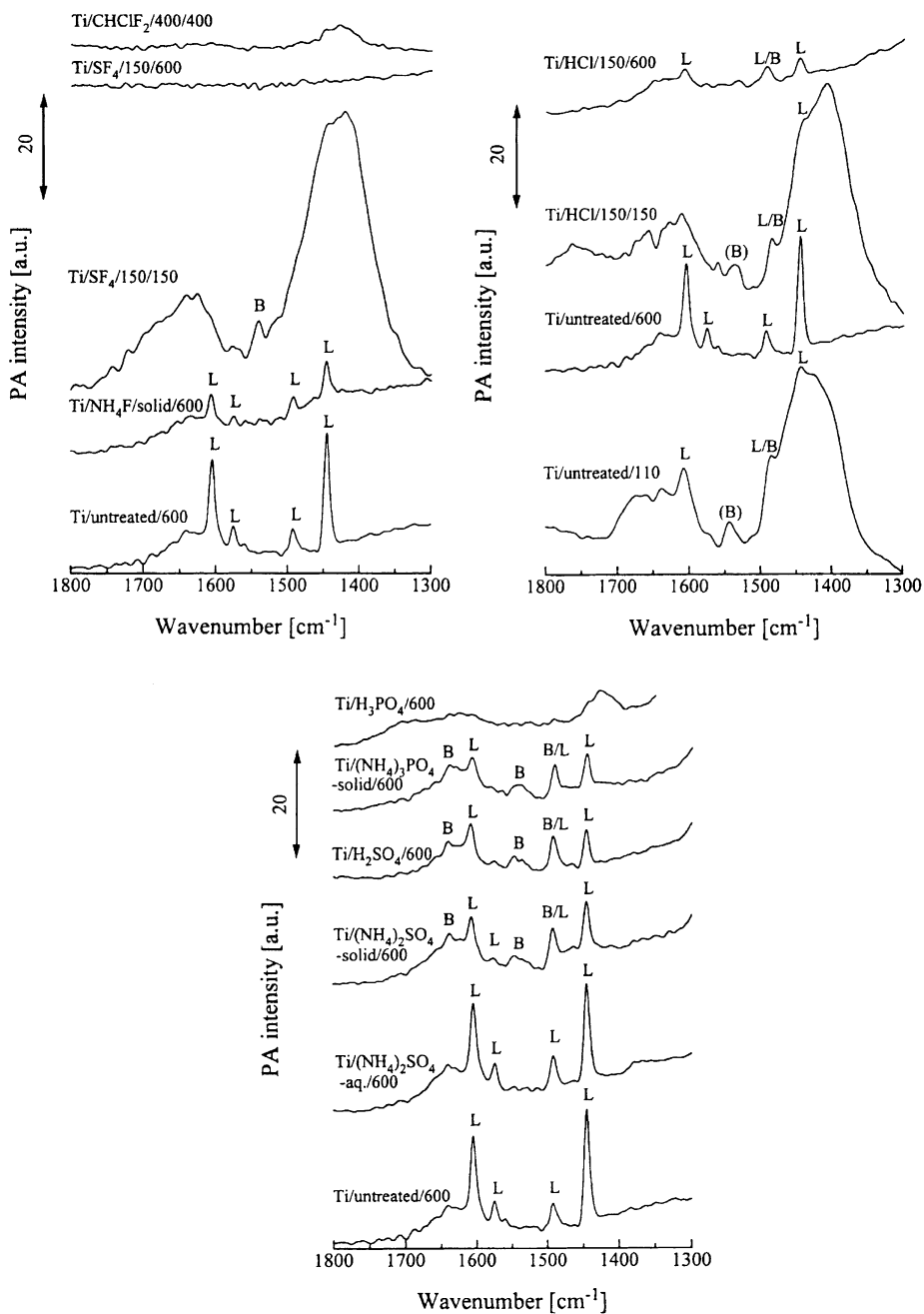


Fig. 83. FT-IR/PAS spectra of pyridine chemisorbed on modified TiO₂ samples (L, B — pyridine chemisorbed on Lewis and Brønsted acid sites, respectively) [728].

structure transition of ethanol on a silver surface was studied by IR laser PAS [731]. FT-IR/PAS is a useful tool for structural studies of hydrogen and/or oxygen chemisorption on the surface of diamond powders [732]. The polymerisation of pyrrole and thiophene on Cu- or Ni-exchanged mordenite was investigated using XPS and IR PAS. Depth-profiling experiments suggested differences in distribution of the polymers in the zeolite channels [733]. The adsorption of pyridine in the channel/cage of zeolites HZSM-5 and HY was studied [734]. FT-IR/PAS studies of the interaction between molybdenum and silica showed the formation of surface silanol groups. Molybdenum impregnation and pore structure were also discussed [735]. CO hydrogenation catalyst precursors prepared by rhodium and molybdenum carbonyls adsorption on zirconia were studied [736].

9. Hyphenated and miscellaneous IR techniques

Determination of molecular identities and quantities in complex mixtures may be the most common problem in chemistry. In most instances, the result of synthetic chemical operations is not a single product, but a distribution of multiple products. Because of the difficulty and importance of the task, multiple analytical techniques are combined to form what are often called hyphenated techniques. Combined analytical techniques utilising FT-IR have been employed for solid, liquid, and gas-phase samples. For solids, variations in composition over the spatial dimensions of the sample can be examined by FT-IR/microscopy. Examination of spectra of solid samples by microscopy is not always sufficient to provide enough information to characterise the sample fully. Further information can often be gained by studying the thermal properties and decomposition products of the sample with thermogravimetric FT-IR (TG/FT-IR). Thermogravimetric analysis (TGA) is used to measure the fraction of sample weight lost as a function of temperature and/or time. The loss of sample weight implies that some portion of the sample is evolved into the surrounding purge gas stream. Conducting the purge gas into an IR sampling cell often enables the identification of the evolved gases and provides insight into the sample thermochemistry.

Joo et al. [737] have studied migration and reduction of formate to form methanol on Cu/ZnO catalysts. Temperature-programmed IR (TPIR) spectroscopy of the copper formate/ZnO indicated the migration of the formate from copper to ZnO in the temperature range below 430 K at which the decomposition of the copper formate began. The experimental results elucidated the synergistic effect between copper and ZnO as well as formate migration onto ZnO and its hydrogenation to methanol on ZnO. The influence of Pt on Ce sulphation has been studied using thermogravimetry and IR spectroscopy [738]. IR experiments allowed concluding that the same sulphate species are formed on Pt/CeO₂ and CeO₂. The deactivation of sulphated zirconia catalysts in the isomerisation of *n*-butane has been studied using a combined TGA/FTIR technique [739]. Two types of sulphur were observed on the surface of deactivated sulphated zirconia catalysts. Deactivation appears to be intimately related to a sulphur species, which is evolved under a flow of N₂ at 873 K. Deactivated sulphated zirconia catalysts can be completely regenerated by selectively burning of the coke at 723 K in O₂. The loss of the sulphur, which is evolved at 873 K results in a catalyst, which is inactive in the isomerisation of *n*-butane [739]. Catalysts deactivated by the loss of this sulphur cannot be regenerated. TGA/FT-IR technique was applied to quantify the amount of carbon deposited during the isomerisation of *n*-butane [740]. As the authors pointed it out, the use of this technique offers distinct advantages in the determination of regeneration conditions. Rhodium surface states (Rh/Al₂O₃) and their adsorbates during NO–CO reaction have been characterised by the in situ IR coupled with TPR technique [741].

Parts a–c of Fig. 84 show the IR spectra of adsorbates, variation in adsorbate intensity with temperature, and variation in the rates of NO conversion and N₂O and CO₂ formation with temperature during the TPR. Flowing NO/CO at 323 K over the prerduced catalyst produced linear CO [Rh⁰–CO] at 2060 cm⁻¹ and bent NO [Rh⁰–NO⁻] at 1706 cm⁻¹ during the first 0.96 min. An increase in the NO/CO exposure time increased the Rh⁰–CO intensity and resulted in the emergence of gem-dicarbonyl [Rh⁺(CO)₂] at 2085 and 2020 cm⁻¹, nitrate species [NO³⁻] on Al₂O₃ at 1617 cm⁻¹, and RhNCO at 2145 cm⁻¹. Following prolonged exposure of the catalyst to 0.5%

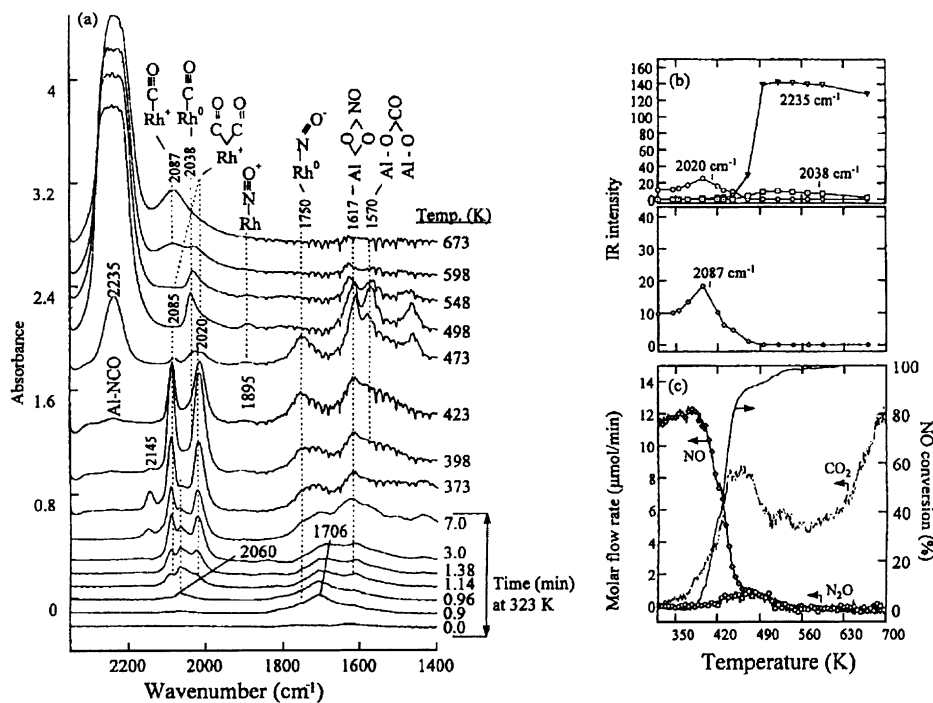


Fig. 84. Experimental results of NO–CO reaction over Rh/Al₂O₃ catalyst: (a) IR spectra of adsorbates during the temperature-programmed reaction of the 0.5% NO/0.5% CO (60 cm³/min) flow at 10 K/min; (b) adsorbate intensity versus temperature; (c) rate of NO conversion and N₂O and CO₂ formation versus temperature [741].

NO/0.5% CO flow at 323 K, Rh⁺(CO)₂, Rh⁰–CO, Rh⁰–NO[–], Rh⁰–NCO, and NO^{3–} approached a steady-state level. Absence of CO₂ during the formation of various adsorbates such as Rh⁺(CO)₂ and NO^{3–} suggests that Rh⁰–O produced from NO dissociation provides adsorbed oxygen for oxidising Rh⁰ to Rh⁺ and forming NO^{3–} species. An increase in the reaction temperature led to an increase in NO conversion and N₂O/CO₂ formation as well as variation in the intensities of Rh⁰–NCO, Rh⁺(CO)₂, Rh⁰–CO, Rh⁰–NO[–], and NO^{3–}. Variation in the intensities of NO and CO adsorbates with temperature and reactant partial pressures indicates the dependence of the redox reaction cycle on temperature and reactant partial pressures [741].

In situ IR and mass spectroscopy (MS) coupled with temperature-programmed reaction (TPR), isotopic temperature-programmed desorption (TPD), step transient, and pulse transient techniques have been used to study the dynamic behaviour of adsorbed species in the NO decomposition reaction on over-

and underchanged Cu-ZSM-5 [742]. It was found out that overchanged Cu-ZSM-5 possessed more Cu⁺ sites, exhibited higher activity and generated Cu⁺ sites at lower temperatures than underchanged Cu-ZSM-5. Both produce similar adsorbates that differ in the rate of formation at different temperatures. The steady-state surface concentrations of adsorbed methoxy intermediates (formed during methanol oxidation) on monolayer catalysts of V₂O₅/(TiO₂, CeO₂, Al₂O₃, and ZrO₂) have been quantified with in situ IR/MS (Figs. 85 and 86) [743].

The direct catalytic decomposition of NO on Rh/Al₂O₃, Rh/C, Pd/Al₂O₃, and Pd/C catalysts was investigated at 673 K by in situ IR coupled with mass spectroscopy MS [744]. NO decomposition on these catalysts initially produced N₂ and adsorbed oxygen. Different catalysts exhibit different capabilities for manipulating adsorbed oxygen. Rh/Al₂O₃ shows little activity for oxygen desorption, resulting in loss of catalyst activity. NO decomposition on Rh/Al₂O₃ produced N₂ initially. As oxygen on the surface

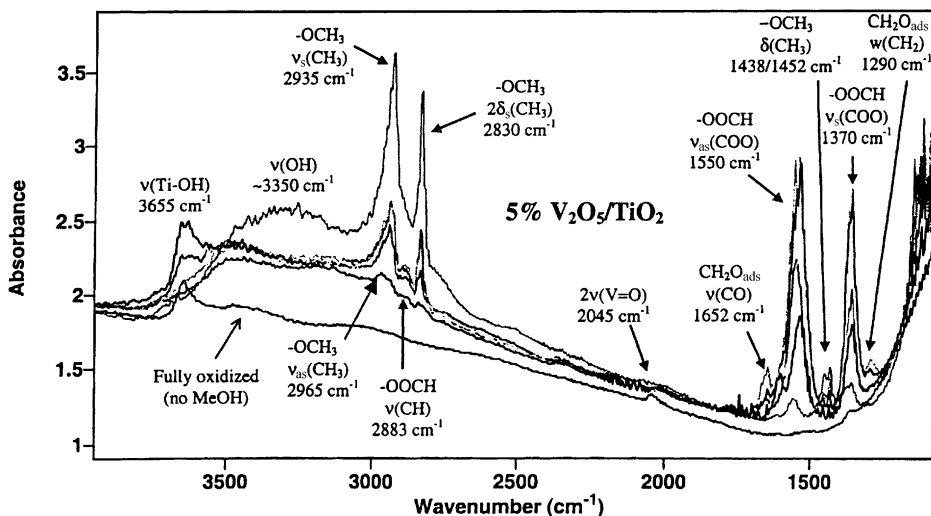


Fig. 85. In situ IR spectra of 5% V_2O_5/TiO_2 during methanol oxidation as a function of temperature (lowest temperatures on top: 373 K, 473 K, 498 K, 523 K, 548 K, and 573 K) [743].

accumulated, $Rh-NO^+$ at 1893 cm^{-1} and $Rh-NO^-$ at 1644 cm^{-1} developed. Rh/C shows the ability for promoting the adsorbed oxygen-carbon reaction, removing oxygen in the form of CO_2 . The adsorbed oxygen on the metal migrated to the support, resulting in development of C-O stretches at 1402 cm^{-1} , which served as the precursor adsorbate for CO_2 formation.

Pd/Al_2O_3 shows some activity for O_2 desorption. As oxygen on the surface accumulated, $Pd-NO^+$ at 1802 cm^{-1} developed (Fig. 87).

Uses of carbon as a support for Pd promotes O_2 desorption, resulting in improvement of NO decomposition activity. The in situ IR results provide evidence to support the behaviour of adsorbed oxygen

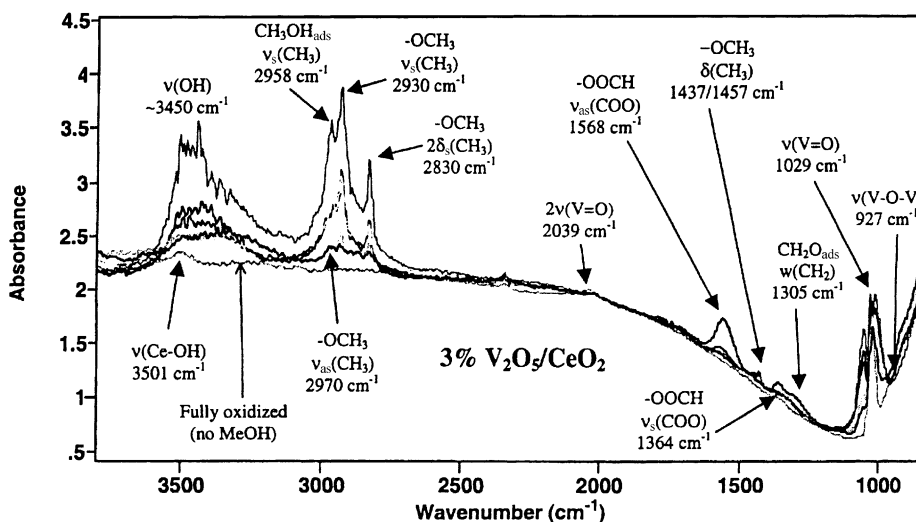


Fig. 86. In situ IR spectra of 3% V_2O_5/CeO_2 during methanol oxidation as a function of temperature (lowest temperatures on top: 373 K, 473 K, 498 K, 523 K, 548 K, and 573 K) [743].

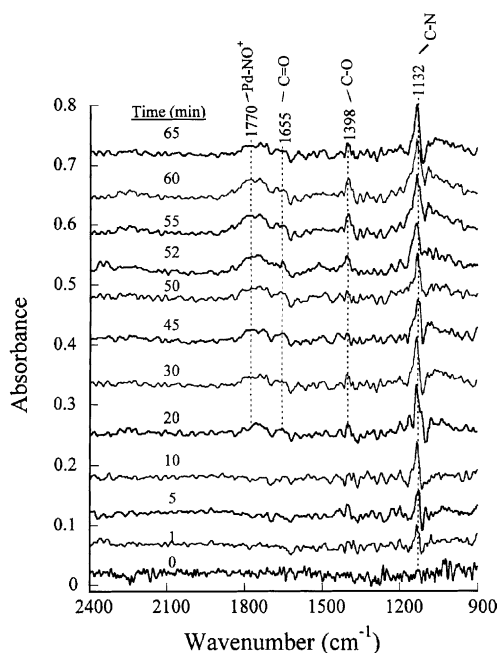


Fig. 87. IR spectra of adsorbates during the step switch from He to 1% NO on Pd/C at 673 K [744].

on carbon-supported Rh and Pd catalysts. Chi and Chuang [745] have studied NO adsorption and reduction with C_3H_6 in the presence of oxygen over CuO/Al_2O_3 . Adsorption IR coupled with MS allows the determination of the dynamic behaviour of adsorbate and product formation during NO/O_2 adsorption, decomposition, and $NO/O_2/C_3H_6$ reaction. Adsorption of NO (CO) and displacement by CO (NO) has been investigated at 523 K on Rh catalysts supported on undoped and W^{6+} -doped TiO_2 , employing transient MS and FT-IR techniques [746]. It is found that, under the experimental conditions employed, four kinds of nitrogen oxide species may coexist in the adsorbed mode, namely, $Rh-NO^-$ (high), $Rh-NO^-$ (low), $Rh(NO)_2$, and $Rh-NO^+$, giving rise to IR bands located at 1770, 1660, 1830/1725, and 1908 cm^{-1} , respectively. Both negatively charged species readily dissociate on reduced surface sites, yielding nitride, and are mainly responsible for N_2 formation in the gas phase. The dinitrosyl species, the formation of which is favoured over partially oxidised surfaces, is related to the production of N_2O . The formation of both N_2 and N_2O requires the presence of reduced surface sites. In the absence of Rh^0 , dissociative adsorption

of NO stops and $Rh-NO^+$ species dominate the catalyst surface. Doping TiO_2 with W^{6+} cations alters the electronic properties of supported Rh crystallites and, concomitantly, the chemisorptive behaviour of the catalyst toward NO and CO. IR coupled with MS allows determination of the form of NO_x storage during NO/O_2 adsorption [747]. NO/O_2 adsorbed as bridging and chelating bidentate nitrates and monobidentate nitrate on Tb_4O_7 , La_2O_3 , and BaO, and as a bridging bidentate nitrate and monodentate nitrate on MgO via the reaction of adsorbed NO with adsorbed oxygen at 298 K. NO/O_2 coadsorbed as a chelating bidentate nitrate on Tb_4O_7 and La_2O_3 , and as a distinctive bridging bidentate nitrate on BaO and MgO via the reaction of adsorbed NO with surface lattice oxygen at 523 K.

Combined in situ IR and online mass spectrometric studies provided simultaneous information of the adsorbed species on $V_2O_5-TiO_2$ catalysts and the composition of the reaction products during the selective catalytic reduction of NO [748]. During the studies of the influence of Rh and Ce promotion of automotive Pd catalyst on its catalytic behaviour under steady state and dynamic operation of FT-IR and MS has been applied [749]. This combined use allowed simultaneous monitoring of the exhaust components.

A combined NMR and in situ IR spectroscopy catalytic study of the conversion of allyl alcohol over zeolite catalysts was reported [750]. The reactivity of adsorbed NO and CO was studied using combined in situ IR spectroscopy and mass spectrometry on Rh/SiO_2 catalysts [751].

Steady-state isotopic transient kinetic analysis (SSITKA) coupled with in situ IR allows determination of rate coefficients, elementary rate constants, surface coverages, and residence times of surface intermediates during heterogeneous ethylene hydroformylation over $Mn-Rh/SiO_2$ catalyst [752].

Temperature-programmed desorption spectroscopy and IRAS were used to study the decomposition of vinyl iodide on Pt(111) surfaces [753]. Cylindrical internal reflection spectroscopy was found to be useful for study of hydroformylation catalysis [754].

Time-resolved FT-IR studied the isotopic exchange of dinitrosyl species adsorbed on a Co-MFI zeolite and gas-phase NO [755]. The interaction of carbon dioxide with alkali modified surfaces to form oxalate intermediates was studied by in situ time-resolved IR

spectroscopy [756]. Picosecond and femtosecond IR techniques were used to characterise energy transfer at surfaces [757]. Time-resolved FT-IR microscopy was used to study in situ the transport and sorption of toluene in individual zeolite ZSM 5 crystals [758] and pyridine in H-ZSM-5 and H-mordenite zeolites [759]. The response of CO adsorbate to heating of the Cu(100) substrate was monitored by picosecond time-resolved FT-IR [760]. The time dependence of vibrational relaxation of deuterated hydroxyls in acidic zeolites and dynamical studies of zeolitic protons and adsorbates was studied by picosecond time-resolved IR [761,762]. Using conventional absorption and picosecond double-resonance spectroscopy in the IR, the reaction kinetics of weak hydrogen bonds in liquids was studied [763]. Laser-induced desorption and interconversion of linear and bridge bonded carbon monoxide on Pt(100) has been studied [764].

10. Second-harmonic generation

Second-harmonic generation (SHG) and sum-frequency generation (SFG) are two second-order nonlinear optical spectroscopy techniques that, because of their high surface specificity, have recently become the important tools for the study of surfaces and interfaces [765–771].

Unlike traditional FT-IR, SFG is sensitive only to interfaces and requires no bulk subtraction. SFG has many advantages over FT-IR with respect to surface/interface studies. This is primarily due to the fact that SFG is forbidden to occur except at the interfacial region making it a true surface sensitive technique. On the other hand, FT-IR requires a bulk subtraction in order to extract surface information. The advantages of SFG are the following:

- provides the IR vibrational spectrum of surface species;
- sub-monolayer surface sensitivity;
- no bulk contributions/ultrahigh vacuum is not required;
- in situ and non-destructive;
- sub-picosecond time resolution for real-time probing of fast surface dynamics;
- good spatial and spectral resolution.

Among the various optical spectroscopies utilised to probe surfaces and interfaces, second-order nonlinear optical techniques have gained wide recognition for their ability to determine the electronic and vibrational structure and dynamics of surfaces. The study of buried interfaces using these techniques offers several significant advantages over conventional surface spectroscopies. The material damage and contamination associated with charged particle beams is eliminated; all pressure ranges are accessible; insulators can be studied without the problem of charging effects; and solid/solid interfaces are accessible owing to the large penetration depth of the optical radiation. Non-invasive, in situ characterisation of thin films, surfaces and interfaces in all pressure regimes is important in the development of new materials and new growth processes.

SHG and SFG are potentially interface-specific at non-destructive power densities. This is most easily seen for centrosymmetric materials, such as metals and elemental semiconductors. In the standard multipole expansion of fields, the electric dipole term is parity-forbidden for such materials, leaving only higher order, non-local contributions (magnetic dipole and electric quadrupole effects). At a surface or interface, the bulk symmetry is broken and electric dipole effects are allowed. Cross-sections for SHG and SFG processes are small, giving typically one signal photon per 10^{13} – 10^{17} incident photons [772]. When large field gradients are present at the surface or interface higher-order second-harmonic (SH) or sum-frequency (SF) signals can be generated in the bulk which are comparable in size to the interface signal.

Excellent reviews and basic principles of SHG and SFG applied to thin films, surfaces and interfaces have been published [773–786]. Heinz [787] has discussed the phenomenology of surface and bulk effects in centrosymmetric media and McGilp [788] has presented a general review of optical techniques for surface and interface characterisation. Surface spectroscopy by nonlinear optics and nonlinear spectroscopy for molecular structure determination has been reviewed by Shen [774,789]. The unique feature of IR–Vis SFG spectroscopy lies in the fact that it enables to perform vibrational spectroscopy on chemical species located specifically at surfaces and interfaces [790–794].

In situ SFG surface vibrational spectroscopy for different polarisation arrangements has been employed

along with low-energy electron diffraction (LEED) measurements and kinetic modelling calculations to study NO adsorption on Pt(111) as a function of NO gas-phase pressure ($p_{\text{NO}} = 10^{-9}$ – 10^{-4} mbar) and substrate temperature ($T_s = 300$ – 400 K) [782]. The observation of a NO stretching vibrational band with a frequency of 1724 cm^{-1} with different signal intensities for ssp and ppp polarisation combinations indicated the presence of tilted NO species at high NO coverages ($\theta \geq 0.5$). At lower coverages ($0.5 > \theta > 0.25$), the adsorption geometry was found to change towards upright NO giving rise to a vibrational band with slightly lower frequencies of 1716 – 1720 cm^{-1} . Experiments were carried out using the SFG spectrometer in a reaction chamber (Fig. 88).

SFG has been used to monitor pressure-dependent changes in the chemisorption of CO and NO over Pt(111) [796]. Bonding which is similar to that in $\text{Pt}_m(\text{CO})_n$ (where $n/m > 1$) clusters and for an incommensurate CO overlayer was observed above 0.01 MPa. Reaction intermediates that form during ethylene, propylene, and *iso*-butene hydrogenation, as well as CO oxidation, at atmospheric pressures and 300 K were monitored by SFG. The dominant reacting species that hydrogenate are the weakly π -bonded olefins, while the strongly chemisorbed alkylidyne and di- σ bonded species are spectators during the reaction. From quantitative measurement of coverages, the absolute turnover rates can be determined.

Adsorption of CO and NO on NiO(111) thin films epitaxially grown on Ni(111) substrate has been studied by IR–Vis SFG and the results were compared with those of infrared reflection absorption spectroscopy (IRAS) [797]. From SFG measurements, the C–O stretching band of adsorbed CO was observed at 2144 cm^{-1} for both p- and s-polarised visible (532 nm) light whereas the adsorbed NO gave the N–O stretching band at 1800 cm^{-1} only for the p-polarised visible light. These observations suggested that the CO molecule was inclined to the surface whereas the tilt angle of NO from the surface normal was smaller than that of CO. The adsorption sites of CO and NO molecules are located on the slopes of trigonal microfacets formed by the reconstruction of the NiO(111) surface. CO adsorbed on Ni(111) instead of NiO(111) was also examined: the SFG signal corresponding to the C–O stretching mode of linearly bonded CO was observed at 2076 cm^{-1}

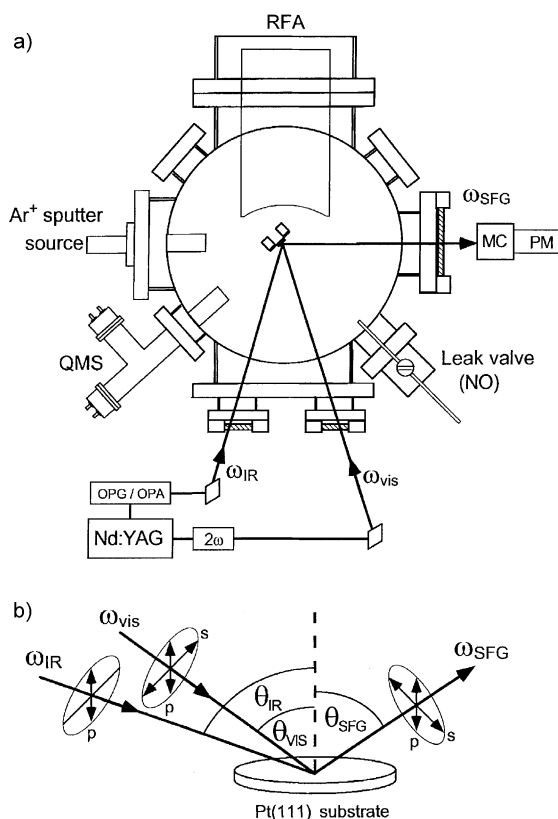


Fig. 88. (a) Schematic diagram of the experimental set-up used for the detection of adsorbed NO on a Pt(111) single-crystal via IR–Vis SFG (RFA: retarding field analyser for Auger electron spectroscopy — AES and low-energy electron diffraction — LEED; QMS: quadrupole mass spectrometer; OPG: optical parametric generator; OPA: optical parametric amplifier). (b) Schematic description of the optical arrangement and the possible excitation/detection polarisation configurations in SFG surface vibrational spectroscopic studies on metal substrates [795].

only for the p-polarised visible light, but that of the bridge-bonded one (at saturation coverage) was not detected by SFG (Fig. 89).

The results of the nonlinear least-squares fit of the experimental data are given by solid lines in Fig. 89(a). It is shown clearly that the asymmetric profile of the SFG signal is due to the interference between the vibrationally resonant and non-resonant terms. It was noted that the non-resonant SFG signal was slightly different between the bare NiO(111) surface and CO-adsorbed surface. It was suggested that the electronic state of the surface changed by

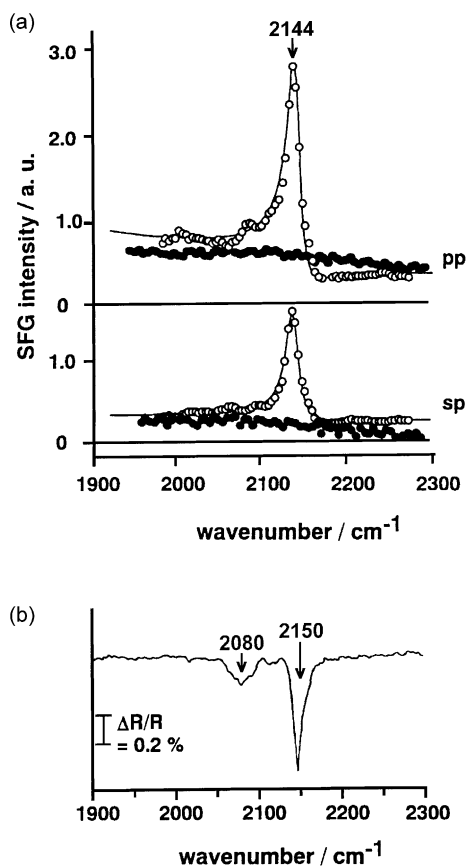


Fig. 89. (a) SFG spectra of CO adsorbed on NiO(111) at 140 K under a continuous flow at 1.33×10^{-5} Pa. The first and second letters in abbreviations pp and sp denote the polarisation directions of Vis (532 nm) and IR lights, respectively. (b) IRAS spectrum of CO adsorbed on NiO(111) after exposure to the saturation coverage of CO (eight layers) at 140 K [797].

the CO adsorption to give the change in the nonresonant SFG signal. The frequency of 2144 cm^{-1} as the CO vibration is in line with IRAS observation (Fig. 89(b)), where the IRAS band at 2150 cm^{-1} is assigned to the C–O stretching mode of CO adsorbed on fully oxidised Ni^{2+} sites of the surface. The SFG spectra did not give the signal around 2080 cm^{-1} , which arises from the CO on less-oxidised sites. The reason for the absence of the 2080 cm^{-1} band on the SFG spectra is ascribed to either the smaller value of the Raman tensor or the smaller number of associated CO molecules, since the intensity of the SFG signal is proportional to the square of the molecular density instead of the linear dependence of IRAS signal.

The combination of a laser-induced temperature jump and subsequent observation by time-resolved SFG spectroscopy enabled to verify the decomposition route of formate on the NiO(111) and Ni(111) surfaces [798]. The transformation of the bidentate/bridging formate to unstable monodentate formate occurred at the instant of irradiation and the feature was ascribed to the shift of the chemical equilibrium caused by the rapid laser-induced temperature jump at the surfaces.

The time-resolved SFG spectroscopy has been applied to the CO/Ni(111) and CO/NiO(111)/Ni(111) systems under the irradiation of picosecond UV and visible laser pulses [799]. The UV irradiation resulted in a highly efficient excitation of molecular vibration of the adsorbed CO, and the transient responses of both the fundamental and hot band signals suggested that the excitation arose from an electronically driven process; the involvement of hot electrons in the excitation of the CO internal stretching mode was proposed (Fig. 90).

A possible mechanism for the process was transient-negative ion resonance. The features induced by the irradiation of visible pulses to CO/Ni(111) were different and were ascribed to a thermal process.

Yuzawa et al. [800] have studied the polarisation characteristics from SFG spectra of clean and regulatively oxidised Ni(100) surface adsorbed by propionate and formate. Both propionate and formate

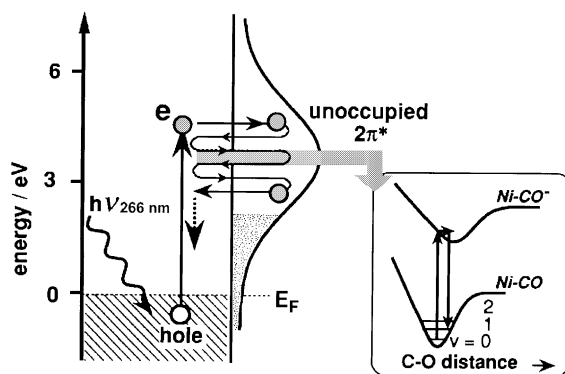


Fig. 90. Possible scheme for the UV-induced transient vibrational excitation of adsorbed CO on Ni(111) surface. A photogenerated hot electron in the metal moves into the $2\pi^*$ level leading to the formation of a temporary negative ion state. The inset illustrates how the internal stretching mode of adsorbed CO is excited during the scattering of the electron [799].

give signals only for p-polarised visible pulses on clean metal and oxygen-saturated surfaces, but signals due to s-polarised visible pulses appeared from the propionate-covered surface as soon as the surface was covered with a monolayer of NiO(100). Vibrational peaks of propionate were located at 2887, 2945, and 2988 cm^{-1} and were assigned to the symmetric stretching mode of CH_2 group, the symmetric stretching mode of CH_3 group, and the degenerate stretching mode of CH_3 group, respectively. The peak of the surface formate was located at 2948 cm^{-1} on the clean metal surface, but another band appeared at 2860 cm^{-1} on oxide-layered surfaces.

Optical IR–Vis SFG vibrational spectroscopy is one of the few surface-specific techniques that can operate in a pressure range from ultrahigh vacuum to ambient conditions [801]. Due to its inherent surface sensitivity and pressure independence, SFG is particularly suited for in situ studies of adsorbates or surface species at elevated pressure or during a catalytic reaction. Rupprechter et al. [801] have described the design of an SFG compatible elevated pressure reactor that was attached to an ultrahigh vacuum surface analysis chamber (Fig. 91).

After preparation and characterisation in UHV, model catalysts can be transferred in vacuum into the reaction cell. The authors have studied the adsorption of CO and NO on Ni and NiO(100) surfaces at low coverages.

SFG determines the changing adsorbate structure as a function of pressure through pressure ranges where other spectroscopic techniques cannot operate. Corrosive chemisorption of CO has been observed along with adsorbate-induced restructuring of the metal surface as the equilibrium shifts toward the possible formation of multiple carbonyl-metal bonds [802]. Several reaction intermediates, and adsorbed species that inhibit the reaction, are detectable during CO oxidation below and above the ignition point. SFG studies of hydrogenation and dehydrogenation of cyclohexene indicate that dehydrogenated cyclohexadiene isomers are important catalytic reaction intermediates and that their altered surface concentration on the Pt(100) surface as compared to the Pt(111) crystal face explores the surface structure sensitivity of dehydrogenation. The combined application of scanning tunnelling microscopy (STM) and SFG at high pressures permits us to bridge the

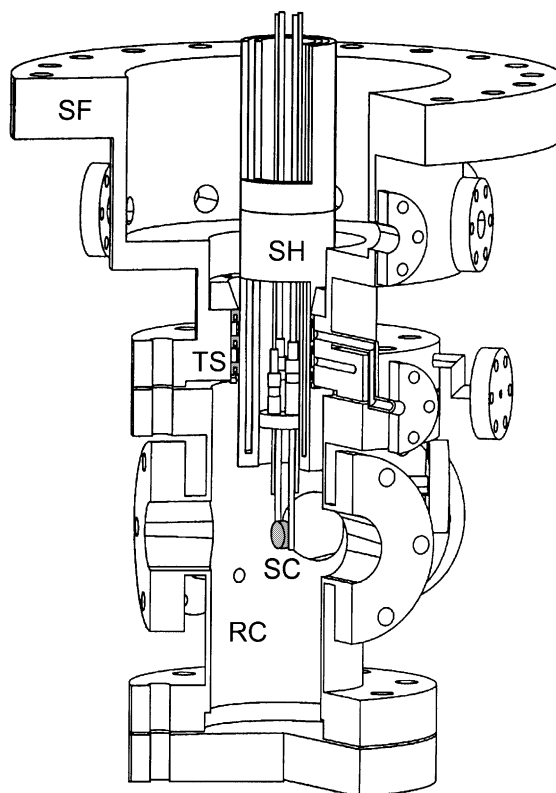


Fig. 91. Cross-section of the SFG-compatible reaction cell: SH — sample holder; SF — sealing flange; TS — Teflon seals; RC — reaction cell; SC — single crystal [801].

pressure gap in surface science and catalytic reaction studies using single crystal surfaces [802].

Su et al. [803] have presented the SFG spectra of CO on Pt(111) as a function of pressure and showed evidence for the reversible formation of carbonyl clusters with a CO/Pt ratio of >1 and for an incommensurate CO layer at high pressures. These species turn over rapidly to produce CO_2 during CO oxidation. Sum frequency spectroscopy was used in an attempt to detect the platinum–carbon vibration of CO adsorbed on Pt(111) [804]. Olefin hydrogenation and CO oxidation over the (111) crystalline face of Pt [805]. Based on the results obtained the authors have presented propylenic moieties formed on Pt(111) and possible reaction pathways for propylene hydrogenation as well as a schematic representation of the hydrogenation of ethylidyne, propylidyne, and isobutylidyne to their respective alkylidenes.

SFG and IR absorption spectra of CO adsorbed on Pd(111) were reported [806]. Adsorption of CO in the surface temperature range 150–230 K results in the appearance of extra peaks in the spectral range of the CO stretching vibration. The conditions of appearance of these peaks, and their stability, were investigated. The extra peaks are assigned to sites at antiphase domain boundaries, in which CO is less bonded than in the regular sites of the domains.

IR–Vis SFG was applied for the first time to monitor CO stretching vibrations on alumina-supported Pd nanoparticles in a pressure range from 10^{-7} to 200 mbar [807]. The adsorption behaviour of Pd aggregates with 3 and 6 nm mean size was dominated by surface defects and two different adsorption sites (twofold bridging and on-top) were identified. The CO adsorption site occupancy on Pd nanocrystals was mainly governed by the gas-phase pressure while the structure of the particles and their temperature had a smaller influence.

Broadband IR SFG spectroscopy was used to investigate the CO-stretch vibration of CO chemisorbed on a Ru(001) surface at coverages as low as 0.001 monolayers (MLs) [808]. Due to the high intensity of the broadband-IR pulses, the $\nu = 1 \rightarrow 2$ hot band of the CO-stretch vibration of CO on pure and oxygen-covered Ru was observed for the first time. The authors have shown that broadband IR SFG can be used to study adsorbates with high sensitivity.

Using time-resolved sum-frequency generation spectroscopy, the C–O stretch vibration of CO adsorbed on a single crystal Ru(001) surface was investigated during femtosecond near-IR laser excitation leading to desorption (Fig. 92) [809].

It was demonstrated for Co/Ru(001) that ultrafast energy transfer at an adsorbate-covered metal surface can be studied by recording vibrational spectra of the adsorbate under conditions where reaction is occurring. Experiments carried out open the way for observing chemical reactions in real time through the vibrations of reactants at the surface and for testing the concept of thermal equilibrium underlying the theory of rate process [809].

SFG was used for in situ detection of CO during heterogeneous oxidation and chemisorption of carbon monoxide on a polycrystalline platinum foil [810,811]. High-pressure CO oxidation on Pt(111) monitored

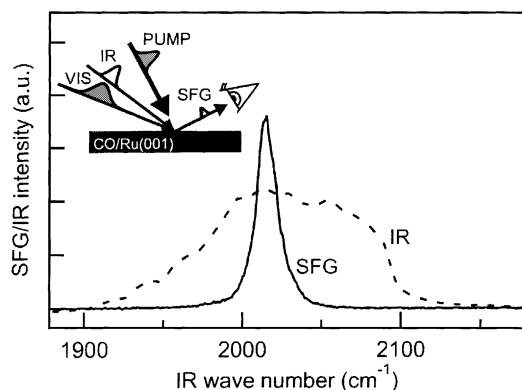


Fig. 92. SFG spectrum of the C–O stretching vibration of $(\sqrt{3} \times \sqrt{3})$ -CO/Ru(001) (14.3 cm^{-1} full peak width at half maximum — FWHM) at 340 K and the spectrum of the 150 fs broadband IR pulse (dashed line) [809].

with IR–Vis SFG [812]. Adsorption and desorption of CO on W(110) has been studied [813].

The laser-induced desorption of CO from Pd(111) at 308 and 532 nm was compared to the thermal desorption by recording FT-IR and SFG spectra of the CO molecules remaining on the surface [814]. There is no photodesorption from a fully ordered CO layer. However, when the CO layer is adsorbed below 270 K, extra sites (assigned to antiphase domain boundaries) appear in addition to the normal sites (assigned to domains), and the photodesorption occurs selectively from the extra sites.

One of the great advantages of vibrational SFG spectroscopy was the application to the investigation of chemical processes taking place on the surfaces of single crystalline oxides, a task which is usually difficult to achieve by other techniques (e.g., IRAS). Domen and Hirose [815] have presented several applications of IR laser pulses to study the kinetics and dynamics of surface chemical reactions (e.g., C_2H_4 on Rh(111) and Pt(111), HCOOH on MgO) (see Fig. 93).

A spectroscopic study of adsorbed CO on Ni(111) was carried out using IR–Vis SFG and IRAS [816]. An anomalous coverage-dependence of the SFG signal intensities of bridged and linear CO was found.

Ethylene hydrogenation on Pt(111) was monitored in situ at high pressure using SFG [817]. SFG has been utilised to monitor the surface species present on platinum and rhodium crystal surfaces during catalytic

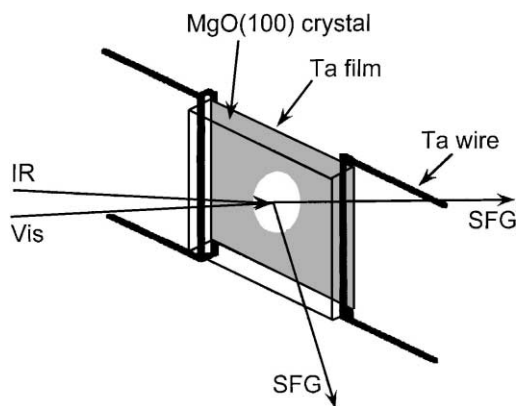


Fig. 93. A sketch of the MgO(100) sample used for the SFG and TPD measurements [815].

reactions at atmospheric pressures [818]. Ethylene hydrogenation to ethane, cyclohexene hydrogenation to cyclohexane and its dehydrogenation to benzene and carbon monoxide oxidation to carbon dioxide have been studied. Strongly bound spectators, weakly bound reaction intermediates, and pressure-dependent changes in the chemical bonding of surface species have all been observed [818]. Examples of ethylene hydrogenation at high pressures over a Pt(1 1 1), CO adsorption on Pt(1 1 1) have been presented [819]. The conversion of di- σ -bonded ethylene ($-\text{CH}_2-\text{CH}_2-$) to ethylidyne ($\equiv\text{CCH}_3$) on the Pt(1 1 1) crystal surface was monitored with IR–Vis SFG in the $\nu(\text{CH})$ frequency range [820]. The spectra show that in addition to the CH_3 and CH_2 symmetric stretch features from ethylidyne and di- σ -bonded ethylene, respectively, there is a high frequency feature around 2957 cm^{-1} during the transformation process. The authors have assigned this feature to the CH_3 asymmetric stretch of ethylidene and/or ethyl. Therefore, there is a third stable species present on the surface during the conversion of di- σ -bonded ethylene to ethylidyne on Pt(1 1 1) [820].

Cremer et al. [821] have reported studies of propylene hydrogenation over Pt(1 1 1) crystal surfaces at atmospheric pressures and 300 K using SFG and STM. Four surface species (2-propyl, π -bonded propylene, di- σ -bonded propylene, and propylidyne) were identified; the first two being implicated as reaction intermediates. The platinum surface structure remains unchanged during the reaction, consistent with the

structure insensitive nature of olefin hydrogenation. Propylene decomposition-induced substantial surface reconstruction. Adsorption and oxidation of CO, hydrocarbon conversion such as ethylene hydrogenation and cyclohexene hydrogenation and dehydrogenation on Pt(1 1 1) has been presented [822]. The experiments demonstrate that the key intermediates of high-pressure catalytic reactions are not present under low-pressure ultrahigh vacuum conditions. Hydrogenation and dehydrogenation of *iso*-butene and cyclohexene on Pt(1 1 1) has been studied [823,824].

Ammonia–water complexes have been detected with SFG at the liquid/vapour interface of concentrated ammonia solutions [825]. SFG spectra taken with the ssp polarisation combination (s-polarised sum frequency signal, s-polarised visible light, p-polarised IR beam) were dominated by the N–H symmetric stretch (ν_1) at 3312 cm^{-1} and a weaker deformation mode ($2\nu_4$) at 3200 cm^{-1} . The free OH peak due to water at 3700 cm^{-1} was suppressed at this concentration, indicating that water molecules were complexed through hydrogen bonds to ammonia at the interface.

Investigations of undoped and doped interfacial structure of a chemisorbed monolayer of C_{60} fullerenes on Ag(1 1 1) have been described in a series of articles [826–830].

Finally, the adsorption phenomena of several thiols (e.g., 12-(4-nitroanilino)dodecanethiol, decanethiol, didecyl disulphide, didecyl sulphide, hexadecane thiol, *n*-alkanethiols, *p*-nitroanilino thiol) onto polycrystalline gold was a subject of several studies [831–836].

11. Adsorption of chelating compounds on mineral oxides surface

Ethylenediaminetetraacetic acid (EDTA) was first synthesised in Germany during the 1930s. Since that time, EDTA and its salts have become important industrial chelating agents [837]. For a long time they were applied in analytical chemistry or with complex metals as chelated micro-nutrients. In a practical sense, metal micro-nutrients may be chemically changed and protected by forming a cage-like structure around the metal ions. This cage-like protective structure will prevent unwanted and harmful reactions from taking place. When protected in this manner,

the metal is considered chelated. This EDTA-type compound property has been applied, among others, in catalytic research, e.g., for zeolite dealumination [838–847] and/or catalyst preparation [848–860].

In our laboratory an original technique of obtaining metal catalysts characterised by small metal crystallites, the so-called double impregnation method (DIM) was elaborated [851]. In contrast to the classical impregnation method (CIM), in the DIM preparation procedure the carrier is preliminary “activated” (modified) by EDTA. Procedures and studies of the catalysts prepared by DIM were published in several papers [851–859].

Adsorption of amines, metal ions in the presence of chelating agents, and chelating agents on the surface of inorganic supports has been confirmed in the literature [861–865].

The catalytic and adsorption properties of inorganic supports, the interaction of its species with the adsorbed components, their reactivity in solid-phase synthesis of complex oxides, and other properties are largely determined by the peculiarities of the local environment of metal atoms in the crystal lattice and isoelectric point of solid surface (IEPS).

Spectroscopic techniques have provided important contributions to the understanding of the influence of preparation conditions on the properties of heterogeneous catalysts. Several bonding schemes have been suggested to explain the adsorption of organics on hydrous solids [864–867]. However, there are few literature data dealing with this problem that are based on IR investigations [868–883]. Preparation of nickel alumina-supported catalysts with high metal dispersion involves adsorption of EDTA or its sodium salt on the γ -Al₂O₃ surface [851,852]. Transmission FT-IR

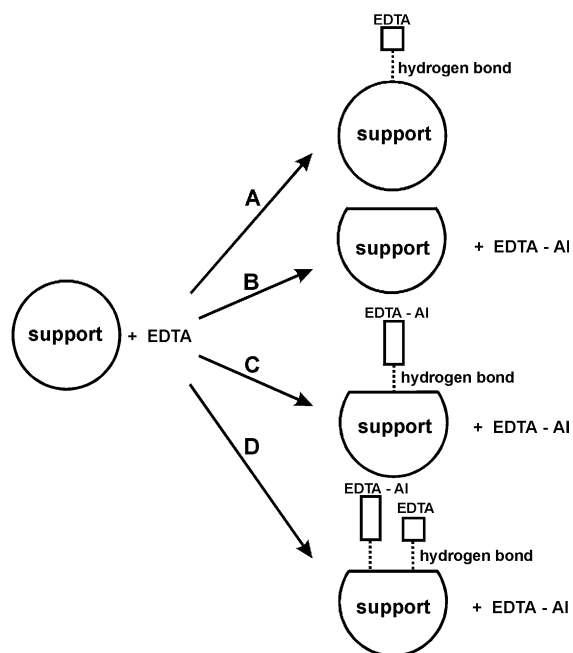


Fig. 94. Schematic representation of the possible route of EDTA inorganic support interaction.

[869,878,881], ATR technique [870], FT-IR/PAS [730] and ²⁷Al NMR [873] have confirmed the adsorption phenomenon of EDTA on gamma alumina and titania surface as well as interaction of chelating molecules with the inorganic support surface.

It is well known that in acidic impregnating solutions there occurs a partial leaching of the support (Fig. 94, route B). Studies carried out has confirmed this phenomena and in some sense they were very unique because obtained data came from the spectroscopic measurements.

Table 7
IEPS of various inorganic oxides [884,885]^a

Literature data [884]		Adsorption	Experimental data [885]	
Oxide	IEPS		Oxide	IEPS
SiO ₂ (h)	1.0–2.0	Cations	V ₂ O ₅	1.8
TiO ₂ (r, a)	~6	Cations or anions	SiO ₂	1.5–3.0
ZrO ₂ (h)	~6.7		TiO ₂	3.0
α , γ -Al ₂ O ₃	7.0–9.0	Anions	ZrO ₂	6.6
MgO	12.1–12.7		ZrO ₂ -La	~7.0
			γ -Al ₂ O ₃	~8.0
			MgO	11.0–12.0

^a (h): hydrous, (r, a): rutile, anatase.

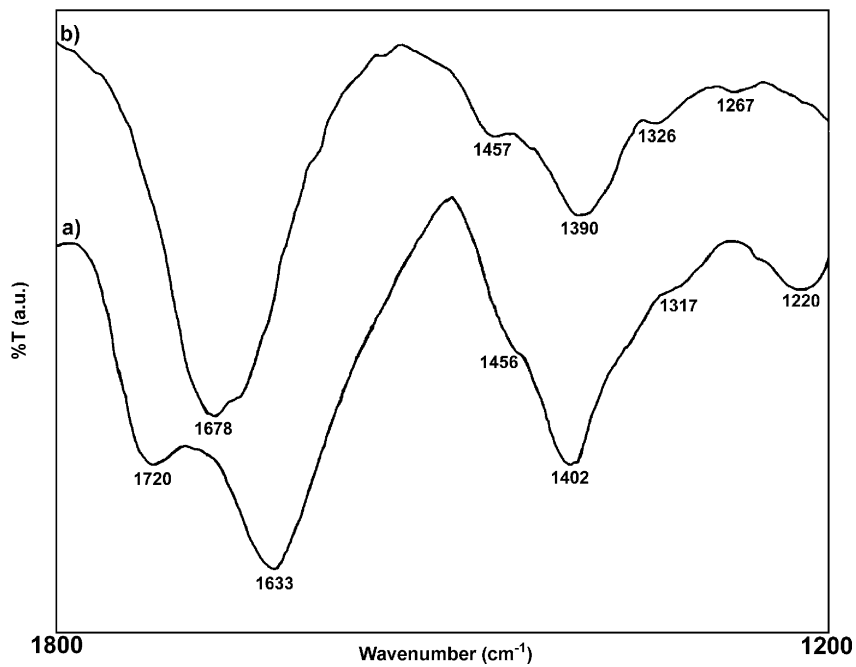


Fig. 95. (NH₄)₂EDTA adsorbed on the surface of: (a) TiO₂; (b) Al₂O₃ [878].

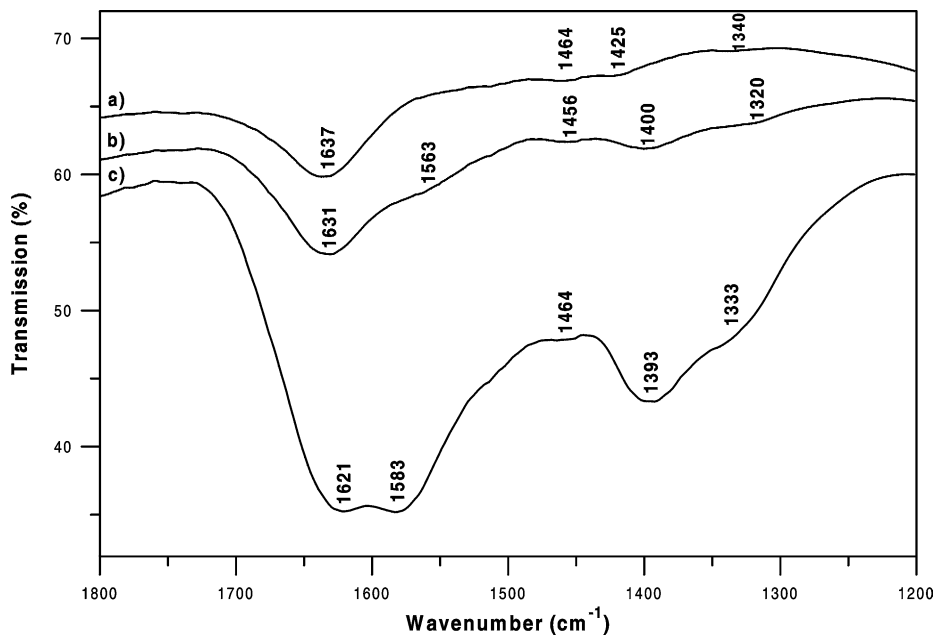


Fig. 96. (NH₄)₂EDTA adsorbed on the surface of: (a) MgO; (b) ZrO₂; (c) ZrO₂-La [886].

The observed changes in the IR spectra of the supported chelates are mainly due to interactions of the chelate carboxyls with inorganic hydroxyl groups. The IEPS has a strong influence on the band position of the adsorbed species. A change of the support is connected with a change of the IEPS, so in each case the

distribution of the existing surface hydroxyl groups is different (Table 7). This is confirmed by the results presented in Figs. 95 and 96.

The most intense bands are those which could be assigned to the stretching vibrations of the COO^- group. Different IEPS of the inorganic oxides causes

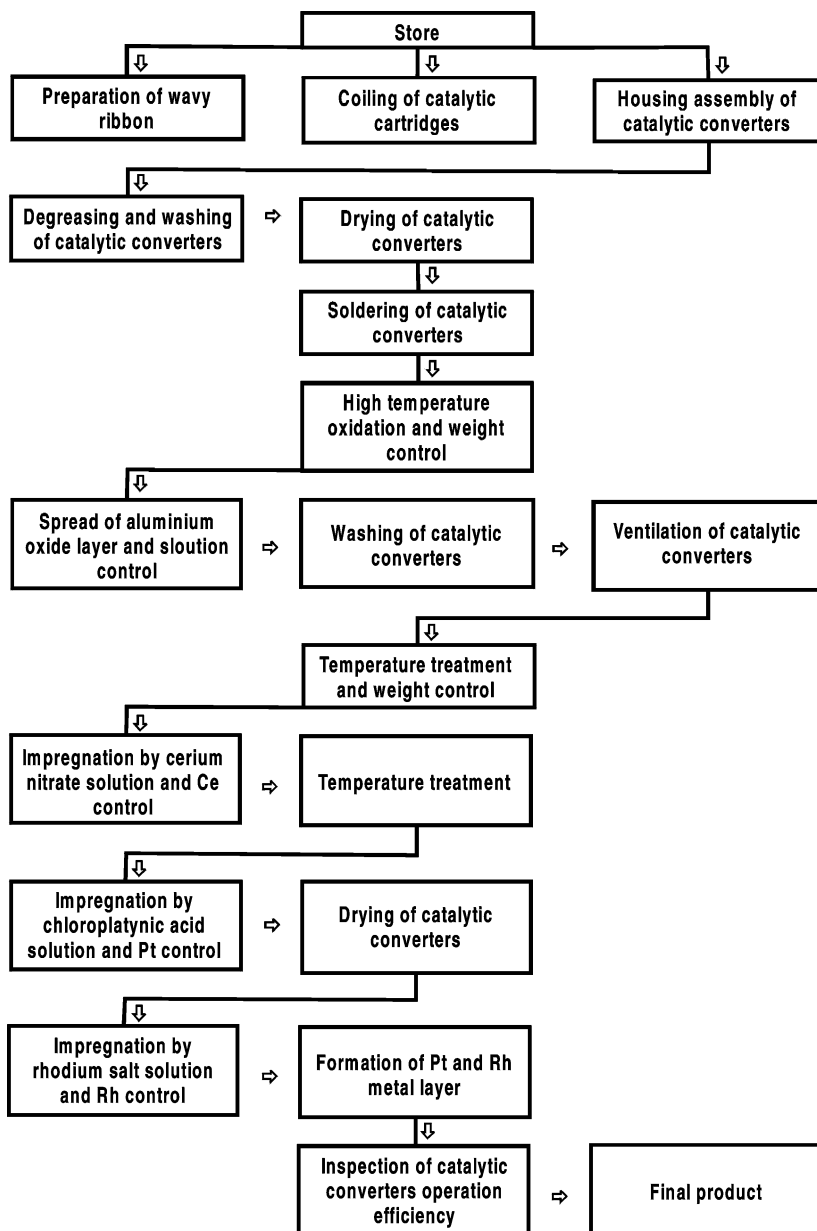


Fig. 97. Scheme of the process of the metal catalytic converters production [883].

diverse adsorption of diammonium salt of EDTA. Due to dependence of the hydroxyl group distribution on the type of support, the adsorption of chelates can be described by different types of interaction [878].

However, those interactions are weak which was confirmed by in situ studies [882]. The results of these fundamental studies are of great importance and have a practical application in the preparation of supported catalysts with a high metal dispersion. The other practical and important application is introducing this base research into the hi-tech technological process of catalytic converter production (Fig. 97) [883].

EDTA adsorption properties were applied in a part of the technological process for the production of an active catalyst.

It should be noted that, aminopolycarboxylic chelating agents e.g., EDTA, have been extensively used in nuclear waste reprocessing to concentrate fission products and actinides from contaminated equipment and cooling systems. Those complexones form strong water-soluble complexes with cationic radionuclides, and depending on the environmental conditions, may alter the adsorption behaviour of these radionuclides and thus facilitate their migration in soil pore waters and groundwaters at or near waste disposal sites [887].

The environmental impact of presented studies should also be emphasised. EDTA is commonly used substance in pharmaceutical and chemical products. This anthropogenic complexing agent is a component of many detergents for the support of bleaching agents [861,888]. Due to its low biodegradability in biological sewage treatment plants it is found in many aquatic environments. EDTA forms stable complexes with the major ions (including heavy metals) and therefore alter the migration of these metals in aquifers because the anionic complexes show a different adsorptions and retardation behaviour than uncomplexed metal [861,888,889].

12. Conclusions

This review tries to present as complete a picture as possible of the actual and the potential use of IR spectroscopic techniques in catalytic research. Recently, Kalinkova [890] has published a paper where she gave a schematic presentation of the application of IR spectroscopy in pharmacy. The application of IR

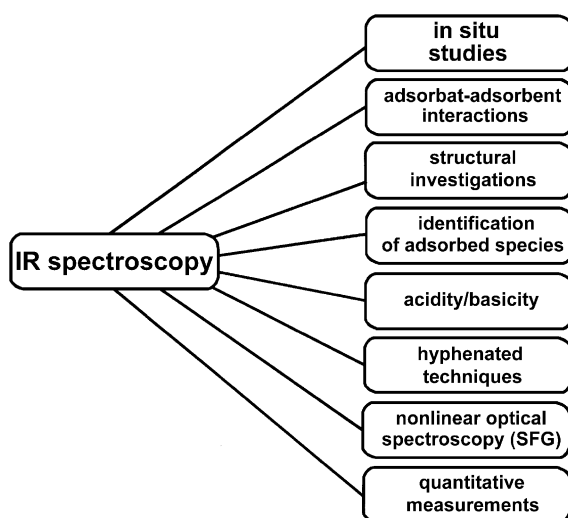


Fig. 98. Application of IR spectroscopy in catalysis and surface science.

in catalysis and surface science can be presented in a similar way (Fig. 98). It is a useful way to summarise the material presented here.

There is no doubt that we can observe an increasing interest in the application of IR in catalysis (Fig. 99).

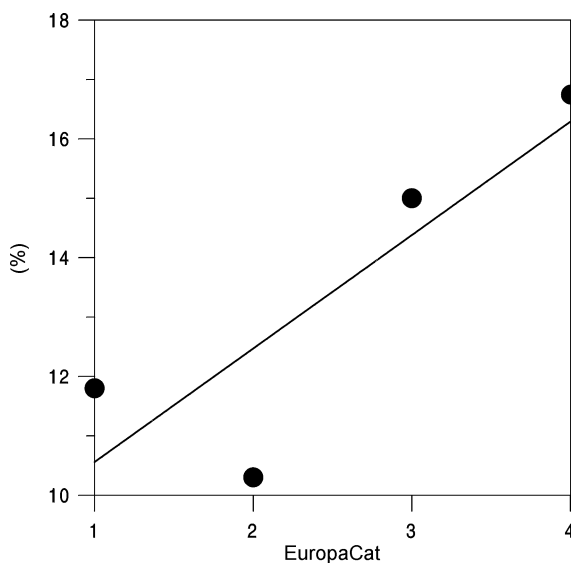


Fig. 99. Estimated percentage of works presented on the following European Congresses on Catalysis, in which IR investigations were included: (1) EuropaCat-I (Montpellier, 1993); (2) EuropaCat-II (Maastricht, 1995); (3) EuropaCat-III (Cracow, 1997); (4) EuropaCat-IV (Rimini, 1999).

Two of the classical IR techniques are still the most popular. They are transmission and diffuse reflectance. This is largely connected of the difficulties encountered with in situ studies, which nevertheless are of increasing significance. Moreover, monitoring of the presence and behaviour of adsorbed molecules on metal surfaces during heterogeneous catalytic reactions is of central importance for elucidating reaction mechanisms. Sum-frequency spectroscopy (SFS) is a type of vibrational spectroscopy that has been used to examine a range of interfacial phenomena that are important in chemical and engineering science. Over the past few years SFS has begun to be applied to problems in heterogeneous catalysis. In particular, the performances of IR–visible sum-frequency generation (SFG), as an interface-specific vibrational spectroscopy, have now been demonstrated for various systems. SFG has spectacularly opened up new investigative routes in surface science (including heterogeneous catalysis) by extending the applicability of vibrational spectroscopy to other types of interfaces which cannot be probed by any of the linear techniques (e.g., IR absorption). SFG can be used to study the vibrational modes and orientations of molecules at interfaces. Unlike traditional FT-IR, SFG is sensitive only to interfaces and requires no bulk subtraction.

Acronyms [900,901]

2D-IR	two-dimensional infrared	CADI	computer-assisted dispersive infrared
A/D	analog-to-digital	CD	circular dichroism
ADC	analog-to-digital converter	CEIR	cryogenically enhanced infrared
ADF	annular dark field	CIR	cylindrical internal reflectance
AE	atomic emission, acoustic emission	CP	cross-polarisation
AFS	atomic fluorescence spectroscopy	CPL	circularly polarised light
AGC	automatic gain control	CW	continuous wave
AIREs	abnormal infrared effects	D/A	digital-to-analog
ALE	atomic layer epitaxy	DAC	diamond anvil cell
ALS	advanced light source	DF	dark field
ASW	acoustic surface wave	DL	detection limit
ATE	automatic test equipment	DLSS	dual light source spectroscopy
ATR	attenuated total reflectance	DLTS	deep-level transient spectroscopy
ATR-FT-IR	attenuated total reflectance Fourier transform infrared spectroscopy	DM	double modulation
ATRS	attenuated total reflection spectroscopy	DOAS	differential optical absorption spectroscopy
Att	attenuated	DR	diffuse reflectance
BAW	bulk acoustic wave	DRA	diffuse reflectance attachment
BF	bright field	DREAS	diffuse reflectance electron absorption spectrometry
		DRIFTS	diffuse reflectance infrared Fourier transform spectroscopy
		DRS	diffuse reflectance spectroscopy
		DUF	diffusion under epitaxial film
		EFT-IR	emission Fourier transform infrared spectroscopy
		EO	electro-optic
		ER	external reflection
		ES	emission spectroscopy
		FFT	fast Fourier transform
		FIR	far-infrared
		FIRE	flame infrared emission spectroscopy
		FT	Fourier transform
		FT-IR	Fourier transform infrared spectroscopy
		FT-IRES	Fourier transform infrared emission spectroscopy
		FT-IR/PAS	Fourier transform infrared photo-acoustic spectroscopy
		FTIR	frustrated total internal reflection
		FT-NIR	Fourier transform near-infrared spectroscopy
		FTR	frustrated total reflection
		FT-RAIRS	Fourier transform reflection–absorption infrared spectroscopy
		FTS	Fourier transform spectroscopy
		FWHH	full peak width at half height
		FWHM	full peak width at half maximum

GC-IR	gas chromatography infrared	RAS	reflection-absorption
GC/FT-IR	gas chromatography/Fourier		spectroscopy
	transform infrared spectroscopy	RA-SHG	second-harmonic generation
GC/FT-IR/MS	gas chromatography/Fourier		rotational anisotropy
	transform infrared spectroscopy/ mass spectroscopy	RDS	reflectance-difference spectroscopy
HPLC/FT-IR	high-performance liquid chromato- graphy/Fourier transform infrared	RI	refractive index
IDL	instrument detection limit	RT	room temperature
ILS	interactivity laser spectroscopy	SAW	surface acoustic wave
IR	infrared spectroscopy	SDR	surface differential reflectance
IRAS	infrared reflection-absorption spectroscopy	SEW	surface electromagnetic wave
IRE	internal reflection element	SEWS	surface electromagnetic wave spectroscopy
IRES	infrared emission spectroscopy	SF	sum frequency
IRS	infrared spectrometry	SFC/FT-IR	supercritical-fluid chromatography/ Fourier transform infrared
IRS	internal reflection spectroscopy		sum frequency generation
IR-Vis/SFG	infrared-visible sum frequency generation	SFG	sum frequency generation
LAMMS	laser micro-mass spectroscopy	SFS	sum frequency spectroscopy
MC	monochromator	SH	second-harmonic
MCA	multichannel analyser	SHG	second-harmonic generation
MCT	mercury cadmium telluride (detector)	S/N	signal-to-noise ratio
MIR	mid-infrared	SRS	surface reflectance spectroscopy
MIR	multiple internal reflection	STAR	simultaneous transmitted and reflected
MIRIRS	multiple internal reflection infrared spectroscopy	STIRS	surface titration by internal reflectance spectroscopy
MIRS	multiple internal reflection spectroscopy	TGS	triglycine sulphate detector
NIR	near-infrared	TPIR	temperature-programmed infrared
NIR	near-infrared spectroscopy	TRIR	time-resolved infrared
NIRA	near-infrared reflectance (reflection) analysis	TRO	time-resolved optical
NIRS	near-infrared (reflectance) spectroscopy	TS	transmission spectroscopy
NLO	nonlinear optics	Utt	unattenuated
OAS	opto-acoustic spectroscopy	VASE	variable angle spectroscopic elipsometry
OES	optical emission spectroscopy	VCD	vibrational circular dichroism
OPA	optical parametric amplifier	ZOPD	zero optical path difference
OPG	optical parametric generator	ZPD	zero path difference
PA/FT-IR	photoacoustic Fourier transform infrared spectroscopy		
PAS	photoacoustic spectroscopy		
PLS	partial least-squares		
PLSR	partial least-squares regression		
RAIRS	reflection-absorption infrared spectroscopy		

Acknowledgements

The author gratefully acknowledges the suggestions given by Prof. Julian Ross, Limerick University, Ireland, Dr. Ben Nieuwenhuys, Leiden University, and also special thanks to Dr. Michael Gagan, Open Manchester University, for his kind help in linguistic improvements. This paper is dedicated to all my co-workers at the Department.

Appendix A. Sample handling

IR is a particularly useful analytical technique because of its enormous versatility. Spectra can be obtained, often non-destructively, on samples in all three states of matter. For a given sample, there will usually be different sampling techniques that can be used to obtain the spectrum, thus permitting the spectroscopist a choice that may be dictated by available accessory equipment, personal preference, or the detailed nature of that particular sample. The quality of the information that can be derived from a spectrum is directly related to the quality of the spectrum itself [891].

Powders, being examined by IR, in transmission, are generally prepared by mulling in liquid paraffin (Nujol), or by grinding with potassium bromide powder [891–893]. The latter is then pressed into a disk. The method of preparation of a powder sample is generally determined by the information required or the chemical/physical stability of the sample. If information on the physical state, e.g., polymorphism, is required then grinding may change the state and mulling is preferable. Some substances, such as base hydrochloride, may exchange halogen with KBr powder, again mulling is preferable. However, most mulling agents contain bands in the spectrum, which may mask bands in the sample spectrum. The transparency of KBr to IR radiation means that it will not contribute to the absorption spectrum (therefore preparation as halide disks potentially loses less information) but the spectral absorption effects of KBr impurities will have to be considered. The principal impurity to be aware of is water, because KBr is highly adsorptive and

hygroscopic. This will be manifested as an absorption at 3440 cm^{-1} , and a somewhat weaker band at 1640 cm^{-1} (Fig. 100).

Even with carefully dried and highly pure KBr, the spectral absorptions due to water are ubiquitous, and must be considered in the interpretation of spectra (Fig. 101). It is also important to store the KBr in a desiccator to minimise water uptake.

Samples dispersed in halide powder must be homogeneously dispersed, with a particle size small enough not to cause scatter (theoretically $<2\text{ }\mu\text{m}$). The strength of an IR absorption spectrum depends on the number of molecules in the beam. With a KBr disk the strength will depend on the amount and homogeneity of the sample dispersed in the KBr powder. The amounts stated below are for guidance only, the bulk density of the sample or other diluents may require these to be varied. They will also have to be varied according to the diameter of the disk required. The weights quoted are for a 16 mm diameter disk (approximately half should be used for the 13 mm diameter disks).

Recommended method [893]:

1. Transfer weighed amounts of sample, $\sim 2\text{ mg}$, and KBr powder, $\sim 300\text{ mg}$ into an agate mortar (or in vibrating ball mill). The KBr powder must be of spectroscopic grade purity, and be spectroscopically dry.
2. Grind the powders together, with an agate pestle, until the sample is well dispersed and the mixture has the consistency of fine flour. With some very hard or crystalline powders this may not be

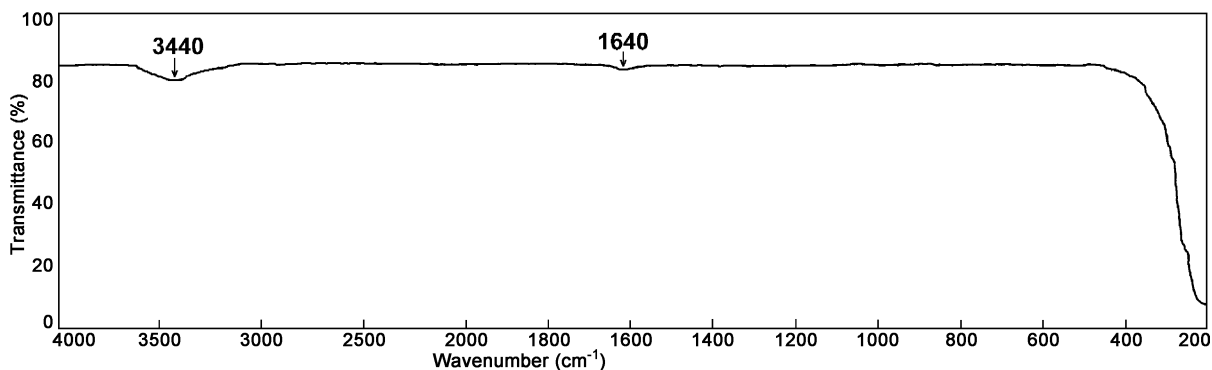


Fig. 100. IR spectrum of potassium bromide (3440 and 1640 cm^{-1} traces of water) [894].

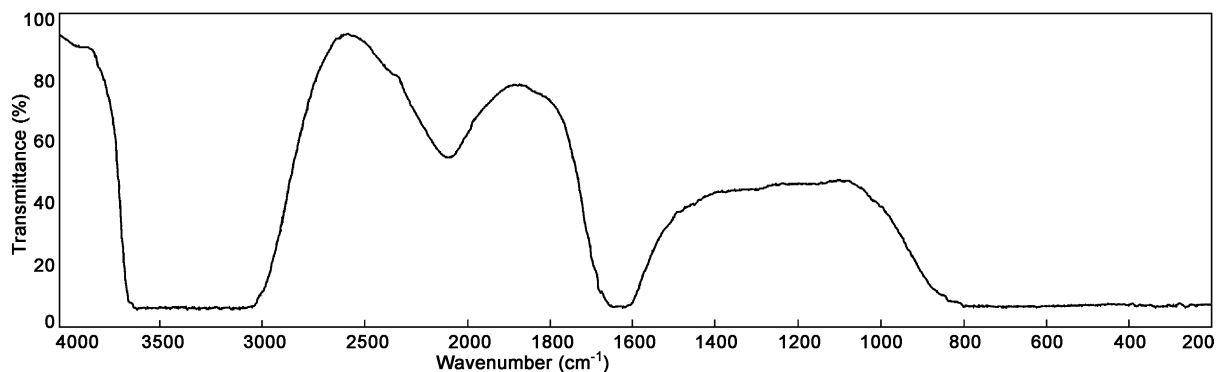


Fig. 101. IR spectrum of distilled water [894].

- possible by hand. If necessary, use mechanical or low-temperature (liquid nitrogen cooled) grinding accessories.
3. Assemble the die, with the lower pellet polished face up (see Fig. 102).
 4. Transfer the ground mixture into the cylinder bore so that it is evenly distributed across the polished face of the lower pellet. Gently inserting the plunger and lightly swivelling can often achieve a flat, even surface.
 5. Insert the second pellet, polished face towards the mixture, into the bore followed by the plunger.

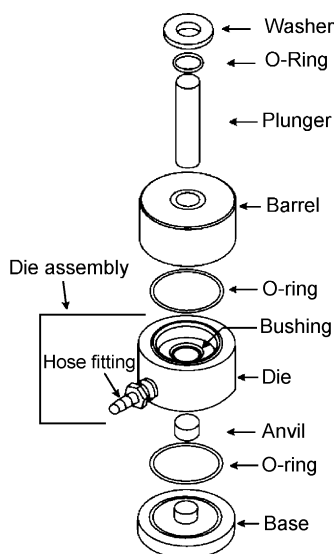


Fig. 102. KBr die assembly.

6. Place the die assembly into a hydraulic press, between the ram and the piston.
7. Ensure that the die is firmly held in the press.
8. Connect a vacuum tube and switch on a high vacuum pump (1.3×10^{-4} kPa).
9. Leave the die assembly under vacuum for approximately 2 min. This removes air from the disk.
10. Increase pressure in the press to 15 tons (10 t for 13 mm die, follow manufacturers instructions for maximum pressure with other diameter dies).
11. After approximately 1 min, slowly release the pressure.
12. Carefully release the vacuum, and remove the die from the press.
13. Dismantle the die, and transfer the KBr disk to a spectrometer disk holder. Avoid touching the faces of the disk.
14. Check that the disk is translucent and that the sample is homogeneously distributed in the disk.
15. Mount the disk holder in the spectrometer.

The spectrum quality is affected by the quality of the disk. The flatness of the baseline is dependent on the particle size and dispersion of the sample in the KBr powder. Check the disk and spectrum for the following faults:

1. If the disk breaks on removal from the die, this indicates that the disk is too thin caused by too little powder, or too much pressure for too long. Remedy this effect by increasing the sample load. Also check that the correct pressure is used.
2. If the disk is not translucent, this can have numerous causes:

- 2.1. Uneven distribution of powder in die;
- 2.2. Too much sample;
- 2.3. Too much KBr powder;
- 2.4. Poorly dispersed sample;
- 2.5. Water in disk;
- 2.6. Pressed at too low pressure or for too short a time.

Re-grinding and pressing with adjusted amounts can remedy all except the last fault. Water in the disk can be present due to a wet sample or wet KBr powder. Small amounts can be removed by the high vacuum step (9). Heating the disk at ~ 373 K for a few minutes and repressing the disk will sometimes remove residual water.

The disk turns brown — this could be due to the sample being an oxidising agent. Check the spectrum for halide degradation and re-examine as a mull if possible.

Truncated bands — if the spectrum contains bands which have a flattened turning point and do not reach 0% T , this is caused by a poorly dispersed sample or holes in the disk. Check the disk visually and if necessary repeat the preparation.

Sloping baseline — this is usually due to a poorly dispersed sample. Some substances are too hard (polymers) or too crystalline (e.g., anthraquinone) to disperse properly. The latter can also cause bands to appear like a first derivative spectrum. This is due to refractive index changes and is known as the Christiansen effect.

The faults listed above have been commonly found, sometimes in publications, but the list is not necessa-

rily exhaustive. Use of other halide salts can overcome some effects, or extend the range of the spectrum examined, e.g., CsI extends the lower wavenumber range from 400 to 200 cm^{-1} . Poor sample preparation can lead to avoidable errors in interpretation of the resultant spectrum. A little care can avoid the need for repetitious sample preparation or embarrassing errors in results.

The mull method is another common technique for the preparation of solid samples, especially solids that are insoluble in the common IR solvents [891,892]. To prepare a mull, the solid sample, presented as a powder, is ground in a mortar and pestle or vibrating ball mill. As with the preparation of a KBr pellet, the grinding must continue until the particles are smaller than the shortest wavelength of the radiation to be used, in order to minimise scattering. After the sample is ground, a small quantity (1–3 drops is usually sufficient) of mulling oil is added to the mixture, and the grinding is continued. Grinding with the oil produces a viscous paste that is pressed as a film between two IR window plates. Precautions should be taken to exclude moisture from the mull preparation, especially if the sample is hygroscopic.

The most common mulling oil is clear mineral oil or paraffin (generally known as Nujol). This is a hydrocarbon oil that absorbs strongly between 3000 and 2800 cm^{-1} , with additional weaker absorptions at 1460 and 1375 cm^{-1} , and an even weaker absorption at 720 cm^{-1} (Fig. 103).

These absorptions will naturally obscure any sample absorptions that occur in these regions. For this reason,

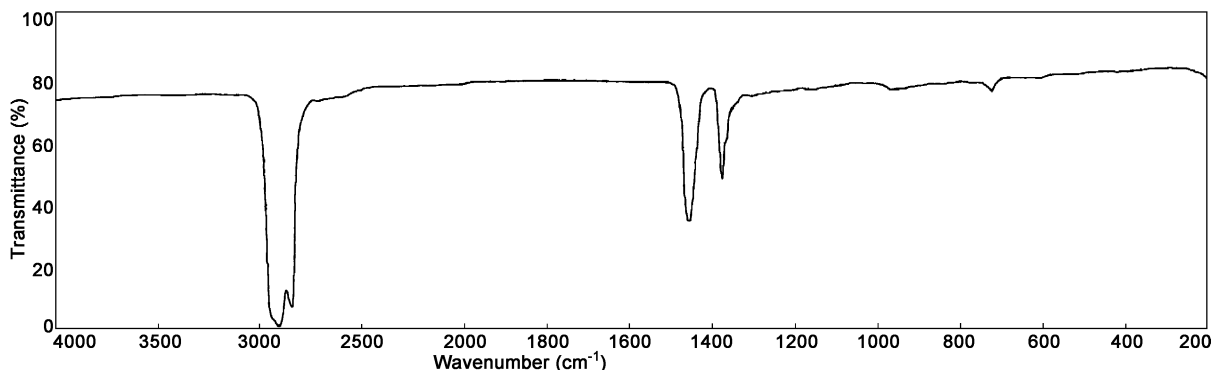


Fig. 103. IR spectrum of paraffin liquid [894,895].

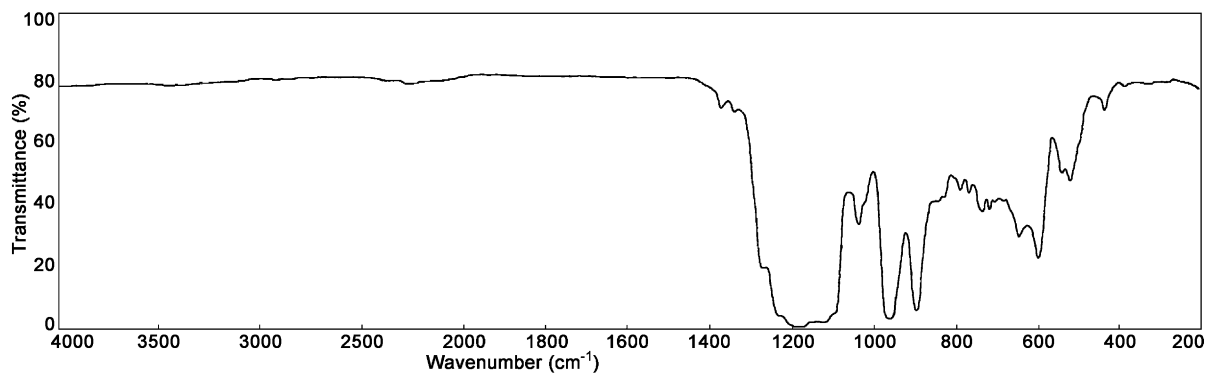


Fig. 104. IR spectrum of kerosene [894].

another mull is often prepared with a mulling agent composed of fluorinated kerosene (Fig. 104).

This oil has a very weak absorption at 2300 cm^{-1} , and strong absorptions at $1300\text{--}1100\text{ cm}^{-1}$, and

fingerprint absorptions (caused by the intense C–F stretching vibrations) from $1000\text{ to }500\text{ cm}^{-1}$. This technique of preparing two mulls to cover the full mid-IR range is called the split-mull method.

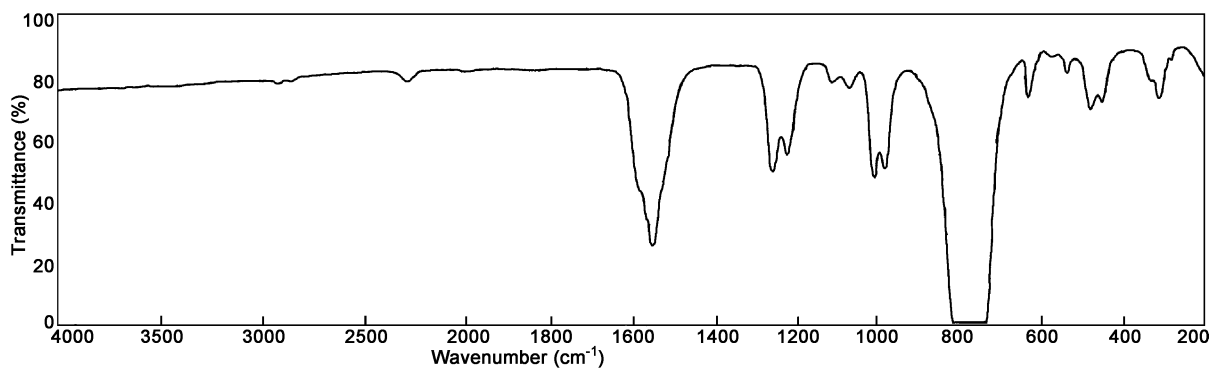


Fig. 105. IR spectrum carbon tetrachloride [894,895].

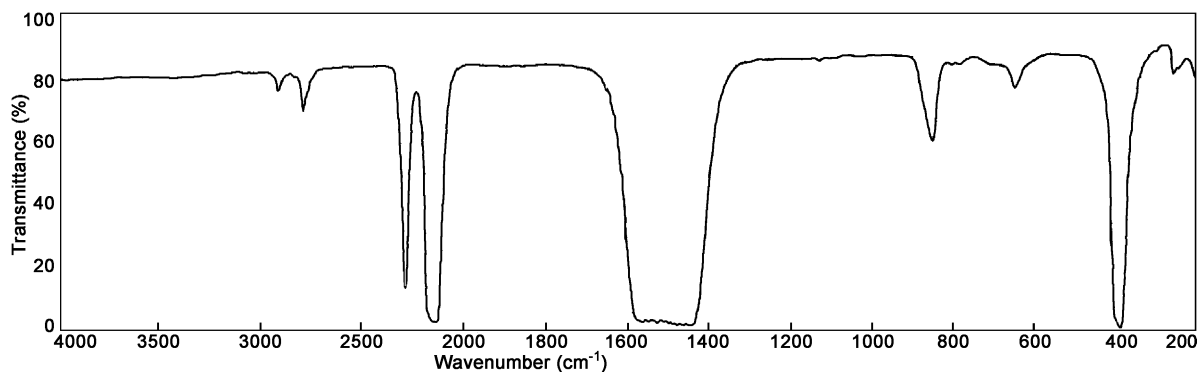


Fig. 106. IR spectrum of carbon disulphide [894,895].

Table 8
Appropriate combinations of sources, beam splitters, and detectors for mid- and far-IR [896]

Region	Source	Beamsplitter	Detector
Mid-IR	Glowbar®, ceramic element, Nerst glower® (both $\sim 6000\text{--}200\text{ cm}^{-1}$)	Ge on KBr substrate ($7400\text{--}350\text{ cm}^{-1}$), Ge on CsI substrate ($6400\text{--}225\text{ cm}^{-1}$)	DTGS (KBr window) ($7400\text{--}350\text{ cm}^{-1}$), DTGS (CsI window) ($6400\text{--}225\text{ cm}^{-1}$), and MCT ($7400\text{--}400\text{ cm}^{-1}$)
Far-IR	Mercury arc lamp ($200\text{--}10\text{ cm}^{-1}$), Glowbar ($6000\text{--}100\text{ cm}^{-1}$)	Metal mesh ($600\text{--}10\text{ cm}^{-1}$), Silicon substrate ($650\text{--}50\text{ cm}^{-1}$), Mylar films ($500\text{--}10\text{ cm}^{-1}$)	DTGS (polyethylene window) ($650\text{--}20\text{ cm}^{-1}$), He bolometer ($100\text{--}10\text{ cm}^{-1}$)

Table 9
IR window materials [897,898]

Material	Transmission range (cm^{-1})	Refractive index (at 5000 cm^{-1})	Properties
AgBr	22 000–286	2.30	A soft crystal; insoluble in H_2O ; darkens upon exposure to UV radiation; will cold flow
AgCl	10 000–360	2.07	Soft crystal that is insoluble in H_2O ; darkens upon exposure to UV radiation; will cold flow
Al_2O_3 (sapphire)	50 000–1650	1.75	Glass-like
BaF_2	67 000–740	1.46	A hard, brittle crystal; insoluble in H_2O ; good resistance to fluorine and fluorides; no fog
CaF_2	77 000–1110	1.42	A strong crystal; resists most acids and alkalis; withstands high pressure; insoluble in H_2O ; no fog
CdTe	10 000–400	2.4	Lower thermal conductivity than ZnSe (used with CO_2 lasers)
CsI	40 000–200	1.74	Soft crystal; soluble in H_2O ; hygroscopic; offers an extended transmission range
GaAs	7000–650	3.33	Hard crystal, can be made amorphous
Ge	5500–600	4.00	A hard and brittle crystal; insoluble in H_2O ; well suited for ATR
Irtran-2	17 000–720	2.26	Insoluble in water; withstands thermal and mechanical shocks; avoid strong oxidisers; fringes induced due to high refractive index
KBr	40 000–400	1.53	Very soft, H_2O soluble crystal; low cost and good transmission range; fogs
KCl	40 000–500	1.46	Hygroscopic; fogs slowly; easy to polish
KRS-5	20 000–250	2.37	A soft crystal, deforms under pressure; good ATR material
LiF	50 000–1700	1.4	Best VuV transmitter available
MgF_2	75 000–1250		
NaCl	40 000–625	1.52	Very soft, H_2O soluble crystal; low cost and good transmission range; fogs
Polyethylene (high density)	625–30	1.54	Resistant to most solvents; difficult to clean thoroughly; inexpensive
Si	10 000–1540, 500–30 (depends on doping)	3.40	A hard and brittle crystal; inert; ideal material for far-IR
SiO_2 (quartz)	65 000–2700	1.42	A hard crystal, clear in the visible
ZnS (Cleartran)	23 800–833	2.26	A water-free form of ZnS
ZnSe (Irtran-4)	20 000–454	2.40	A hard and brittle crystal; inert; ideal material for ATR

The mull method is very simple and can be used rapidly, especially in research protocols and in quality control, as well as in educational settings. The common mulling oils are very stable, and chemical reactions with most samples are rare.

If a solid sample can be dissolved in a suitable solvent, it is possible to measure its IR spectrum with one of the appropriate cells for liquid samples [891,892]. There is no perfect solvent for IR spectroscopy in terms of transparency in the mid-IR region, however. Historically, among the most useful have been carbon tetrachloride (Fig. 105), CCl_4 (with a broad band centred at 1550 cm^{-1} , and a strong broad absorption at 750 cm^{-1}) and carbon disulphide (Fig. 106), CS_2 (with sharp, moderate absorptions near 350 and 2200 cm^{-1} , and a broad absorption centred at 1570 cm^{-1}).

It is possible to view an entire mid-IR spectrum with a split-solution technique using these two solvents that is analogous to the split-mull technique. Alternative solvents, that may also be used, and may be more readily accessible, are chloroform, methylene chloride (dichloromethane), and perchloroethylene. In each of these cases, the IR transparency is not as good as CCl_4 .

The preparation of samples as films is especially useful for polymers [891,892]. Films can be prepared by several methods that include casting, rolling, pressing, and hot melting. The cast film is the most common, and is prepared by dissolving the sample in a moderate to high volatility solvent. A drop of the solution is placed on an IR window such as a NaCl or KBr window, and the solvent is allowed to evaporate. A thin film of the sample forms on the window, which is not covered with another plate as in the case of a mull. The window containing the film is placed in the “V” holder in the instrument sample compartment to measure the spectrum.

Another sample preparation technique that is valuable for the analysis of polymeric samples is pyrolysis. In this method, the sample is heated in a test tube (or commercial pyrolyser) to produce destructive distillation and decomposition. The more volatile products will be driven off, and may be captured for analysis in an evacuated gas cell.

The spectra of the gaseous and liquid products are then measured. Identification of the polymer sample is usually done through a comparison with a library of pyrolyzates. More details about sample handling in IR

spectroscopy can be found in the literature [891–894] (Tables 8 and 9).

References

- [1] R.L. Carter, *Molecular Symmetry and Group Theory*, Wiley, New York, 1998.
- [2] J.M. Chalmers, G. Dent, *Industrial Analysis with Vibrational Spectroscopy*, The Royal Society of Chemistry, Cambridge, 1997.
- [3] F.M. Mirabella, *Modern Techniques in Applied Molecular Spectroscopy*, Wiley, New York, 1998.
- [4] J. Workman Jr., A.W. Springsteen, *Applied Spectroscopy: A Compact Reference for Practitioners*, Academic Press, San Diego, CA, 1998.
- [5] B.C. Smith, *Fundamentals of Fourier Transform Infrared Spectroscopy*, CRC Press, Boca Raton, FL, 1996.
- [6] G. Socrates, *Infrared Characteristic Group Frequencies: Tables and Charts*, Wiley, Chichester, 1994.
- [7] K. Nakamoto, *Infrared and Raman Spectra of Inorganic and Coordination Compounds*, 5th Edition, Wiley, New York, 1997.
- [8] N.P.G. Roeges, *A Guide to the Complete Interpretation of Infrared Spectra of Organic Structures*, Wiley, Chichester, 1994.
- [9] B. Smith, *Infrared Spectral Interpretation: A Systematic Approach*, CRC Press, Boca Raton, FL, 1999.
- [10] R.A. Nyquist, R.O. Kagel, C.L. Putzig, *The Handbook of Infrared and Raman Spectra of Inorganic Compounds and Organic Salts*, Academic Press, San Diego, CA, 1997.
- [11] W. Suetaka, *Surface Infrared and Raman Spectroscopy: Methods and Applications*, Plenum Press, New York, 1995.
- [12] B. Stuart, B. George, P. McIntyre, *Modern Infrared Spectroscopy*, Wiley, Chichester, 1998.
- [13] www.ijvs.com.
- [14] www.ijvs/links.htm.
- [15] F.A. Miller, *Anal. Chem.* 64 (1992) 824A.
- [16] P.A. Wilks Jr., *Anal. Chem.* 64 (1992) 833A.
- [17] P.R. Griffiths, *Anal. Chem.* 64 (1992) 868A.
- [18] R.P. Eischens, W.A. Pliskin, S.A. Francis, *J. Chem. Phys.* 22 (1954) 1786.
- [19] J.A. Lercher, *Ch. Grundling*, G. Eder-Mirth, *Catal. Today* 27 (1996) 353 and references cited therein.
- [20] B.M. Abu-Zied, *Appl. Catal. A* 198 (2000) 139.
- [21] A.M. de Aguilar Cruz, J.G. Eon, *Appl. Catal. A* 167 (1998) 203.
- [22] M. Agunaou, B. Mernari, J.M. Tatibouet, *Appl. Catal. A* 196 (2000) 87.
- [23] W.S. Ahn, D.H. Lee, T.J. Kim, J.H. Kim, G. Seo, R. Ryoo, *Appl. Catal. A* 181 (1999) 39.
- [24] G.O. Alptekin, A.M. Herring, D.L. Williamson, T.R. Ohno, R.L. McCormick, *J. Catal.* 181 (1999) 104.
- [25] D. Andreeva, V. Idakiev, T. Tabakova, A. Andreev, R. Giovanoli, *Appl. Catal. A* 134 (1996) 275.
- [26] A. Antinolo, P. Canizares, F. Carrillo-Hermosilla, J. Fernández-Baeza, F.J. Funez, A. de Lucas, A. Otero, L. Rodriguez, J.L. Valverde, *Appl. Catal. A* 193 (2000) 139.

- [27] P. Atanasova, R.L. Cordero, L. Mintchev, T. Halachev, A.L. Agudo, *Appl. Catal. A* 159 (1997) 269.
- [28] P. Atanasova, T. Tabakova, C. Vladov, T. Halachev, A.L. Agudo, *Appl. Catal. A* 161 (1997) 105.
- [29] E. Baburek, J. Novakova, *Appl. Catal. A* 190 (2000) 241.
- [30] O.M. Bade, R. Blom, *Appl. Catal. A* 161 (1997) 249.
- [31] S.H. Baeck, W.Y. Lee, *Appl. Catal. A* 168 (1998) 171.
- [32] G. Baronetti, L. Briand, U. Sedran, H. Thomas, *Appl. Catal. A* 172 (1998) 265.
- [33] N.H. Batis, H. Batis, A. Ghorbel, *Appl. Catal. A* 147 (1996) 347.
- [34] J.J. Benitez, A. Diaz, Y. Laurent, J.A. Odriozola, *Appl. Catal. A* 176 (1999) 177.
- [35] K. Blazsik, B. Torok, G. Szakonyi, M. Bartók, *Appl. Catal. A* 182 (1999) 53.
- [36] E. Boellaard, A.M. van der Kraan, A.B.P. Sommen, J.H.B.J. Hoebink, G.B. Martin, J.W. Geus, *Appl. Catal. A* 179 (1999) 175.
- [37] M. Bowker, C.R. Bicknell, P. Kerwin, *Appl. Catal. A* 136 (1996) 205.
- [38] M.C.J. Bradford, M.A. Vannice, *Appl. Catal. A* 142 (1996) 97.
- [39] G. Centi, P. Mazzoli, S. Perathoner, *Appl. Catal. A* 165 (1997) 273.
- [40] G. Centi, S. Perathoner, *Appl. Catal. A* 124 (1995) 317.
- [41] T.-H. Chang, F.-Ch. Leu, *Appl. Catal. A* 180 (1999) 123.
- [42] Y.-C. Chang, A.-N. Ko, *Appl. Catal. A* 190 (2000) 149.
- [43] H.-Y. Chen, X. Wang, W.M.H. Sachtler, *Appl. Catal. A* 194–195 (2000) 159.
- [44] H.-B. Chiang, M.-D. Lee, *Appl. Catal. A* 154 (1997) 55.
- [45] St.G. Christoskova, N. Danova, M. Georgieva, O.K. Argirov, D. Mahandzhiev, *Appl. Catal. A* 128 (1995) 219.
- [46] St.G. Christoskova, M. Stoyanova, N. Danova, O. Argirov, *Appl. Catal. A* 173 (1998) 101.
- [47] J.R. Combes, L.D. White, C.P. Tipp, *Langmuir* 15 (1999) 7870.
- [48] R.A. Comelli, S.A. Canavese, S.R. Vaudagna, N.S. Figoli, *Appl. Catal. A* 135 (1996) 287.
- [49] A. Corma, A. Martinez, C. Martinez, *Appl. Catal. A* 134 (1996) 169.
- [50] L.M. Cornaglia, C.R. Carrara, J.O. Petunchi, E.A. Lombardo, *Appl. Catal. A* 183 (1999) 177.
- [51] S. Damyanova, A. Spojakina, K. Jiratova, *Appl. Catal. A* 125 (1995) 257.
- [52] Ch.B. Dart, M.E. Davis, *Appl. Catal. A* 143 (1996) 53.
- [53] D. Das, G. Ravichandran, D.K. Chakrabarty, *Appl. Catal. A* 131 (1995) 335.
- [54] B. Demirel, S. Fang, E.N. Givens, *Appl. Catal. A* 201 (2000) 177.
- [55] C. Dossi, A. Fusi, G. Moretti, S. Recchia, R. Psaro, *Appl. Catal. A* 188 (1999) 107.
- [56] V. Ermini, E. Finocchio, S. Sechi, G. Busca, S. Rossini, *Appl. Catal. A* 198 (2000) 67.
- [57] A. Fasi, J.T. Kiss, B. Torok, I. Palinko, *Appl. Catal. A* 200 (2000) 189.
- [58] P. Fejes, J.B. Nagy, K. Kovacs, G. Vanko, *Appl. Catal. A* 145 (1996) 155.
- [59] Z.R. Finelli, C.A. Querini, N.S. Figoli, R.A. Comelli, *Appl. Catal. A* 187 (1999) 115.
- [60] L.M. Gandia, M.A. Vicente, A. Gil, *Appl. Catal. A* 196 (2000) 281.
- [61] L. Gang, G. Xinwen, W. Xiangsheng, Z. Qi, B. Xinhe, H. Xiuwen, L. Liwu, *Appl. Catal. A* 185 (1999) 11.
- [62] A. Ghanbari-Siahkali, A. Philippou, J. Dwyer, M.W. Anderson, *Appl. Catal. A* 192 (2000) 57.
- [63] A.C.L. Gomez, E.F. S-Aguiar, S.C. Menezes, D. Cardoso, *Appl. Catal. A* 148 (1997) 373.
- [64] F. Goncalves, P.R.S. Medeiros, J.G. Eon, L.G. Appel, *Appl. Catal. A* 193 (2000) 195.
- [65] M.L. Granados, E.E. Wolf, *Appl. Catal. A* 131 (1995) 263.
- [66] D. Gulkova, Z. Vit, *Appl. Catal. A* 125 (1995) 61.
- [67] A.F. Gusovius, T.C. Watling, R. Prins, *Appl. Catal. A* 188 (1999) 187.
- [68] A. Hakuli, A. Kytokivi, A.O.I. Krause, *Appl. Catal. A* 190 (2000) 219.
- [69] A.W. Heinen, J.A. Peters, H. van Bekkum, *Appl. Catal. A* 194–195 (2000) 193.
- [70] G.P. Heitmann, G. Dahlhoff, W.F. Holderich, *Appl. Catal. A* 185 (1999) 99.
- [71] W.F. Holderich, J. Tjoe, *Appl. Catal. A* 184 (1999) 257.
- [72] J. Houzvicka, R. Klik, L. Kubelkova, V. Ponec, *Appl. Catal. A* 150 (1997) 101.
- [73] M.J. Iglesias, G. De la Puente, E. Fuente, J.J. Pis, *Vib. Spectrosc.* 17 (1998) 41.
- [74] K. Inumaru, M. Misono, T. Okuhara, *Appl. Catal. A* 149 (1997) 133.
- [75] N.J. Jebarathinam, M. Eswaramoorthy, V. Krishnasamy, *Appl. Catal. A* 145 (1996) 57.
- [76] F.C. Jentoft, H. Schmelz, H. Knozinger, *Appl. Catal. A* 161 (1997) 167.
- [77] S.-J. Jong, S. Cheng, *Appl. Catal. A* 126 (1995) 51.
- [78] Y. Kim, H. Kim, J. Lee, K. Sim, Y. Han, H. Paik, *Appl. Catal. A* 155 (1997) 15.
- [79] M. Kimura, T. Nakato, T. Okuhara, *Appl. Catal. A* 165 (1997) 227.
- [80] I. Kiricsi, A. Fudala, Z. Konya, K. Hernadi, P. Lentz, J.B. Nagy, *Appl. Catal. A* 203 (2000) L1.
- [81] A.-N. Ko, C.H. Hu, J. Chen, *Appl. Catal. A* 184 (1999) 211.
- [82] P. Kovacheva, K. Arishtirova, N. Davidova, *Appl. Catal. A* 149 (1997) 277.
- [83] P. Kovacheva, K. Arishtirova, N. Davidova, *Appl. Catal. A* 178 (1999) 111.
- [84] E. Leclercq, A. Rives, E. Payen, R. Hubaut, *Appl. Catal. A* 168 (1998) 279.
- [85] M.I. Levinbuk, M.L. Pavlov, L.M. Kustov, J.P. Fraissard, T.V. Vasina, A.V. Kazakov, Y.I. Azimova, Y.Y. Smorodinskaya, *Appl. Catal. A* 172 (1998) 177.
- [86] J. Li, N.J. Coville, *Appl. Catal. A* 181 (1999) 201.
- [87] J. Li, W. Zhang, L. Gao, P. Gu, K. Sha, H. Wan, *Appl. Catal. A* 165 (1997) 411.
- [88] W. Li, K. Oshihara, W. Ueda, *Appl. Catal. A* 182 (1999) 357.
- [89] Y. Li, J.N. Armor, *Appl. Catal. A* 183 (1999) 107.
- [90] Q. Liang, K. Chen, W. Hou, Q. Yan, *Appl. Catal. A* 166 (1998) 191.

- [91] A.A.G. Lima, M. Nele, E.L. Moreno, H.M.C. Andrade, Appl. Catal. A 171 (1998) 31.
- [92] G. Lischke, B. Parltitz, U. Lohse, E. Schreier, R. Fricke, Appl. Catal. A 166 (1998) 351.
- [93] A. Loaiza-Gil, B. Fontal, F. Rueda, J. Mendialdua, R. Casanova, Appl. Catal. A 177 (1999) 193.
- [94] U. Lohse, I. Pitsch, E. Schreier, B. Parltitz, K.-H. Schnabel, Appl. Catal. A 129 (1995) 189.
- [95] R. Long, S. Zhou, Y. Huang, W. Weng, H. Wan, K. Tsai, Appl. Catal. A 133 (1995) 269.
- [96] T. Lopez, P. Bosch, F. Tzompantzi, R. Gomez, J. Navarrete, E. Lopez-Salinas, M.E. Llanos, Appl. Catal. A 197 (2000) 107.
- [97] J.M. Lopez Nieto, A. Dejoz, M.I. Vazquez, Appl. Catal. A 132 (1995) 41.
- [98] E. Lopez-Salinas, J.G. Hernandez-Cortez, I. Schifter, E. Torres-Garcia, J. Navarrete, A. Gutierrez-Carrillo, T. Lopez, P.P. Lottici, D. Bersani, Appl. Catal. A 193 (2000) 215.
- [99] A. Lugstein, A. Jentys, H. Vinek, Appl. Catal. A 176 (1999) 119.
- [100] S. Luukkanen, P. Homanen, M. Haukka, T.A. Pakkanen, A. Deronzier, S. Chadron-Noblat, D. Zsoldos, R. Ziessel, Appl. Catal. A 185 (1999) 157.
- [101] G.C. Maiti, M. Berns, Appl. Catal. A 127 (1995) 219.
- [102] N.K. Mal, V. Ramaswamy, S. Ganapathy, A.V. Ramaswamy, Appl. Catal. A 125 (1995) 233.
- [103] R.V. Malyala, C.V. Rode, M. Arai, S.G. Hegde, R.V. Chaudhari, Appl. Catal. A 193 (2000) 71.
- [104] R.L. McCormick, G.O. Alptekin, A.M. Herring, T.R. Ohno, S.F. Dec, J. Catal. 172 (1997) 160.
- [105] F.M.T. Mendes, M. Schmal, Appl. Catal. A 151 (1997) 393.
- [106] J.M. Miller, L.J. Lakshmi, Appl. Catal. A 190 (2000) 197.
- [107] H.K. Mishra, K.M. Parida, Appl. Catal. A 184 (1999) 219.
- [108] A. Montes, Z. Gabelica, A. Rodriguez, G. Giannetto, Appl. Catal. A 169 (1998) 87.
- [109] S. Morin, P. Ayrault, N.S. Gnep, M. Guisnet, Appl. Catal. A 166 (1998) 281.
- [110] S.R. Mukai, T. Masuda, I. Ogino, K. Hashimoto, Appl. Catal. A 165 (1997) 219.
- [111] A. Music, J. Batista, J. Levec, Appl. Catal. A 165 (1997) 115.
- [112] S. Myllyoja, T.A. Pakkanen, J. Mol. Catal. A 156 (2000) 195.
- [113] K.V. Narayana, A. Venugopal, K.S. Rama Rao, S.K. Masthan, V.V. Rao, P.K. Rao, Appl. Catal. A 167 (1998) 11.
- [114] S. Narayanan, K. Krishna, Appl. Catal. A 174 (1998) 221.
- [115] S. Narayanan, K. Krishna, Appl. Catal. A 198 (2000) 13.
- [116] S. Narayanan, A. Sultana, Q.T. Le, A. Auroux, Appl. Catal. A 168 (1998) 373.
- [117] R.J. Nash, M.E. Dry, C.T. O'Connor, Appl. Catal. A 134 (1996) 285.
- [118] J.A. Navio, G. Colon, M. Macias, C. Real, M.I. Litter, Appl. Catal. A 177 (1999) 111.
- [119] F. Niu, H. Hofmann, Appl. Catal. A 128 (1995) 107.
- [120] R.A. Overbeek, P.A. Warringa, M.J.D. Crombag, L.M. Visser, A.J. van Dillen, J.W. Geus, Appl. Catal. A 135 (1996) 209.
- [121] I. Palinko, B. Torok, G.K.S. Prakash, G.A. Olah, Appl. Catal. A 174 (1998) 147.
- [122] K. Pamin, A. Kubacka, Z. Olejniczak, J. Haber, B. Sulikowski, Appl. Catal. A 194–195 (2000) 137.
- [123] C. Pecharroman, I. Sobrados, J.E. Iglesias, T. Gonzalez-Carreno, J. Sanz, J. Phys. Chem. B 103 (1999) 6160.
- [124] E.L. Pires, J.C. Magalhaes, U. Schuchardt, Appl. Catal. A 203 (2000) 231.
- [125] L.R. Pizzio, C.V. Caceres, M.N. Blanco, Appl. Catal. A 167 (1998) 283.
- [126] F. Quignard, O. Graziani, A. Choplin, Appl. Catal. A 182 (1999) 29.
- [127] M. Quiroga, M.R. Capeletti, N. Figoli, U. Sedran, Appl. Catal. A 177 (1999) 37.
- [128] R. Raja, P. Ratnasamy, Appl. Catal. A 143 (1996) 145.
- [129] S. Recchia, C. Dossi, A. Fusi, L. Sordelli, R. Psaro, Appl. Catal. A 182 (1999) 41.
- [130] B.M. Reddy, M.V. Kumar, K.J. Ratnam, Appl. Catal. A 181 (1999) 77.
- [131] J.S. Reddy, S. Sayari, Appl. Catal. A 128 (1995) 231.
- [132] M.A. Reiche, T. Burgi, A. Baiker, A. Scholz, B. Schnyder, A. Wokaun, Appl. Catal. A 198 (2000) 155.
- [133] Z. Sarbak, Appl. Catal. A 124 (1995) 245.
- [134] J. Sarkany, Appl. Catal. A 188 (1999) 369.
- [135] F. Schekler-Nahama, O. Clause, D. Commereuc, J. Saussey, Appl. Catal. A 167 (1998) 237.
- [136] U. Seidler, M. Koch, E. Brunner, B. Staudte, H. Pfeifer, Microporous Mesoporous Mater. 35–36 (2000) 341.
- [137] F. Simard, U.A. Sedran, J. Sepulveda, N.S. Figoli, H.I. de Lasa, Appl. Catal. A 125 (1995) 81.
- [138] F. De Smet, P. Ruiz, B. Delmon, M. Devillers, Appl. Catal. A 172 (1998) 333.
- [139] Z. Sobalik, A.A. Belhekar, Z. Tvaruzkova, B. Wichterlova, Appl. Catal. A 188 (1999) 175.
- [140] V.I. Sobolev, K.A. Dubkov, E.A. Paukshtis, L.V. Pirutko, M.A. Rodkin, A.S. Kharitonov, G.I. Panov, Appl. Catal. A 141 (1996) 185.
- [141] M. Suvanto, J. Raty, T.A. Pakkanen, Appl. Catal. A 181 (1999) 189.
- [142] J. Taguchi, T. Okuhara, Appl. Catal. A 194–195 (2000) 89.
- [143] J.-M. Tatibouet, Ch. Montalescot, K. Bruckman, Appl. Catal. A 138 (1996) L1.
- [144] C.P. Tipp, P. Kazmaier, M.L. Hair, Langmuir 12 (1996) 6404.
- [145] C.P. Tipp, P. Kazmaier, M.L. Hair, Langmuir 12 (1996) 6407.
- [146] C.P. Tipp, J.R. Combes, Langmuir 14 (1998) 7348.
- [147] B. Torok, A. Molnar, N. Balogh, I. Kiricsi, I. Palinko, L.I. Horvath, Appl. Catal. A 158 (1997) L17.
- [148] M. Trombetta, T. Armadori, A.G. Alejandre, J.R. Solis, G. Busca, Appl. Catal. A 192 (2000) 125.
- [149] R.P. Viswanath, P. Wilson, Appl. Catal. A 201 (2000) 23.
- [150] L.D. White, C.P. Tripp, J. Colloid Interface Sci. 224 (2000) 417.
- [151] L.D. White, C.P. Tripp, J. Colloid Interface Sci. 227 (2000) 237.
- [152] M.A. Uguina, D.P. Serrano, G. Ovejero, R. Van Grieken, M. Camacho, Appl. Catal. A 124 (1995) 391.
- [153] E. Unneberg, S. Kolboe, Appl. Catal. A 124 (1995) 345.
- [154] G.D. Yadav, V.V. Bokade, Appl. Catal. A 147 (1996) 299.

- [155] G.D. Yadav, N. Kirthivasan, *Appl. Catal. A* 154 (1997) 29.
- [156] M.-G. Yang, I. Nakamura, K. Fujimoto, *Appl. Catal. A* 144 (1996) 221.
- [157] P.-W. Yen, T.-Ch. Chou, *Appl. Catal. A* 182 (1999) 217.
- [158] M.I. Zaki, M.A. Hasan, L. Pasupulety, *Appl. Catal. A* 198 (2000) 247.
- [159] K. Zama, Y. Imada, A. Fukuoka, M. Ichikawa, *Appl. Catal. A* 194–195 (2000) 285.
- [160] J. Zheng, J.-L. Dong, Q.-H. Xu, Y. Liu, A.-Z. Yan, *Appl. Catal. A* 126 (1995) 141.
- [161] M. Paulis, M. Martin, D.B. Soria, A. Diaz, J.A. Odriozola, M. Montes, *Appl. Catal. A* 180 (1999) 411.
- [162] F. Schekler-Nahama, O. Clause, D. Commereuc, J. Saussey, *Appl. Catal. A* 167 (1998) 247.
- [163] M.D. Wildberger, T. Mallat, U. Gobel, A. Baiker, *Appl. Catal. A* 168 (1998) 69.
- [164] R.T. Yang, W.B. Li, N. Chen, *Appl. Catal. A* 169 (1998) 215.
- [165] W. Zhang, P.G. Smirniotis, *Appl. Catal. A* 168 (1998) 113.
- [166] V.A. Veeffkind, M.L. Smidt, J.A. Lercher, *Appl. Catal. A* 194–195 (2000) 319.
- [167] T. Halachev, P. Atanasova, A. Lopez Agudo, M.G. Arias, J. Ramirez, *Appl. Catal. A* 136 (1996) 161.
- [168] J.-L. Li, T. Inui, *Appl. Catal. A* 137 (1996) 105.
- [169] J. Ramirez, P. Castillo, L. Cedeno, R. Cuevas, M. Castillo, J.M. Palacios, A. Lopez-Agudo, *Appl. Catal. A* 132 (1995) 317.
- [170] J. Bodis, J. Zsako, Cs. Nemeth, J. Mink, *Vib. Spectrosc.* 9 (1995) 197.
- [171] W. Daniell, U. Schubert, R. Glockler, A. Meyer, K. Noweck, H. Knozinger, *Appl. Catal. A* 196 (2000) 247.
- [172] O. Dulaurent, M. Nawdali, A. Bouane, D. Bianchi, *Appl. Catal. A* 201 (2000) 271.
- [173] G. Larsen, E. Lotero, R.D. Parra, L.M. Petkovic, H.S. Silva, S. Raghavan, *Appl. Catal. A* 130 (1995) 213.
- [174] N.T. Dung, D. Tichit, B.H. Chiche, B. Coq, *Appl. Catal. A* 169 (1998) 179.
- [175] V.A. Ivanov, A. Pieplu, J.C. Lavalley, P. Nortier, *Appl. Catal. A* 131 (1995) 323.
- [176] F. Fally, V. Perrichon, H. Vidal, J. Kaspar, G. Blanco, J.M. Pintado, S. Bernal, G. Colon, M. Daturi, J.C. Lavalley, *Catal. Today* 59 (2000) 373.
- [177] E.K. Poels, D.S. Brands, *Appl. Catal. A* 191 (2000) 83.
- [178] F. Wang, T. Tsai, *Appl. Catal. A* 201 (2000) 91.
- [179] N. Arsenova, H. Bludau, W.O. Haag, H.G. Karge, *Microporous Mesoporous Mater.* 23 (1998) 1.
- [180] N. Arsenova-Hartel, H. Bludau, R. Schumacher, W.O. Haag, H.G. Karge, E. Brunner, U. Wild, *J. Catal.* 191 (2000) 326.
- [181] I. Hannus, *Appl. Catal. A* 189 (1999) 263.
- [182] E. Baburek, J. Novakova, *Appl. Catal. A* 185 (1999) 123.
- [183] M. Trombetta, G. Busca, M. Lenarda, L. Storaro, R. Ganzerla, L. Povesan, A.J. Lopez, M. Alcantara-Rodríguez, E. Rodríguez-Castellón, *Appl. Catal. A* 193 (2000) 55.
- [184] M. Trombetta, G. Busca, M. Lenarda, L. Storaro, M. Pavan, *Appl. Catal. A* 182 (1999) 225.
- [185] O.A. Anunziata, L.B. Pierella, R.G. Marino, *Appl. Catal. A* 165 (1997) 35.
- [186] A. Auroux, J. Datka, *Appl. Catal. A* 165 (1997) 473.
- [187] J.M. Campelo, F. Lafont, J.M. Marinas, M. Ojeda, *Appl. Catal. A* 192 (2000) 85.
- [188] P. Canizares, A. Carrero, P. Sanchez, *Appl. Catal. A* 190 (2000) 93.
- [189] P. Concepcion, J.M.L. Nieto, A. Mifsud, J. Perez-Pariente, *Appl. Catal. A* 151 (1997) 373.
- [190] J.K.A. Dapaah, Y. Uemichi, A. Ayame, H. Matsushashi, M. Sugioka, *Appl. Catal. A* 187 (1999) 107.
- [191] A. Dejoz, J.M. Lopez Nieto, F. Marquez, M.I. Vazquez, *Appl. Catal. A* 180 (1999) 83.
- [192] C. Flego, L. Galasso, R. Millini, I. Kiricsi, *Appl. Catal. A* 168 (1998) 323.
- [193] C. Flego, I. Kiricsi, W.O. Parker Jr., M.G. Clerici, *Appl. Catal. A* 124 (1995) 107.
- [194] Z. Fu, D. Yin, Y. Yang, X. Guo, *Appl. Catal. A* 124 (1995) 59.
- [195] S.P. Ghorpade, V.S. Darshane, S.G. Dixit, *Appl. Catal. A* 166 (1998) 135.
- [196] Y.-G. Li, W.-H. Xie, S. Yong, *Appl. Catal. A* 150 (1997) 231.
- [197] T. Lopez, J. Navarrete, R. Gomez, O. Novaro, F. Figueras, H. Armendariz, *Appl. Catal. A* 125 (1995) 217.
- [198] H.B. Mostad, M. Stocker, A. Karlsson, T. Rorvik, *Appl. Catal. A* 144 (1996) 305.
- [199] B. Paweewan, P.J. Barrie, L.F. Gladden, *Appl. Catal. A* 167 (1998) 353.
- [200] B. Paweewan, P.J. Barrie, L.F. Gladden, *Appl. Catal. A* 185 (1999) 259.
- [201] L.M. Rodriguez, J. Alcaraz, M. Hernandez, M. Dufaux, Y.B. Taarit, M. Vrinat, *Appl. Catal. A* 189 (1999) 53.
- [202] J.R. Sohn, H.W. Kim, M.Y. Park, E.H. Park, J.T. Kim, S.E. Park, *Appl. Catal. A* 128 (1995) 127.
- [203] M.-T. Tran, N.S. Gnep, G. Szabo, M. Guisnet, *Appl. Catal. A* 171 (1998) 207.
- [204] J. Xie, S. Kaliaguine, *Appl. Catal. A* 148 (1997) 415.
- [205] S. Damyanova, J.L.G. Fierro, *Appl. Catal. A* 144 (1996) 59.
- [206] K. Hashimoto, Y. Hanada, Y. Minami, Y. Kera, *Appl. Catal. A* 141 (1996) 57.
- [207] K. Segawa, T. Shimura, *Appl. Catal. A* 194–195 (2000) 309.
- [208] N.V. Economidis, D.A. Pena, P.G. Smirniotis, *Appl. Catal. B* 23 (1999) 123.
- [209] K.B. Fogash, G. Yaluris, M.R. Gonzalez, P. Ouraipryvan, D.A. Ward, E.I. Ko, J.A. Dumesic, *Catal. Lett.* 32 (1995) 241.
- [210] J.M. Gallardo Amores, V. Sanchez Escribano, G. Ramis, G. Busca, *Appl. Catal. B* 13 (1997) 45.
- [211] G.P. Heitmann, G. Dahlhoff, W.F. Holderich, *J. Catal.* 186 (1999) 12.
- [212] Yu. Isaev, J.J. Fripiat, *J. Catal.* 182 (1999) 257.
- [213] S.M. Jung, P. Grange, *Catal. Today* 59 (2000) 305.
- [214] M.A. Kuehne, S.M. Babitz, H.H. Kung, J.T. Miller, *Appl. Catal. A* 166 (1998) 293.
- [215] L. Lietti, I. Nova, G. Ramis, L. Dall'Acqua, G. Busca, E. Giamello, P. Forzatti, F. Bregani, *J. Catal.* 187 (1999) 419.
- [216] R.Q. Long, R.T. Yang, *Catal. Lett.* 59 (1999) 39.
- [217] C.A. Muller, M. Schneider, T. Mallat, A. Baiker, *J. Catal.* 189 (2000) 221.
- [218] M. Nagai, Y. Goto, A. Irisawa, S. Omi, *J. Catal.* 191 (2000) 128.

- [219] M.A. Reiche, P. Hug, A. Baiker, *J. Catal.* 192 (2000) 400.
- [220] A.V. Salker, W. Weisweiler, *Appl. Catal. A* 203 (2000) 229.
- [221] R.B. Watson, U.S. Ozkan, *J. Catal.* 191 (2000) 12.
- [222] S. Yamauchi, T. Mori, H. Yamamura, *Appl. Catal. A* 132 (1995) 21.
- [223] G. Ramis, M.A. Larrubia, in: L. Petrov, Ch. Bonev, G. Kadinov (Eds.), *Heterogeneous Catalysis, Proceedings of the Ninth International Symposium, Varna, September 23–27, 2000*, Institute of Catalysis, Bulgarian Academy of Science, Sofia, 2000, pp. 647–652.
- [224] M.C.N. Amorim de Carvalho, F.B. Passos, M. Schmal, *Appl. Catal. A* 193 (2000) 265.
- [225] J.A. Anderson, C. Fergusson, I. Rodriguez-Ramos, A. Guerrero-Ruiz, *J. Catal.* 192 (2000) 344.
- [226] H. Berndt, A. Martin, A. Bruckner, E. Schreier, D. Muller, H. Kosslick, G.-U. Wolf, B. Lucke, *J. Catal.* 191 (2000) 384.
- [227] G. Colon, I. Ferino, E. Rombi, E. Selli, L. Forni, P. Magnoux, G. Guisnet, *Appl. Catal. A* 168 (1998) 81.
- [228] T. Cseri, S. Bekkassy, F. Figueras, E. Cseke, L.-Ch. de Menorval, R. Dutartre, *Appl. Catal. A* 132 (1995) 141.
- [229] M. Daturi, G. Busca, G. Groppi, P. Forzatti, *Appl. Catal. B* 12 (1997) 325.
- [230] B.H. Davis, R.A. Keogh, S. Alerasool, D.J. Zalewski, D.E. Day, P.K. Doolin, *J. Catal.* 183 (1999) 45.
- [231] E. Dumitriu, V. Hulea, I. Fechet, C. Catrinescu, A. Auroux, J.-F. Lacaze, C. Guimon, *Appl. Catal. A* 181 (1999) 15.
- [232] E. Dumitriu, V. Hulea, S. Kaliaguine, M.M. Huang, *Appl. Catal. A* 135 (1996) 57.
- [233] X. Fang, F. Li, L. Luo, *Appl. Catal. A* 146 (1996) 297.
- [234] K. Hashimoto, N. Toukai, *Appl. Catal. A* 180 (1999) 367.
- [235] G.P. Heitmann, G. Dahlhoff, J.P.M. Niederer, W.F. Holderich, *J. Catal.* 194 (2000) 122.
- [236] M.J. Hernado, C. Pasquera, C. Blanco, I. Benito, F. Gonzalez, *Appl. Catal. A* 141 (1996) 175.
- [237] P.D. Hopkins, J.T. Miller, B.L. Meyers, G.J. Ray, R.T. Roginski, M.A. Kuehne, H.H. Kung, *Appl. Catal. A* 136 (1996) 29.
- [238] J.-K. Jeon, K.-E. Jeong, Y.-K. Park, S.-K. Ihm, *Appl. Catal. A* 124 (1995) 91.
- [239] M. Jiang, T. Tatsumi, *J. Phys. Chem. B* 102 (1998) 10879.
- [240] M.S. Kaba, M.A. Barteau, W.Y. Lee, I.K. Song, *Appl. Catal. A* 194–195 (2000) 129.
- [241] Ch. Kwak, J.J. Lee, J.S. Bae, K. Choi, S.H. Moon, *Appl. Catal. A* 200 (2000) 233.
- [242] M. Laniecki, M. Malecka-Grycz, F. Domka, *Appl. Catal. A* 196 (2000) 293.
- [243] G. Larsen, E. Lotero, S. Raghavan, R.D. Parra, C.A. Queini, *Appl. Catal. A* 139 (1996) 201.
- [244] W. Liu, Y. Xu, *J. Catal.* 185 (1999) 386.
- [245] X. Liu, R.E. Truitt, *J. Am. Chem. Soc.* 119 (1997) 9856.
- [246] V. Loddo, G. Marci, C. Martin, L. Palmisano, V. Rives, A. Scalfani, *Appl. Catal. B* 20 (1999) 29.
- [247] T. Lopez, F. Tzompantzi, J. Navarrete, R. Gomez, J.L. Boldu, E. Munoz, O. Novaro, *J. Catal.* 181 (1999) 285.
- [248] E. Lopez-Salinas, J.G. Hernandez-Cortez, Ma.A. Cortes-Jacome, J. Navarrete, Ma.E. Llanos, A. Vazquez, H. Armendariz, T. Lopez, *Appl. Catal. A* 175 (1998) 43.
- [249] Y. Ma, Q.L. Wang, W. Jiang, B. Zuo, *Appl. Catal. A* 165 (1997) 199.
- [250] J. Martinez-Triguero, M.J. Diaz-Cabanias, M.A. Cambolor, V. Fornes, Th.L.M. Maesen, A. Corma, *J. Catal.* 182 (1999) 463.
- [251] J. Medina-Valtierra, M.A. Sanchez, J.A. Montoya, J. Navarrete, J.A. de los Reyes, *Appl. Catal. A* 158 (1997) L1.
- [252] J. Medina-Valtierra, O. Zaldivar, M.A. Sánchez, J.A. Montoya, J. Navarrete, J.A. de los Reyes, *Appl. Catal. A* 166 (1998) 387.
- [253] M. Moraes, W.De S.F. Pinto, W.A. Gonzalez, L.M.P.M. Carmo, N.M.R. Pastura, E.R. Lachter, *Appl. Catal. A* 138 (1996) L7.
- [254] M.L. Ocellii, S. Biz, A. Auroux, P.S. Iyer, *Appl. Catal. A* 179 (1999) 117.
- [255] Y.Ch. Park, H.-K. Rhee, *Appl. Catal. A* 179 (1999) 145.
- [256] J. Santamaria Gonzalez, M. Martinez Lara, M. Lopez Granados, J.L.G. Fierro, A. Jimenez Lopez, *Appl. Catal. A* 144 (1996) 365.
- [257] A. Severino, A. Esculcas, J. Rocha, J. Vital, L.S. Lobo, *Appl. Catal. A* 142 (1996) 255.
- [258] M. Shirai, K. Aoki, K. Torii, M. Arai, *Appl. Catal. A* 187 (1999) 141.
- [259] J.R. Sohn, S.Y. Lee, *Appl. Catal. A* 164 (1997) 127.
- [260] M. Tajima, M. Niwa, Y. Fujii, Y. Koinuma, R. Aizawa, S. Kushiyaama, S. Kobayashi, K. Mizuno, H. Ohuchi, *Appl. Catal. B* 12 (1997) 263.
- [261] K. Tao, W. Li, X. Li, X. Qi, *Appl. Catal. A* 139 (1996) 43.
- [262] B. Torok, I. Kiricsi, A. Molnar, G.A. Olah, *J. Catal.* 193 (2000) 132.
- [263] R. Ueda, T. Kusakari, K. Tomishige, K. Fujimoto, *J. Catal.* 194 (2000) 14.
- [264] T. Ushikubo, K. Wada, *Appl. Catal. A* 124 (1995) 19.
- [265] S. Vergne, A. Berreghis, J. Tantet, C. Canaff, P. Magnoux, M. Guisnet, N. Davis, R. Noirost, *Appl. Catal. B* 18 (1998) 37.
- [266] A. Vimont, F. Thibault-Starzyk, J.C. Lavalley, *J. Phys. Chem. B* 104 (2000) 286.
- [267] J. Wang, Q. Li, J. Yao, *Appl. Catal. A* 184 (1999) 181.
- [268] F.-S. Xiao, G. Pang, T. Ji, X. Meng, W. Pang, R. Xu, *Appl. Catal. A* 133 (1995) 305.
- [269] M. Yurdakoc, M. Akcay, Y. Tonbul, K. Yurdakoc, *Turk. J. Chem.* 23 (1999) 319.
- [270] H.W. Zanthoff, S. Schaefer, G.-U. Wolf, *Appl. Catal. A* 164 (1997) 105.
- [271] M. Ziolk, J. Kujawa, J. Czyniewska, I. Nowak, A. Aboulayt, O. Saur, J.C. Lavalley, *Appl. Catal. A* 171 (1998) 109.
- [272] S. Ramirez, M. Viniegra, J.M. Dominguez, P. Schacht, L.Ch. De Menorval, *Catal. Lett.* 66 (2000) 25.
- [273] K.M. Bulanin, J.C. Lavalley, J. Lamotte, L. Mariey, N.M. Tsyganienko, A.A. Tsyganienko, *J. Phys. Chem. B* 102 (1998) 6809.
- [274] C. Binet, M. Daturi, J.-C. Lavalley, *Catal. Today* 50 (1999) 207.
- [275] C. Pophal, T. Yogo, K. Yamada, K. Segawa, *Appl. Catal. B* 16 (1998) 177.
- [276] P. KaBner, M. Berns, *Appl. Catal. A* 139 (1996) 107.
- [277] U. Bentrup, A. Martin, B. Lucke, *Topics Catal.* 11/12 (2000) 139.

- [278] V. Parvulescu, S. Coman, P. Grange, V.I. Parvulescu, *Appl. Catal. A* 176 (1999) 27.
- [279] H. Berndt, G. Lietz, B. Lucke, J. Volter, *Appl. Catal. A* 146 (1996) 351.
- [280] G. Busca, G. Martra, A. Zecchina, *Catal. Today* 56 (2000) 361.
- [281] T. Jarecka, J. Datka, *Appl. Catal. A* 184 (1999) 203.
- [282] R. Navarro, B. Pawelec, J.L.G. Fierro, P.T. Vasudevan, *Appl. Catal. A* 148 (1996) 23.
- [283] Z. Sarbak, *Appl. Catal. A* 159 (1997) 147.
- [284] Z. Sarbak, *Appl. Catal. A* 164 (1997) 13.
- [285] H.K. Heinichen, W.F. Hölderich, *J. Catal.* 185 (1999) 408.
- [286] A.I. Ivanov, G.W. Graham, M. Shelef, *Appl. Catal. B* 21 (1999) 243.
- [287] B. Coq, D. Tichit, S. Ribet, *J. Catal.* 189 (2000) 117.
- [288] M.P. Vorob'eva, A.A. Greish, A.V. Ivanov, L.M. Kustov, *Appl. Catal. A* 199 (2000) 257.
- [289] D.B. Akolekar, *Appl. Catal. A* 171 (1998) 261.
- [290] M.R. Albert, *J. Catal.* 189 (2000) 158.
- [291] O. Alexeev, D.-W. Kim, G.W. Graham, M. Shelef, B.C. Gates, *J. Catal.* 185 (1999) 170.
- [292] J.A. Anderson, C. Marquez-Alvarez, M.J. Lopez-Munoz, I. Rodriguez-Ramos, A. Guerrero-Ruiz, *Appl. Catal. B* 14 (1997) 189.
- [293] G.J. Arteaga, J.A. Anderson, C.H. Rochester, *J. Catal.* 189 (2000) 195.
- [294] G. Berhault, F. Mauge, J.-C. Lavalley, M. Lacroix, M. Breyse, *J. Catal.* 189 (2000) 431.
- [295] F. Boccuzzi, A. Chiorino, M. Manzoli, D. Andreeva, T. Tabakova, in: L. Petrov, Ch. Bonev, G. Kadinov (Eds.), *Heterogeneous Catalysis, Proceedings of the Ninth International Symposium, Varna, September 23–27, 2000*, Institute of Catalysis, Bulgarian Academy of Science, Sofia, 2000, pp. 725–730.
- [296] F. Boccuzzi, S. Coluccia, G. Martra, N. Ravasio, *J. Catal.* 184 (1999) 316.
- [297] F. Boccuzzi, G. Martra, C.P. Papalia, N. Ravasio, *J. Catal.* 184 (1999) 327.
- [298] E. Boellaard, A.M. van der Kraan, J.W. Geus, *Appl. Catal. A* 147 (1996) 207.
- [299] E. Boellaard, F.Th. van de Scheur, A.M. van der Kraan, J.W. Geus, *Appl. Catal. A* 171 (1998) 333.
- [300] V.Yu. Borovkov, M. Jiang, Y. Fu, *J. Phys. Chem. B* 103 (1999) 5010.
- [301] M.C. Campa, D. Pietrogiamomi, S. Tuti, G. Ferraris, V. Indovina, *Appl. Catal. B* 18 (1998) 151.
- [302] B.D. Chandler, A.B. Schabel, C.F. Blanford, L.H. Pignolet, *J. Catal.* 187 (1999) 367.
- [303] Y. Chen, K. Tomishige, K. Yokoyama, K. Fujimoto, *Appl. Catal. A* 165 (1997) 335.
- [304] Y.-G. Chen, K. Tomishige, K. Yokoyama, K. Fujimoto, *J. Catal.* 184 (1999) 479.
- [305] F.K. Chong, J.A. Anderson, C.H. Rochester, *J. Catal.* 190 (2000) 327.
- [306] A. Dandekar, M.A. Vannice, *Appl. Catal. B* 22 (1999) 179.
- [307] O. Dulaurent, D. Bianchi, *Appl. Catal. A* 196 (2000) 271.
- [308] O. Dulaurent, K. Chandès, Ch. Bouly, D. Bianchi, *J. Catal.* 192 (2000) 262.
- [309] O. Dulaurent, K. Chandès, Ch. Bouly, D. Bianchi, *J. Catal.* 192 (2000) 273.
- [310] O. Dulaurent, X. Courtois, V. Perrichon, D. Bianchi, *J. Phys. Chem. B* 104 (2000) 6001.
- [311] C. Elmasides, D.I. Kondarides, W. Grunert, X.E. Verykios, *J. Phys. Chem. B* 103 (1999) 5227.
- [312] R.T. Figueiredo, M.L. Granados, J.L.G. Fierro, L. Vigos, P.R. de la Piscina, N. Homs, *Appl. Catal. A* 170 (1998) 145.
- [313] M. Frank, M. Baumer, *Phys. Chem. Chem. Phys.* 2 (2000) 3723.
- [314] Z. Gandao, B. Coq, L.Ch. de Menorval, D. Tichit, *Appl. Catal. A* 147 (1996) 395.
- [315] T.F. Guidry, G.L. Price, *J. Catal.* 181 (1999) 16.
- [316] K. Hadjiivanov, H. Knozinger, *J. Phys. Chem. B* 102 (1998) 10936.
- [317] K. Hadjiivanov, H. Knozinger, *J. Catal.* 191 (2000) 480.
- [318] K. Hadjiivanov, M. Mihaylov, D. Klissurski, P. Stefanov, N. Abadjieva, E. Vassileva, L. Mintchev, *J. Catal.* 185 (1999) 314.
- [319] K. Hajiivanov, B.M. Reddy, H. Knozinger, *Appl. Catal. A* 188 (1999) 355.
- [320] A. Holmgren, B. Andersson, D. Duprez, *Appl. Catal. B* 22 (1999) 215.
- [321] V. Indovina, M. Occhiuzzi, D. Pietrogiamomi, S. Tuti, *J. Phys. Chem. B* 103 (1999) 9967.
- [322] E.L. Jablonski, A.A. Castro, O.A. Scelza, S.R. de Miguel, *Appl. Catal. A* 183 (1999) 189.
- [323] G. Jacobs, F. Ghadiali, A. Pisanu, A. Borgna, W.E. Alvarez, D.E. Resasco, *Appl. Catal. A* 188 (1999) 79.
- [324] G. Jacobs, F. Ghadiali, A. Pisanu, C.L. Padro, A. Borgna, W.E. Alvarez, D.E. Resasco, *J. Catal.* 191 (2000) 116.
- [325] R.-M. Jao, L.-J. Leu, J.-R. Chang, *Appl. Catal. A* 135 (1996) 301.
- [326] K.-D. Jung, A.T. Bell, *J. Catal.* 193 (2000) 207.
- [327] H. Kalies, N. Pinto, G.M. Pajonk, D. Bianchi, *Appl. Catal. A* 202 (2000) 197.
- [328] M. Kantcheva, M.U. Kucukkal, S. Suzer, *J. Catal.* 190 (2000) 144.
- [329] P. Li, Y. Xiang, V.H. Grassian, S.C. Larsen, *J. Phys. Chem. B* 103 (1999) 5058.
- [330] H. Liu, A.I. Kozlov, A.P. Kozlova, T. Shido, K. Asakura, Y. Iwasawa, *J. Catal.* 185 (1999) 252.
- [331] J.R. Monnier, J.W. Medlin, Y.-J. Kuo, *Appl. Catal. A* 194–195 (2000) 463.
- [332] R. Navarro, B. Pawelec, J.L.G. Fierro, P.T. Vasudevan, J.F. Cambra, P.L. Arias, *Appl. Catal. A* 137 (1996) 269.
- [333] R.M. Navarro, B. Pawelec, J.M. Trejo, R. Mariscal, J.L.G. Fierro, *J. Catal.* 189 (2000) 184.
- [334] A.J. Pardey, M. Fernandez, J. Alvarez, C. Urbina, D. Moronta, V. Leon, M. Haukka, T.A. Pakkanen, *Appl. Catal. A* 199 (2000) 275.
- [335] B. Pawelec, L. Daza, J.L.G. Fierro, J.A. Anderson, *Appl. Catal. A* 145 (1996) 307.
- [336] H. Praliand, S. Mikhailenko, Z. Chajar, M. Primet, *Appl. Catal. B* 16 (1998) 359.
- [337] F. Prinetto, G. Ghiotti, S. De Rossi, G. Di Modica, *Appl. Catal. B* 14 (1997) 225.

- [338] A.I. Serykh, O.P. Tkachenko, V.Yu. Borovkov, V.B. Kazansky, Kh.M. Minachev, Ch. Hippe, N.I. Jaeger, G. Schulz-Ekloff, in: L. Petrov, Ch. Bonev, G. Kadinov (Eds.), *Heterogeneous Catalysis, Proceedings of the Ninth International Symposium, Varna, September 23–27, 2000*, Institute of Catalysis, Bulgarian Academy of Science, Sofia, 2000, pp. 471–476.
- [339] M.A.P. Silva, R.A. MelloVieira, M. Schmal, *Appl. Catal. A* 190 (2000) 177.
- [340] T.R.O. de Souza, S.M. de Oliveira Brito, H.M.C. Andrade, *Appl. Catal. A* 178 (1999) 7.
- [341] S. Sun, N. Tsubaki, K. Fujimoto, *Appl. Catal. A* 202 (2000) 121.
- [342] T. Ueckert, R. Lamber, N.I. Jaeger, U. Schubert, *Appl. Catal. A* 155 (1997) 75.
- [343] Z. Wu, Y. Chu, S. Yang, Z. Wei, C. Li, Q. Xin, *J. Catal.* 194 (2000) 23.
- [344] S. Yang, C. Li, J. Xu, Q. Xin, *J. Phys. Chem. B* 102 (1998) 6986.
- [345] A. Yee, S.J. Morrison, H. Idriss, *J. Catal.* 191 (2000) 30.
- [346] Z.C. Zhang, B.C. Beard, *Appl. Catal. A* 188 (1999) 229.
- [347] E. Yoda, J.N. Kondo, F. Wakabayashi, K. Domen, *Appl. Catal. A* 194–195 (2000) 275.
- [348] V. Labalme, N. Benhamou, N. Guilhaume, E. Grabowski, M. Primet, *Appl. Catal. A* 133 (1995) 351.
- [349] K.K. Bando, K. Soga, K. Kunimori, H. Arakawa, *Appl. Catal. A* 175 (1998) 67.
- [350] G. Martra, *Appl. Catal. A* 200 (2000) 275.
- [351] M.A.S. Baldanza, L.F. de Mello, A. Vannice, F.B. Noronha, M. Schmal, *J. Catal.* 192 (2000) 64.
- [352] D. Spielbauer, G.A.H. Mekhemer, M.I. Zaki, H. Knozinger, *Catal. Lett.* 40 (1996) 71.
- [353] E. Guglielminotti, F. Boccuzzi, M. Manzoli, F. Pinna, M. Scarpa, *J. Catal.* 192 (2000) 149.
- [354] Z. Schay, H. Knozinger, L. Gucci, G. Pal-Borbely, *Appl. Catal. B* 18 (1998) 263.
- [355] A. Trunschke, D.L. Hoang, J. Radnik, H. Lieske, *J. Catal.* 191 (2000) 456.
- [356] K.M. Neyman, P. Strodel, S.Ph. Ruzankin, N. Schlensog, H. Knozinger, N. Rosch, *Catal. Lett.* 31 (1995) 273.
- [357] A. Benitez, J. Ramirez, J.L.G. Fierro, A. Lopez Agudo, *Appl. Catal. A* 144 (1996) 343.
- [358] K. Eguchi, T. Kondo, T. Hayashi, H. Arai, *Appl. Catal. B* 16 (1998) 69.
- [359] K. Hadjiivanov, P. Concepcion, H. Knozinger, *Topics Catal.* 11/12 (2000) 123.
- [360] K. Hashimoto, K. Fukuhara, Y. Fujiwara, H. Kominami, H. Mishima, Y. Kera, *Appl. Catal. A* 165 (1997) 451.
- [361] C. Henriques, M.F. Ribeiro, C. Abreu, D.M. Murphy, F. Pognant, J. Saussey, J.C. Lavaley, *Appl. Catal. B* 16 (1998) 79.
- [362] S.-J. Huang, A.B. Walters, M.A. Vannice, *J. Catal.* 192 (2000) 29.
- [363] V.I. Parvulescu, P. Oelker, P. Grange, B. Delmon, *Appl. Catal. B* 16 (1998) 1.
- [364] B. Pawelec, R. Navarro, J.L.G. Fierro, P.T. Vasudevan, *Appl. Catal. A* 168 (1998) 205.
- [365] J. Ramirez, R. Contreras, P. Castillo, T. Klimova, R. Zarate, R. Luna, *Appl. Catal. A* 197 (2000) 69.
- [366] M. Shimokawabe, K. Tadokoro, *Appl. Catal. A* 166 (1998) 215.
- [367] E.A. Efthimiadis, S.C. Christoforou, A.A. Nikolopoulos, I.A. Vasalos, *Appl. Catal. B* 22 (1999) 91.
- [368] A. Raj, T.H.N. Le, S. Kaliaguine, A. Auroux, *Appl. Catal. B* 15 (1998) 259.
- [369] J.B. Peri, in: J.R. Anderson, M. Boudart (Eds.), *Catalysis*, Springer, Berlin, 1984, pp. 172–220.
- [370] J.E. Mapes, R.P. Eischens, *J. Phys. Chem.* 58 (1954) 1059.
- [371] R.P. Eischens, S.A. Francis, W.A. Pliskin, *J. Phys. Chem.* 60 (1956) 194.
- [372] R.P. Eischens, W.A. Pliskin, *Adv. Catal.* 10 (1958) 1.
- [373] E.P. Parry, *J. Catal.* 2 (1963) 371.
- [374] A. Zecchina, D. Scarano, *Surf. Sci.* 166 (1986) 347.
- [375] J.C.S. Wong, J.T. Yates Jr., *J. Phys. Chem.* 99 (1995) 12640.
- [376] D.B. Mawhinney, J.A. Rossin, K. Gerhart, J.T. Yates Jr., *Langmuir* 15 (1999) 4617.
- [377] L. Marchese, S. Bordiga, S. Coluccia, G. Martra, A. Zecchina, *J. Chem. Soc., Faraday Trans.* 89 (1993) 3483.
- [378] S.S.C. Chuang, M.A. Brundage, M.W. Balakos, G. Srinivas, *Appl. Spectrosc.* 49 (1995) 1151.
- [379] R. Mariscal, H.R. Reinhoudt, A.D. van Langeveld, J.A. Moulijn, *Vib. Spectrosc.* 16 (1998) 119.
- [380] Q. Sun, Ch.-W. Liu, W. Pan, Q.-M. Zhu, J.-F. Deng, *Appl. Catal. A* 171 (1998) 301.
- [381] J.A. Lercher, V. Veeffkind, K. Fajferweg, *Vib. Spectrosc.* 19 (1999) 107.
- [382] G. Mirth, F. Eder, J.A. Lercher, *Appl. Spectrosc.* 48 (1994) 194.
- [383] Yu.E. Gorbaty, G.V. Bondarenko, *Appl. Spectrosc.* 53 (1999) 908.
- [384] H. Yoshida, T. Yamazaki, S. Ozawa, *J. Colloid Interface Sci.* 224 (2000) 261.
- [385] W.Z. Weng, M.S. Chen, Q.G. Yan, T.H. Wu, Z.S. Chao, Y.Y. Liao, H.L. Wan, *Catal. Today* 63 (2000) 317.
- [386] A. Dombi, Z.A. Fekete, I. Kiricsi, *Appl. Catal. A* 193 (2000) L5.
- [387] G. Laurency, F. Lukacs, R. Roulet, *Anal. Chim. Acta* 359 (1998) 275.
- [388] O. Bache, M. Ystenes, *Appl. Spectrosc.* 48 (1994) 985.
- [389] G.J. Millar, D. Newton, G.A. Bowmaker, R.P. Cooney, *Appl. Spectrosc.* 48 (1994) 827.
- [390] Harrick Scientific Corporation. <http://www.haricksci.com>.
- [391] International Crystal Laboratories, USA.
- [392] Reflex Analytical Corporation, USA. www.reflexusa.com.
- [393] In Situ Research and Instruments, USA.
- [394] <http://www.remspec.com>.
- [395] G. Busca, *Catal. Today* 27 (1996) 323.
- [396] M.J. Weaver, *Topics Catal.* 8 (1999) 65.
- [397] H.D. Lutz, H. Haeuseler, *Trends Appl. Spectrosc.* 2 (1998) 59.
- [398] H.D. Lutz, H. Haeuseler, *J. Mol. Struct.* 511–512 (1999) 69.
- [399] P. Dumas, M.K. Weldon, Y.J. Chabal, G.P. Williams, *Surf. Rev. Lett.* 6 (1999) 225.
- [400] J.C. Lavalley, *Catal. Today* 27 (1996) 377.
- [401] C. Morterra, G. Magnacca, *Catal. Today* 27 (1996) 497.

- [402] M. Akcay, M. Yurdakoc, Y. Tonbul, K. Yurdakoc, D. Honicke, *Spectrosc. Lett.* 31 (1998) 1719.
- [403] A. Aranzabe, P. Román, A.T. Aguayo, C. Martin, V. Rives, *Spectrosc. Lett.* 30 (1997) 963.
- [404] S. Irusta, A. Boix, B. Pierini, C. Caspani, J. Petunchi, *J. Catal.* 187 (1999) 298.
- [405] J. Liu, P. Ying, Q. Xin, C. Li, *Appl. Spectrosc.* 53 (1999) 40.
- [406] C.L.T. da Silva, V.L.L. Camorim, J.L. Zotin, M.L.R.D. Pereira, A.C. Faro Jr., *Catal. Today* 57 (2000) 209.
- [407] E. Zhao, Yu. Isaev, A. Sklyarov, J.J. Fripiat, *Catal. Lett.* 60 (1999) 173.
- [408] R. Barthos, F. Lonyi, J. Engelhardt, J. Valyon, *Topics Catal.* 10 (2000) 79.
- [409] S.M. Jung, O. Dupont, P. Grange, *Appl. Catal. A* 208 (2001) 393.
- [410] S. Scire, C. Crisafulli, R. Maggiore, S. Minico, S. Galvagno, *Appl. Surf. Sci.* 136 (1998) 311.
- [411] J.M. Saniger, *Mater. Lett.* 22 (1995) 109.
- [412] S. Srinivasan, C.R. Narayanan, A.K. Datye, *Appl. Catal. A* 132 (1995) 289.
- [413] D.B. Mawhinney, J.A. Rossin, K. Gerhart, J.T. Yates Jr., *Langmuir* 16 (2000) 2237.
- [414] L.C. Varanda, M. Jafelicci Jr., R. Magnani, M.R. Davolos, F.A. Sigoli, R.F.C. Marques, R.H.M. Godoi, *J. Non-Cryst. Solids* 247 (1999) 227.
- [415] P. Thomasson, O.S. Tyagi, H. Knozinger, *Appl. Catal. A* 181 (1999) 181.
- [416] X. Gao, S.R. Bare, J.L.G. Fierro, M.A. Banares, I.E. Wachs, *J. Phys. Chem. B* 102 (1998) 5653.
- [417] S. Shoval, S. Yariv, K.H. Michaelian, I. Lapidés, M. Boudeuille, G. Panczer, *J. Colloid Interface Sci.* 212 (1999) 523.
- [418] T. Sugino, A. Kido, N. Azuma, A. Ueno, Y. Udagawa, *J. Catal.* 190 (2000) 118.
- [419] B.M. Reddy, B. Chowdhury, I. Ganesh, E.P. Reddy, T.C. Rojas, A. Fernandez, *J. Phys. Chem. B* 102 (1998) 10176.
- [420] Y. Toda, T. Ohno, F. Hatayama, H. Miyata, *Appl. Catal. A* 207 (2001) 273.
- [421] L.J. Burcham, J. Datka, I.E. Wachs, *J. Phys. Chem. B* 103 (1999) 6015.
- [422] L. Dong, Y. Hu, F. Xu, D. Lu, B. Xu, Z. Hu, Y. Chen, *J. Phys. Chem. B* 104 (2000) 78.
- [423] M. Wojciechowska, B. Czajka, M. Pietrowski, M. Zielinski, *Catal. Lett.* 66 (2000) 147.
- [424] L. Lupan, G. Munteanu, in: A. Andreev, L. Petrov, Ch. Bonev, G. Kadinov, I. Mitov (Eds.), *Heterogeneous Catalysis, Proceedings of the Eighth International Symposium, Varna, October 5–9, 1996, Institute of Catalysis, Bulgarian Academy of Sciences, Sofia, 1996*, pp. 55–60.
- [425] H. Ishikawa, J.N. Kondo, K. Domen, *J. Phys. Chem. B* 103 (1999) 3229.
- [426] A.M. Ferrari, S. Huber, H. Knozinger, K.M. Neyman, N. Rosch, *J. Phys. Chem. B* 102 (1998) 4548.
- [427] S. Golay, R. Doepper, A. Renken, *Appl. Catal. A* 172 (1998) 97.
- [428] Z.-F. Pei, V. Ponec, *Appl. Surf. Sci.* 103 (1996) 171.
- [429] O. Klug, W. Forsling, *Langmuir* 15 (1999) 6961.
- [430] J.K. Cox, C.P. Tripp, *Appl. Spectrosc.* 54 (2000) 144.
- [431] M. Kantacheva, K. Hadjiivanov, F. Audry, J.C. Lavalley, in: A. Andreev, L. Petrov, Ch. Bonev, G. Kadinov, I. Mitov (Eds.), *Heterogeneous Catalysis, Proceedings of the Eighth International Symposium, Varna, October 5–9, 1996, Institute of Catalysis, Bulgarian Academy of Sciences, Sofia, 1996*, pp. 31–36.
- [432] M.I. Zaki, M.A. Hasan, F.A. Al. Sagheer, L. Pasupulety, *Langmuir* 16 (2000) 430.
- [433] C.-C. Chuang, W.-C. Wu, M.-C. Huang, I.-C. Huang, J.-L. Lin, *J. Catal.* 185 (1999) 423.
- [434] Y. Chi, S.S.C. Chuang, *J. Phys. Chem. B* 104 (2000) 4673.
- [435] I.V. Babich, Yu.V. Plyuto, A.D. Van Langeveld, J.A. Moulijn, *Appl. Surf. Sci.* 115 (1997) 267.
- [436] R. Molina, M.A. Centeno, G. Poncelet, *J. Phys. Chem. B* 103 (1999) 6036.
- [437] R. Molina, G. Poncelet, *J. Phys. Chem. B* 103 (1999) 11290.
- [438] F. Verpoort, T. Haemers, P. Roose, J.-P. Maes, *Appl. Spectrosc.* 53 (1999) 1528.
- [439] S. Suvanto, T.A. Pakkanen, L. Backman, *Appl. Catal. A* 177 (1999) 25.
- [440] M. Kaltchev, W.T. Tysoc, *J. Catal.* 193 (2000) 29.
- [441] A. Martinez-Arias, M. Fernandez-Garcia, J. Soria, J.C. Conesa, *J. Catal.* 182 (1999) 367.
- [442] J.M. Hill, J. Shen, R.M. Watwe, J.A. Dumesic, *Langmuir* 16 (2000) 2213.
- [443] M. Li, J. Shen, W. Ji, *Thermochim. Acta* 345 (2000) 19.
- [444] E.V. Benvenuti, L. Franken, C.C. Moro, *Langmuir* 15 (1999) 8140.
- [445] J. Shen, J.M. Hill, R.M. Watwe, S.G. Podkolzin, J.A. Dumesic, *Catal. Lett.* 60 (1999) 1.
- [446] K.K. Bando, K. Sayama, H. Kusama, K. Okabe, H. Arakawa, *Appl. Catal. A* 165 (1997) 391.
- [447] I.A. Fisher, A.T. Bell, *J. Catal.* 172 (1997) 222.
- [448] H. Kusama, K.K. Bando, K. Okabe, H. Arakawa, *Appl. Catal. A* 205 (2001) 285.
- [449] H. Kusama, K. Okabe, H. Arakawa, *Appl. Catal. A* 207 (2001) 85.
- [450] N. Nomura, T. Tagawa, S. Goto, *Appl. Catal. A* 166 (1998) 321.
- [451] L.Z. Gao, C.T. Au, *J. Catal.* 189 (2000) 1.
- [452] E. Finocchio, M. Daturi, C. Binet, J.C. Lavalley, G. Blanchard, *Catal. Today* 52 (1999) 53.
- [453] A.-N. Ko, C.-L. Yang, W. Zhu, H. Lin, *Appl. Catal. A* 134 (1996) 53.
- [454] W. Zhang, P.G. Smirniotis, *J. Catal.* 182 (1999) 70.
- [455] Z. Konya, I. Hannus, A. Molnar, I. Kiricsi, *Appl. Catal. A* 146 (1996) 323.
- [456] S.S.C. Chuang, M.A. Brundage, M.W. Balakos, *Appl. Catal. A* 151 (1997) 333.
- [457] I. Kiricsi, C. Flego, G. Bellussi, *Appl. Catal. A* 126 (1995) 401.
- [458] M. Baldi, E. Finocchio, Ch. Pistarino, G. Busca, *Appl. Catal. A* 173 (1998) 61.
- [459] Ph. Maetz, R. Touroude, *Appl. Catal. A* 149 (1997) 189.
- [460] N.E. Fouad, P. Thomasson, H. Knozinger, *Appl. Catal. A* 196 (2000) 125.

- [461] N.E. Fouad, P. Thomasson, H. Knozinger, *Appl. Catal. A* 194–195 (2000) 213.
- [462] P. Ferreira-Aparicio, I. Rodriguez-Ramos, J.A. Anderson, A. Guerrero-Ruiz, *Appl. Catal. A* 202 (2000) 183.
- [463] L. Basini, A. Guarinoni, A. Aragno, *J. Catal.* 190 (2000) 284.
- [464] M.A. Ulla, R. Spretz, E. Lombardo, W. Daniell, H. Knozinger, *Appl. Catal. B* 29 (2001) 217.
- [465] G. Busca, E. Finocchio, V. Lorenzelli, G. Ramis, M. Baldi, *Catal. Today* 49 (1999) 453.
- [466] Z. Zhao, Y. Yamada, Y. Teng, A. Ueda, K. Nakagawa, T. Kobayashi, *J. Catal.* 190 (2000) 215.
- [467] S. Krishnamoorthy, M.D. Amiridis, *Catal. Today* 51 (1999) 203.
- [468] S. Krishnamoorthy, J.A. Rivas, M.D. Amiridis, *J. Catal.* 193 (2000) 264.
- [469] A. Martin, U. Bentrup, A. Bruckner, B. Lucke, *Catal. Lett.* 59 (1999) 61.
- [470] D. Carmello, E. Finocchio, A. Marsella, B. Cremaschi, G. Leofanti, M. Padovan, G. Busca, *J. Catal.* 191 (2000) 354.
- [471] E. Finocchio, N. Rossi, G. Busca, M. Padovan, G. Leofanti, B. Cremaschi, A. Marsella, D. Carmello, *J. Catal.* 179 (1998) 606.
- [472] V. Ermini, E. Finocchio, S. Sechi, G. Busca, S. Rossini, *Appl. Catal. A* 190 (2000) 157.
- [473] M. Baldi, F. Milella, G. Ramis, V. Sanchez Escribano, G. Busca, *Appl. Catal. A* 166 (1998) 75.
- [474] K.Y. Jung, S.B. Park, *Appl. Catal. B* 25 (2000) 249.
- [475] M. El-Maazawi, A.N. Finken, A.B. Nair, V.H. Grassian, *J. Catal.* 191 (2000) 138.
- [476] V. Augugliaro, S. Coluccia, V. Loddo, L. Marchese, G. Martra, L. Palmisano, M. Schiavello, *Appl. Catal. B* 20 (1999) 15.
- [477] K. Early, V.I. Kovachuk, F. Lonyi, S. Deshmukh, J.L. d'Itri, *J. Catal.* 182 (1999) 219.
- [478] C. Morterra, G. Cerrato, S. Di Ciero, *Appl. Surf. Sci.* 126 (1998) 107.
- [479] C. Morterra, G. Cerrato, S. Di Ciero, *Appl. Surf. Sci.* 126 (1998) 107.
- [480] P. Concepcion, K. Hadjiivanov, H. Knozinger, *J. Catal.* 184 (1999) 172.
- [481] X. Mugniery, T. Chafik, M. Primet, D. Bianchi, *Catal. Today* 52 (1999) 15.
- [482] G.A. Savelieva, K.K. Tenchev, L.A. Petrov, A.S. Sass, in: A. Andreev, L. Petrov, Ch. Bonev, G. Kadinov, I. Mitov (Eds.), *Heterogeneous Catalysis, Proceedings of the Eighth International Symposium, Varna, October 5–9, 1996*, Institute of Catalysis, Bulgarian Academy of Sciences, Sofia, 1996, pp. 299–304.
- [483] L.L. Sheu, Z. Karpiński, W.M.H. Sachtler, *J. Phys. Chem.* 93 (1989) 4890.
- [484] L.L. Sheu, W.M.H. Sachtler, *J. Mol. Catal.* 81 (1993) 267.
- [485] C. Hippe, T. Ueckert, R. Lamber, N.I. Jaeger, G. Schulz-Ekloff, U. Schubert, in: A. Andreev, L. Petrov, Ch. Bonev, G. Kadinov, I. Mitov (Eds.), *Heterogeneous Catalysis, Proceedings of the Eighth International Symposium, Varna, October 5–9, 1996*, Institute of Catalysis, Bulgarian Academy of Sciences, Sofia, 1996, pp. 643–648.
- [486] M. Mihaylov, K. Hadjiivanov, D. Klissurski, in: L. Petrov, Ch. Bonev, G. Kadinov (Eds.), *Heterogeneous Catalysis, Proceedings of the Ninth International Symposium, Varna, September 23–27, 2000*, Institute of Catalysis, Bulgarian Academy of Science, Sofia, 2000, pp. 387–392.
- [487] K. Nagase, Y. Zheng, Y. Kodama, J. Kakuta, *J. Catal.* 187 (1999) 123.
- [488] J. Rasko, J. Bontovics, *Catal. Lett.* 58 (1999) 27.
- [489] M. Kantcheva, S. Sayan, *Catal. Lett.* 60 (1999) 27.
- [490] G.J. Arteaga, J.A. Anderson, C.H. Rochester, *Catal. Lett.* 58 (1999) 189.
- [491] O. Dularent, D. Bianchi, *Appl. Catal. A* 207 (2001) 211.
- [492] G.J. Arteaga, J.A. Anderson, C.H. Rochester, *J. Catal.* 184 (1999) 268.
- [493] O. Dularent, K. Chandes, Ch. Bouly, D. Bianchi, *J. Catal.* 188 (1999) 237.
- [494] P. Araya, C. Weissmann, *Catal. Lett.* 68 (2000) 33.
- [495] W.F. Lin, T. Iwasita, W. Vielstich, *J. Phys. Chem. B* 103 (1999) 3250.
- [496] T. Chafik, O. Dularent, J.L. Gass, D. Bianchi, *J. Catal.* 179 (1998) 503.
- [497] S. Todorova, G. Kadinov, in: L. Petrov, Ch. Bonev, G. Kadinov (Eds.), *Heterogeneous Catalysis, Proceedings of the Ninth International Symposium, Varna, September 23–27, 2000*, Institute of Catalysis, Bulgarian Academy of Science, Sofia, 2000, pp. 169–174.
- [498] A.K. Tripathi, V.S. Kamble, N.M. Gupta, *J. Catal.* 187 (1999) 332.
- [499] A. Erdohelyi, K. Fodor, S. Suru, *Appl. Catal. A* 139 (1996) 131.
- [500] J. Weigel, C. Frohlich, A. Baiker, A. Wokaun, *Appl. Catal. A* 140 (1996) 29.
- [501] E. Boellaard, A.M. van der Kraan, J.W. Geus, *Appl. Catal. A* 147 (1996) 229.
- [502] N.-Y. Topsøe, H. Topsøe, *Topics Catal.* 8 (1999) 267.
- [503] J. Rasko, *Catal. Lett.* 56 (1998) 11.
- [504] H. Kusama, K.K. Bando, K. Okabe, H. Arakawa, *Appl. Catal. A* 197 (2000) 255.
- [505] K. Tomishige, Y.-G. Chen, K. Fujimoto, *J. Catal.* 181 (1999) 91.
- [506] C. Crisafulli, S. Scire, R. Maggiore, S. Minico, S. Galvagno, *Catal. Lett.* 59 (1999) 21.
- [507] K. Nagaoka, T. Karasuda, K.-I. Aika, *J. Catal.* 181 (1999) 160.
- [508] M. Waqif, P. Bazin, O. Saur, J.C. Lavalley, G. Blanchard, O. Touret, *Appl. Catal. B* 11 (1997) 193.
- [509] E. Laperdrix, A. Sahibed-dine, G. Costentin, O. Saur, M. Bensitel, C. Nedez, A.B.M. Saad, J.C. Lavalley, *Appl. Catal. B* 26 (2000) 71.
- [510] T.-Ch. Yu, H. Shaw, *Appl. Catal. B* 18 (1998) 105.
- [511] Y. Wang, A.B.M. Saad, O. Saur, J.C. Lavalley, B.A. Morrow, *Appl. Catal. B* 16 (1998) 279.
- [512] E. Laperdrix, I. Justin, G. Costentin, O. Saur, J.C. Lavalley, A. Aboulayt, J.L. Ray, C. Nedez, *Appl. Catal. B* 17 (1998) 167.
- [513] Z.R. Ismagilov, V.V. Kuznetsov, D.A. Arendarskii, S.R. Khairulin, M.A. Kerzhentsev, in: A. Andreev, L. Petrov,

- Ch. Bonev, G. Kadinov, I. Mitov (Eds.), *Heterogeneous Catalysis, Proceedings of the Eighth International Symposium*, Varna, October 5–9, 1996, Institute of Catalysis, Bulgarian Academy of Sciences, Sofia, 1996, pp. 425–430.
- [514] J.A. Anderson, C.H. Rochester, Z. Wang, *J. Mol. Catal. A* 139 (1999) 285.
- [515] J.A. Anderson, F.K. Chong, C.H. Rochester, *J. Mol. Catal. A* 140 (1999) 65.
- [516] L.P.A.F. Elst, S. Eijssbouts, A.D. van Langeveld, J.A. Moulijn, *J. Catal.* 196 (2000) 95.
- [517] Z. Sarbak, *Appl. Catal. A* 177 (1999) 85.
- [518] J.V. Ibarra, C. Royo, A. Monzon, J. Santamaria, *Vib. Spectrosc.* 9 (1995) 191.
- [519] Z. Wang, C.H. Rochester, J.A. Anderson, *J. Catal.* 184 (1999) 213.
- [520] C.L. Li, O. Novaro, E. Munoz, J.L. Boldu, X. Bokhimi, J.A. Wang, T. Lopez, R. Gomez, *Appl. Catal. A* 199 (2000) 211.
- [521] L. Becker, H. Forster, *Appl. Catal. A* 153 (1997) 31.
- [522] H.G. Karge, W. NieBen, H. Bludau, *Appl. Catal. A* 146 (1996) 339.
- [523] M. Guisnet, P. Dege, P. Magnoux, *Appl. Catal. B* 20 (1999) 1.
- [524] H.S. Cerqueira, P. Ayrault, J. Datka, P. Magnoux, M. Guisnet, *J. Catal.* 196 (2000) 149.
- [525] K. Hadjiivanov, H. Knozinger, *Catal. Lett.* 58 (1999) 21.
- [526] V.B. Kazansky, V.Yu. Borovkov, A.I. Serikh, R.A. van Santen, B.G. Anderson, *Catal. Lett.* 66 (2000) 39.
- [527] C. Otero Arean, G. Turnes Palomino, A. Zecchina, S. Borgia, F.X. Llabres i Xamena, C. Paze, *Catal. Lett.* 66 (2000) 231.
- [528] M.V. Konduru, S.S.C. Chuang, *J. Catal.* 187 (1999) 436.
- [529] J.N. Kondo, E. Yoda, H. Ishikawa, F. Wakabayashi, K. Domen, *J. Catal.* 191 (2000) 275.
- [530] G. Spoto, F. Geobaldo, S. Bordiga, C. Lamberti, D. Scarano, A. Zecchina, *Topics Catal.* 8 (1999) 279.
- [531] A.G. Panov, J.J. Fripiat, *Catal. Lett.* 57 (1999) 25.
- [532] Y. Huang, R.R. Poissant, P. Qiu, *Langmuir* 16 (2000) 889.
- [533] N. Arsenova-Hartel, H. Bludau, R. Schumacher, W.O. Haag, H.G. Karge, E. Brunner, U. Wild, *J. Catal.* 191 (2000) 326.
- [534] B.-L. Su, V. Norberg, C. Hansenne, *Langmuir* 16 (2000) 1132.
- [535] P. Marturano, A. Kogelbauer, R. Prins, *J. Catal.* 190 (2000) 460.
- [536] P. Marturano, L. Drozdova, A. Kogelbauer, R. Prins, *J. Catal.* 192 (2000) 236.
- [537] A. Satsuma, A.D. Cowan, N.W. Cant, D.L. Trimm, *J. Catal.* 181 (1999) 165.
- [538] B. Tsyntarski, D. Klissurski, K. Hadjiivanov, in: L. Petrov, Ch. Bonev, G. Kadinov (Eds.), *Heterogeneous Catalysis, Proceedings of the Ninth International Symposium*, Varna, September 23–27, 2000, Institute of Catalysis, Bulgarian Academy of Science, Sofia, 2000, pp. 133–138.
- [539] J.W. Yoo, Ch.W. Lee, J.-S. Chang, S.-E. Park, J. Ko, *Catal. Lett.* 66 (2000) 169.
- [540] S. Chavan, D. Srinivas, P. Ratnasamy, *J. Catal.* 192 (2000) 286.
- [541] B. Ganemi, E. Bjornbom, J. Paul, *Appl. Catal. B* 17 (1998) 293.
- [542] P.S. Chintawar, H.L. Greene, *Appl. Catal. B* 14 (1997) 37.
- [543] R.M. Mihalyi, H.K. Beyer, Y. Nainska, V. Mavrodinova, Ch. Minchev, *React. Kinet. Catal. Lett.* 68 (1999) 355.
- [544] R. Zavoianu, E. Angelescu, C. Nenu, N. Nastase, in: L. Petrov, Ch. Bonev, G. Kadinov (Eds.), *Heterogeneous Catalysis, Proceedings of the Ninth International Symposium*, Varna, September 23–27, 2000, Institute of Catalysis, Bulgarian Academy of Science, Sofia, 2000, pp. 447–452.
- [545] B. Paze, B. Sazak, A. Zecchina, J. Dwyer, *J. Phys. Chem. B* 103 (1999) 9978.
- [546] M. Trombetta, A.G. Alejandre, J.R. Solis, G. Busca, *Appl. Catal. A* 198 (2000) 81.
- [547] J.N. Kondo, H. Ishikawa, E. Yoda, F. Wakabayashi, K. Domen, *J. Phys. Chem. B* 103 (1999) 8538.
- [548] P.A. Weyrich, W.F. Holderich, *Appl. Catal. A* 158 (1997) 145.
- [549] L. Mariey, J. Lamotte, T. Chevreau, J.C. Lavalley, *React. Kinet. Catal. Lett.* 59 (1996) 241.
- [550] A. Beres, Z. Konya, I. Hannus, A. Molnar, I. Kiricsi, *Appl. Catal. A* 146 (1996) 331.
- [551] C. Paze, G.T. Palomino, A. Zecchina, *Catal. Lett.* 60 (1999) 139.
- [552] S. Kowalak, M. Łaniecki, M. Pawłowska, K.J. Balkus Jr., A. Khanmamedova, in: A. Andreev, L. Petrov, Ch. Bonev, G. Kadinov, I. Mitov (Eds.), *Heterogeneous Catalysis, Proceedings of the Eighth International Symposium*, Varna, October 5–9, 1996, Institute of Catalysis, Bulgarian Academy of Sciences, Sofia, 1996, pp. 793–798.
- [553] Z. Fu, J. Chen, D. Yin, D. Yin, L. Zhang, Y. Zhang, *Catal. Lett.* 66 (2000) 105.
- [554] X. Zhang, Z. Zhang, J. Suo, S. Li, *Catal. Lett.* 66 (2000) 175.
- [555] K. Shimizu, H. Kawabata, A. Satsuma, T. Hattori, *Appl. Catal. B* 19 (1998) L87.
- [556] G. Diaz, R. Perez-Hernandez, A. Gómez-Cortes, M. Benaissa, R. Mariscal, J.L.G. Fierro, *J. Catal.* 187 (1999) 1.
- [557] J.H. Holles, M.A. Switzer, R.J. Davis, *J. Catal.* 190 (2000) 247.
- [558] E. Novak, D. Sprinceana, F. Solymosi, *Appl. Catal. A* 149 (1997) 89.
- [559] M. Moran-Pineda, S. Castillo, T. Lopez, R. Gomez, C. Borboa, O. Novaro, *Appl. Catal. B* 21 (1999) 79.
- [560] J.-L. Freysz, J. Saussey, J.-C. Lavalley, P. Bourges, *J. Catal.* 197 (2001) 131.
- [561] K. Almusaiter, S.S.C. Chuang, *J. Catal.* 184 (1999) 189.
- [562] K.A. Almusaiter, S.S.C. Chuang, C.-D. Tan, *J. Catal.* 189 (2000) 247.
- [563] D.I. Kondarides, T. Chafik, X.E. Verykios, *J. Catal.* 191 (2000) 147.
- [564] D.I. Kondarides, T. Chafik, X.E. Verykios, *J. Catal.* 193 (2000) 303.
- [565] K. Almusaiter, S.S.C. Chuang, *J. Catal.* 180 (1998) 161.
- [566] D.B. Akolekar, S.K. Bhargava, *Appl. Catal. A* 207 (2001) 355.
- [567] T. Gerlach, F.-W. Schutze, M. Baerns, *J. Catal.* 185 (1999) 131.
- [568] L.J. Lobree, I.-C. Hwang, J.A. Reimer, A.T. Bell, *Catal. Lett.* 63 (1999) 233.

- [569] E.V. Rebrov, A.V. Simakov, N.N. Sazonova, E.S. Stoyanov, *Catal. Lett.* 58 (1999) 107.
- [570] X. Wang, H. Chen, W.M.H. Sachtler, *Appl. Catal. B* 29 (2001) 47.
- [571] R. Burch, T.C. Watling, *Appl. Catal. B* 17 (1998) 131.
- [572] L.J. Lobree, A.W. Aylor, J.A. Reimer, A.T. Bell, *J. Catal.* 181 (1999) 189.
- [573] S. Hodjati, K. Vaezzadeh, C. Petit, V. Pitchon, A. Kiebbenann, *Catal. Today* 59 (2000) 323.
- [574] E. Fiedel, H. Persson, B. Westerberg, L. Olsson, M. Skoglundh, *Catal. Lett.* 66 (2000) 71.
- [575] E. Friedell, M. Skoglundh, B. Westerberg, S. Johansson, G. Smedler, *J. Catal.* 183 (1999) 196.
- [576] S. Hodjati, P. Bernhardt, C. Petit, V. Pitchon, A. Kiennemann, *Appl. Catal. B* 19 (1998) 221.
- [577] K. Hadjiivanov, H. Knozinger, B. Tsyntsarski, L. Dimitrov, *Catal. Lett.* 62 (1999) 35.
- [578] V.A. Sadykov, E.A. Paukshtis, S.A. Beloshapkin, G.M. Alikina, S.A. Veniaminov, R.V. Bunina, E.V. Lunina, A.N. Kharlanov, V.V. Lunin, V.A. Matyshak, A.Ya. Rozovskii, in: A. Andreev, L. Petrov, Ch. Bonev, G. Kadinov, I. Mitov (Eds.), *Heterogeneous Catalysis, Proceedings of the Eighth International Symposium, Varna, October 5–9, 1996*, Institute of Catalysis, Bulgarian Academy of Sciences, Sofia, 1996, pp. 347–352.
- [579] G.J. Millar, A. Canning, G. Rose, B. Wood, L. Trewartha, I.D.R. Mackinnon, *J. Catal.* 183 (1999) 169.
- [580] S. Matsumoto, Y. Ikeda, H. Suzuki, M. Ogai, N. Miyoshi, *Appl. Catal. B* 25 (2000) 115.
- [581] H.-Y. Chen, T. Voskoboinikov, W.M.H. Sachtler, *J. Catal.* 186 (1999) 91.
- [582] D.K. Captain, M.D. Amiridis, *J. Catal.* 184 (1999) 377.
- [583] R.Q. Long, R.T. Yang, *J. Phys. Chem. B* 103 (1999) 2232.
- [584] F.C. Meunier, V. Zuzaniuk, J.P. Breen, M. Olsson, J.R.H. Ross, *Catal. Today* 59 (2000) 287.
- [585] J. Pasel, V. Speer, Ch. Albrecht, F. Richter, H. Papp, *Appl. Catal. B* 25 (2000) 105.
- [586] K. Shimizu, H. Kawabata, A. Satsuma, T. Hattori, *J. Phys. Chem. B* 103 (1999) 5240.
- [587] G. Busca, G. Martra, A. Zecchina, *Catal. Today* 56 (2000) 361.
- [588] R.Q. Long, R.T. Yang, *J. Catal.* 194 (2000) 80.
- [589] R.Q. Long, R.T. Yang, *J. Catal.* 190 (2000) 22.
- [590] M. Kantcheva, K. Hadjiivanov, D. Klissurski, in: A. Andreev, L. Petrov, Ch. Bonev, G. Kadinov, I. Mitov (Eds.), *Heterogeneous Catalysis, Proceedings of the Eighth International Symposium, Varna, October 5–9, 1996*, Institute of Catalysis, Bulgarian Academy of Sciences, Sofia, 1996, pp. 371–376.
- [591] B. Chakraborty, B. Viswanathan, *Catal. Today* 49 (1999) 253.
- [592] S.A. Bagshaw, R.P. Cooney, *Proc. SPIE Int. Soc. Opt. Eng.* 2089 (1993) 162.
- [593] E. Brunner, *Catal. Today* 38 (1997) 361.
- [594] B. Lee, J.N. Kondo, F. Wakabayashi, K. Domen, *Catal. Lett.* 59 (1999) 51.
- [595] G. Srinivas, S.S.C. Chuag, *J. Phys. Chem.* 98 (1994) 3024.
- [596] A. Baysar, G.L. Schrader, *Turk. J. Chem.* 18 (1994) 223.
- [597] A. Bielanski, J. Datka, B. Gil, A. Malecka-Lubanska, A. Micek-Ilnicka, *Catal. Lett.* 57 (1999) 61.
- [598] R. Zavoianu, C. Dias, M. Portela, in: L. Petrov, Ch. Bonev, G. Kadinov (Eds.), *Heterogeneous Catalysis, Proceedings of the Ninth International Symposium, Varna, September 23–27, 2000*, Institute of Catalysis, Bulgarian Academy of Science, Sofia, 2000, pp. 411–416.
- [599] G.J. Millar, J.B. Metson, G.A. Bowmaker, R.P. Cooney, *J. Catal.* 147 (1994) 404.
- [600] P. Li, Y. Chen, S. Chen, M. Gong, L. Li, J. Zhou, Y.J. Chen, *Natl. Gas Chem.* 4 (1995) 302.
- [601] J.A. Chudek, M.W. McQuire, G.W. McQuire, C.H. Rochester, *J. Chem. Soc., Faraday Trans.* 90 (1994) 3699.
- [602] Y. Wang, Z. Song, D. Ma, H. Luo, D. Liang, X. Bao, *J. Mol. Catal. A* 149 (1999) 51.
- [603] N.-Y. Topsoe, H. Topsoe, *J. Mol. Catal. A* 141 (1999) 95.
- [604] T.C. Schilke, I.A. Fisher, A.T. Bell, *J. Catal.* 184 (1999) 144.
- [605] I.A. Fisher, A.T. Bell, *J. Catal.* 184 (1999) 357.
- [606] K.K. Bando, K. Soga, K. Kunimori, N. Ichikuni, K. Okabe, H. Kusama, K. Sayama, H. Arakawa, *Appl. Catal. A* 173 (1998) 47.
- [607] J. Nakamura, K. Aikawa, K. Sato, T. Uchijima, *Stud. Surf. Sci. Catal.* 90 (1994) 495.
- [608] K. Rahkamaa, R.L. Keiski, T. Salmi, in: L. Petrov, Ch. Bonev, G. Kadinov (Eds.), *Heterogeneous Catalysis, Proceedings of the Ninth International Symposium, Varna, September 23–27, 2000*, Institute of Catalysis, Bulgarian Academy of Science, Sofia, 2000, pp. 121–126.
- [609] M. Ziolek, O. Saur, J. Lamotte, J.C. Lavalley, *J. Chem. Soc., Faraday Trans.* 90 (1994) 1029.
- [610] L.M. Cornaglia, C.R. Carrara, J.O. Petunchi, E.A. Lombardo, *Catal. Today* 57 (2000) 313.
- [611] G. Ramis, G. Busca, V. Lorenzelli, *J. Chem. Soc., Faraday Trans.* 90 (1994) 1293.
- [612] G. Busca, A. Zecchina, *Catal. Today* 20 (1994) 61.
- [613] Y.G. Noskov, M.L. Terekhova, E. Petrov, *Kinet. Katal.* 34 (1993) 1001.
- [614] G. Eder-Mirth, *Collect. Czech. Chem. Commun.* 60 (1995) 421.
- [615] V.A. Bell, J.S. Feeley, M. Deeba, R.J. Farrauto, *Catal. Lett.* 29 (1994) 15.
- [616] A. Martin, D. Gutschick, N.L. Jaeger, G. Schulz-Ekloff, H. Miessner, B. Luecke, *Catal. Lett.* 27 (1994) 119.
- [617] J.V. Ibarra, C. Royo, A. Monzan, J. Santamaria, *Vib. Spectrosc.* 9 (1995) 191.
- [618] M.D. Driessen, V.H. Grassian, *J. Phys. Chem. B* 102 (1998) 1418.
- [619] L. Palmisano, M. Schiavello, A. Sciafani, G. Martra, E. Borello, S. Coluccia, *Appl. Catal. B* 3 (1994) 117.
- [620] L. Basini, *Catal. Today* 41 (1998) 277.
- [621] C.A. Koh, J.A. Zollweg, K.E. Gubbins, *Stud. Surf. Sci. Catal.* 87 (1994) 61.
- [622] Ph. Maetz, J. Saussey, J.C. Lavalley, R.J. Touroude, *J. Catal.* 147 (1994) 48.
- [623] P.C. Ford, J.S. Bridgewater, S. Massick, J. Marhenke, *Catal. Today* 49 (1999) 419.

- [624] C. Force, J.P. Belzunegui, J. Sanz, A. Martinez-Arias, J. Soria, *J. Catal.* 197 (2001) 192.
- [625] E. Fernandez Lopez, V. Sanchez Escribano, C. Resini, J.M. Gallardo-Amores, G. Busca, *Appl. Catal. B* 29 (2001) 251.
- [626] J.R. Zoeller, N.L. Buchanan, T.J. Dickson, K.K. Ramming, *Catal. Today* 49 (1999) 431.
- [627] P.A. Connor, K.D. Dobson, A.J. McQuillan, *Langmuir* 15 (1999) 2402.
- [628] U. Wolf, R. Leiberich, J. Seeba, *Catal. Today* 49 (1999) 411.
- [629] W. Huber, A. Bubendorf, A. Grieder, D. Obrecht, *Anal. Chim. Acta* 393 (1999) 213.
- [630] J. Thomasson, C. Coin, H. Kahraman, P.M. Fredericks, *Fuel* 79 (2000) 685.
- [631] N. Osaka, M. Akita, K. Itoh, *J. Phys. Chem. B* 102 (1998) 6817.
- [632] A. Rodes, R. Gomez, J.M. Feliu, M.J. Weaver, *Langmuir* 16 (2000) 811.
- [633] A. Siokou, R.M. Nix, *J. Phys. Chem. B* 103 (1999) 6984.
- [634] M. Akita, S. Hiramoto, N. Osaka, K. Itoh, *J. Phys. Chem. B* 103 (1999) 10189.
- [635] H. Wijnja, C.P. Schultness, *Spectrochim. Acta A* 55 (1999) 861.
- [636] C.A. Mims, M.D. Weisel, F.M. Horiman, J.H. Sinfelt, J.M. White, *J. Phys. Chem.* 97 (1993) 12656.
- [637] M.V. Biber, W. Stumm, *Environ. Sci. Technol.* 28 (1994) 763.
- [638] P. Heger, G. Marx, *Fresenius J. Anal. Chem.* 365 (1999) 103.
- [639] G.-Q. Lu, S.-G. Sun, L.-R. Cai, S.-P. Chen, Z.-W. Tian, *Langmuir* 16 (2000) 778.
- [640] J. Szanyi, D.W. Goodman, *J. Phys. Chem.* 98 (1994) 2972.
- [641] J. Szanyi, W.K. Kuhn, D.W. Goodman, *J. Phys. Chem.* 98 (1994) 2978.
- [642] X. Xu, P. Chen, D.W. Goodman, *J. Phys. Chem.* 98 (1994) 9242.
- [643] M.J. Weaver, *Surf. Sci.* 437 (1999) 215.
- [644] X. Liu, R.E. Truitt, *J. Am. Chem. Soc.* 119 (1997) 9856.
- [645] D.H. Lee, R.A. Condrate Sr., *Mater. Lett.* 23 (1995) 241.
- [646] G.J. Hutchings, I.D. Hudson, D.G. Timms, *Catal. Lett.* 61 (1999) 219.
- [647] G. Mul, F. Kapteijn, J.A. Moulijn, *Carbon* 37 (1999) 401.
- [648] A. Dandekar, M.A. Vannice, *J. Catal.* 183 (1999) 344.
- [649] A. Dandekar, R.T.K. Baker, M.A. Vannice, *J. Catal.* 184 (1999) 421.
- [650] S. Nishiyama, T. Hara, S. Tsuruya, M. Masai, *J. Phys. Chem. B* 103 (1999) 4431.
- [651] B.D. Chandler, A.B. Schabel, L.H. Pignolet, *J. Catal.* 193 (2000) 186.
- [652] A.A. Tsyganenko, E.E. Platero, C.O. Arean, E. Garrone, A. Zecchina, *Catal. Lett.* 61 (1999) 187.
- [653] B.W.L. Southward, R.J. Nash, C.T. O'Connor, *Appl. Catal. A* 135 (1996) 177.
- [654] B. Li, R.D. Gonzalez, *Catal. Today* 46 (1998) 55.
- [655] D.J. Zalewski, S. Alerasool, P.K. Doolin, *Catal. Today* 53 (1999) 419.
- [656] M. Marwood, R. Doepper, A. Renken, *Appl. Catal. A* 151 (1997) 223.
- [657] Z. Tian, O. Dewaele, G.B. Marin, *Catal. Lett.* 57 (1999) 9.
- [658] B. Klingenberg, M.A. Vannice, *Appl. Catal. B* 21 (1999) 19.
- [659] S.-J. Huang, A.B. Walters, M.A. Vannice, *Appl. Catal. B* 26 (2000) 101.
- [660] S.-J. Huang, A.B. Walters, M.A. Vannice, *Catal. Lett.* 64 (2000) 77.
- [661] N. Koizumi, K. Takahashi, M. Yamazaki, M. Yamada, *Catal. Today* 45 (1998) 313.
- [662] F.C. Meunier, J.P. Breen, V. Zuzaniuk, M. Olsson, J.R.H. Ross, *J. Catal.* 187 (1999) 493.
- [663] M.A. Centeno, I. Carrizosa, J.A. Odriozola, *Appl. Catal. B* 19 (1998) 67.
- [664] W.E.J. van Kooten, H.C. Krijnsen, C.M. van den Bleek, H.P.A. Calis, *Appl. Catal. B* 25 (2000) 125.
- [665] H. Mahzoul, J.F. Brilhac, P. Gilot, *Appl. Catal. B* 20 (1999) 47.
- [666] A. Fisher, M. Maciejewski, T. Burgi, T. Mallat, A. Baiker, *J. Catal.* 183 (1999) 373.
- [667] H. Schneider, S. Tsuchudin, M. Schneider, A. Wokaun, A. Baiker, *J. Catal.* 147 (1994) 5.
- [668] N. Topsoe, *Science* 265 (1994) 1217.
- [669] M.A. Centeno, I. Carrizosa, J.A. Odriozola, *Appl. Catal. B* 29 (2001) 307.
- [670] K. Beck, H. Pfeifer, B. Staudte, *Microporous Mater.* 2 (1993) 1.
- [671] J.J. Benitez, L. Carrizosa, J.A. Odriozola, *Appl. Surf. Sci.* 84 (1995) 391.
- [672] M. Amblard, R. Burch, B.W.L. Southward, *Catal. Today* 59 (2000) 365.
- [673] S.F. Parker, A. Amorelli, Y.D. Amos, C. Hughes, N. Porter, J.R. Walton, *J. Chem. Soc., Faraday Trans.* 91 (1995) 517.
- [674] D. Robert, S. Parra, C. Pulgarin, A. Krzton, J.V. Weber, *Appl. Surf. Sci.* 167 (2000) 51.
- [675] Ch. Peuker, *J. Mol. Struct.* 349 (1995) 317.
- [676] J.P. Blitz, S.M. Augustine, *Spectroscopy* 9 (1994) 28.
- [677] L. Basini, A.J. Aragno, *J. Chem. Soc., Faraday Trans.* 90 (1994) 787.
- [678] L.E. Skaare Rygh, L. Gausemel, O.H. Ellestad, P. Klæboe, C.J. Nielsen, E. Ryter, *J. Mol. Struct.* 349 (1995) 325.
- [679] J.J. Benitez, I. Carrizosa, J.A. Odriozola, *Appl. Spectrosc.* 48 (1994) 1208.
- [680] V.Y. Borovkov, V.B. Kazansky, *Catal. Lett.* 23 (1994) 107.
- [681] V.B. Kazansky, V.Y. Borovkov, E.G. Derouane, *Catal. Lett.* 19 (1993) 327.
- [682] J.J. Benitez, M.A. Centeno, J.A. Odriozola, *Catal. Lett.* 34 (1995) 379.
- [683] M. Sanati, A. Andersson, *J. Mol. Catal.* 81 (1993) 51.
- [684] C. Peuker, *J. Mol. Struct.* 349 (1995) 317.
- [685] V.B. Kazansky, V.Y. Borovkov, N. Sokolova, N.I. Jaeger, G. Schulz-Ekloff, *Catal. Lett.* 23 (1994) 263.
- [686] M. Kurhinen, T. Venalainen, T.A. Pakkanen, *J. Phys. Chem.* 98 (1994) 10237.
- [687] M.B. Mitchell, V.R. Chakravarthy, M.G. White, *Langmuir* 10 (1994) 4523.
- [688] D.O. Henderson, R. Mu, Y.S. Tung, G.C. Huston, *Appl. Spectrosc.* 49 (1995) 444.
- [689] H.S. Han, S.W. Han, Ch.H. Kim, K. Kim, *Langmuir* 16 (2000) 1149.

- [690] M. Fernandez-Garcia, A. Martinez-Arias, C. Belver, J.A. Anderson, J.C. Conesa, J. Soria, *J. Catal.* 190 (2000) 387.
- [691] L.M. Petkovic, G. Larsen, *J. Catal.* 191 (2000) 1.
- [692] M. Paulis, L.M. Gandia, A. Gil, J. Sambeth, J.A. Odriozola, M. Montes, *Appl. Catal. B* 26 (2000) 37.
- [693] S. Kotrel, M.P. Rosynek, J.H. Lunsford, *J. Catal.* 191 (2000) 55.
- [694] J. Kiviaho, M.K. Niemela, M. Reinikainen, T.A. Pakkanen, *Appl. Catal. A* 149 (1997) 353.
- [695] M.A. Centeno, S. Delsarte, P. Grange, *J. Phys. Chem. B* 103 (1999) 7214.
- [696] A. Dandekar, R.T.K. Baker, M.A. Vannice, *J. Catal.* 183 (1999) 131.
- [697] M. Kurhinen, T.A. Pakkanen, *Appl. Catal. A* 192 (2000) 97.
- [698] J. Kiviaho, M.K. Niemela, Y. Morioka, K. Kataja, *Appl. Catal. A* 144 (1996) 93.
- [699] M. Schmal, M.A.S. Baldanza, M.A. Vannice, *J. Catal.* 185 (1999) 138.
- [700] A. Valente, A.M. Botelho do Rego, M.J. Reis, L.F. Silva, A.M. Ramos, J. Vital, *Appl. Catal. A* 207 (2001) 221.
- [701] R. Stangl, W. Platter, V. Wittwer, *J. Non-Cryst. Solids* 186 (1995) 256.
- [702] J. Bodis, Cs. Nemeth, J. Mink, G. Keresztury, P. Tetenyi, *J. Mol. Struct.* 410–411 (1997) 179.
- [703] R.L. Frost, J.T. Klopogge, *Spectrochim. Acta A* 55 (1999) 2195.
- [704] J.T. Klopogge, R.L. Frost, *Appl. Catal. A* 184 (1999) 61.
- [705] R.L. Frost, J.T. Klopogge, S.C. Russell, J.L. Sztetu, *Tchermochim. Acta* 329 (1999) 47.
- [706] R. Stangl, W. Platter, V. Wittwer, *J. Non-Cryst. Solids* 186 (1995) 256.
- [707] <http://www.mtecpas.com>.
- [708] S.J. McGovern, B.S.H. Royce, J.B. Bezinger, *Appl. Surf. Sci.* 18 (1984) 401.
- [709] D. Noble, *Anal. Chem.* 66 (1994) 757A.
- [710] J.F. McClelland, R.W. Jones, S. Luo, L.M. Seaverson, in: P.B. Coleman (Ed.), *Practical Sampling Techniques in Infrared Analysis*, CRC Press, Boca Raton, FL, 1993, pp. 107–144.
- [711] Nicolet FT-IR Application Note, AN-8718.
- [712] R.A. Palmer, Y. Jiang, *J. Phys. IV* 4 (1994) 337.
- [713] E.Y. Jian, R.A. Palmer, J.L. Chao, *J. Appl. Phys.* 78 (1995) 460.
- [714] R.A. Palmer, E.Y. Jiang, J.L. Chao, *Proc. SPIE Int. Soc. Opt. Eng.* 2089 (1993) 250.
- [715] J.F. McClelland, R.W. Jones, S. Ochiai, *Proc. SPIE Int. Soc. Opt. Eng.* 2089 (1993) 302.
- [716] P.J. Stout, R.A. Crocombe, *Proc. SPIE Int. Soc. Opt. Eng.* 2089 (1993) 300.
- [717] G.M. Story, C. Marcott, I. Noda, *Proc. SPIE Int. Soc. Opt. Eng.* 2089 (1993) 242.
- [718] E.M. Eyring, S.M. Riseman, F.E. Massoth, in: T.E. Whyte Jr., R.A. Dalla Betta, E.G. Derouane, R.T.K. Baker (Eds.), *Catalytic Materials: Relationship Between Structure and Reactivity*, ACS Symposium Series No. 248, New York, 1984, pp. 399–410.
- [719] J.B. Benziger, S.J. McGovern, B.S.H. Royce, in: M.L. Deviney, J.L. Gland (Eds.), *Catalyst Characterization Science*, ACS Symposium Series No. 288, New York, 1985, pp. 449–463.
- [720] I. Gillis-D'Hamers, K.C. Vrancken, E.F. Vansant, G. De Roy, *J. Chem. Soc., Faraday Trans.* 88 (1992) 2047.
- [721] Y. Nishikawa, K. Kimura, A. Matsuda, T. Kenpo, *Appl. Spectrosc.* 46 (1992) 1695.
- [722] L.T. Petkovska, M.S. Trtica, M.M. Stoiljkovic, G.S. Ristic, S.S. Miljanc, *J. Quant. Spectrosc. Radiat. Transfer* 54 (1995) 509.
- [723] Y.X. Li, J.R. Schlup, K.J. Klabunde, *Langmuir* 7 (1991) 1394.
- [724] M.M. Mokhtar, E.F. Vansant, *Colloids Surf. A* 96 (1995) 253.
- [725] M.M. Mohamed, *Spectrochim. Acta A* 51 (1995) 1.
- [726] M.M. Mohamed, E.F. Vansant, *Colloids Surf. A* 96 (1995) 253.
- [727] P. Fejes, J.B. Nagy, J. Halasz, A. Oszko, *Appl. Catal. A* 175 (1998) 89.
- [728] A. Hess, E. Kemnitz, *Appl. Catal. A* 149 (1997) 373.
- [729] A. Hess, E. Kemnitz, *J. Catal.* 149 (1994) 449.
- [730] J. Ryzkowski, *Proc. SPIE Int. Soc. Opt. Eng.* 2089 (1993) 182.
- [731] A.R. Zhu, C.W. Hu, Z.Y. Wang, in: X. Xie, S.Y. Tong, M.A. Van Hove (Eds.), *Structure of Surfaces IV, Proceedings of the Fourth International Conference*, World Scientific, Singapore, 1994, pp. 248–254.
- [732] T. Ando, S. Inoue, M. Ishii, M. Kamo, Y. Sato, O. Yamada, T. Nakano, *J. Chem. Soc., Faraday Trans.* 89 (1993) 749.
- [733] G.J. Millar, G.F. McCann, C.M. Hobbs, G.A. Bowmaker, R.P. Cooney, *J. Chem. Soc., Faraday Trans.* 90 (1994) 2579.
- [734] H.P. Wang, E.M. Eyring, H. Huai, *Appl. Spectrosc.* 45 (1991) 883.
- [735] G.M.S. El Shaftei, M.M. Mokhtar, *Colloids Surf. A* 94 (1995) 267.
- [736] T. Zerlia, A. Carimati, S. Marengo, S. Martinengo, L. Zanderighi, *Stud. Surf. Sci. Catal.* 48 (1989) 943.
- [737] O.-S. Joo, K.-D. Jung, S.-H. Han, S.-J. Uhm, D.-K. Lee, S.-K. Ihm, *Appl. Catal. A* 135 (1996) 273.
- [738] P. Bazin, O. Saur, J.C. Lavalley, G. Blanchard, V. Visciglio, O. Touret, *Appl. Catal. B* 13 (1997) 265.
- [739] B. Li, R.D. Gonzalez, *Appl. Catal. A* 165 (1997) 291.
- [740] B. Li, R.D. Gonzalez, *Appl. Catal. A* 174 (1998) 109.
- [741] K.A. Almusaiter, S.S.C. Chuang, *J. Phys. Chem. B* 104 (2000) 2265.
- [742] M.V. Konduru, S.S.C. Chuang, *J. Phys. Chem. B* 103 (1999) 5802.
- [743] L.J. Burcham, I.E. Wachs, *Catal. Today* 49 (1999) 467.
- [744] K. Almusaiter, R. Krishnamurthy, S.S.C. Chuang, *Catal. Today* 55 (2000) 291.
- [745] Y. Chi, S.S.C. Chuang, *J. Catal.* 190 (2000) 75.
- [746] T. Chafik, D.I. Kondarides, X.E. Verykios, *J. Catal.* 190 (2000) 446.
- [747] Y. Chi, S.S.C. Chuang, *J. Phys. Chem. B* 104 (2000) 4673.
- [748] N.Y. Topsoe, H. Topsoe, J.A. Dumesic, *J. Catal.* 151 (1995) 226.

- [749] S. Tagliaferri, R.A. Koppel, A. Baiker, *Appl. Catal. B* 15 (1998) 159.
- [750] M.W. Anderson, J. Dwyer, G.J. Hutchings, D.F. Lee, M. Makarova, B. Zibrowius, *Catal. Lett.* 31 (1995) 377.
- [751] G. Srinivas, S.S.C. Chuang, S. Debnath, *J. Catal.* 148 (1994) 748.
- [752] S.A. Hedrick, S.S.C. Chuang, M.A. Brundage, *J. Catal.* 185 (1999) 73.
- [753] F. Zaera, N. Bernstein, *J. Am. Chem. Soc.* 116 (1994) 4881.
- [754] M. Don, H. Chien, M.G. Richmond, *J. Mol. Catal.* 88 (1994) 133.
- [755] M. Iwamoto, Y. Hosino, *Chem. Lett.* 8 (1995) 729.
- [756] O. Axelsson, Y. Shao, J. Paul, F.M. Hoffmann, *J. Phys. Chem.* 99 (1995) 7028.
- [757] R.R. Cavanagh, T.A. Germer, J.C. Stephenson, *Vib. Spectrosc.* 9 (1995) 77.
- [758] G. Muller, T. Narbeshuber, G. Mirth, J.A. Lercher, *J. Phys. Chem.* 98 (1994) 7436.
- [759] W. Niessen, H.G. Karge, *Stud. Surf. Sci. Catal.* 84 (1994) 1191.
- [760] T.A. Germer, J.C. Stephenson, E.J. Heilweil, R.R. Cavanagh, *J. Chem. Phys.* 101 (1994) 1704.
- [761] M. Bonn, M.J.P. Brugmans, A.W. Kleyn, R.A. van Santen, A. Legendijk, *Stud. Surf. Sci. Catal.* 84 (1994) 493.
- [762] M. Bonn, H.J. Bakker, K. Domen, C. Hirose, A.W. Kleyn, R.A. van Santen, *Catal. Rev.-Sci. Eng.* 40 (1998) 127.
- [763] G. Seifert, H. Graener, *J. Phys. Chem.* 98 (1994) 11827.
- [764] R.V. Kasza, J. Shapter, K. Griffiths, P.R. Norton, J.J. Solan, *Surf. Sci.* 321 (1994) 1239.
- [765] P.S. Cremer, X. Su, G.A. Somorjai, Y.R. Shen, *J. Mol. Catal. A* 131 (1998) 225.
- [766] P.W. Jacobs, G.A. Somorjai, *J. Mol. Catal. A* 131 (1998) 5.
- [767] G.A. Somorjai, *Chem. Rev.* 96 (1996) 1223.
- [768] G.A. Somorjai, *J. Phys. Chem.* 94 (1990) 1013.
- [769] G.A. Somorjai, *J. Phys. Chem. B* 104 (2000) 2969.
- [770] G.A. Somorjai, U. Starke, *Pure Appl. Chem.* 64 (1992) 509.
- [771] G.A. Somorjai, M.X. Yang, *J. Mol. Catal. A* 115 (1997) 389.
- [772] G. Lupke, *Surf. Sci. Rep.* 35 (1999) 75.
- [773] Y.R. Shen, *The Principles of Nonlinear Optics*, Wiley, New York, 1984.
- [774] Y.R. Shen, in: T. Hansch, M. Inguscio (Eds.), *Frontiers in Laser Spectroscopy*, North-Holland, Amsterdam, 1994, pp. 139–165.
- [775] Y.R. Shen, *Ann. Rev. Mater. Sci.* 16 (1986) 69.
- [776] Y.R. Shen, *Nature* 337 (1989) 519.
- [777] Y.R. Shen, *Ann. Rev. Phys. Chem.* 40 (1989) 327.
- [778] Y.R. Shen, *Surf. Sci.* 299 (1994) 551.
- [779] Y.R. Shen, *Appl. Phys. A* 59 (1994) 541.
- [780] T. Rasing, *Appl. Phys. A* 59 (1994) 531.
- [781] J.F. McGilp, M. Cavanagh, J.R. Power, J.D. O'Mahony, *Appl. Phys. A* 59 (1994) 401.
- [782] J.F. McGilp, *J. Phys. D* 29 (1996) 1812.
- [783] Y.R. Shen, *Solid State Commun.* 59 (1994) 541.
- [784] J.F. McGilp, *Thin Solid Films* 313–314 (1998) 533.
- [785] Y.R. Shen, *Appl. Phys. B* 68 (1999) 295.
- [786] M.J. Shultz, C. Schnitzer, D. Simonelli, S. Baldelli, *Int. Rev. Phys. Chem.* 19 (2000) 123.
- [787] T.F. Heinz, Second-order nonlinear optical effects at surfaces and interfaces, in: H.-E. Ponath, G. Stegeman (Eds.), *Nonlinear Surface Electromagnetic Phenomena*, Elsevier, Amsterdam, 1991, p. 353 (Chapter S).
- [788] J.F. McGilp, *Prog. Surf. Sci.* 49 (1995) 1.
- [789] Y.R. Shen, in: R.W. Field, E. Hirota, J.P. Maier, S. Tsuchiya (Eds.), *Nonlinear Spectroscopy for Molecular Structure Determination*, Blackwell Science, Oxford, 1998, pp. 249–271.
- [790] Y.R. Shen, *Solid State Commun.* 102 (1997) 221.
- [791] Y.R. Shen, *Proc. Natl. Acad. Sci. USA* 93 (1996) 12104.
- [792] E.W.M. van der Ham, Q.H.F. Vreken, E.R. Eliel, *Opt. Lett.* 21 (1996) 1448.
- [793] C. Hirose, A. Bandara, S. Katano, J. Kubota, A. Wada, K. Domen, *Appl. Phys. B* 68 (1999) 559.
- [794] A. Bandara, J. Kubota, A. Wada, K. Domen, C. Hirose, *Appl. Phys. B* 68 (1999) 573.
- [795] U. Metka, M.G. Schweitzer, H.-R. Vilpp, J. Wolfrum, *Zeit. Phys. Chem.* 214 (2000) 865.
- [796] G.A. Somorjai, *Appl. Surf. Sci.* 121/122 (1997) 1.
- [797] A. Bandara, S. Dobashi, J. Kubota, K. Onda, A. Wada, K. Domen, C. Hirose, S.S. Kano, *Surf. Sci.* 387 (1997) 312.
- [798] K. Domen, A. Bandara, J. Kubota, K. Onda, A. Wada, S.S. Kano, C. Hirose, *Surf. Sci.* 427–428 (1999) 349.
- [799] A. Bandara, J. Kubota, K. Onda, A. Wada, S.S. Kano, K. Domen, C. Hirose, *Surf. Sci.* 427–428 (1999) 331.
- [800] T. Yuzawa, T. Shioda, J. Kubota, K. Onda, A. Wada, K. Domen, C. Hirose, *Surf. Sci.* 416 (1998) L1090.
- [801] G. Rupprechter, T. Dellwig, H. Unterhalt, H.-J. Freund, *Stud. Surf. Sci. Catal.* 130 (2000) 3131.
- [802] G.A. Somorjai, X. Su, K.R. McCrea, K.B. Rider, *Topics Catal.* 8 (1999) 23.
- [803] X. Su, J. Jensen, M.X. Yang, M.B. Salmeron, Y.R. Shen, G.A. Somorjai, *Faraday Discuss.* 105 (1996) 263.
- [804] C.T. Williams, Y. Yang, C.D. Bain, *Catal. Lett.* 61 (1999) 7.
- [805] P.S. Cremer, X. Su, G.A. Somorjai, Y.R. Shen, *J. Mol. Catal. A* 131 (1998) 225.
- [806] B. Bourguignon, S. Carrez, B. Dragnea, H. Dubost, *Surf. Sci.* 418 (1998) 171.
- [807] T. Dellwig, G. Rupprechter, H. Unterhalt, H.-J. Freund, *Phys. Rev. Lett.* 85 (2000) 776.
- [808] Ch. Hess, M. Bonn, S. Funk, M. Wolf, *Chem. Phys. Lett.* 325 (2000) 139.
- [809] M. Bonn, Ch. Hess, S. Funk, J.H. Miners, B.N.J. Persson, M. Wolf, G. Ertl, *Phys. Rev. Lett.* 84 (2000) 4653.
- [810] H. Harle, A. Lehnert, U. Metka, H.-R. Volpp, L. Willms, J. Wolfrum, *Appl. Phys. B* 68 (1999) 567.
- [811] H. Harle, A. Lehnert, U. Metka, H.-R. Volpp, L. Willms, J. Wolfrum, *Chem. Phys. Lett.* 293 (1998) 26.
- [812] X. Su, P.S. Cremer, Y.R. Shen, G.A. Somorjai, *J. Am. Chem. Soc.* 119 (1997) 3994.
- [813] U. Schroder, P. Guyot-Sionnest, *Surf. Sci.* 421 (1999) 53.
- [814] S. Carrez, B. Dragnea, W.Q. Zheng, H. Dubost, B. Bourguignon, *Surf. Sci.* 440 (1999) 151.
- [815] K. Domen, C. Hirose, *Appl. Catal. A* 160 (1997) 153.
- [816] S. Katano, A. Bandara, J. Kubota, K. Onda, A. Wada, K. Domen, C. Hirose, *Surf. Sci.* 427–428 (1999) 337.

- [817] P.S. Cremer, X. Su, Y.R. Shen, G.A. Somorjai, *J. Am. Chem. Soc.* 118 (1996) 2942.
- [818] Z. Chen, D.H. Gracias, G.A. Somorjai, *Appl. Phys. B* 68 (1999) 549.
- [819] G.A. Somorjai, *Cattech* 3 (1999) 84.
- [820] P. Cremer, C. Stanners, J.W. Niemantsverdriet, Y.R. Shen, G. Somorjai, *Surf. Sci.* 328 (1995) 111.
- [821] P.S. Cremer, B.J. McIntyre, M. Salmeron, Y.-R. Shen, G.A. Somorjai, *Catal. Lett.* 34 (1995) 11.
- [822] G.A. Somorjai, G. Rupprechter, *J. Phys. Chem. B* 103 (1999) 1623.
- [823] P.S. Cremer, X. Su, Y.R. Shen, G.A. Somorjai, *J. Chem. Soc., Faraday Trans.* 92 (1996) 4717.
- [824] X. Su, K. Kung, J. Lahtinen, R.H. Shen, G.A. Somorjai, *Catal. Lett.* 54 (1998) 9.
- [825] D. Simonelli, M.J. Shultz, *J. Chem. Phys.* 112 (2000) 6804.
- [826] D.B.Y. Caudano, A. Peremans, P.A. Thiry, P. Dumas, A. Tadjeddine, *J. Phys. B* 29 (1996) 5023.
- [827] A. Peremans, Y. Caudano, P.A. Thiry, P. Dumas, W.-Q. Zhang, A. Le Rille, A. Tadjeddine, *Phys. Rev. Lett.* 78 (1997) 2999.
- [828] Y. Caudano, A. Peremans, P.A. Thiry, P. Dumas, W.Q. Zeng, A. De Rille, A. Tadjeddine, *Physica Mag.* 20 (1998) 31.
- [829] A. Peremans, Y. Caudano, P. Dumas, W.-Q. Zheng, A. Le Rille, P.A. Thiry, A. Tadjeddine, *Proc. SPIE* 3272 (1998) 35.
- [830] C. Silien, Y. Caudano, J.-L. Longueville, S. Bouzidi, F. Wiame, A. Peremans, P.A. Thiry, *Surf. Sci.* 427–428 (1999) 79.
- [831] O. Dannenberger, J.J. Wolf, M. Buck, *Langmuir* 14 (1998) 4679.
- [832] Ch. Jung, O. Dannenberger, Y. Xu, M. Buck, M. Grunze, *Langmuir* 14 (1998) 1103.
- [833] I. Bohm, A. Lampert, M. Buck, F. Eisert, M. Grunze, *Appl. Surf. Sci.* 141 (1999) 237.
- [834] O. Dannenberger, M. Buck, M. Grunze, *J. Phys. Chem. B* 103 (1999) 2202.
- [835] Ch. Humbert, M. Buck, A. Calderone, J.-P. Vigneron, V. Munier, B. Champagne, W.-Q. Zheng, A. Tadjeddine, P.A. Thiry, A. Peremans, *Phys. Stat. Sol. A* 175 (1999) 129.
- [836] M. Himmelhaus, F. Eisert, M. Buck, M. Grunze, *J. Phys. Chem. B* 104 (2000) 576.
- [837] J.R. Hart, *Ullmann's Encyclopedia of Industrial Chemistry*, 5th Edition, Vol. 10, VCH, Weinheim, 1987, pp. 95–101.
- [838] G.T. Kerr, *J. Phys. Chem.* 72 (1968) 2594.
- [839] G.T. Kerr, *J. Phys. Chem.* 73 (1969) 2780.
- [840] R. Beaumont, D. Barthomeuf, *J. Catal.* 26 (1972) 218.
- [841] R. Beaumont, D. Barthomeuf, *J. Catal.* 27 (1972) 45.
- [842] D. Barthomeuf, R. Beaumont, *J. Catal.* 30 (1973) 288.
- [843] D. Barthomeuf, B.-H. Ha, *J. Chem. Soc., Faraday Trans. 1* 69 (1973) 2147.
- [844] B. Czerwinska, J.M. Berak, J. Sznajder, M. Oblicka, J. Meisner, *Przem. Chem.* 54 (1975) 293.
- [845] L. Kubelkova, L. Dudikova, Z. Bastl, G. Borbely, H.K. Beyer, *J. Chem. Soc., Faraday Trans. 1* 83 (1987) 511.
- [846] L. Kubelkova, V. Seidl, G. Borbely, H.K. Beyer, *J. Chem. Soc., Faraday Trans. 1* 84 (1988) 1447.
- [847] J. Datka, B. Gil, J. Zlamaniec, B. Batamack, J. Fraissard, P. Massiani, *Polish J. Chem.* 73 (1999) 1535.
- [848] M. Matsumura, H. Ohnishi, K. Hanafusa, H. Tsubomura, *Bull. Soc. Chem. Jpn.* 60 (1987) 2001.
- [849] F.M. Bautista, J.M. Campelo, A. Garcia, R. Guardeno, D. Luna, J.M. Marinas, *J. Catal.* 125 (1990) 171.
- [850] T. Shimizu, K. Hiroshima, T. Honma, T. Mochizuki, M. Yamada, *Catal. Today* 45 (1998) 271.
- [851] J. Barcicki, D. Nazimek, W. Grzegorzczak, T. Borowiecki, R. Frak, M. Pielach, *React. Kinet. Catal. Lett.* 17 (1989) 169.
- [852] J. Ryzkowski, *React. Kinet. Catal. Lett.* 40 (1989) 189.
- [853] J. Ryzkowski, D. Nazimek, *React. Kinet. Catal. Lett.* 44 (1991) 427.
- [854] J. Ryzkowski, T. Borowiecki, *React. Kinet. Catal. Lett.* 49 (1993) 127.
- [855] J. Ryzkowski, W. Grzegorzczak, D. Nazimek, *Appl. Catal. A* 126 (1995) 341.
- [856] J. Ryzkowski, T. Borowiecki, D. Nazimek, *Ads. Sci. Technol.* 14 (1996) 113.
- [857] D. Nazimek, J. Ryzkowski, *Stud. Surf. Sci. Catal.* 119 (1998) 623.
- [858] J. Ryzkowski, T. Borowiecki, *Adsorp. Sci. Technol.* 16 (1998) 759.
- [859] J. Ryzkowski, T. Borowiecki, A. Machocki, D. Nazimek, *Annales UMCS, LIV/LV* (1999/2000) 85.
- [860] L. Coulier, V.H.J. de Beer, J.A.R. van Veen, J.W. Niemantsverdriet, *J. Catal.* 197 (2001) 26.
- [861] B. Nowack, L. Sigg, *J. Colloid Interface Sci.* 177 (1996) 106.
- [862] J. Koubek, J. Volf, J. Pasek, *J. Catal.* 38 (1975) 385.
- [863] H.A. Elliott, C.P. Huang, *J. Colloid Interface Sci.* 70 (1979) 29.
- [864] A.R. Bowers, C.P. Huang, *J. Colloid Interface Sci.* 105 (1985) 197.
- [865] A.R. Bowers, C.P. Huang, *J. Colloid Interface Sci.* 110 (1986) 575.
- [866] R. Kumert, W. Stumm, *J. Colloid Interface Sci.* 75 (1980) 373.
- [867] G. Furrer, W. Stumm, *Chimia* 37 (1983) 338.
- [868] J. Ryzkowski, D. Nazimek, G. Keresztury, *Proceedings of the Seventh International Symposium on Heterogeneous Catalysis*, Bourgas, September 28–October 1, 1991, pp. 361–366.
- [869] J. Ryzkowski, G. Keresztury, in: H.M. Heise, E.H. Korte, H.W. Siesler (Eds.), *Proceedings of the Eighth International Conference on Fourier Transform Spectroscopy*, Proc. SPIE Int. Soc. Opt. Eng. 1575 (1992) 540.
- [870] J. Ryzkowski, *React. Kinet. Catal. Lett.* 51 (1993) 501.
- [871] J. Ryzkowski, in: J.E. Bertie, H. Wieser (Eds.), *Proceedings of the Ninth International Conference on Fourier Transform Spectroscopy*, Proc. SPIE Int. Soc. Opt. Eng. 2089 (1993) 418.
- [872] J. Ryzkowski, in: J.E. Bertie, H. Wieser (Eds.), *Proceedings of the Ninth International Conference on Fourier Transform Spectroscopy*, Proc. SPIE Int. Soc. Opt. Eng. 2089 (1993) 504.
- [873] J. Ryzkowski, *React. Kinet. Catal. Lett.* 56 (1995) 241.
- [874] J. Ryzkowski, in: A. Andreev, L. Petrov, Ch. Bonev, G. Kadinov, I. Mitov (Eds.), *Proceedings of the Eighth International Symposium on Heterogeneous Catalysis*, Institute of Catalysis, Bulgarian Academy of Sciences, Sofia, 1996, pp. 637–642.

- [875] J. Ryzkowski, D. Nazimek, G. Keresztury, *Microchim. Acta* 14 (1997) 223.
- [876] J. Ryzkowski, D. Nazimek, *Microchim. Acta* 14 (1997) 227.
- [877] J. Ryzkowski, T. Borowiecki, G. Keresztury, *Microchim. Acta* 14 (1997) 229.
- [878] J. Ryzkowski, *Vib. Spectrosc.* 17 (1998) 187.
- [879] J. Ryzkowski, T. Borowiecki, *Adsorp. Sci. Technol.* 16 (1998) 759.
- [880] J. Ryzkowski, T. Borowiecki, A. Machocki, D. Nazimek, *Annales UMCS, LIV/LV* (1999/2000) 85.
- [881] J. Ryzkowski, *Vib. Spectrosc.* 22 (2000) 55.
- [882] J. Ryzkowski, B. Janda, *Vib. Spectrosc.* 22 (2000) 163.
- [883] J. Ryzkowski, *Pol. J. Environ. Stud.* 9 (Suppl. I) (2000) 57.
- [884] J.-P. Brunelle, *Pure Appl. Chem.* 50 (1978) 1211.
- [885] J. Ryzkowski, S. Pasieczna, Unpublished data.
- [886] J. Ryzkowski, Unpublished data.
- [887] D.C. Girvin, P.L. Gassman, H. Bolton Jr., *Clays and Clay Minerals* 44 (1996) 757.
- [888] S.C. Wolf, K.-A. Kovar, *J. Planar Chromatogr.* 7 (1994) 286.
- [889] Y. Nishikawa, T. Okumura, *J. Chromatogr. A* 690 (1995) 109.
- [890] G.N. Kalinkova, *Vib. Spectrosc.* 19 (1999) 307.
- [891] W.D. Perkins, in: P.B. Coleman (Ed.), *Practical Sampling Techniques for Infrared Analysis*, CRC Press, Boca Raton, FL, 1993, pp. 11–53.
- [892] T. Bruno, *Appl. Spectrosc. Rev.* 34 (1999) 34.
- [893] G. Dent, *Internet J. Vib. Spectrosc.* 1 (1996). <http://www.ijvs.com/volume1/edition1/section1.html#feature1>.
- [894] BDH Chemicals Ltd., Information Leaflet.
- [895] B. Schrader, *Raman/Infrared Atlas of Organic Compounds*, VCH, Weinheim, 1989.
- [896] *Encyclopedia of Analytical Science*, Vol. 4, Academic Press, San Diego, CA, 1995, pp. 2153–2240.
- [897] <http://www.lbl.gov/~mmartin/bl1.4/Irwindows.html>.
- [898] W.J. Tropf, M.E. Thomas, in: P. Klocek (Ed.), *Inorganic Optical Materials*, *Crit. Rev. Opt. Sci. Technol.* CR64 (1996) 137–164.
- [899] <http://216.46.231.181/resource/glossary.asp>.
- [900] J. Ryzkowski, *Appl. Catal. A* 110 (1994) N2.
- [901] J. Ryzkowski, *Appl. Catal. A* 135 (1996) N2.

Glossary

This glossary contains definitions of many important FT-IR terms [5,899].

100% line: is calculated by rationing two background spectra taken under identical conditions. Ideally, the result is a flat line at 100% transmittance. The slope and noise of 100% lines are measured to ascertain the quality of spectra and the health of an instrument.

Absorbance: units used to measure the amount of IR radiation absorbed by a sample. Absorbance is commonly used as the y-axis unit in IR spectra. Absorbance is defined by Beer's law,

and is linearly proportional to concentration. This is why spectra plotted in absorbance units should be used in quantitative analysis.

Absorbance spectrum: absorbance is related to transmittance as follows: $A = \log(1/T)$ where A is absorbance and T is transmittance. Transmittance spectra are calculated by rationing a sample single beam spectrum to a background spectrum. Absorbance is linearly proportional to concentration (see Beer's law), and are the units that should be used for quantitative analysis.

Absorption: refers to the loss of light that occurs when it passes through a medium due to its conversion to another energy form (most often heat energy).

Air bearing: a device used in some interferometers to reduce friction between the moving mirror and its housing. In this particular device, the moving mirror and its shaft are supported on a cushion of air.

Air cooled source: a type of IR source used in IR spectrometers. This source typically consists of coil of wire or a small ceramic piece through which electricity passes, causing it to give off heat. It is said to be "air cooled" since air currents in the instrument affect its temperature.

Alignment: the adjustment of accessory components (mirrors and lenses) to bring all of their optical axes in line and maximise its performance.

Analog-to-digital converter (ADC): is used to convert an interferogram signal from volts (the analog signal) into a series of base 2 numbers (a digital signal), the language that a computer understands. ADCs are characterised by the number of "bits" that the digitised output contains.

Analyte: the molecule of interest when performs a quantitative analysis.

Angle of incidence: the angle that forms between a ray of the light striking a surface and the normal (the line perpendicular to the surface at that point).

Angular divergence: the spreading out of an IR beam as it travels through the FT-IR. Angular divergence contributes to noise in high-resolution spectra.

Antireflection coating: a thin film coating that, when applied to an optical material, increases the transmittance by reducing the surface reflectance.

Aperture: an opening in an optical system.

Aperture, angular (AA): the maximum angle of light rays that pass through an optical element, lens, aperture, etc.

Aperture, numerical (NA): a mathematical formula for the direct comparison of objectives for resolving power and optical throughput. $NA = n \sin(\frac{1}{2}AA)$.

Apodisation functions: are multiplied times an interferogram to reduce the amount of sidelobes in a spectrum. Different types of apodisation functions include boxcar, triangle, Beer–Norton, Happ–Genzel, and Bessel. The use of apodisation functions unavoidably reduces the resolution of a spectrum.

ATR: stands for attenuated total reflectance, and is a reflectance sampling technique. In ATR, IR radiation impinges on a prism of IR transparent material of high refractive index. Because of internal reflectance, the light reflects off the surface of the crystal at least once before leaving it. The IR radiation sets

- up an evanescent wave that penetrates a small distance above and below the crystal surface. Samples brought into contact with the surface will absorb the evanescent wave giving rise to an IR spectrum. This sampling technique is useful for liquids, polymer films, and semisolids.
- Background spectrum:** a single beam spectrum acquired with no sample in the IR beam. The purpose of a background spectrum is to measure the contribution of the instrument and environment to the spectrum. These effects are removed from a sample spectrum by ratiating the sample single beam spectrum to the background spectrum.
- Bandwidth:** the spectral width of wavelengths transmitted by a bandpass filter, usually specified as the width at 50% of peak transmittance.
- Band-rejection filter:** a filter that suppresses (normally by reflection), a given range of wavelengths, transmitting only those above and below that band.
- Bandpass filter:** an optical filter, which allows transmittance over a particular wavelength range while restricting the transmittance of wavelengths above and below this range. These are also called interference filters.
- Baseline correction:** a spectral manipulation technique used to correct spectra with sloped or curving baselines. The user must draw a function parallel to the baseline, then this function is subtracted from the spectrum.
- Beam attenuator:** a mirror designed to decrease the flux density or power per unit area of a beam by absorption and scattering.
- Beamsplitter:** any optical device that reflects part of radiation impinging upon it, and transmits the other part. Beamsplitters are used in Michelson interferometers to send IR radiation to the moving mirror and fixed mirror respectively.
- Beer's law:** the equation that relates the absorbance of a sample to its concentration. Its form is $A = \epsilon lc$ where A stands for absorbance, ϵ for absorptivity, l for pathlength, and c for concentration. Beer's law is the equation used in FT-IR quantitative analysis to perform calibrations and to predict unknown concentrations.
- Calibration:** the process in quantitative analysis by which the peak heights and areas in a spectrum are correlated with the concentrations of analytes in standards. After calibration, the concentration of the analyte in unknown samples can be predicted.
- Calibration curve:** a plot of absorbance versus concentration used in a calibration. If the plot is linear, it means Beer's law has been followed, and that the plot can be used to predict the concentration of unknown samples.
- Capillary thin film:** a transmission sampling technique used to obtain spectra of liquids. Typically, a drop of liquid is placed between two KBr windows, and the windows and sample are placed directly into the IR beam. The capillary action of the liquid holds the two windows together, hence the name of the technique.
- Cast films:** a transmission sampling technique used to analyse polymer films. The polymer is dissolved in a solvent, and the solution is evaporated onto a KBr window giving a polymer film. The window/film combination is then placed directly in the IR beam.
- Centerburst:** the sharp, intense part of an interferogram. The size of the centerburst is directly proportional to the amount of IR radiation striking the detector.
- Cepstrum:** the result obtained when a reverse Fourier transform is performed on a spectrum. Cepstrums are used in the deconvolution process.
- Chamber:** refers to an enclosed, usually airtight, vessel (as in the diffuse reflectance chamber) where a sample is contained.
- Chromatogram:** a plot of detector response versus time. The response is typically proportional to amount of material coming out of a gas or liquid chromatograph. These devices are interfaced to FT-IRs to give hyphenated techniques.
- Chromatograph:** a device used to separate complex mixtures into their components. Chromatographs measure chromatograms, which are plots of detector response versus time. Chromatographs can be used to quantify the concentration of molecules in a sample.
- Coadding:** the process of adding interferograms together to achieve an improvement in signal-to-noise ratio.
- Condenser:** the optic in a microscope that focuses light onto the sample.
- Constructive interference:** a phenomenon that occurs when two waves occupy the same space and are in phase with each other. Since the amplitudes of waves are additive, the two waves will add together to give a resultant wave which is more intense than either of the individual waves. This phenomenon causes the centerburst seen in interferograms.
- Critical angle (θ_c):** $\theta_c = \sin^{-1}(n_2/n_1)$, where n_2 and n_1 are the refractive indices of two materials at the interface (n_2 being of the higher refractive material).
- Cross-validation:** when using factor analysis, the process by which the optimal number of factors is determined. Essentially, leaving specific standards out of the calculation, then actual performs calibrations and calculated concentrations are compared.
- Curve-fitting:** a method used to try and determine the number, shape, position, width, and height of a group of IR bands that overlap to give one broad band. The technique involves making initial estimate of the parameters, then using a least-squares-fitting routine to optimise the parameters.
- Deconvolution:** a way of mathematically enhancing the resolution of a spectrum to visualise spectral features that overlap to give a broad band. The calculation involves the use of cepstrums.
- Depth of penetration:** in ATR, a measure of how far-IR radiation penetrates into the sample. More precisely, it is the depth at which the evanescent wave has decreased to 37% of its original value. Depth of penetration is affected by a number of things including the wavenumber of IR radiation, the refractive index of the ATR crystal, and the angle of incidence of the light impinging on the sample.
- Depth profiling:** the ability of some sampling techniques (e.g., ATR and photoacoustic spectroscopy) to obtain spectra from different depths within a sample non-destructively. This allows the change in composition with depth to be studied.
- Derivative:** in mathematics, a plot of the slope of a function versus its x -axis values. In FT-IR, the derivative of a spectrum gives sharp features at the x -axis value of greatest absorbance. Thus, derivatives are used in peak picking and library searching.

- Destructive interference:** a phenomenon that occurs when two waves occupy the same space. Since the amplitudes of waves are additive, if the two waves are out of phase with each other, the resultant wave will be less intense than either of the individual waves.
- Diamond anvil cell:** a device used to prepare samples for transmission sampling by IR microscopy. The cell consists of two diamonds with flat faces. The sample is placed on one diamond face, and the second diamond face is brought into contact with the sample to squish it. The entire assembly is then placed in the IR beam of the IR microscope.
- Diffraction:** the bending of light around the edge of an opaque body, or through a narrow slit, resulting in a series of alternately high and low intensities in the shadow of the obstacle.
- Diffuse reflectance:** the phenomenon that takes place when IR radiation reflects off a rough surface. The light is transmitted, absorbed, scattered, and reflected by the surface. The light approaches the surface from one direction, but the diffusely reflected light leaves the surface in all directions. A reflectance sampling technique known as DRIFTS is based on this phenomenon.
- Dispersive instruments:** IR spectrometers that use a grating or prism to disperse IR radiation into its component wavenumbers before detecting the radiation. This type of instrument was dominant before the development of FT-IR.
- DRIFTS:** stands for diffuse reflectance Fourier transform IR spectroscopy, a reflection sampling technique that makes use of the phenomenon of diffuse reflectance, and is used primarily on powders and other solid samples.
- DTGS:** deuterated triglycine sulphate pyroelectric detectors are the most common detectors used in FT-IR instruments. They are chosen for their ease of use, good sensitivity, wide spectral responsivity, and excellent linearity. DTGS measures the heating effect of radiation and whose response is independent of wavelength.
- Dynamic range:** for an interferogram, it is the ratio of the large centerburst signal at zero optical path difference to the smallest recorded signal (which must be greater than the noise for any benefit from signal averaging). The A/D used must have sufficient precision to measure the entire range as any clipping or distortion of the largest signal affects the whole spectrum.
- Electric vector:** the electric part of electromagnetic radiation (light). It is the electric vector that interacts with molecules to give rise to IR spectra.
- Evanescent wave:** in ATR, the standing wave of radiation set up in the ATR crystal. The evanescent wave penetrates beyond the crystal surface into any sample brought into contact with the surface. As a result, the IR spectrum of the sample can be obtained.
- External standards:** a technique of quantitative analysis where the standards are run at a different point in time than the unknown samples.
- Factor analysis:** a method of multicomponent quantitative analysis.
- Far-IR:** IR radiation between 400 and 10 cm^{-1} .
- Felgett (multiplex) advantage:** an advantage of FT-IR instrument compared to scanning/single channel dispersive instruments. It is based on the fact that in FT-IR all the wavenumbers of light are detected at once.
- Fourier transform:** the calculation performed on an interferogram to turn it into an IR spectrum. The calculation involves a mathematical integral.
- Fourier transform infrared (FT-IR):** a method of obtaining IR spectra by first measuring the interferogram of the sample using an interferometer, then performing a Fourier transform on the interferogram to obtain the spectrum.
- Fluorolube:** polymer of trifluorovinyl chloride $(-\text{CF}_2-\text{CFCl}-)_x$ used for the preparation of mulls. Unlike Nujol, it does not mask CH stretch bands.
- Full spectrum search:** in library searching, the use of entire spectra when comparing unknown and library spectra. The advantage of this method is that the use of all the spectral data points gives a more accurate comparison.
- Functional groups:** structural fragments within a molecule that has unique reactivity or properties. For instance, the carbonyl group in acetone is an example of a functional group. The main use of IR spectroscopy is the detection of specific functional groups within molecules.
- Functional group chromatogram:** in GC-FT-IR, a plot of the absorbance in a specific wavenumber range versus time. Typically, the wavenumber range is chosen to correspond the absorbance of a specific functional group.
- Full width at half height:** a way of measuring the width of an IR band. The width of the band is measured at half the maximum absorbance value of the band. The peak width at full height of some gas-phase molecules is used to measure the resolution that an IR spectrometer has attained.
- GC-FT-IR:** stands for gas chromatography-Fourier transform infrared, a type of hyphenated technique. GC-FT-IR involves interfacing a gas chromatograph (GC) to an FT-IR to obtain the spectra of sample molecules as they come out of the GC. By combining the two techniques, complex mixtures can be analysed quickly.
- Germanium:** a brittle metallic element of a greyish-white colour having semiconductor properties. This element has a refractive index of 4.0 and is used in ATR accessories to measure high refractive index samples.
- Gram-Schmidt chromatogram:** in GC-FT-IR, a plot of total IR absorbance versus time. This chromatogram is used to determine how many sample components were detected by the FT-IR.
- Grazing angle reflection:** occurs when the IR beam bounces off a reflective substrate and passes through a sample at angles between 60 and 80° . This is best suited for films with thicknesses between 20 \AA and $0.5\text{ }\mu\text{m}$ that are on a metallic substrate.
- Heat and pressure films:** a transmission sampling technique used to obtain spectra of polymers. Polymer samples are heated under pressure until they flow and form a thin film. The film is then placed directly in the IR beam.
- Hit quality index (HQI):** in library searching, the number that shows how closely matched a library spectrum is to an unknown spectrum.
- HPLC-FT-IR:** stands for high-pressure liquid chromatography-Fourier transform infrared. This is a hyphenated technique

where a high-pressure liquid chromatograph is interfaced to an FT-IR, which detects molecules as they leave the chromatograph.

Hyphenated techniques: when an FT-IR is interfaced to another instrument that also performs chemical or physical analyses, a hyphenated technique is born. The name derives from the fact that the new technique is usually abbreviated with a hyphen and the letter FT-IR, such as GC–FT-IR. By interfacing FT-IRs to other instruments, more information about a sample can be obtained more quickly than using the two instruments to analyse the sample separately.

Index of refraction: the ratio of the velocity of radiation in a vacuum to its velocity in the medium through which it passes.

Infrared chromatogram: a plot of IR absorbance versus time. The hyphenated techniques GC–FT-IR and HPLC-FT-IR generate IR chromatograms. IR chromatograms are used to determine at what points in time the FT-IR detected something coming out of the chromatograph. Functional group chromatograms and Gram–Schmidt chromatograms are examples of IR chromatograms.

Infrared microscope: a microscope specially designed to handle visible and IR radiation. The microscope is interfaced to an FT-IR and used to visually examine and take the IR spectrum of small (less than 250 μm in diameter) samples.

Infrared microscopy: also known as IR microspectroscopy. The technique of using an IR microscope to obtain the IR spectrum of microscopic samples.

Infrared radiation: the portion of the electromagnetic (light) spectrum from 14000 to 10 cm^{-1} . This type of light is higher in wavenumber than radio and microwaves, but is smaller in wavenumber than visible light. The far-IR is found between 400 and 10 cm^{-1} , the mid-IR is between 400 and 4000 cm^{-1} , and the near-IR is between 4000 and 14000 cm^{-1} . IR radiation is the same thing as heat.

Infrared spectrometer: an instrument that is used to obtain the IR spectrum of a sample. The instrument typically consists of a source of IR radiation, a sample compartment to allow the radiation to interact with a sample, a means of determining the intensity of radiation as a function of wavenumber, and a way of displaying the spectrum of the sample.

Infrared spectroscopy: the study of the interaction of IR radiation with matter.

Infrared spectrum: a plot of measured IR intensity versus wavenumber. The features in an IR spectrum correlate with the presence of functional groups in a molecule, which is why IR spectra can be interpreted to determine molecular structure.

Instrument response function: the portion of a background spectrum due to the instrument. The instrument's components, such as mirrors, detector, and beamsplitter all contribute features to the instrument response function.

Interferogram: a plot of IR detector response versus optical path difference. The fundamental measurement obtained by an FT-IR is an interferogram. Interferograms are Fourier transformed to give IR spectra.

Interferometer: an optical device that causes two beams of light to travel different distances (optical path difference). The light beams are combined allowing constructive interference and

destructive interference to take place. By changing the optical path difference using the interferometer, an interferogram is measured.

Internal reflection: the phenomenon whereby light passing through material of high refractive index reflects off the surface of the material rather than passing out of it. Internal reflection takes place in fibre optics and in ATR.

Internal standards: a technique used in quantitative analysis. A known amount of a known substance called the "internal standard" is added to all standards and unknowns. The calibration curve is plotted with the ratio of the analyte's absorbance to the internal standard absorbance on the y-axis. By rationing the two absorbances measured at the same time, fluctuations in the instrument or sampling that may have affected absorbance values are cancelled out.

Jacquinot advantage: this is the throughput advantage of FT-IRs over traditional spectrometers that require a slit aperture. The advantage varies as wavenumber and depends on resolution (because of slit width changes). In practice, any advantage will also depend on source dimensions.

K matrix: a multicomponent quantitative analysis technique, also known as "classical least-squares" or CLS. In this method, absorbance is expressed as a function of concentration, and a least-squares fit is performed to obtain the calibration.

KBr pellet: a transmission sampling technique most commonly used on powders and other solids. The technique involves grinding the sample and KBr, diluting the sample in the KBr, then pressing the mixture to produce a transparent pellet. The pellet is then placed directly in the IR beam.

Kramers–Kronig transform: a mathematical calculation performed on specular reflectance spectra to get rid of restraints. The result of the calculation is an "n spectrum", which is a plot of refractive index versus wavenumber, and a "k spectrum" which is the true absorbance spectrum of the sample.

KRS-5: the trade name for thallium bromide iodide. It is commonly used as an ATR crystal. It is a very toxic substance, and should be handled with great care.

Kubelka–Munk units: units used to measure the intensity of diffusely reflected light. The Kubelka–Munk equation relates Kubelka–Munk units to the concentration and scattering factor of a sample. The scattering factor is determined by the particle size, shape, and packing density of the sample, and can be difficult to control. Kubelka–Munk units should be used when performing quantitative DRIFTS analyses.

Least-squares fit: a technique used to develop mathematical models of reality. By definition, a least-squares fit will provide the best model available. In FT-IR, least-squares fits are used in multicomponent quantitative analysis to model the correlation between IR spectra and concentration (calibration).

Library searching: a process in which an unknown spectrum is compared to a collection of known spectra kept in a spectral library. The comparison gives a number called the hit quality index, which represents how closely related two spectra are to each other. If a match is of high quality, it is possible to identify an unknown sample using library searching.

Matrix: surrounding substance within which the sample material is contained.

MCT: photoconductive detector (HgCdTe), which has a response that is markedly dependent upon wavelength.

Mechanical bearing: a device used in some interferometers to reduce friction between the moving mirror and its housing. In this particular device, the moving mirror and its shaft are typically held in place by ball bearings.

Microscope mapping: using an IR microscope to obtain spectra at different points in a sample. Often times a special computer-controlled microscope stage is used to obtain spectra at precise spatial intervals. The result of microscope mapping is a molecular map, which is a plot of absorbance at a specific wavenumber versus position on the sample.

Mid-infrared: IR radiation between 4000 and 400 cm^{-1} .

Mirror displacement: the distance that the mirror in an interferometer has moved from zero path difference.

Molecular maps: plots of absorbance at a specific wavenumber versus location on a sample. Usually obtained using microscope mapping.

Monochromator: a device used in dispersive instruments to separate an IR light beam into its component wavenumbers. A grating or prism is used for this purpose.

Mull: a transmission sampling technique where the sample is ground, then dispersed in an oil or mulling agent. The oil/sample mixture is then sandwiched between two KBr windows and placed in the IR beam.

Mulling agent/mulling oil: oil that is added to a ground sample for the preparation of mulls.

Multiplex (Felgett) advantage: is an advantage of FT-IR compared to dispersive instruments. It is based on the fact that in an FT-IR all the wavenumbers of light are detected at once.

Near-infrared: IR radiation between 14 000 and 4000 cm^{-1} .

Normalised: the process of dividing all the absorbance values in a spectrum by the largest absorbance value. This resets the y-axis scale from 0 to 1. Normalisation is often performed on spectra before library searching.

Nujol: a liquid paraffin (refined mineral oil) used for the preparation of mulls. Nujol is not always the best mulling agent as it masks any CH stretch bands that would otherwise be seen in the sample spectrum.

Objective: the optic in a microscope that collects light after it has interacted with the sample.

Optical distance: physical distance multiplied by the index of refraction of the medium.

Optical path difference: the difference in distance that two light beams travel in an interferometer.

P matrix: a multicomponent quantitative analysis technique, also known as “inverse least-squares” or ILS. In this method, concentration is expressed as a function of absorbance, and a least-squares fit is performed to obtain the calibration.

Peak editing: a process typically performed after a GC-FT-IR or HPLC-FT-IR run. IR chromatograms are viewed to determine when sample molecules were detected by the FT-IR. Then, the spectra acquired during the time when a sample was detected are coadded to improve signal-to-noise ratio.

Peak-to-peak noise: a noise measurement often made on a 100% line. It is measured as the difference between the lowest and highest noise value in a specific wavenumber range. When

obtained under controlled conditions, peak-to-peak noise is an excellent measure of spectrum quality and instrument health.

Photoacoustic spectroscopy (PAS): detecting a sample's IR spectrum by “listening” to the sound made when the sample absorbs IR radiation. A highly sensitive microphone is used as a detector, and the spectra are similar to absorbance spectra. This technique can be used for quantitative analysis. Carbon black is commonly used a reference material.

Polariser: a device converting ordinary light into a polarised light. Typical IR polarisers feature a ZnSe substrate with thin gold wires deposited on its surface.

Quantitative analysis: the use of peak heights, band ratios, or peak areas to calculate the amount of substance in an unknown sample.

Reference spectrum: in spectral subtraction, the spectrum of a substance that is subtracted from the spectrum of a mixture (sample spectrum). Often, the reference spectrum is of a solvent.

Reflectance sampling: a method of obtaining IR spectra by bouncing the IR beam off of the sample.

Reflection-absorption: a reflection sampling technique used on thin films coated on shiny metal surfaces. The IR beam passes through the film, reflects off the metal, and then passes through the film a second time before reaching the detector. This technique is also known as “double-transmission”.

Resolution: a measure of how well an IR spectrometer can distinguish spectral features that are close together. For instance, if two features are 4 cm^{-1} apart and can be discerned easily, the spectrum is said to be at least 4 cm^{-1} resolution. Resolution in FT-IR is determined by optical path difference.

Resolution, spectral: the ability of an instrument to distinguish between two spectral features that are close to each other in wavenumber. Resolution is measured in terms of the closest two features that can be distinguished. In FT-IR high resolution is denoted by small numbers, e.g., 0.01 cm^{-1} . Low resolution is denoted by large numbers, e.g., 64 cm^{-1} . In FT-IR, resolution is determined by the optical path difference.

Reststrahlen: derivative shaped spectral features that occasionally appear in specular reflectance spectra. Reststrahlen is caused by how a sample's refractive index changes in the vicinity of an absorbance band. The Kramers-Kronig transform can be used to remove reststrahlen from spectra.

Sample single beam spectrum: a single beam spectrum obtained with a sample in the IR beam. These spectra are typically rationed against background spectra to obtain absorbance or transmittance spectra.

Sample spectrum: in spectral subtraction, the spectrum of a mixture from which the reference spectrum is subtracted.

Sampling depth: in photoacoustic spectroscopy (PAS), the depth in the sample from which 63% of the photoacoustic signal is measured.

Scan: the process of measuring an interferogram with an FT-IR. Typically, this involves moving the mirror in the interferometer back and forth once.

Sealed liquid cells: a transmission sampling technique used to obtain the spectra of liquids. The cell consists of two KBr windows held apart a fixed distance by a gasket. The cell is filled with liquid then placed in the IR beam.

- Search algorithm:** in library searching, the mathematical calculation used to compare two spectra and produce a hit quality index, which measures how closely matched two spectra are to each other.
- Search report:** the end product of a library search. A search report ranks the quality of library matches using the hit quality index then presents these results in a table. Most software packages allow visual comparison of the unknown spectrum and the best library matches.
- Sidelobes:** spectral features that appear to the sides of an absorbance band as undulations in the baseline. Sidelobes are caused by having to truncate an interferogram, and can be removed from a spectrum by multiplying the spectrum's interferogram times an apodisation function.
- Signal-to-noise ratio (SNR):** the ratio of signal in a spectrum, usually measured as the intensity of an absorbance band, to noise measured at a nearby point in the baseline. SNR is a measure of the quality of a spectrum, and can be used to ascertain the quality of an IR spectrometer if it is measured under controlled conditions.
- Silicon:** element, atomic number 14, atomic weight 28.09, greyish metallic semiconductor. A very hard, inert crystal with a refractive index of 3.42, Silicon is very useful for far-IR in the range 400–30 cm^{-1} .
- Single beam spectrum:** the spectrum that is obtained after Fourier transforming an interferogram. Single beam spectra contain features due to the instrument, the environment, and the sample (if there is one in the beam).
- Smoothing:** a spectral manipulation technique used to reduce the amount of noise in a spectrum. It works by calculating the average absorbance (or transmittance) of a group of data points called the "smoothing window", and plotting the average absorbance (or transmittance) versus wavenumber. The size of the smoothing window determines the number of data points to use in the average, and hence the amount of smoothing. The "smoothing algorithm" determines how the average is calculated.
- Spectral subtraction:** a spectral manipulation technique where the absorbances of a reference spectrum are subtracted from the absorbances of a sample spectrum. The idea is to remove the bands due to the reference material from the sample spectrum. This is done by simply calculating the difference in absorbance between the two spectra, then plotting this difference versus wavenumber. The reference spectrum is often multiplied times a subtraction factor so that the reference material bands subtract out properly.
- Specular reflectance:** the type of reflectance that takes place off smooth, shiny surfaces, such as that of mirrors. By definition, in specular reflectance the angle of incidence of light equals the angle of reflectance of light. Specular reflectance, as a reflection sampling technique, can be used to obtain IR spectra.
- Split mulls:** the technique of using two different mulling oils, namely Nujol and Fluorolube to obtain two mulls of the same sample. These two oils are transparent in different wavenumber ranges. By splicing the spectra of the two mulls together, a spectrum free of most mulling oil absorbances can be obtained.
- Standards:** in quantitative analysis, samples that contain known concentrations of the analyte. The absorbance of these samples is measured and then used in a calibration.
- Subtraction factor:** in spectral subtraction, a number that is multiplied times the reference spectrum before it is subtracted from the sample spectrum. The purpose of the subtraction factor is to match the absorbances of the reference material in the two spectra so the reference bands subtract out cleanly. Also known as the "scale factor".
- Subtrahend:** see reference spectrum.
- Thermal wave:** in photoacoustic spectroscopy, the heat deposited in a sample due to IR absorption that travels towards the surface of the sample. It is caused by the fact that heat is conducted from areas of high temperature to areas of low temperature.
- Throughput advantage (Jacquinot advantage):** an advantage of FT-IR over dispersive instruments due to the fact that in FT-IR all the radiation strikes the detector at once, enhancing signal-to-noise ratio.
- Transmission:** a physical phenomenon where radiation passes through a body. When producing a transmission spectrum a proportion of the energy is absorbed by the sample, while the remainder travels on to the detector.
- Transmission sampling:** a sampling method where the IR beam passes through the sample before it is detected. Samples are typically diluted or flattened to adjust the absorbance values to a measurable range.
- Transmittance:** a unit used to measure the amount of IR radiation transmitted by a sample. It is often used as the *y*-axis unit in IR spectra. Transmittance is not linearly proportional to concentration, and spectra plotted in these units should not be used for quantitative analysis.
- Transmittance spectrum:** transmittance is defined by the following equation: $T = I/I_0$ where T is the transmittance, I_0 the IR intensity measured without a sample in the beam, and I the IR intensity measured with a sample in the beam. Transmittance spectra are calculated by rationing a sample single beam spectrum to a background spectrum. These spectra are plotted as % T versus wavenumbers. Transmittance is not linearly proportional to concentration, and transmittance spectra should not be used for quantitative analysis.
- Water cooled source:** an IR source whose temperature is controlled by a flow of water or other cooling liquid.
- Wavelength:** one wavelength is the distance between two identical points on two adjacent identical waves in a beam.
- Wavenumber:** is defined as $1/\text{wavelength}$. The units of wavenumbers are cm^{-1} , and are most commonly used as the *x*-axis unit in IR spectra. $1 \mu\text{m} = 1000 \text{ nm} = 10\,000 \text{ cm}^{-1}$; $5 \mu\text{m} = 5000 \text{ nm} = 2000 \text{ cm}^{-1}$.
- Wings:** the portion of an interferogram where there is little or no intensity.
- Zero path difference (ZPD), or zero optical path difference (ZOPD):** the mirror displacement at which the optical path difference for the two beams in an interferometer is zero. At ZPD, ZOPD, the detector signal is often very large, the centerburst.